APPLICATION OF DYNAMICAL SYSTEMS THEORY

TO NONLINEAR AIRCRAFT DYNAMICS

Thesis by

Craig C. Jahnke

In Partial Fulfillment of the Requirements

for the Degree of

Doctor of Philosophy

California Institute of Technology

Pasadena, California

1990

(Submitted January 5, 1990)

I would like to thank NASA Dryden Flight Research Center for helping support this research and for providing the F-14 aerodynamic data. I would also like to thank Professor Fred E. C. Culick for editing this thesis and his helpful and supportive comments. Finally I would like to thank my wife Sharon for her support and encouragement while I was writing this thesis.

ABSTRACT

A continuation method has been used to determine the steady states of three nonlinear aircraft models: a general aviation aircraft with a canard configuration, a generic jet fighter, and the F-14. The continuation method calculated the steady states of the aircraft as functions of the control surface deflections. Bifurcations of these steady states were determined and shown to cause instabilities which resulted in qualitative changes in the state of the aircraft. A longitudinal instability which resulted in a deep stall was determined for the general aviation aircraft. Roll-coupling and high angle of attack instabilities were determined for the generic jet fighter, and wing rock, directional divergence and high angle of attack instabilities were determined for the F-14.

Knowledge of the control surface deflections at which bifurcations occurred was used to either put limits on the control surface deflections or to program the control surface deflections such that a combination of control surface deflections at which bifurcations occur could not be attained. Simple control systems were included in the aircraft models to determine the effects of control systems on the instabilities of each aircraft. Steady spin modes were determined for each aircraft. A successful recovery technique was determined for the general aviation aircraft, but no successful recovery technique could be found for the F-14.

TABLE OF CONTENTS

page

LIST OF SYMBOLS

b - wing span

c - wing chord

g - gravitational acceleration

I_x - moment of inertia about aircraft x-axis

I_y - moment of inertia about aircraft y-axis

I_z - moment of inertia about aircraft z-axis

ℓ - roll moment

m - pitch moment

M - aircraft mass

n - yaw moment

p - roll rate

q - pitch rate

Q - dynamic pressure

r - yaw rate

S - wing surface area

T - applied thrust

V - aircraft speed

W - aircraft weight

X - force along aircraft x-axis

Y - force along aircraft y-axis

Z - force along aircraft z-axis

α - angle of attack

β - angle of sideslip

δa - aileron deflection

δe - elevator deflection

δr - rudder deflection

θ - pitch angle

ϕ - roll angle

ψ - yaw angle

I. INTRODUCTION

1.1 HISTORY OF FLIGHT

1.1.1 Development of the First Aircraft

The first significant advances towards human flight were made in the nineteenth century, when Sir George Cayley (1783-1857) made engravings showing the basis for a fixed wing aircraft (Culick [1988]). The aircraft included a vertical tail for directional stability and a horizontal tail for longitudinal stability. Cayley also realized that the wings should not provide the thrust for the aircraft. This was a major advance as previous aircraft had been modelled after birds and included flapping wings for thrust. Cayley actually built several gliders that flew and one carried a man.

Alphonse Penaud (1850-1880) made several important contributions to human flight. Penaud rediscovered that longitudinal stability can be provided by an aft horizontal tail and gave the first correct discussion of this result. He also built and flew many model aircraft. Among these models was the first aircraft in which the thrust was provided by a propellor. Penaud built several stable powered model aircraft which led most later aircraft builders to seek an inherently stable aircraft (Culick [1988]).

Otto Lilienthal (1848-1896) was an exception to this rule. He made many successful gliding flights because he realized that the pilot must learn how to fly. He also gathered the first quantitative data on the lift and drag of airfoils. The

airfoil sections he analyzed were modelled on bird wings which led to the use of thin highly cambered airfoil sections. This was a logical approach, but led to poor choices of airfoil sections, a problem that plagued aircraft designers for years. The Wright brothers used Lilienthal's data on the lift and drag of airfoils to design their early gliders. Lilienthal had a significant effect on the Wright brothers' development of the first human-carrying aircraft. It is often stated that Lilienthal's death in a glider crash in 1896 renewed Wilbur's interest in flight (Howard [1987]).

While the Wright brothers were influenced by Lilienthal's work, they were unique in their approach to the problem of human flight in several ways. The Wright brothers' concern with the control of the aircraft instead of stability was a major difference between their work and previous efforts. This concern led them to develop a movable canard, the first elevator, for controlling pitching motions. Lilienthal had been concerned with the control of his gliders, but his only method of control was the movement of his body, which changed the location of the center of gravity of the aircraft. Other efforts completely ignored the control issues and concentrated on stability.

The Wright brothers also realized that the lateral motions of the aircraft, (i.e., roll and yaw motions), were important, while previous work considered only pitching motions. A wing warping mechanism was designed by the Wrights which allowed the pilot to control rolling motions and was essentially the first aileron. The Wrights patented their wing warping system and could be said to have held

back the entire United States effort to build better aircraft by their defense of this patent during the years prior to World War I. The patent stopped any other manufacturer from selling an aircraft with ailerons for several years. Patent fights stopped Glen Curtis from selling his aircraft, which had the first modern aileron (Howard [1987]).

While the Wright brothers developed a good understanding of the dynamics of an aircraft, they never wrote down quantitative expressions describing the motions of an aircraft. Bryan published the first complete analysis of the pitch stability of an aircraft in 1903. This was several months before the Wright brothers' first flight, but was unknown to them and did not influence aircraft design for several years (Culick [1988]). The first aircraft inventors built airplanes by trial and error and generally ended up with failures. The Wright brothers were an exception, and their work is an excellent example of a thorough, well thought research program.

When the Wright brothers first flew in 1903 they were far ahead of their contemporaries. The Wrights continued working on their aircraft in an effort to improve its performance and endurance. They tried to keep their accomplishments secret because they wanted to sell their invention to the military and did not want their secret stolen. In 1905 the Wrights were ready to sell their invention to the military, but the military was not interested. The Wrights kept their success so secret that nobody in Washington believed flight was possible, and their obsession with secrecy prevented them from giving a demonstration until a contract was signed.

The Wrights spent the next several years trying to sell their aircraft to the United States and European militaries. The process was very time consuming, so neither brother had much time to work on their aircraft. By this time the Wrights were also involved with several patent suits. The result was that the Wrights could no longer work on their aircraft and their contemporaries started to catch up to them. Finally, the Wrights got a contract with the United States and French militaries. They then spent a great deal of their time training pilots, again causing them to put off working on their aircraft.

The Wright brothers' aircraft were eventually surpassed for several reasons. They did not have enough time to improve on their design and Wilbur's untimely death in 1912 caused Orville to spend most of his time on business matters. The Wrights were also reluctant to change the design of their aircraft. While the aircraft was a remarkable achievement when it was first designed, it was difficult to fly and required an experienced pilot. The Wrights' aircraft continued to be canard configurations and used wing warping for roll control. French designs soon surpassed the Wrights with aircraft characterized by aft tails for longitudinal stability and control and ailerons instead of wing warping for roll control. The majority of aircraft used by the allies in World War I were French built because they had the best designs.

1.1.2 Development of Modern Aircraft

Aircraft design procedures changed radically after World War I as inventors

were replaced by trained scientists. The question of whether manned flight was possible had been answered and aircraft designers now concentrated on building better aircraft. The hard part of this problem was that it was not clear what constituted a better airplane. One early question was: is it desirable to have a stable airplane? There were adherents to both sides of this conflict and both sides had valid points. People who favored unstable airplanes thought that control was more important, as the Wrights had, and were more concerned with maneuverability than ease of flying. Indeed, many modern aircraft are designed to be unstable without their flight control systems to obtain a more maneuverable aircraft. Adherents of stable aircraft eventually prevailed as the endurance of aircraft increased because pilots became fatigued flying unstable aircraft for long distances.

By the 1930's aircraft designers were using both wind tunnels and analytical techniques to design better airplanes. Aircraft were becoming much faster as a result of more streamlined designs and the cantilever wing, which made monoplanes feasible. Wing spans were also reduced relative to the overall length of the aircraft. This combination of high speed, low aspect ratio wings caused fighter aircraft of the late 1930's to exhibit instabilities related to inertial coupling. The instabilities were especially prevalent during rolling maneuvers and came to be called roll-coupling instabilities. Many aircraft were lost in roll-coupling instabilities causing the instability to become a major focus of aeronautical research in

the 1950's. Attempts to analyze the roll-coupling instability will be discussed in Section 1.2.

Stalls have been a problem for aircraft designers and pilots since the first attempts at flying manned gliders. Stalls often lead to a phenomenon called a stall/spin in which the aircraft loses lateral and directional stability after the wing stalls. This loss of stability causes the aircraft to experience increasing roll and yaw rates which, if not checked, can lead to a fully developed spin. Many early aircraft pioneers, including Otto Lilienthal, were killed in crashes caused by the stall/spin phenomenon. Stall/spins were particularly dangerous in most early gliders because the designers, excluding the Wrights, tended to concentrate on the stability of the aircraft and neglect the control. As a result it was usually impossible to control the lateral rotations caused by the stall/spin, resulting in many crashes. Stall/spins continued to be poorly understood in the early days of manned flight. Pilots needed a great deal of flying experience to learn how to avoid stalling the aircraft or deal with stall/spin phenomenon when they occurred. Unfortunately, for many pilots the first experience with a stall proved fatal.

Stalling was a major concern of the Wright brothers and caused their emphasis on controlling their aircraft. They wanted to be able to recover from a stall if they got into one. Their efforts were not always successful. A crash during one of the Wright brothers early flights is thought to have been the result of a stall/spin (Howard [1987]). Nobody was seriously injured in the crash, as the aircraft was fairly close to the ground at the time of the stall. As aircraft became more reliable

pilots went to higher altitudes and a new phenomenon, called a steady spin, was discovered. A steady spin is a steady state of an aircraft characterized by high rotation rates and a helical flight path about a vertical axis (see Figure 1.1). An aircraft generally enters a steady spin after the transient motions of a stall/spin, with the steady spin becoming fully developed in a few rotations. Spins proved deadly because it is impossible to get out of fully developed spins in many aircraft.

Spins continued to be a problem even as aeronautics became better understood. Two hundred fighter and trainer aircraft were lost in post stall/spin accidents from 1966 to 1970 resulting in 100 fatalities [Adams, 1972]. The spin problem actually became more difficult in modern fighter aircraft because the moment of inertia in yaw is 20 times greater in a 1969 aircraft than in a 1949 aircraft, which causes the spins in modern aircraft to contain more momentum. Meanwhile, rudder size and moment arm have remained approximately the same (Chambers, Bowman, and Anglin [1969]).

One of the difficulties with spins is that it is a highly nonlinear phenomenon. The flow field is very complex resulting in nonlinear aerodynamic coefficients and large rotation rates that make inertial coupling an important part of the aircraft dynamics. Each aircraft also exhibits unique spin characteristics. Most aircraft exhibit phugoid and short period modes in low angle of attack flight and instabilities of theses modes can be treated in the same general way, while the spin behavior of each aircraft design is unique. For example, increasing the dihedral of the horizontal tail might improve the spin behavior of one aircraft

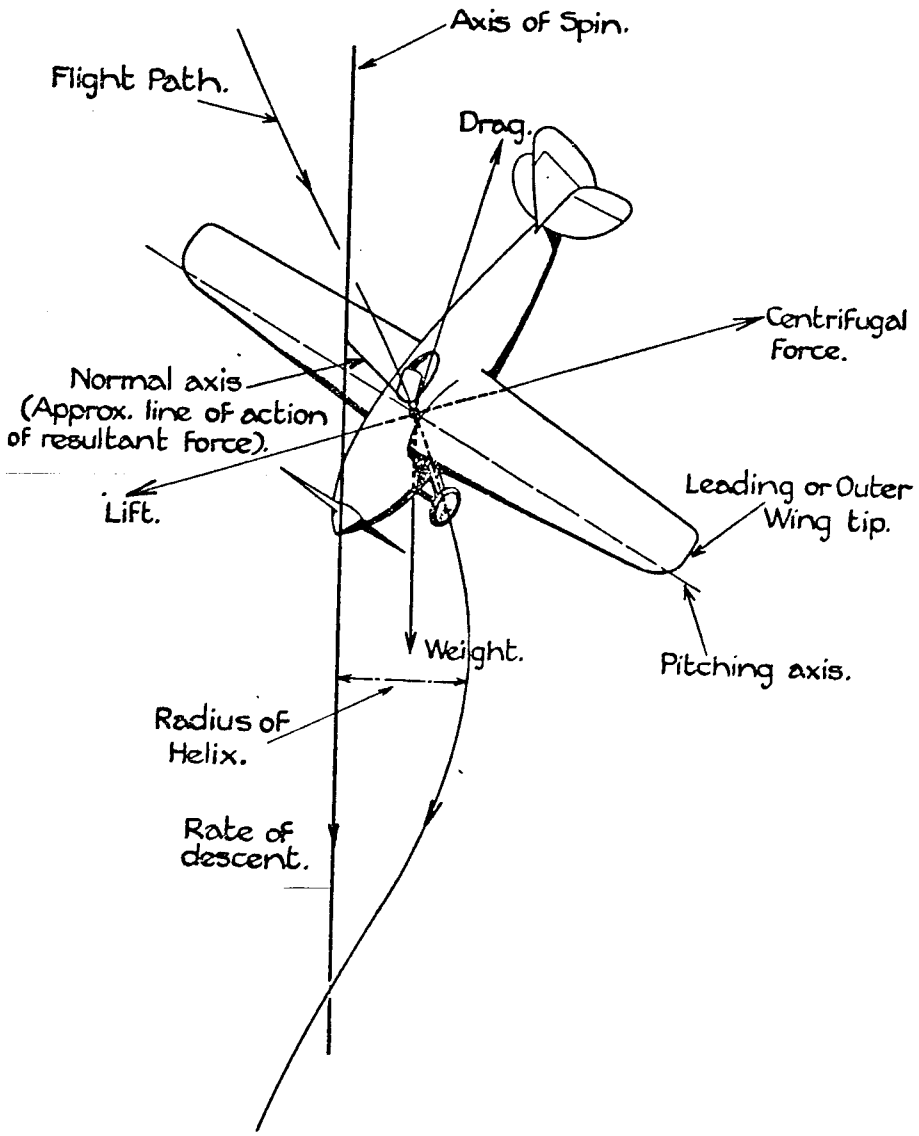

Figure 1.1: Flight path and force balance of a steady spin (Irving [1933]).

while degrading the spin behavior of another aircraft. Thus, most of the research on spins has concentrated on specific airplanes. Previous attempts to analyze the spin phenomenon will be discussed in Section 1.3.

Control theory and aircraft design have been closely linked since the early 1900's. The Wright brothers attempted to design a control system for their aircraft which would have functioned as an autopilot, but their efforts were not very successful (Howard [1987]). The first functioning control system was an autopilot designed by the Sperry brothers and demonstrated in 1914. The demonstration consisted of Sperry standing in the cockpit with his arms above his head while his mechanic walked out on the wing in an attempt to upset the aircraft (Nelson [1989]).

Control systems have grown tremendously in scope and design since that first functioning control system. Most airplanes today have extensive flight control systems and some aircraft cannot be flown without their flight control systems. This is particularly true of high performance jet fighters. Control systems are designed to give aircraft desirable stability and control characteristics and can significantly alter the dynamics of the aircraft. Linear control theory is used to design most control systems, even in nonlinear flight regimes. The general approach is to linearize the equations of motion for a particular flight regime and determine the feedback gains which give the aircraft desirable operating characteristics. For example, the lateral equations of motion are neglected when analyzing the short

period instability, while the longitudinal equations of motion are neglected when studying the Dutch roll instability.

1.2 The Roll-Coupling Instability

Roll-coupling instabilities were first studied by William Phillips [1948]. The difficulty of studying the roll-coupling instability is that it is a nonlinear phenomenon. Linearized equations of motion, which were generally used for analyzing aircraft motion, could not be used to study roll-coupling. Phillips' approach was to use the simplest set of equations that retained the roll-coupling behavior. He analyzed the three moment equations (see Section 3.1) and neglected the remaining equations. A linear aerodynamic model was used and the inertial terms, which were typically neglected, were retained to preserve the roll-coupling behavior.

Phillips assumed a constant roll rate, which identically satisfied the rolling moment equation, and used the roll rate as a parameter in the pitching and yawing moment equations. By choosing the roll rate as a parameter, he changed the three-dimensional nonlinear system into a two-dimensional linear system containing a parameter. The resulting system is analogous to a pair of coupled mass-spring systems where the variables are the pitch and yaw angles. Phillips assumed small angles of pitch and yaw and expanded the moment coefficients in terms of these angles. Phillips found, by analyzing the response of the system for various roll rates, that critical roll rates existed above which either pitching or yawing motions became unstable. The mode with the lowest stability became unstable and

the critical roll rate was given by the lower of the pitching or yawing natural frequencies.

Subsequent research attempted to calculate the sideslip deviations caused by the roll coupling instability. Large deviations in sideslip had been observed in flight and had resulted in loss of the vertical tail on several aircraft. Sideslip deviations cause the vertical tail to be at an angle of incidence to the flight path and result in significant vertical tail loads. Aircraft designers were interested in predicting the maximum sideslip in order to calculate the maximum expected tail load and design the tail accordingly. The general approach was to run flight simulations of maneuvers involving roll-coupling and record the maximum sideslip deviations (Stone [1953], Pinsker [1958], Rhoads and Schuler [1957]). While these results did not add to the basic understanding of roll-coupling instabilities given by Phillips, they did show that current methods for estimating maximum sideslip deviations were inadequate. In particular, they showed that inertia terms were essential for predicting the response of the aircraft and the behavior of the aircraft is much more violent if the initial pitch rate is nonzero.

Welch and Wilson [1957] and Westerwick [1957] attempted to reduce the effects of roll-coupling with flight control systems. The idea was to use elevator and rudder feedback to keep the pitch and yaw rates small, thus reducing the inertial moments during a maneuver. This approach only applies when purely rolling motion is desired. It is more common to want a combination of rolling and pitching or yawing, such as in a rolling pull-out. This approach also assumes that

there exists sufficient elevator and rudder power to keep the pitch and yaw rates small. This is not always the case and in many flight regimes, specifically high angle of attack flight, it is certainly not the case.

Analysis of the roll-coupling problem became easier with the introduction of the concept of pseudosteady states. A pseudosteady state is a steady state of the fifth order equations of motion (see Section 3.1.3). Pinsker [1958] and Rhoads and Schuler [1957] showed that Phillips' critical roll rates could be obtained by analyzing the pseudosteady states of an aircraft. Pseudosteady states can be plotted as a function of the control surface deflections and critical control surface deflections at which instabilities occured could be determined. Analysis of the pseudosteady states also gave the values of all variables at the jump, not just the critical roll rate.

Obtaining the pseudosteady states for an aircraft involves solving a system of five coupled nonlinear algebraic equations. This is a difficult problem and most researchers simplified the equations of motion as much as possible. Inertia in roll was generally neglected and only linear aerodynamic models were analyzed. It was generally assumed that the angles of attack and sideslip were small so the tangent of the angle could be replaced by the angle itself (Pinsker [1958], Welch and Wilson [1957], Gates and Minka [1959]). The resulting system could be reduced to a polynomial equation involving the roll rate, which could be solved to determine the pseudosteady state roll rate. All other variables could be determined from the roll rate. This analysis showed the existence of multiple pseudosteady states

for fixed control surface deflections. Critical control surface deflections were obtained by determining which control surface deflections caused the appearance or disappearance of pseudosteady states.

The above results were all limited by the use of linear aerodynamic models. Schy and Hannah [1977] extended the above results by analyzing aerodynamic models which were nonlinear functions of the angle of attack and linear functions of the angle of sideslip. Nonlinear aerodynamic coefficients made it necessary to solve a system of two coupled nonlinear algebraic equations, which can be done quickly with the help of a computer. Young, Schy and Johnson [1980] used this method to study the roll-coupling instability and calculated curves of steady states as functions of the aileron deflection. Multiple curves of steady states were shown to exist for zero aileron and rudder deflections and an elevator deflection of negative 3.1 degrees. Angles of attack for these steady states ranged from 5 to 85 degrees. The 5 degree angle of attack steady state represents straight level flight while the other steady states represent steady spins. Straight level flight was the only stable steady state as the spins were all unstable. Jump phenomena related to roll-coupling were only shown to occur for pitch down maneuvers, which involve negative angles of attack. This was also shown by Pinsker [1958].

1.3 Previous Spin Research

Early researchers discovered many qualitative properties of steady spins (Irving [1933]). They recognized the steady spin as an equilibrium state and studied

the balance of forces and moments. These studies showed that an airplane in a steady spin follows a helical path with the lift force balancing the centrifugal force and the drag balancing the weight (see Figure 1.1). Force balance could always be maintained by changing the radius and rotation rate of the spin, so the existence of a steady spin depends on whether or not the moments could be balanced. Early researchers also knew that it was often impossible to get out of a spin because the flow over the fin and rudder was blocked by the horizontal tail, thus eliminating yaw control. Their solution to this problem was to design aircraft with larger vertical tails.

While early researchers had a good intuitive understanding of the spin, they could not do much quantative research. Early attempts at analyzing the spin behavior of aircraft used linearized equations of motion and generally obtained poor results. This would be expected because inertial coupling and nonlinear aerodynamics are both important to the spin behavior of an aircraft. Computers made it possible to use numerical simulations to study the tendency of an aircraft to go into a spin (Scher and Anglin [1959], Grantham and Scher [1960], Grantham and Grafton [1965]). Calculated results were compared to spin tunnel results and full scale flight tests. There was often poor correlation between the three types of results. Simulation studies suffered from poor aerodynamic data because it was difficult to model the complex flow fields of a spin in a wind tunnel. Spin tunnel tests were usually at different Reynolds numbers than the full scale flight tests,

which is cited as a possible cause of the discrepencies between full scale and spin tunnel tests (Scher and Anglin [1959]).

More recently, attempts have been made to determine the spin modes of an aircraft by determining its steady states, as was done in studies of the roll-coupling instability. Analyzing spins is more difficult than analyzing the roll-coupling instability as more complex aerodynamic models must be used to represent the forces and moments in this highly nonlinear flow. Adams [1972] developed a numerical routine which determined the spin modes of various aircraft by searching for steady states that represented the helical path of a spin. This method for determining the spin modes of an aircraft is much more efficient than determining the spin modes with simulations.

Adams determined the spin modes of four different aircraft, but his results did not compare very well with flight tests. He attributed the discrepencies to insufficient aerodynamic models. Rotary balance data were not included in any of the aerodynamic models, which is a probable source of the difference between the numerical results and flight tests. Chambers, Bowman, and Anglin [1969] have shown that rotary balance data are required to model aerodynamic forces and moments in a spin. In particular, they showed that damping in yaw is a nonlinear function of the yaw rate and that the interaction between the vertical and horizontal tails provides the autorotative forces in a spin.

Tischler and Barlow [1981] went the opposite route and included rotary balance data in their analysis, but used more simplified equations of motion. They

determined steady spin modes by searching for states of the aircraft where the moments were balanced. Force balance was maintained by assuming that the side force was negligible while balancing the longitudinal forces by adjusting the spin radius and rate of descent. These simplified equations of motion predicted the spin modes for a general aviation aircraft fairly accurately. Tischler and Barlow's results were much better than Adam's, who used more complete equations of motion but no rotary balance data. This seems to indicate the necessity of using rotary balance data in the analysis of the spin modes of an aircraft.

1.4 Approach of This Research

The previous methods of analyzing aircraft dynamics tend to be specific to one type of motion. The equations of motion are usually simplified to study one type of motion. This is an effective method for studying specific phenomena, such as roll-coupling, but requires the researcher to have some previous knowledge of the phenomena. Also, some instabilities might be missed because of simplifications undertaken in the analysis. For example, the roll-coupling instability was determined in flight, often with fatal results, because linearized equations of motion, used for most early analysis, could not predict the instability.

The present research retains the complete equations of motion in an effort to search for any instabilities that might occur. This is possible with the use of continuation methods, which are numerical techniques for determining the steady states of systems of differential equations as a function of a parameter of the

system. Guicheteau [1981], Carroll and Mehra [1982], Planeaux [1988], and Jahnke and Culick [1988] have used continuation methods to analyze the equations of motion for an aircraft. Their results have shown the value of this approach for analyzing nonlinear aircraft dynamics. Bifurcations, which cause the system to exhibit qualitatively different behavior, often occur as a parameter is varied. Many types of bifurcations exist and each type causes the behavior of the system to change in specific ways. Dynamical systems theory provides a methodology for determining which types of bifurcations occur in a system and their effect on the dynamics of the system and will be used in this thesis to interpret the effects of bifurcations on the motions of an aircraft.

The remainder of this report is divided into six main sections. Section II will introduce the main ideas of dynamical systems theory and the numerical techniques which were used in this thesis. Section III will describe the equations of motion and aerodynamic models which were used in this thesis. Results for the three aerodynamic models discussed in Section III will be presented in Sections IV, V, and VI. Particular emphasis is placed on the roll-coupling and high angle of attack dynamics of each aircraft. Simple linear feedback control systems are included in some of the analysis to determine the effect of feedback control in nonlinear flight regimes. Section VII summarizes the major findings of this work.

II. THEORY

2.1 DYNAMICAL SYSTEMS THEORY

The following section introduces the main points of dynamical systems theory. While the following information is well known to mathematicians, it is generally less well known to engineers. This information is presented with the latter group in mind, to summarize the basis for the results presented in this paper. Important theorems of dynamical systems theory will be presented, but proofs will not be given. Proofs for the various theorems can be found in Guckenheimer and Holmes [1983], Wiggins [1988], and Ioos and Joseph [1980]. Most of the following discussion will involve the practical consequences of dynamical systems theory with aircraft dynamics in mind. Simple examples will be discussed to introduce phenomena that will be encountered in the results presented in Sections IV, V, and VI.

2.1.1 Definition of a Dynamical System

A dynamical system is a set of ordinary differential equations of the form

$$\dot{x} = f(x, t; \mu) \tag{2.1.1}$$

where x is an n-dimensional vector, $\dot{x}$ represents differentation of x with respect to time, f is an n-dimensional vector field, t is time, and μ is an m-dimensional parameter. Many physical systems, including the equations of motion for an aircraft, can be modelled by dynamical systems. These systems are characterized by

nonlinear vector fields that depend on one or more parameters and are difficult to analyze. Dynamical systems theory provides a methodology for analyzing nonlinear dynamical systems and has proven effective in analyzing many nonlinear physical systems. Bifurcations, periodic motions and chaotic motions have been predicted and verified for, among others, the periodically forced Duffing equation and the Lorenz equations (Guckenheimer and Holmes [1983]).

In this discussion of dynamical systems theory, only those concepts that are applicable to the analysis of the equations of motion for an aircraft will be introduced. With this in mind, only dynamical systems with time independent vector fields will be discussed. Dynamical systems of this type are called autonomous and have the form

$$\dot{x} = f(x;\mu). \tag{2.1.2}$$

This will limit the analysis of the equations of motion to maneuvers with controls fixed, but this is already a difficult problem and a good place to start the analysis. Also, dynamical systems theory has only proven effective in analyzing time periodic systems, which are not applicable to general transient aircraft maneuvers.

Concepts and techniques from dynamical systems theory that have been used to analyze the equations of motion for an aircraft will be introduced in the following sections. The concepts will be discussed for a general vector field (i.e., $f(x;\mu)$), and examples for one and two-dimensional vector fields will be given. Illustrations with elementary examples avoids obscuring the concepts with details, and allows clear graphical presentation of the results. All vector fields are assumed to be

smooth in the following discussion, where smooth means that the vector field and all of its derivatives are continuous. This allows us to ignore questions about the required degree of differentiability of the vector field for the theorems introduced in this section and results in a clearer introduction to dynamical systems theory.

2.1.2 Phase Space

The phase space of a dynamical system is the Euclidean space of the dependent variables of the vector field. Thus, the phase space has the same dimension as the system and each axis represents one of the dependent variables. The phase space for the equations of motion for an aircraft is twelve-dimensional with the axes representing the variables $(p, q, r, \alpha, \beta, V, \theta, \phi, \psi, x, y, z)$ (see Section 3.1). Figure 2.1.1 shows the phase space for a two-dimensional system with artificial examples of solution curves. A solution curve for a system is determined by integrating the system with respect to time from some initial condition.

Since solution curves are determined by integrating the system, solution curves are smooth for smooth vector fields. Solution curves in phase space cannot intersect in finite times because of the uniqueness of solutions to ordinary differential equations. This is easy to see in the two-dimensional case shown in Figure 2.1.2. At each point (x, y) the values of $\dot{x}$ and $\dot{y}$ are unique and determine the direction of the solution curve through that point. If a solution curve intersects itself, there must be two values of the vector $(\dot{x}, \dot{y})$, as shown at the point (x_o, y_o), a condition not allowed by uniqueness of the vector field.

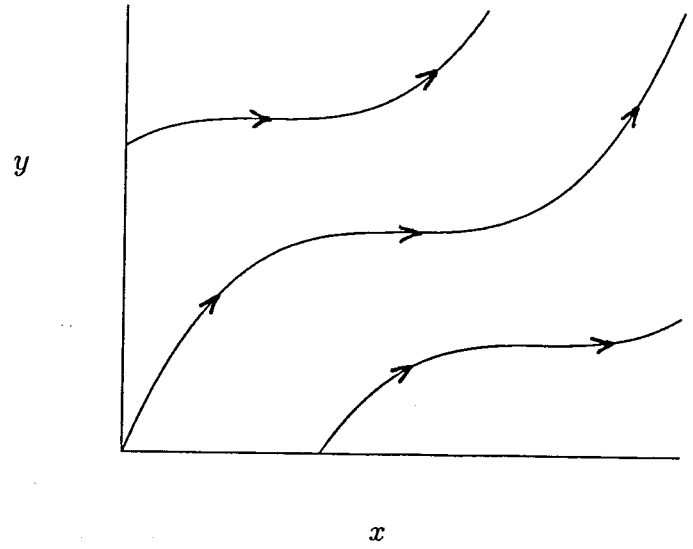

Figure 2.2.1: Phase space with several integral curves.

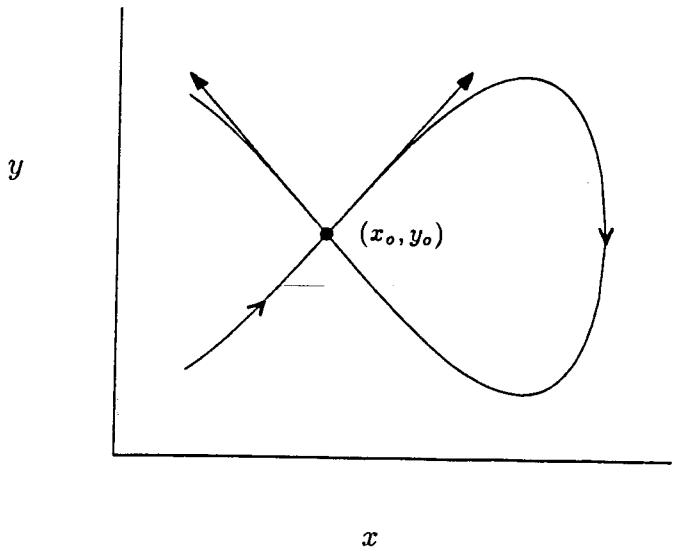

Figure 2.1.2: Solution curves for a nonunique vector field.

Solution curves of a dynamical system show the evolution of the system for given initial conditions. For many systems, and surely for an aircraft, it is im-

possible to determine the solution curves analytically, as this requires integrating the system of simultaneous nonlinear equations. Numerical integration is then required to determine the solution curves of the system. This may be practical for small, relatively simple systems, but for large systems it is practically impossible to determine the solution curves for all initial conditions in the phase space and all parameter values.

One more shortcoming of phase space representations is that for systems of dimension four or higher, it is not possible to show the entire phase space in one plot. It is necessary to show the phase space in two or three-dimensional projections which makes it much more difficult to interpret the dynamical behavior in the phase space. Phase space representations are extremely useful for two-dimensional systems and have been effective in analyzing perturbations of two-dimensional integrable systems. This method has been widely used to study the forced Duffing equation and bifurcations, periodic motions, and chaotic motions have been predicted and verified (Guckenheimer and Holmes [1983]). In this report, phase space techniques will be used to develop certain theoretical techniques, but will not be used extensively to present results for the dynamics of an aircraft.

2.1.3 Fixed Points

The first step in analyzing a complex system, according to dynamical systems theory, is to determine the fixed points of the system. Fixed points of a dynamical

system are points in phase space where all time derivatives are zero. Fixed points are also called zeros and equilibrium points. A fixed point for the equations of motion for an aircraft is a state of the aircraft where all translational and rotational accelerations are zero and the roll and pitch angles are constant. The differential equation governing the yaw angle is decoupled from the force and moment equations, so a constant yaw angle is not required at a fixed point. This is a result of the definition of the Euler angles and will be discussed in Section 3.1. Trimmed flight and steady spins are both examples of fixed points for aircraft motions.

Fixed points describe the equilibrium states of the system but provide no direct information about the transient response of the system. Some information about the transient response of the system can be inferred from the fixed points, because in many cases a maneuver involves going from one fixed point to another. Thus, in many cases the fixed points can be used to predict the final state of the system after a parameter is changed. For example, if the elevator is deflected in trimmed flight the fixed points for the new elevator setting can be used to predict the possible new angles of attack for the aircraft.

The fixed points of a dynamical system can be determined by setting all time derivatives equal to zero and solving the resulting set of algebraic equations. For the system

$$\dot{x} = f(x;\mu) \tag{2.1.3}$$

the fixed points can be determined by solving the equation

$$f(x;\mu) = 0. \tag{2.1.4}$$

This reduces the problem from solving a system of nonlinear differential equations to one of finding the zeros of a nonlinear function. This is still a substantial problem, but the zeros of nonlinear functions have been studied for many years. Many theoretical and numerical techniques have been developed and will be used in this study.

The most important result for the study of the fixed points of nonlinear dynamical systems is the Implicit Function Theorem. The Implict Function Theorem can be stated as follows, where F represents the function in equation (2.1.4) (Ioos and Joseph, Chapter 2):

Let $F: R^n \times R^m \to R^n$ satisfy, for some $\rho_1 > 0, \rho_2 > 0$ sufficiently small:

a) $F(x_o;\mu_o) = 0$,

b) $F_x(x_o,\mu_o)$ has a bounded inverse,

c) $F(x;\mu)$ and $F_x(x;\mu)$ continuous for $|x - x_o| < \rho_1$ and $|\mu - \mu_o| < \rho_2$.

Then there exists $x = x(\mu)$ for all $|\mu - \mu_o| < \rho_2$ such that:

i) $x(\mu_o) = x_o$,

ii) $F(x(\mu);\mu) = 0$,

iii) For $|\mu - \mu_o| < \rho_2$ there is no solution other than $x(\mu)$,

iv) $x(\mu)$ is continuous.

A proof of the Implicit Function Theorem can be found in most advanced calculus books and will not be given here. The theorem means that if the system obtained by linearizing about the fixed point has nonzero Jacobian determinant, then there is a unique curve of fixed points in a small region around that fixed point. This is shown graphically in Figure 2.1.3. The existence of continuous curves of fixed points is central to continuation methods and will be discussed in greater detail in Section 2.2.1. It is important to note that the Implicit Function Theorem is only valid in a small region around the fixed point. The statement that a single branch of fixed points exists applies only to this small region. In many nonlinear dynamical systems there is more than one fixed point for a given parameter value. The theorem implies that multiple branches of fixed points cannot intersect in a small region around a fixed point where the conditions of the theorem are met. Thus, we can expect to find separated branches of fixed points for many nonlinear dynamical systems. The following example should make the above points clear.

Consider the unforced Duffing equation,

$$\begin{aligned} \dot{x} &= y, \\ \dot{y} &= \mu\, x - x^3 - y, \end{aligned} \tag{2.1.5}$$

which models a mass-spring system with a nonlinear spring. The variables (x, y) represent the displacement and velocity of the mass respectively. Fixed points of this system are determined by solving the set of equations

$$\begin{aligned} 0 &= y, \\ 0 &= \mu\, x - x^3 - y. \end{aligned} \tag{2.1.6}$$

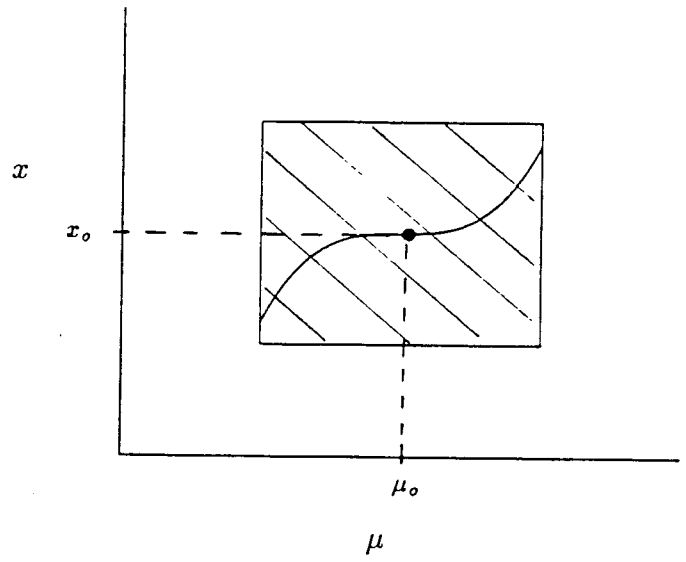

Figure 2.1.3: Graphical representation of the Implicit Function Theorem.

For $\mu < 0$ there is one fixed point: $(x, y) = (0, 0)$, and for $\mu > 0$ there are three fixed points: $(x, y) = (0, 0), (\sqrt{\mu}, 0), (-\sqrt{\mu}, 0)$. These fixed points can be plotted on what is called a bifurcation diagram, a plot of the fixed points of the system as a function of one of the parameters of the system. The bifurcation diagram for the Duffing equation is shown in Figure 2.1.4. Because the y variable is zero for all fixed points, it is not shown.

Several characteristics of nonlinear dynamical systems, which were mentioned above, are evident in the bifurcation diagram for the Duffing equation. The first is that the fixed points are continuous functions of the parameters of the system. When μ is zero two branches of fixed points intersect, seeming to contradict the uniqueness result of the Implicit Function Theorem. However, the Implicit Function Theorem does not hold at this point because the Jacobian determinant is

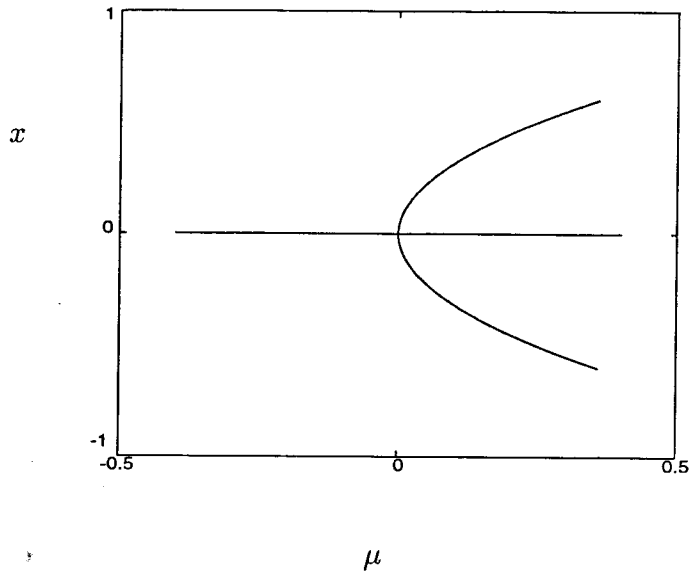

Figure 2.1.4: Bifurcation diagram for the Duffing equation.

zero. The fixed point $(x, y; \mu) = (0, 0, 0)$ is what is called a bifurcation point and will be discussed in Section 2.1.5. Another characteristic of nonlinear dynamical systems evident in the bifurcation diagram of the Duffing equation is the existence of multiple fixed points for a given parameter value. For values of μ that are greater than zero there are three fixed points. While the three fixed points merge as μ goes to zero and the two branches of fixed points intersect, this is not always the case. A nonlinear system may have branches of fixed points that never intersect. The equations of motion for an aircraft contain both intersecting and non-intersecting branches of fixed points.

2.1.4 Stability of Fixed Points

Once the fixed points of a dynamical system have been found it is important

to determine their stability. The stability of a fixed point determines whether the state of the system is attracted to the fixed point or repelled from it. There are two general types of stability. Global stability characterizes the stability of a fixed point for any initial condition in the phase space, while local stability characterizes the stability of a fixed point in a small region around the fixed point.

The global stability of a fixed point is very useful, but difficult to compute. One method of computing the global stability of a fixed point is Liapunov's Method. Liapunov's method involves computing the direction of the vector field on a curve around the fixed point. If the vector field points inward on all curves around the fixed point, the fixed point is globally stable. If the vector field points outward on all curves around the fixed point, the fixed point is globally unstable. The difficulty of Liapunov's method is finding a family of curves such that the vector field always points inward or outward on the curves. Indeed it is not always possible to find such a family of curves for a given fixed point. The method is very successful for two-dimensional systems, but will not be used on the equations of motion for an aircraft. All of the stability results for fixed points of the equations of motion for an aircraft will be local.

The local stability of a fixed point is very easy to calculate by using the Hartman-Grobman Theorem (Guckenheimer and Holmes, Chapter 1). The theorem states that the stability of a fixed point of a nonlinear system can be calculated by determining the eigenvalues of the system obtained by linearizing about the fixed point, as long as no eigenvalues have zero real parts. A fixed point is stable

if the real parts of all eigenvalues are less than zero and unstable if any eigenvalue has a real part that is greater than zero. Two-dimensional phase plots of the various stability types are shown in Figure 2.1.5. If one or more eigenvalues have zero real parts, the Center Manifold Theorem is used to determine the stability of the fixed point, a matter discussed in Section 2.1.6.

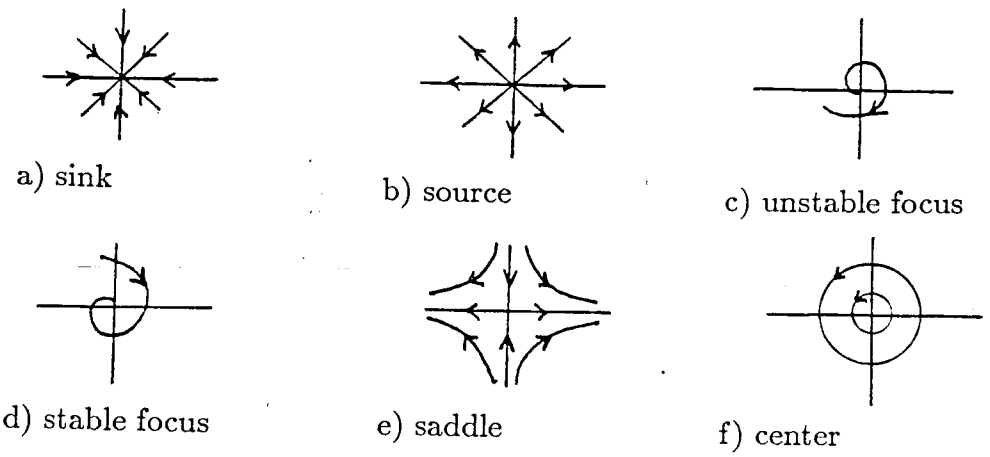

Figure 2.1.5: Stability types for a linear system.

Linearizing a system at a fixed point involves calculating the Jacobian at that point. For the nonlinear dynamical system

$$\dot{x} = f(x;\mu), \tag{2.1.7}$$

the linearized system about the fixed point (x_o, μ_o) is given by

$$\dot{u} = f_x(x_o, \mu_o)\, u \tag{2.1.8}$$

where $u = x - x_o$ and $f_x(x_o, \mu_o)$ is the Jacobian of $f(x, \mu)$ evaluated at (x_o, μ_o). Note that this is simply a Taylor expansion about the fixed point where $f(x_o; \mu_o)$

is zero because (x_o, μ_o) is a fixed point. The linearized system for the Duffing equation is

$$\begin{pmatrix} \dot{u} \\ \dot{v} \end{pmatrix} = \begin{pmatrix} 0 & 1 \\ \mu_o - 3\,x_o^2 & -1 \end{pmatrix} \begin{pmatrix} u \\ v \end{pmatrix} \tag{2.1.9}$$

where $u = x - x_o$ and $v = y - y_o$. The eigenvalues of this system are

$$\lambda_{1,2} = -\frac{1}{2} \pm \frac{1}{2}\sqrt{1 - 4(3\,x_o^2 - \mu_o)}. \tag{2.1.10}$$

It is important to notice that the eigenvalues of the linearized system are continuous functions of the parameters of the system. This is true for all smooth vector fields and will be important to the discussion of continuation methods in Section 2.2.1. The eigenvalues for the fixed point $(x_o, y_o) = (0, 0)$ are given by $\lambda_{1,2} = -\frac{1}{2} \pm \frac{1}{2}\sqrt{1 + 4\,\mu_o}$. Thus for $\mu < 0$ the fixed point $(x_o, y_o) = (0, 0)$ is stable and for $\mu > 0$ the fixed point $(x_o, y_o) = (0, 0)$ is unstable. The eigenvalues for the fixed points $(x_o, y_o) = (\pm\sqrt{\mu_o}, 0)$ are given by $\lambda_{1,2} = -\frac{1}{2} \pm \frac{1}{2}\sqrt{1 - 8\,\mu_o}$. These fixed points are stable for all positive values of μ. The stability of the fixed points can be shown on a bifurcation diagram by plotting stable fixed points with solid lines and unstable fixed points with dashed lines. This convention is shown in Figure 2.1.6 for the Duffing equation and will be used throughout this thesis.

2.1.5 Bifurcations of Fixed Points

The Implicit Function Theorem states that if the linearized system at a fixed point is nonsingular, there is a unique curve of fixed points through that point. If the linearized system at a fixed point is singular (i.e., its Jacobian vanishes),

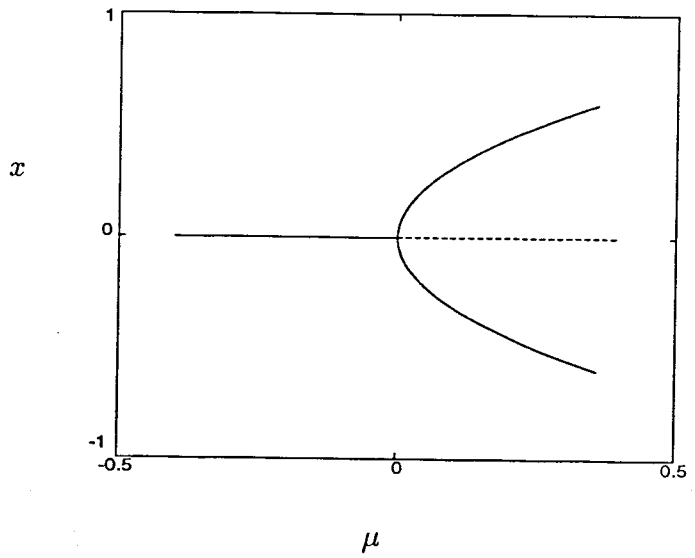

Figure 2.1.6: Bifurcation diagram for the Duffing equation; —— stable, – – – unstable.

the Implicit Function Theorem does not apply and qualitative changes may occur in the structure of the fixed points, such as two branches of fixed points intersecting. These changes are called bifurcations and lead to qualitative changes in the response of the system. We have already seen an example of a bifurcation in the Duffing equation. The bifurcation occurs when μ is zero and is characterized by the intersection of two branches of fixed points. The bifurcation also causes a change in the stability of one branch of fixed points. This can be seen in Figure 2.1.6 by following the branch of fixed points where x is zero from negative to positive values of μ.

Changes in the structure of the fixed points at a bifurcation point can best be understood by studying the Taylor expansion of the vector field. We will use

a one-dimensional vector field with a one-dimensional parameter for this purpose. Calculations are simple for a one-dimensional system and the results are the same for bifurcations in an n-dimensional system if only one real eigenvalue is zero at the bifurcation point. This is a result of the Center Manifold Theorem, which will be discussed in Section 2.1.6. Bifurcations with a pair of complex eigenvalues having zero real parts will be discussed using a two-dimensional system later in this section. Bifurcations with more than one zero eigenvalue or pair of complex eigenvalues having zero real parts are more complicated and are outside the scope of this work.

Assume that the one-dimensional system

$$\dot{x} = f(x;\mu) \tag{2.1.11}$$

has a fixed point at $(x,\mu) = (0,0)$. This can be obtained for an arbitrary fixed point, (x_o,μ_o), by the linear transformation

$$(x,\mu) \to (x + x_o, \mu + \mu_o). \tag{2.1.12}$$

Here we assume that the fixed point is at the origin $(0,0)$; the Taylor expansion of the vector field near this fixed point is

$$\begin{aligned} f(x;\mu) = {} & f_x(0,0)\ x + f_\mu(0,0)\ \mu + \frac{1}{2} f_{xx}(0,0)\ x^2 \\ & + f_{x\mu}(0,0)\ x\ \mu + \frac{1}{2} f_{\mu\mu}(0,0)\ \mu^2 + \cdots . \end{aligned} \tag{2.1.13}$$

If $f_x(0,0)$ and $f_\mu(0,0)$ are both nonzero the dynamical system in a small region around the fixed point can be expressed as

$$\dot{x} = f_x(0,0)\ x + f_\mu(0,0)\ \mu \tag{2.1.14}$$

and the fixed points of the approximate system are given by the formula

$$x = -\frac{f_\mu(0,0)}{f_x(0,0)}\ \mu. \tag{2.1.15}$$

The curve of fixed points through the point $(0,0)$ is approximated by a line, so only one curve of fixed points passes through $(0,0)$, as implied by the Implicit Function Theorem.

If $f_x(0,0)$ is identically zero, second order terms in x must be included in the Taylor expansion and the approximate system is

$$\dot{x} = f_\mu(0,0)\ \mu + \frac{1}{2} f_{xx}(0,0)\ x^2. \tag{2.1.16}$$

The fixed points of the approximate system lie on the curve

$$\mu = -\frac{f_{xx}(0,0)}{2f_\mu(0,0)}\ x^2. \tag{2.1.17}$$

Solutions of this equation depend on the sign of the terms $f_{xx}(0,0)$ and $f_\mu(0,0)$. Both terms are assumed to be positive in this discussion and a plot of this case is shown in Figure 2.1.7. The stability of a fixed point can be determined by linearizing equation 2.1.16 at that point. Linearizing about the fixed point (x_o, μ_o) results in the equation

$$\dot{u} = f_{xx}(0,0) x_o u$$

where $u = x - x_o$. It is clear that fixed points where x_o is greater than zero are unstable and fixed points where x_o is less than zero are stable (recall that $f_{xx}(0,0) > 0$). Note that the stability of the origin cannot be determined by

the linearized system because the Jacobian (here simply $\frac{df}{dx}$) is zero at the origin. This type of bifurcation is known as a saddle-node bifurcation because two fixed points are created or destroyed as the parameter is varied. Here as μ is increased through zero, two fixed points are destroyed, one of which is a saddle (unstable fixed point) and the other is a node (stable fixed point). Saddle-node bifurcations are also called turning points and folds.

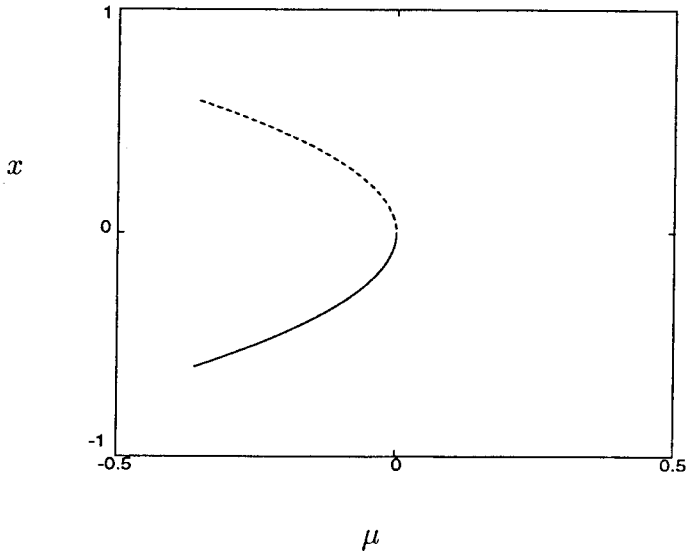

Figure 2.1.7: Bifurcation diagram of the saddle-node bifurcation, —— stable, – – – unstable.

Several effects of the saddle-node bifurcation on the structure of the fixed points of the system are common to most bifurcations. The linear part of the Taylor expansion about the bifurcation point is zero, so the structure of the fixed points becomes nonlinear. This allows many changes in the structure of the fixed points; branches of fixed points may intersect, undergo changes in stability or new

branches may appear. The exact changes that occur depend on the local structure of the vector field in a small region around the bifurcation point. As more terms vanish in the Taylor expansion about the bifurcation point, the structure of the fixed points becomes more complicated. There are many types of bifurcations and the changes that occur in the structure of the fixed points are special to each bifurcation. It is necessary to determine which type of bifurcation occurs before changes in the structure of the fixed points can be determined. The following examples will show the changes that occur in the structure of the fixed points for some common bifurcations relevant to the analysis of aircraft dynamics.

Assume that the dynamical system

$$\dot{x} = f(x;\mu)$$

has a fixed point at the origin and that the vector field is such that $f_x(0,0)$ and $f_\mu(0,0)$ are both zero. The approximate dynamical system in a small region around the bifurcation point is

$$\dot{x} = \frac{1}{2} f_{xx}(0,0)\ x^2 + f_{x\mu}(0,0)\ x\ \mu + \frac{1}{2} f_{\mu\mu}(0,0)\ \mu^2. \tag{2.1.18}$$

The fixed points of the approximate system are given by

$$x = -\frac{f_{x\mu}(0,0)}{2f_{xx}(0,0)}\ \mu\ (1 \pm D) \tag{2.1.19}$$

where

$$D = \sqrt{1 - \frac{4f_{xx}(0,0)f_{\mu\mu}(0,0)}{f_{x\mu}^2(0,0)}}. \tag{2.1.20}$$

If D is greater than zero, two curves of fixed points intersect at the bifurcation point with different tangents. The bifurcation diagram for $D = 1$ (i.e., $f_{\mu\mu}(0,0) = 0$) is shown in Figure 2.1.8. A bifurcation of this type is called a transcritical bifurcation and is characterized by the transverse intersection of two branches of fixed points which change stability at the bifurcation point. Recall that this analysis is only valid in a small region around the fixed point. If higher order terms were included in the expansion, the branches of fixed points could be curved. This analysis only gives the slopes of the curves at the bifurcation point; if there is more than one slope at the fixed point, there must be more than one branch of fixed points going through that point.

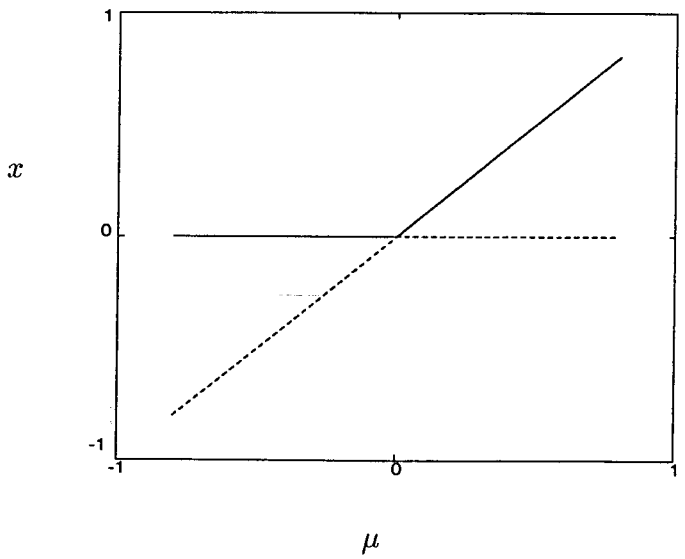

Figure 2.1.8: Bifurcation diagram of the transcritical bifurcation, —— stable, – – – unstable.

If $D = 0$, there is only one slope at the bifurcation point. This is a degener-

ate case and higher order terms must be included in the expansion to determine whether there is only one branch of fixed points or if two branches intersect tangentially at the the bifurcation point. This is called a cusp-point bifurcation and is shown in Figure 2.1.9 (Ioos and Joseph [1980]). Transcritical bifurcations are much more common than cusp-point bifurcations because the cusp-point bifurcation requires a special relationship between the second derivatives of $f(x;\mu)$. If D is less than zero there are no curves through the bifurcation point and the bifurcation point is an isolated fixed point.

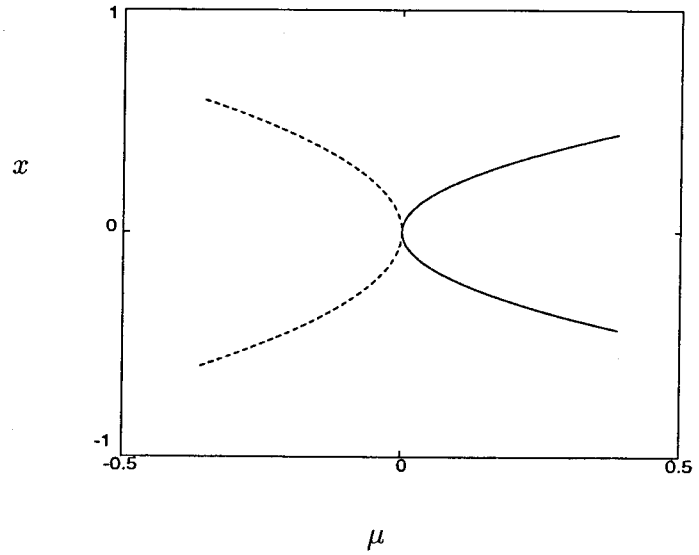

Figure 2.1.9: Bifurcation diagram for the cusp point bifurcation, —— stable, – – – unstable.

Another bifurcation that commonly occurs in physical problems is the pitchfork bifurcation. We have already seen this bifurcation in the Duffing equation. The local form of the dynamical system in the neighborhood of a pitchfork bifur-

cation is

$$\dot{x} = f_{x\mu}(0,0)\ x\ \mu + \frac{1}{6} f_{xxx}(0,0)\ x^3, \tag{2.1.21}$$

as all lower order derivatives are zero at the bifurcation point. One possible bifurcation diagram for a pitchfork bifurcation is shown in Figure 2.1.10. One characteristic of the fixed points near a pitchfork bifurcation is the transverse intersection of two branches of fixed points, such that on one branch $\mu_x(x_o) = 0$. Because of this condition there will be one fixed point for parameter values on one side of the bifurcation and three fixed points for parameter values on the other side of the bifurcation.

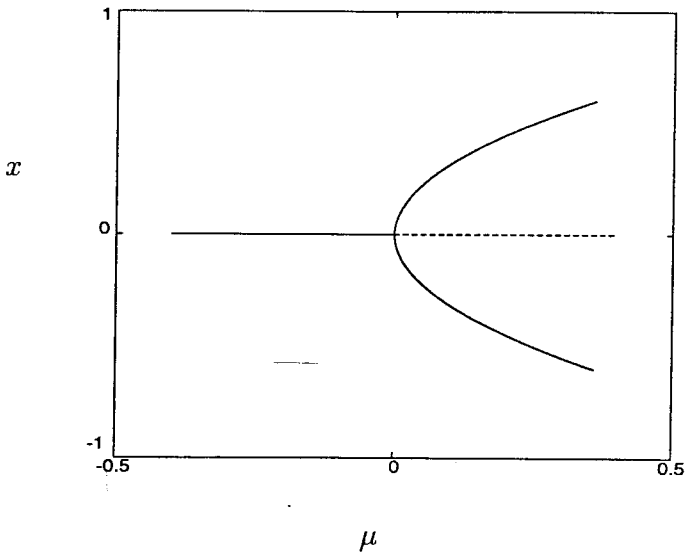

Figure 2.1.10: Bifurcation diagram for the pitchfork bifurcation, —— stable, – – – unstable.

These examples should make it clear that the local structure of the vector field at the bifurcation point determines the effect of the bifurcation on the fixed

points of the system. The structure of the fixed points near the bifurcation point becomes more complex as more derivatives of the vector field equal zero at the bifurcation point. An unlimited number of terms could be zero, resulting in very complicated solution structures. Those possibilities will not be discussed here, as they rarely occur in physical systems. Saddle-node and pitchfork bifurcations are the only one-dimensional bifurcations that have been found for the equations of motion for an aircraft.

The above discussion has been limited to one-dimensional vector fields so only one real eigenvalue could be zero at a bifurcation point. In systems of dimension two or greater, more than one eigenvalue could be zero at a bifurcation point. It is rare for two real eigenvalues to be zero at a bifurcation point, and analyzing this situation is very involved. For these reasons, and because bifurcations for which two real eigenvalues equal zero have not arisen in the analysis of the equations of motion for an aircraft, bifurcations with two or more zero real eigenvalues will not be discussed here. A thorough discussion of bifurcations with multiple zero eigenvalues is given in Guckenheimer and Holmes [1983].

Another difference between one-dimensional systems and systems of dimension two or greater is that complex eigenvalues cannot occur in one-dimensional systems, whereas they are common in systems of dimension two or greater. Also, since complex eigenvalues come in pairs, the real parts of two complex eigenvalues must change signs at the same time. The response of a dynamical system in the neighborhood of a fixed point with a pair of complex eigenvalues having zero real

parts can be determined by studying the Taylor expansion of the system at the fixed point. For simplicity we will examine the behavior of the two-dimensional system

$$\begin{pmatrix} \dot{x} \\ \dot{y} \end{pmatrix} = \begin{pmatrix} \mu & -\omega \\ \omega & \mu \end{pmatrix} \begin{pmatrix} x \\ y \end{pmatrix} + \begin{pmatrix} (x-y)\,(x^2+y^2) \\ (x+y)\,(x^2+y^2) \end{pmatrix} \tag{2.1.22}$$

where μ is a parameter and ω is a constant. This system has a fixed point at $(x, y) = (0, 0)$ for all values of μ. The eigenvalues of the system obtained by linearizing about this fixed point are

$$\lambda_{1,2} = \mu \pm i\omega \tag{2.1.23}$$

where $i = \sqrt{-1}$. This shows that the fixed point $(x, y) = (0, 0)$ is stable for μ less than zero and unstable for μ greater than zero. The eigenvalues have zero real parts if μ equals zero so a bifurcation must occur at the point $(x, y; \mu) = (0, 0; 0)$.

Recall that the Implicit Function Theorem does not apply at fixed points where one or more real eigenvalues equal zero, because the Jacobian matrix is not invertible. It is then possible to have multiple branches of fixed points intersecting at the bifurcation point as we found for the transcritical and pitchfork bifurcations. At a bifurcation point where two complex eigenvalues have zero real parts and nonzero complex parts the Jacobian matrix is invertible so the Implicit Function Theorem will apply. In the above system, for example, the determinant of the Jacobian matrix is equal to $\mu^2 + \omega^2$, so the matrix is invertible at the bifurcation point (i.e., for $\mu = 0$). Then, by the Implicit Function Theorem, only one curve of fixed points can go through the bifurcation point.

To get an idea of what might occur at this type of bifurcation point, it is useful to study the behavior of the linearized system at the bifurcation point. The linearized system is

$$\begin{pmatrix} \dot{x} \\ \dot{y} \end{pmatrix} = \begin{pmatrix} 0 & -\omega \\ \omega & 0 \end{pmatrix} \quad \begin{pmatrix} x \\ y \end{pmatrix} \tag{2.1.24}$$

which is simply the equation for a harmonic oscillator. The solution curves for this system are a family of periodic orbits as shown in Figure 2.1.11. The addition of higher order terms to the system would likely change the solution structure, but some periodic orbits might still exist.

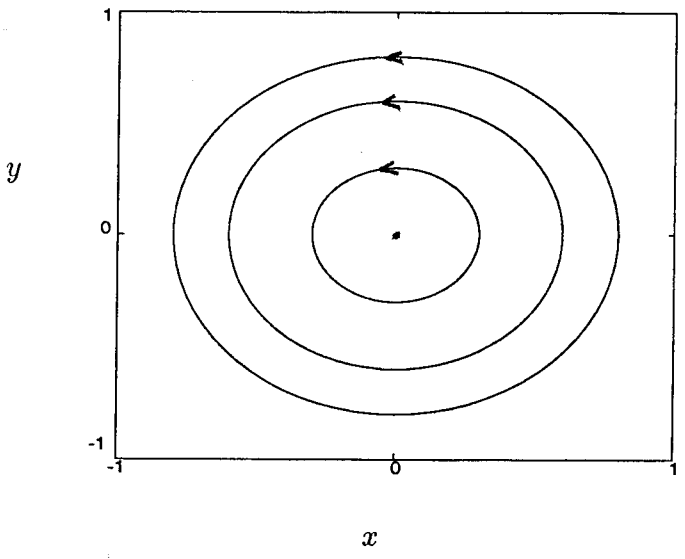

Figure 2.1.11: Solution curves for the harmonic oscillator.

It will be easier to find periodic orbits if the system is transformed into polar coordinates. The polar coordinates are defined by the formulas

$$\begin{aligned} x &= r\cos\theta, \\ y &= r\sin\theta, \end{aligned} \tag{2.1.25}$$

so the transformation to polar coordinates is

$$\begin{pmatrix} \dot{r} \\ \dot{\theta} \end{pmatrix} = \begin{pmatrix} \cos\theta & \sin\theta \\ -\frac{1}{r}\sin\theta & \frac{1}{r}\cos\theta \end{pmatrix} \begin{pmatrix} \dot{x} \\ \dot{y} \end{pmatrix}. \tag{2.1.26}$$

Application of this transformation produces the system

$$\begin{aligned} \dot{r} &= \mu r + r^3, \\ \dot{\theta} &= \omega + \mu + r^2. \end{aligned} \tag{2.1.27}$$

For μ, r small, $\dot{\theta}$ is essentially constant, so the system can be analyzed by considering only the first equation.

The fixed points for r are given by $r = 0, \sqrt{\mu}$, (only positive values of r have meaning) and the bifurcation diagram for this is shown in Figure 2.1.12. If the equation for $\dot{\theta}$ is added to the system, the fixed points where r is greater than zero will be turned into periodic orbits. This situation is shown in Figure 2.2.13. This type of bifurcation is called a Hopf bifurcation and is often encountered in the analysis of the equations of motion for an aircraft. This is only one of many possible bifurcations that could occur when the linearized system has one pair of complex eigenvalues with zero real parts. The structure of the periodic orbits will change depending on the form of the equation for $\dot{r}$; another example is shown in Figure 2.1.14. This example is highly degenerate and is not likely to occur as it requires more terms in the vector field to be zero at the bifurcation point.

2.1.6 Center Manifold Techniques

Examples of the different types of bifurcations of fixed points discussed in the previous section were either one or two-dimensional. The dimension of the system

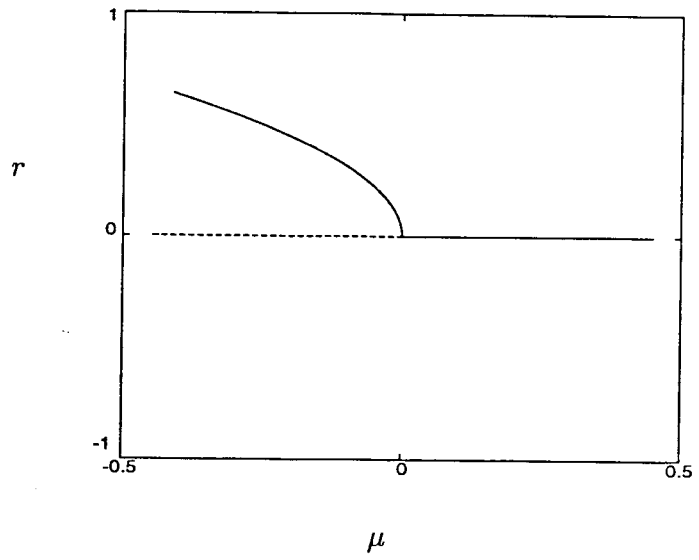

Figure 2.1.12: Bifurcation diagram for equation 2.1.27.

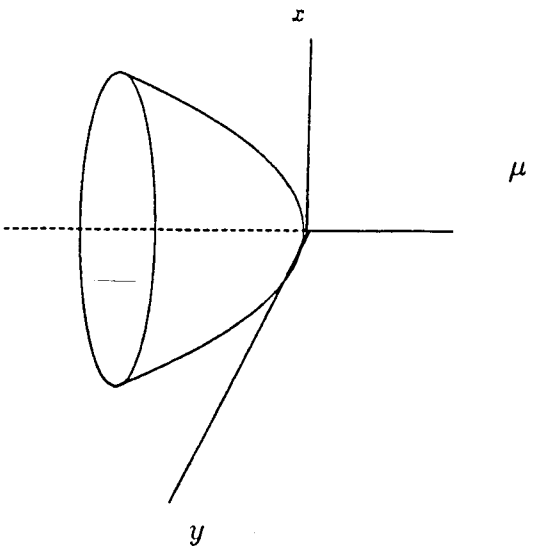

Figure 2.1.13: Bifurcation diagram for the Hopf bifurcation.

equalled the number of eigenvalues having real parts equal to zero. A logical question would be: what happens if a system of dimension greater than one has

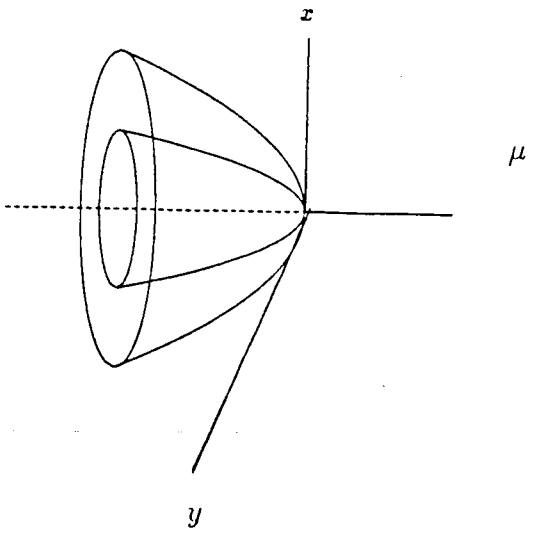

Figure 2.1.14: Bifurcation diagram for a degenerate Hopf bifurcation.

one zero eigenvalue? For example, what can we deduce about the structure of the fixed points of the equations of motion for an aircraft in a neighborhood of a fixed point with one zero eigenvalue? This is exactly the question that the Center Manifold Theorem answers. It happens that to analyze the structure of the fixed points in the neighborhood of a fixed point with one or more eigenvalues having real parts equal to zero, it is sufficient to study a system with dimension equal to the number of eigenvalues for which the real parts vanish (Guckenheimer and Holmes [1983]). This means that if a fixed point of the equations of motion for an aircraft has one eigenvalue with real part equal to zero then the response of the aircraft in a neighborhood of that fixed point can be determined by studying a one-dimensional system.

Some new concepts must be introduced before the methodology for determin-

ing the lower dimensional system can be discussed. The first concept is that of an invariant manifold. An invariant manifold is a curve in phase space such that a motion started on that curve will remain on the curve for all time. The integral curves shown in Figure 2.1.1 are one type of invariant manifold. Any fixed point is also an invariant manifold because if the system starts at a fixed point it will stay there forever.

The Center Manifold Theorem is based on the existence of three invariant manifolds of a fixed point. For a linear system, they are defined as

$$E^s = span\{\text{eigenvectors whose eigenvalues have real part} < 0\}$$

$$E^c = span\{\text{eigenvectors whose eigenvalues have real part} = 0\}$$

$$E^u = span\{\text{eigenvectors whose eigenvalues have real part} > 0\}$$

and are called the stable, center, and unstable eigenspaces. For example, consider the linear system

$$\begin{pmatrix} \dot{x} \\ \dot{y} \end{pmatrix} = \begin{pmatrix} 1 & 0 \\ 0 & -1 \end{pmatrix} \quad \begin{pmatrix} x \\ y \end{pmatrix}. \tag{2.1.28}$$

The eigenvalues are $\lambda = 1, -1$, so the stable and unstable eigenspaces are both one dimensional and the center eigenspace is the null space. The eigenvector corresponding to the positive eigenvalue is $(x, y) = (1, 0)$, and the eigenvector corresponding to the negative eigenvalue is $(x, y) = (0, 1)$. Thus, the stable eigenspace is the y-axis and the unstable eigenspace is the x-axis. This is shown graphically in Figure 2.1.15.

For a nonlinear system the stable, center, and unstable manifolds of a fixed point are curves in phase space and can be related to the eigenvectors of the

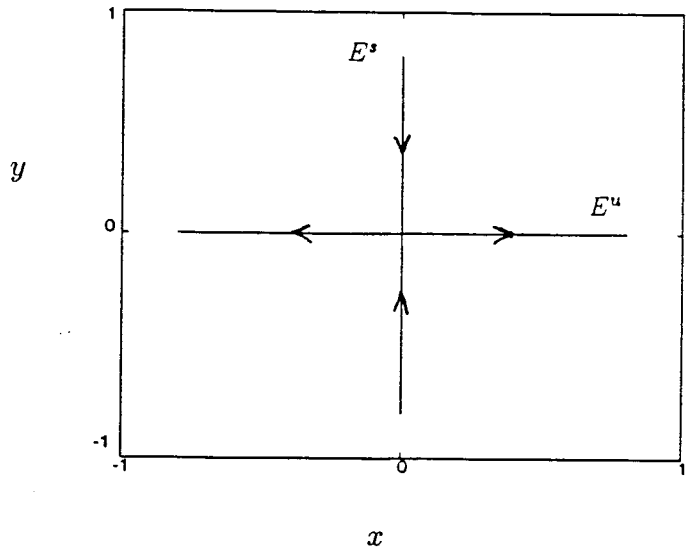

Figure 2.1.15: Stable and Unstable eigenspaces of equation 2.1.28.

linearized system. The stable manifold of a fixed point of a nonlinear system is defined as the invariant manifold containing the fixed point such that if the system starts on the invariant manifold it will asymptotically approach the fixed point as time goes to infinity. The unstable manifold is defined in the same manner, but the system asymptotically approaches the fixed point as time goes to negative infinity. Mathematically, the stable and unstable manifolds can be represented as

$$W^s = \{x | x \to x_o \text{ as } t \to \infty\}$$

$$W^u = \{x | x \to x_o \text{ as } t \to -\infty\}.$$

The stable and unstable manifolds for the nonlinear and linearized problems are related by the Stable and Unstable Manifold Theorems for a Fixed Point (Guckenheimer and Holmes [1983]). The result of the theorems is that the stable and unstable manifolds of the nonlinear system are tangent to the stable and

unstable manifolds of the linearized system. This makes sense intuitively, as the behavior of a nonlinear system in a neighborhood of a fixed point is approximated by the system obtained by linearizing about the fixed point if no eigenvalues have zero real parts.

The following example will illustrate the above concepts. Consider the nonlinear system

$$\begin{aligned} \dot{x} &= x, \\ \dot{y} &= -y + x^2. \end{aligned} \tag{2.1.29}$$

Linearizing about the fixed point, $(0,0)$, gives the system

$$\begin{aligned} \dot{x} &= x, \\ \dot{y} &= -y, \end{aligned} \tag{2.1.30}$$

whose stable and unstable manifolds are

$$E^s = \{(x,y)|x = 0\}$$

$$E^u = \{(x,y)|y = 0\}.$$

Solutions of the nonlinear system can be determined explicitly by eliminating time from the two equations to obtain the equation

$$\frac{dy}{dx} = \frac{-y}{x} + x \tag{2.1.31}$$

whose solution is

$$y(x) = \frac{1}{3}x^2 + \frac{c}{x}. \tag{2.1.32}$$

The unstable manifold of the origin can be determined by choosing the value of c such that the solution curve goes through the origin. This gives a value of zero for c, so the unstable manifold is given by the equation

$$y = \frac{1}{3}x^2. \tag{2.1.33}$$

Note that the slope of the unstable manifold at the origin is zero, so the unstable manifold of the nonlinear system is tangent to the unstable manifold of the linearized system as stated by the Stable and Unstable Manifold Theorem for a Fixed Point. The stable manifold can be determined by noting that if x is initially zero, the solution stays on the y-axis and approaches the origin as time goes to infinity. The stable manifolds of the nonlinear and the linearized systems are also tangent, and in this particular case they are identical.

The center manifold of a fixed point of a nonlinear system is an invariant manifold that contains the fixed point and is tangent to the center eigenspace of the linearized system. This definition is analogous to the definition of the stable and unstable manifolds of a fixed point of a nonlinear system, but no information about the evolution of the system on the center manifold is included in the definition. No information about the evolution of the system on the center manifold can be given without examining the nonlinear terms of the system because the linear terms on the center manifold are zero by definition. For example, consider the system

$$\dot{x} = x^2. \tag{2.1.34}$$

Linearizing about the fixed point $x = 0$ gives

$$\dot{x} = 0 \tag{2.1.35}$$

which has one zero eigenvalue so there is a one-dimensional center manifold containing the fixed point and the stable and unstable manifolds are both equal to the

null space. No information about the stability of the fixed point can be obtained from the linearized system as all the linear terms are zero. It is necessary to examine the higher order terms of the system on the center manifold to determine the stability of the fixed point. The stability of the fixed point can be determined by calculating the sign of $\dot{x}$ on the center manifold. In this case $\dot{x}$ is always positive, so if x is initially negative, the system will approach the fixed point, while if x is initially positive, the value of x will increase with time. This is shown on the phase plot in Figure 2.1.16. It is interesting that the initial condition of the system on the center manifold can determine whether the system is attracted to or repelled from the fixed point.

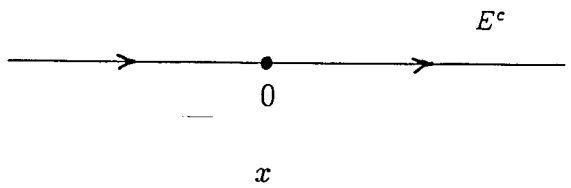

Figure 2.1.16: Center manifold of equation 2.1.34.

A system is always attracted to the fixed point along the stable manifold of the fixed point and always repelled from the fixed point on the unstable manifold. If the unstable manifold is not equal to the null space, there must be at least one eigenvalue of the linearized system that has real part greater than zero so the fixed

point is unstable. If the unstable manifold is the null space, then the stability of the fixed point will be determined by the behavior of the system on the center manifold because the system is always attracted to the fixed point along the stable manifold. For example, consider the system

$$\begin{aligned} \dot{x} &= x^2, \\ \dot{y} &= -y. \end{aligned} \tag{2.1.36}$$

Linearizing the system about the fixed point at the origin gives

$$\begin{pmatrix} \dot{u} \\ \dot{v} \end{pmatrix} = \begin{pmatrix} 0 & 0 \\ 0 & -1 \end{pmatrix} \begin{pmatrix} u \\ v \end{pmatrix} . \tag{2.1.37}$$

This system has a one-dimensional stable manifold and a one-dimensional center manifold. The phase diagram for this system, Figure 2.1.17, shows that the y-axis is the stable manifold so the system is attracted to the x-axis, which is the center manifold. The dynamics of the system in the neighborhood of the fixed point are determined by the dynamics on the center manifold because the system asymptotically approaches the center manifold for all initial conditions in a neighborhood of the fixed point.

It was relatively easy to determine the center manifold of the fixed points in the previous examples. This is not generally the case, so we now turn to a methodology for determining the center manifold of a general fixed point (Guckenheimer and Holmes [1983]). Assume a nonlinear system has a fixed point at the origin and that the linearized system about the origin has n eigenvalues (real or

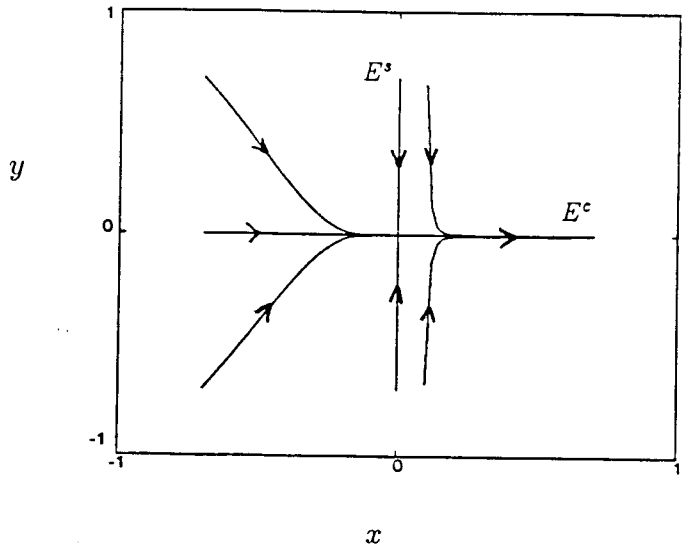

Figure 2.1.17: Solution curves of equation 2.1.36.

complex) with zero real parts and m eigenvalues with negative real parts. The system can then be written

$$\begin{aligned} \dot{x} &= Ax + f(x,y), \\ \dot{y} &= By + g(x,y), \end{aligned} \tag{2.1.38}$$

where x is an n-dimensional vector, y is an m-dimensional vector, A is an $n \times n$ matrix with eigenvalues having zero real parts, and B is an $m \times m$ matrix with eigenvalues having negative real parts. Also assume that $f(x,y)$ and $g(x,y)$ are both zero at the origin and do not contain any linear terms. The original $n+m$-dimensional system must be in Jordan normal form before it can be separated in this manner. This is a relatively simple operation described in the example of Appendix I.

The Center Manifold Theorem (Guckenheimer and Holmes, page 127) proves that an n-dimensional center manifold of the fixed point at the origin exists for

this system. The theorem also proves that the center manifold is a smooth curve for smooth systems, so the center manifold for this system can be represented by

$$y = h(x). \tag{2.1.39}$$

Differentiating this equation with respect to time gives

$$\dot{y} = Dh(x)\dot{x} \tag{2.1.40}$$

where $Dh(x)$ represents the derivative of $h(x)$ with respect to x. Recall that both x and $h(x)$ are vectors. Thus, for example, for the four-dimensional system where

$$x = (x_1, x_2)$$

$$y = (y_1, y_2)$$

the center manifold is

$$h(x) = \begin{pmatrix} h_1(x_1, x_2) \\ h_2(x_1, x_2) \end{pmatrix}$$

and

$$Dh(x) = \begin{pmatrix} \frac{dh_1}{dx_1} & \frac{dh_1}{dx_2} \\ \frac{dh_2}{dx_1} & \frac{dh_2}{dx_2} \end{pmatrix}.$$

Substituting equations 2.1.38 and 2.1.39 into equation 2.1.40 gives

$$Dh(x)[Ax + f(x, h(x))] = Bh(x) + g(x, h(x)). \tag{2.1.41}$$

This is a nonlinear functional equation for the center manifold, to be solved for $h(x)$. Solving this equation is usually more difficult than finding the solution to the original dynamical system, but there is a method for computing the center manifold in a small neighborhood of the fixed point to any required degree of

accuracy (Guckenheimer and Holmes, page 131). The method involves approximating the center manifold with a power series expansion and will be illustrated in the following example.

Consider the following system:

$$\begin{aligned} \dot{x} &= x^2 y, \\ \dot{y} &= -y + x^2, \end{aligned} \tag{2.1.42}$$

which has a fixed point at the origin. Linearizing about the origin gives the system

$$\begin{aligned} \dot{u} &= 0, \\ \dot{v} &= -v, \end{aligned} \tag{2.1.42a}$$

where $u = x-0$, $v = y-0$. This linearized system has eigenvalues zero and negative one and the center and stable eigenspaces are the x and y axes, respectively. Existence of a one-dimensional center manifold containing the origin of the form

$$W^c = \{(x, h(x)) | h(0) = Dh(0) = 0\}$$

is proven by the Center Manifold Theorem. The first derivative, $Dh(x)$, of the center manifold is zero at the fixed point because in this example the center manifold is tangent to the center eigenspace, which is perpendicular to the stable eigenspace. Expressing the center manifold in a neighborhood of the fixed point by a power series expansion gives the local description of the center manifold

$$h(x) = ax^2 + bx^3 + \cdots \tag{2.1.43}$$

Values of a and b can be determined by substituting this expression into the functional equation for the center manifold. For this system we have

$$Dh(x) = 2ax + 3bx^2 + \cdots,$$

and writing equation 2.1.42 in the form of equation 2.1.38 by separating the linear and nonlinear parts gives

$$\dot{x} = (0)x + x^2 y,$$

$$\dot{y} = (-1)y + x^2,$$

so the unknows in equation 2.1.38 are

$$A = 0, \qquad B = -1, \qquad f = x^2 y, \qquad g = x^2.$$

Thus, the functional equation, (2.1.41), can be written,

$$\begin{aligned}(2ax + 3bx^2 + \cdots)[ax^4 + bx^5 + \cdots] \\ + ax^2 + bx^3 + \cdots - x^2 = 0.\end{aligned} \tag{2.1.44}$$

For this equation to hold, the coefficients of each power of x must vanish. Collecting equal powers of x gives

$$x^2: \quad a - 1 = 0 \qquad \Rightarrow \quad a = 1$$

$$x^3: \quad b = 0.$$

The center manifold near the fixed point can then be written

$$h(x) = x^2 + O(|x|^4). \tag{2.1.45}$$

Substituting this into the $\dot{x}$ equation gives the equation governing the system on the center manifold:

$$\dot{x} = x^4 + O(x^6). \tag{2.1.46}$$

Stability of the fixed point in the complete system can now be determined by determining its stability on the center manifold. Small perturbations from

the origin will decay if the initial perturbation is negative and grow if the initial perturbation is positive, so the fixed point is unstable. The phase diagram in a neighborhood of the fixed point is shown in Figure 2.1.18. It is important to notice that the stability of the origin could not be determined by analyzing the linearized system (equation 2.1.42a) because one eigenvalue has zero real part. The above example shows how to calculate the center manifold for a simple two dimensional system. Calculations are similiar for higher dimensional problems, with the scalar terms being replaced by vectors and matrices.

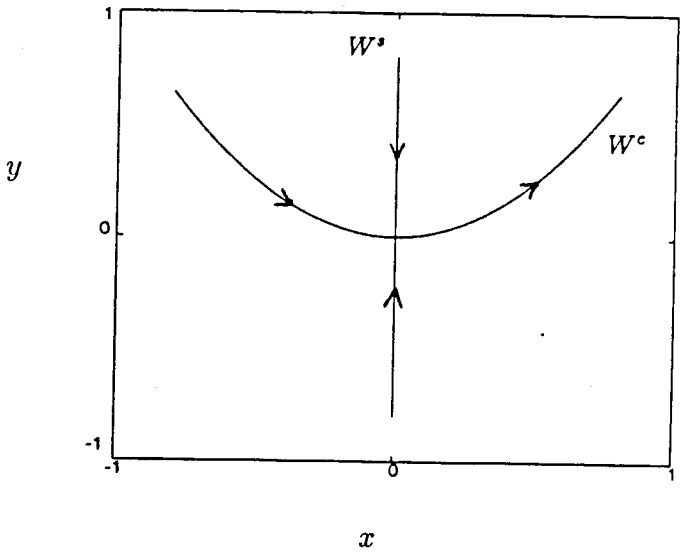

Figure 2.1.18: Stable and center manifolds of equation 2.1.42.

The remaining question is: how can we calculate the center manifold for systems containing parameters? Consider the system

$$\begin{aligned} \dot{x} &= Ax + f(x, y, \mu), \\ \dot{y} &= By + g(x, y, \mu), \end{aligned} \tag{2.1.47}$$

where the eigenvalues for A and B have real parts which are zero and negative respectively, and the origin is a fixed point. This system can be rewritten as the higher dimensional system by treating μ as variable:

$$\begin{aligned} \dot{x} &= Ax + f(x, y, \mu), \\ \dot{y} &= By + g(x, y, \mu), \\ \dot{\mu} &= 0. \end{aligned} \tag{2.1.48}$$

Introducing μ as a new dependent variable has changed the problem in two important ways. The terms $x\mu$ and $y\mu$ are now nonlinear terms, and the center manifold will be higher dimensional because the eigenvalues of the linearized equation for the evolution of the parameter μ are zero. This increases the dimension of the center manifold to the dimension of x plus the dimension of μ.

Locally the center manifold can then be expressed as

$$W^c = \{(x, \mu, h(x, \mu) | h(0, 0) = Dh(0, 0) = 0\},$$

so we have the system

$$\begin{aligned} \dot{x} &= Ax + f(x, h(x, \mu), \mu) \\ \dot{y} &= Bh(x, \mu) + g(x, h(x, \mu), \mu) = D_x h(x, \mu)\dot{x} \\ \dot{\mu} &= 0. \end{aligned} \tag{2.1.49}$$

The functional equation for the center manifold is then

$$D_x h(x, \mu)[Ax + f(x, h(x, \mu), \mu)] - Bh(x, \mu) - g(x, h(x, \mu), \mu) = 0, \tag{2.1.50}$$

and we get an equation on the center manifold of the form,

$$\begin{aligned} \dot{x} &= Ax + f(x, h(x, \mu), \mu) \\ \dot{\mu} &= 0. \end{aligned} \tag{2.1.51}$$

Appendix I contains a sample calculation of the center manifold for a system depending on parameters.

2.2 Numerical Methods

This section introduces the numerical methods which were used in this research. The techniques are not new, but may not be familiar. This section will introduce the important concepts of each method. More complete discussions of continuation methods are given in the works of Keller [1977] and Doedel and Kernevez, which supplied much of the basis for Section 2.2.1. Numerical integration techniques are discussed by Wylie [1975]. Algorithms for solving linear sytems and calculating eigenvalues were taken from Press, Flannery, Teukolsky, and Vetterling [1988], along with the two-dimensional curve fit which was used to fit the aerodynamic data discussed in Chapter III.

2.2.1 Continuation Methods

Continuation methods are a direct result of the Implicit Function Theorem, which proves that if the Jacobian of a nonlinear system at a fixed point is non-singular, then there exists a unique curve of fixed points containing the known fixed point. This result is only valid in a small region around the fixed point, as shown in Figure 2.2.1. The curve of fixed points can be extended by applying the Implicit Function Theorem at a fixed point near the end the curve known to exist through the fixed point (x_o, μ_o). The curve can then be extended in a region around this new point, as shown in Figure 2.2.2. This procedure can be repeated

to prove the existence of a continuous curve of fixed points as long as the Jacobian at each fixed point on the curve is nonsingular. Fixed points where the linearized solution is singular are bifurcation points and the structure of the fixed points can change drastically at these points as discussed in Section 2.1.5. Continuation past bifurcation points will be discussed later in this section.

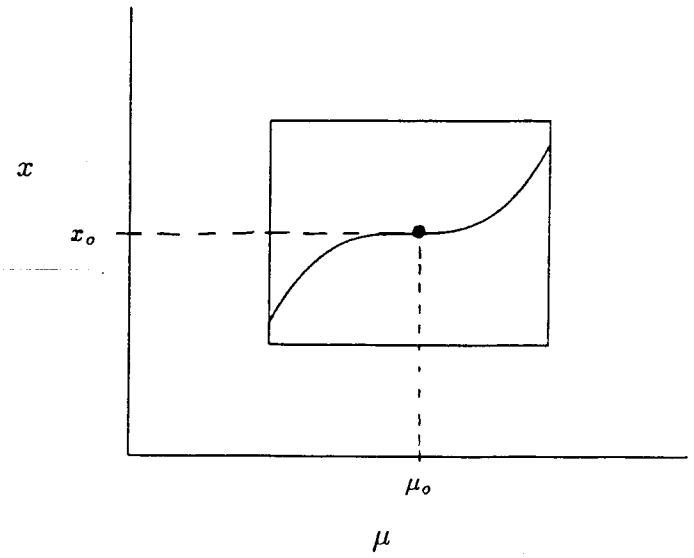

Figure 2.2.1: Graphical representation of the Implicit Function Theorem.

Assume that the dynamical system

$$\dot{x} = f(x;\mu) \tag{2.2.1}$$

has a curve of fixed points as shown in Figure 2.2.3 and that the Jacobian at the fixed point (x_o, μ_o) is nonsingular. This curve of fixed points can represented by

$$x = x(\mu) \tag{2.2.2}$$

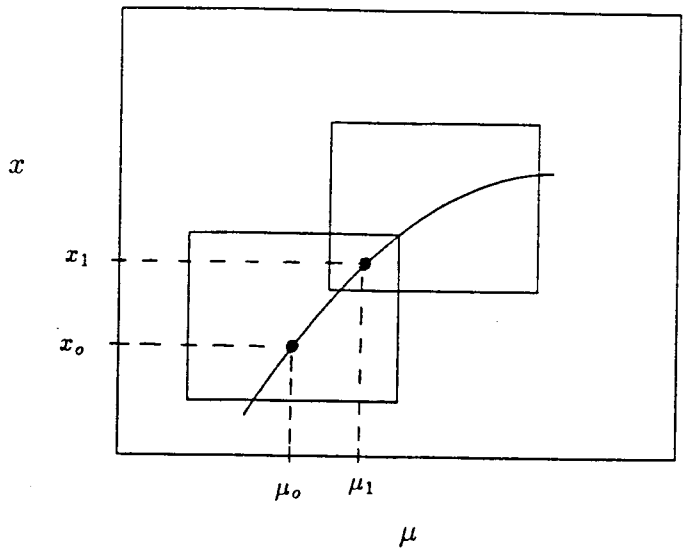

Figure 2.2.2: Extension of a curve of fixed points by the Implicit Function Theorem.

where $x(\mu_o) = x_o$, so fixed points of equation 2.2.1 are given by the solutions of

$$f(x(\mu), \mu) = 0. \tag{2.2.3}$$

If the fixed point (x_o, μ_o) is known, a new fixed point on the curve can be approximated by linear extrapolation from the known fixed point as shown in Figure 2.2.4. The approximate fixed point can be calculated with the formula

$$x = x_o + x_\mu(x_o, \mu_o)(\mu - \mu_o), \tag{2.2.4}$$

where $x_\mu(x_o, \mu_o)$ is the slope of the curve, $x(\mu)$, at the fixed point (x_o, μ_o). This slope can be determined by taking the total derivative of equation 2.2.3

$$f_x(x(\mu), \mu)x_\mu(\mu) + f_\mu(x(\mu), \mu) = 0, \tag{2.2.5}$$

which can be solved for $x_\mu(\mu)$ to give

$$x_\mu(\mu) = -f_x^{-1}(x(\mu), \mu) f_\mu(x(\mu), \mu). \tag{2.2.6}$$

Because the implicit function theorem holds at the fixed point (x_o, μ_o) the matrix $f_x(x_o, \mu_o)$ is invertible and the slope of the curve can be determined at this point.

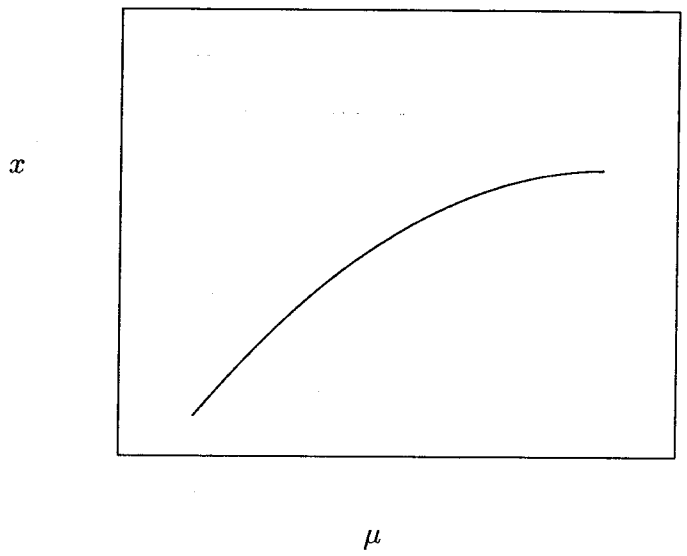

Figure 2.2.3: Fixed points of equation 2.2.1.

Newton's method can be used to reduce the error between the approximate fixed point and the true fixed point if the initial estimate is close enough to the true fixed point. Initial estimates can be made more accurate by reducing the step size, $\mu - \mu_o$, in equation 2.2.4. Newton's method is a simple iterative technique, which can be described as follows. Assume that the approximate fixed point (x_1, μ_1) is known (see Figure 2.2.4). The Taylor expansion about this point is

$$f(x, \mu_1) = f(x_1, \mu_1) + f_x(x_1, \mu_1)(x - x_1) + \cdots \tag{2.2.7}$$

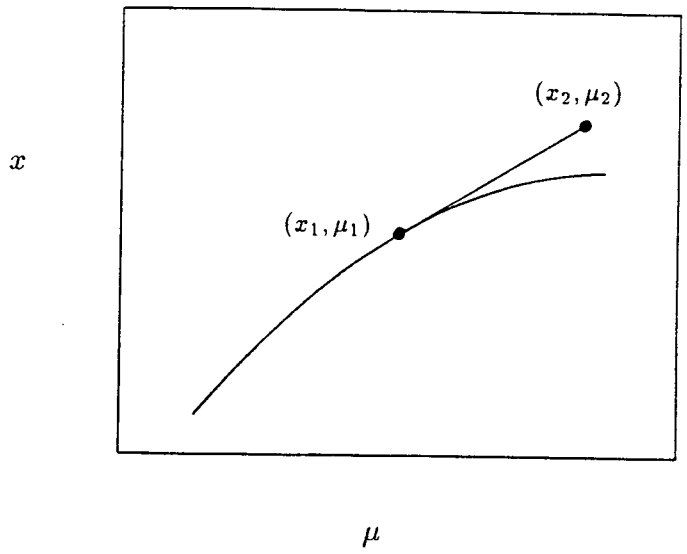

Figure 2.2.4: Extension of a curve of fixed points.

Note that the parameter is held constant in this expansion. Neglecting higher order terms and evaluating the equation at the unknown fixed point, (x_2, μ_1), we have the equation,

$$f(x_1, \mu_1) + f_x(x_1, \mu_1)(x_2 - x_1) = 0, \tag{2.2.8}$$

which can be solved for x_2 to give

$$x_2 = x_1 - f_x^{-1}(x_1, \mu_1) f(x_1, \mu_1). \tag{2.2.9}$$

The value of x_2 calculated with this expression is not the exact fixed point, but is a better approximation than is x_1. Repeating this calculation with x_1 replaced by x_2, we find an even better approximation to the fixed point. Equation 2.2.9 can be written as an iterative equation,

$$x_{\nu+1} = x_\nu - f_x^{-1}(x_\nu, \mu_1) f(x_\nu, \mu_1), \tag{2.2.10}$$

where $\nu = 1, \cdots, N$. By choosing N sufficiently large, the error between the true fixed point and the approximation $x_{\nu+1}$ can be made arbitrarily small. Newton's method has quadratic convergence so N is usually less than ten. Figure 2.2.5 shows a graphical representation of Newton's method.

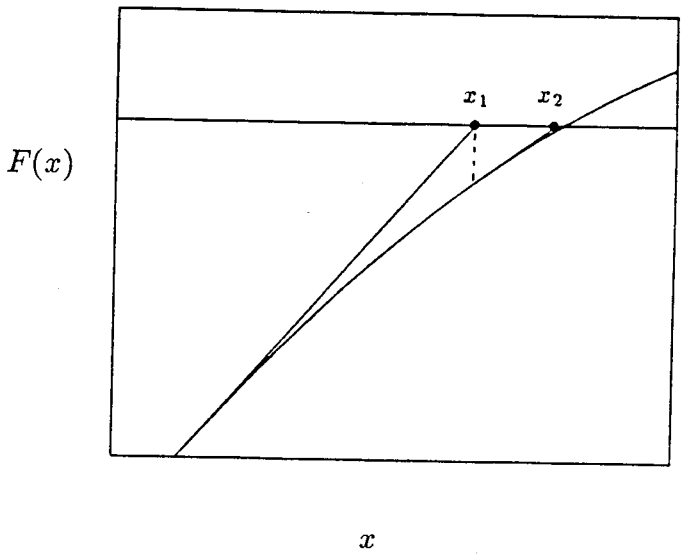

Figure 2.2.5: Graphical representation of Newton's method.

This procedure could be used to calculate curves of fixed points as long as no bifurcation points are encountered. Recall that the Jacobian is zero at bifurcation points, so equation 2.2.6 cannot be used to calculate the slope of the curve of fixed points at a bifurcation point. There is a relatively simple solution to this problem. The slope at each fixed point can be determined by numerical approximation. Assume that two fixed points are known, as shown in Figure 2.2.6; then the slope

of the curve can be approximated by

$$x_\mu(\mu_1) = \frac{x_2 - x_1}{\mu_2 - \mu_1}. \tag{2.2.11}$$

This equation can be used at a bifurcation point and is a much more efficient method for computing the slope than equation 2.2.6 which requires a matrix inversion.

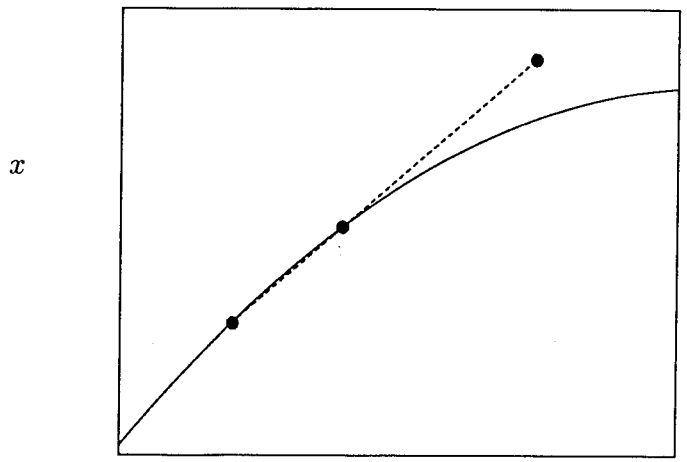

Figure 2.2.6: Approximation to the slope of a curve.

Numerical problems still occur at bifurcation points because Newton's method only works if the linearized system at the fixed point is invertible. This problem can be avoided at saddle-node bifurcations by choosing a different continuation parameter. The saddle-node bifurcation is special because the slope of the curve of fixed points is unique at a saddle-node bifurcation, whereas it is not

at pitchfork or transcritical bifurcations. In the preceeding discussion the continuation parameter had been the natural parameter of the problem, μ. This is not the only choice of continuation parameter. Any independent variable or natural parameter could be used as the continuation parameter. It happens that the arc length is a good choice for the continuation parameter, where the arc length is defined as a variable running along the curve of fixed points as shown in Figure 2.2.7.

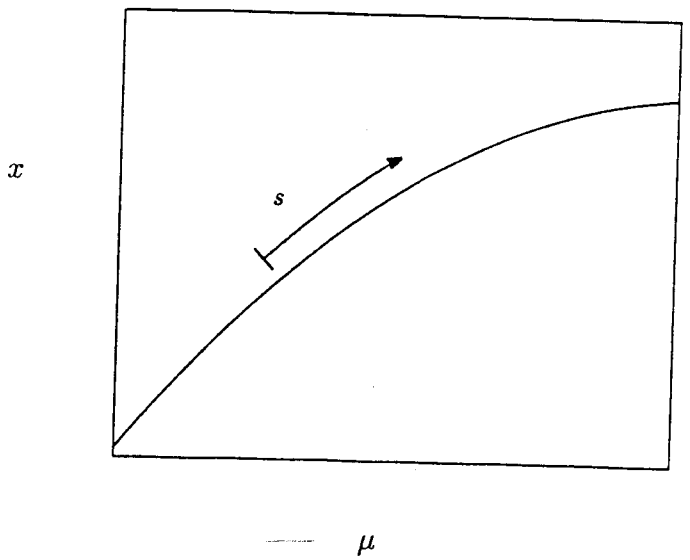

Figure 2.2.7: Definition of the arc length.

Fixed points of equation 2.2.1 will be solutions of

$$f(x(s), \mu(s)) = 0 \tag{2.2.12}$$

where, s, is the arc length. Because μ is not known, equation 2.2.12 has one more unknown than equations. One more equation is required before unique solutions

to equation 2.2.12 can be found. The remaining equation, due to Keller [1977], can be written at the fixed point (x_j, μ_j) as

$$(x_j - x_{j-1})\dot{x}_{j-1} + (\mu_j - \mu_{j-1})\dot{\mu}_{j-1} - \Delta s = 0, \tag{2.2.13}$$

where $\dot{x} = \frac{dx}{ds}$, $\dot{\mu} = \frac{d\mu}{ds}$ and Δs is the step size along the curve. Numerical difference formulas can be used to compute $\dot{x}$ and $\dot{\mu}$ as

$$\begin{aligned} \dot{x}_{j-1} &= \frac{1}{\Delta s}(x_{j-1} - x_{j-2}), \\ \dot{\mu}_{j-1} &= \frac{1}{\Delta s}(\mu_{j-1} - \mu_{j-2}). \end{aligned} \tag{2.2.14}$$

Combining equations 2.2.12 through 2.2.14 results in the expanded system

$$\begin{aligned} &f(x_j, \mu_j) = 0 \\ &(x_j - x_{j-1})(x_{j-1} - x_{j-2}) + (\mu_j - \mu_{j-1})(\mu_{j-1} - \mu_{j-2}) - (\Delta s)^2 = 0. \end{aligned} \tag{2.2.15}$$

The Jacobian of equation 2.2.15 in terms of x_j and μ_j is

$$\begin{pmatrix} f_x(x_j, \mu_j) & f_\mu(x_j, \mu_j) \\ (x_{j-1} - x_{j-2}) & (\mu_{j-1} - \mu_{j-2}) \end{pmatrix}$$

which is nonsingular not only when f_x is nonsingular but also when f_x is singular but f_μ is nonsingular. This is the condition at a saddle-node bifurcation, so using arc length as the continuation parameter makes it possible to compute past saddle-node bifurcations. This is especially important for analyzing the equations of motion for an aircraft, as many saddle-node bifurcations occur in that system. Indeed saddle-node bifurcations are common in many physical systems and cause important system dynamics as we shall see in Chapters IV, V, and VI.

Numerical difficulties can occur at transcritical and pitchfork bifurcations because the Jacobian of equation 2.2.15 is singular when both f_x and f_μ are

singular. It is sometimes possible to continue the curve of fixed points through bifurcation points where the Jacobian is singular because the Jacobian is generally not singular at other fixed points in the neighborhood of the bifurcation point. Newton's method can be used at these surrounding fixed points if the initial estimate is close enough to the actual fixed point. The region of convergence of Newton's method in the neighborhood of the bifurcation point, (x_o, μ_o), is shown in Figure 2.2.8 (Keller [1977]). Continuation past the bifurcation can be attained if the step size is such that the initial estimate of the fixed point is within the region of convergence on the opposite side of the bifurcation point as shown in Figure 2.2.8. Continuation past pitchfork bifurcations has been accomplished in the presesnt work (see Chapters V and VI).

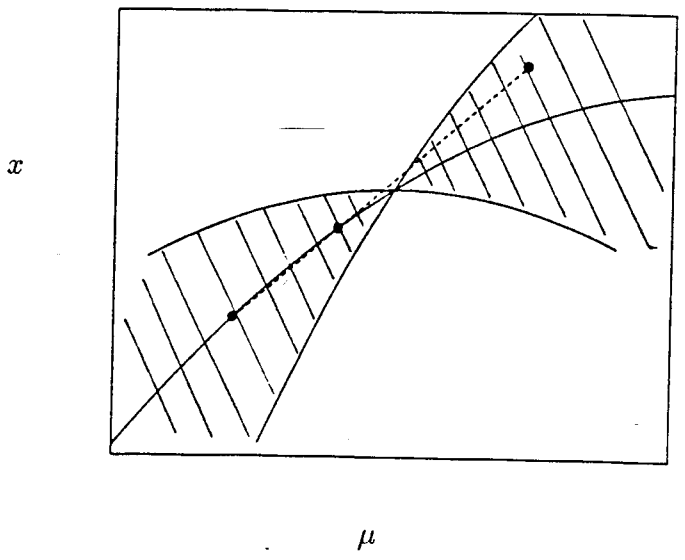

Figure 2.2.8: Continuation past a bifurcation point.

Step size selection (i.e., magnitude of Δs) is important for efficient use of the continuation method described above. The step size must be chosen so the initial estimate of the fixed point is within the region of convergence of Newton's method, which depends on the local structure of the vector field. Thus the required step size for convergence will change along the curve of fixed points. One method for assuring convergence along the entire curve is to pick the smallest step size required for convergence and use it to determine the entire curve. It is more efficient to use a variable step size. The following routine of Keller [1977] was used in this research

$$\Delta s_{j+1} = 2^{(\frac{4-\nu_j}{3})}\Delta s_j, \tag{2.2.16}$$

where ν_j is the number of iterates of Newton's method required for convergence at the j^{th} point. This routine maintains a balance between the number of points needed to determine the curve of fixed points and the numbers of Newton iterates required at each point. If the Newton iterates fail to converge at an approximated fixed point, the step size is cut in half and another attempt to determine the next fixed point is made. This process is repeated until either the next fixed point is found or a specified minimum step size is reached; nonconvergence is then signalled and the routine stopped.

2.2.2 Iterative Methods

The discussion of continuation methods in Section 2.2.1 involves the assumption that at least one fixed point of the system is known. In our applications, it is

usually possible to determine the trim condition of an aircraft analytically, so this point can be used as the starting point for the continuation method. Determining a spin mode for an aircraft is a much more difficult task, as the full equations of motion and nonlinear aerodynamic coefficients must be used in any analysis of the spin modes of an aircraft. This complexity usually requires the use of iterative techniques for determining the spin modes of an aircraft as discussed in Section 1.3.

The iterative technique of Young, Schy, and Johnson [1980] was used in this work to determine possible spin modes for the generic jet fighter of that reference. This technique was designed for an aerodynamic model which did not include rotary balance data or nonlinear sideslip effects, and the equations of motion were simplified by assuming no gravity, small sideslip, and constant speed. While these are severe restrictions, and certainly not valid for studying spin modes, it was generally possible to converge to solutions of the full equations of motion when solutions of these simplified equations were used as a first guess.

2.2.3 Numerical Simulations

Numerical simulations have been used extensively in this work to verify the results of the fixed point analysis. The same equations of motion are used in the simulations and the fixed point analysis, but the aerodynamic coefficients are slightly different in some cases. Continuation methods require smooth first derivatives, so all aerodynamic coefficients had to be approximated with smooth

functions. Numerical simulations do not require smooth functions so linear interpolation is used to fit the aerodynamic data in the numerical simulations for the F-14. Linear fits are much less computationally intensive than smooth fits, so linear fits allowed simulations to be run more efficiently.

Large local curvature is often introduced into the aerodynamic data when approximated with smooth curves. This is particularly true of polynomial fits. Local curvature of the aerodynamic coefficients could affect the dynamics of the aircraft, so running simulations with linear data fits was used to check whether or not the bifurcations determined by the continuation method are introduced by local curvatures in the aerodyamic data caused by the data fit. A fourth order Runge-Kutta scheme was used for all simulations (Wylie [1975]).

III. MODEL OF AIRCRAFT DYNAMICS

3.1 Equations of Motion

The motions of a rigid aircraft are governed by the forces and moments acting on the aircraft. Equations governing these motions can be derived by applying Newton's law to the aircraft, which results in the twelfth order system

$$\vec{F} = M\ddot{\vec{x}},$$

$$\vec{N} = I\ddot{\vec{\theta}},$$

where $\vec{x}$ and $\vec{\theta}$ represent the translational and rotational position of the aircraft, M the mass, I the rotational inertia tensor, $\vec{F}$ the force and $\vec{N}$ the moment acting on the aircraft. Forces and moments acting on the aircraft are functions of the state of the aircraft which includes the rotational and translational degrees of freedom along with deflections of any control surfaces. Most aircraft have three control surfaces; ailerons to control rolling motions, an elevator to control pitching motions, and a rudder to control yawing motions. Thus, the equations of motion for an aircraft include nine degrees of freedom: three translational, three rotational, and three control surface deflections.

The force and moment equations are written in an inertial reference frame (i.e., earth fixed), but it is more convenient to use a reference frame which is fixed to the aircraft. This is because I is constant in this system. Also, the forces and moments acting on an aircraft are usually expressed by expansions in the state of the aircraft relative to an axis system which is fixed to the aircraft

and the control surface deflections. The transformation of the force and moment equations from an inertial reference frame to a reference frame which is fixed to the aircraft (noninertial) is shown in Appendix II. This transformation does not change the order of the system, but several assumptions can be made to reduce the order of the system from twelve to nine. The lateral and longitudinal position of the aircraft, (x, y), do not influence the dynamics of the aircraft so the order of the system can be reduced to ten. Air density, which is a function of altitude, z, will be assumed constant in this study, along with gravity, thus reducing the system to ninth order.

3.1.1 Eighth Order Equations of Motion

The ninth order equations of motion are

- translational acceleration:

$$\dot{\alpha} = q - (r\sin\alpha + p\cos\alpha)\tan\beta + \frac{QS}{MV\cos\beta}(C_Z\cos\alpha - C_X\sin\alpha)$$
$$+\frac{g}{V\cos\beta}(\sin\alpha\sin\theta + \cos\alpha\cos\theta\cos\phi) - \frac{T\sin\alpha}{MV\cos\beta}$$

$$\dot{\beta} = p\sin\alpha - r\cos\alpha + \frac{QS}{MV}(-C_X\cos\alpha\sin\beta + C_Y\cos\beta - C_Z\sin\alpha\sin\beta)$$
$$+\frac{g}{V}(\cos\alpha\sin\beta\sin\theta + \cos\beta\cos\theta\sin\phi - \sin\alpha\sin\beta\cos\theta\cos\phi) - \frac{T\cos\alpha\sin\beta}{MV}$$

$$\dot{V} = \frac{QS}{M}(C_X\cos\alpha\cos\beta + C_Y\sin\beta + C_Z\sin\alpha\cos\beta) + \frac{T\cos\alpha\cos\beta}{M}$$
$$+g(\sin\beta\cos\theta\sin\phi - \cos\alpha\cos\beta\sin\theta + \sin\alpha\cos\beta\cos\theta\cos\phi)$$

-rotational acceleration:

$$\dot{p} = \frac{I_Y - I_Z}{I_X}qr + \frac{QSb}{I_X}C_\ell$$

$$\dot{q} = \frac{I_Z - I_X}{I_Y}pr + \frac{QSc}{I_Y}C_m$$

$$\dot{r} = \frac{I_X - I_Y}{I_Z} pq + \frac{QSb}{I_Z} C_n$$

-Euler angles:

$$\dot{\theta} = q\cos\phi - r\sin\phi$$

$$\dot{\phi} = p + (q\sin\phi + r\cos\phi)\tan\theta$$

$$\dot{\psi} = (q\sin\phi + r\cos\phi)\sec\theta.$$

The Euler angles determine the rotational orientation of the aircraft relative to the inertial reference frame (i.e., earth fixed) and determine the direction of gravity relative to the axis system which is fixed to the aircraft. It is easy to see that the equation for the yaw angle, ψ, is decoupled from the rest of the equations. This is a result of the definition of the Euler angles, (θ, ϕ, ψ). The final result of a series of rotations depends on the order in which they are applied. For example, pitching up by 90 degrees and then rolling 90 degrees results in a different orientation than first rolling 90 degrees and then pitching up by 90 degrees. For applications to aircraft dynamics, the usual convention for Euler angle rotations is the sequence: yaw, pitch, roll (see Appendix II).

There are other possible conventions, but this particular choice has the benefit that the yaw angle decouples from the rest of the equations of motion. Yawing an aircraft does not change the direction of the gravity vector relative to the aircraft, because the yaw rotation is about the gravity vector. This is only true if the yaw rotation is applied first in the sequence defining the convention for Euler angles. This definition of Euler angles also results in convenient forms for the linearized equations for rotations about body axes (yaw, pitch, and roll). The eighth order

equations of motion are then given by the above system of equations without the equation for the yaw angle.

3.1.2 Sixth Order Equations of Motion

Neglecting the influence of gravity decouples Euler's equations from the translational and rotational acceleration equations. This reduces the system to the six coupled equations

$$\begin{aligned}
\dot{\alpha} =& q - (r\sin\alpha + p\cos\alpha)\tan\beta - \frac{T\sin\alpha}{MV\cos\beta} \\
&+ \frac{QS}{MV\cos\beta}(C_Z\cos\alpha - C_X\sin\alpha) \\
\dot{\beta} =& p\sin\alpha - r\cos\alpha - \frac{T\cos\alpha\sin\beta}{MV} \\
&+ \frac{QS}{MV}(-C_X\cos\alpha\sin\beta + C_Y\cos\beta - C_Z\sin\alpha\sin\beta) \\
\dot{V} =& \frac{QS}{M}(C_X\cos\alpha\cos\beta + C_Y\sin\beta + C_Z\sin\alpha\cos\beta) + \frac{T\cos\alpha\cos\beta}{M} \\
\dot{p} =& \frac{I_Y - I_Z}{I_X}qr + \frac{QSb}{I_X}C_\ell \\
\dot{q} =& \frac{I_Z - I_X}{I_Y}pr + \frac{QSc}{I_Y}C_m \\
\dot{r} =& \frac{I_X - I_Y}{I_Z}pq + \frac{QSb}{I_Z}C_n.
\end{aligned}$$

Gravity has been neglected in many previous studies of aircraft dynamics, mainly because it simplifies the equations of motion. Studies have also shown that gravity is negligible for some types of maneuvers, particularly roll-coupling instabilities (Hacker and Oprisiu [1974]), but no studies have been made of the effect of gravity on the steady states of an aircraft. Later in this work we will compare results from the six and eight degree of freedom equations to determine if and when gravity has a significant effect on the fixed points of the system.

3.1.3 Fifth Order Equations of Motion

Another common simplification to the equations of motion for an aircraft is the assumption of constant velocity. Several techniques have been used in previous works to satisfy the condition of constant velocity. Most works simply ignore the velocity equation altogether while some assume that the thrust equals the drag ($T = X\cos\alpha + Z\sin\alpha$) and substitute this relation into the equations for $\dot{\alpha}$ and $\dot{\beta}$. In this work we assume that the thrust is varied in such a way that the velocity remains constant. The required thrust can be determined by setting the equation for $\dot{V}$ equal to zero and solving for the thrust to obtain

$$T = -\frac{QS}{\cos\alpha\cos\beta}(C_X\cos\alpha\cos\beta + C_Z\sin\alpha\cos\beta + C_Y\sin\beta).$$

Note that setting the thrust equal to the drag only satisfies the condition of constant velocity when the sideslip angle is zero.

Substituting this relation into the equations for $\dot{\alpha}$ and $\dot{\beta}$ gives the fifth order system

$$\begin{aligned}
\dot{\alpha} &= q - (r\sin\alpha + p\cos\alpha)\tan\beta + \frac{QS}{MV\cos\alpha\cos\beta}(C_Z + C_Y\sin\alpha\tan\beta)\\
\dot{\beta} &= p\sin\alpha - r\cos\alpha + \frac{QS}{MV\cos\beta}C_Y\\
\dot{p} &= \frac{I_Y - I_Z}{I_X}qr + \frac{QS}{I_X}C_\ell\\
\dot{q} &= \frac{I_Z - I_X}{I_Y}pr + \frac{QS}{I_Y}C_m\\
\dot{r} &= \frac{I_X - I_Y}{I_Z}pq + \frac{QS}{I_Z}C_n.
\end{aligned}$$

The thrust required to keep the velocity constant can be monitored along the curves of fixed points to see if the required thrust is physically possible. Fixed

points of the fifth order equations will be compared to fixed points of the eighth order equations to see if and when the fifth order equations are a valid approximation.

3.2 Aerodynamic Models

3.2.1 General Aviation Aircraft Having a Canard Configuration

Aerodynamic data for a general aviation canard configuration aircraft was obtained from Chambers, Yip, and Moul [1983]. Only the longitudinal coefficients will be used in this work as all of the necessary lateral coefficients were not provided in the reference. The longitudinal aerodynamic model has the form,

$$C_X = C_X(\alpha) + \delta e C_{X_{\delta e}}(\alpha)$$

$$C_Z = C_Z(\alpha) + \delta e C_{Z_{\delta e}}(\alpha)$$

$$C_m = C_m(\alpha) + C_T C_{m_T}(\alpha) + \delta e C_{m_{\delta e}}(\alpha) + \frac{c}{2V} q C_{m_q}(\alpha)$$

where C_T is the thrust coefficient, which is defined as

$$C_T = \frac{T}{QS}.$$

Polynomial fits of several coefficients are shown in Figure 3.2.1.

3.2.2 Generic Jet Fighter

Aerodynamic data for a generic jet fighter were obtained from Young, Schy, and Johnson [1980]. The aerodynamic data are nonlinear functions of the angle of attack and are reported in increments of 5 degrees for angles of attack from

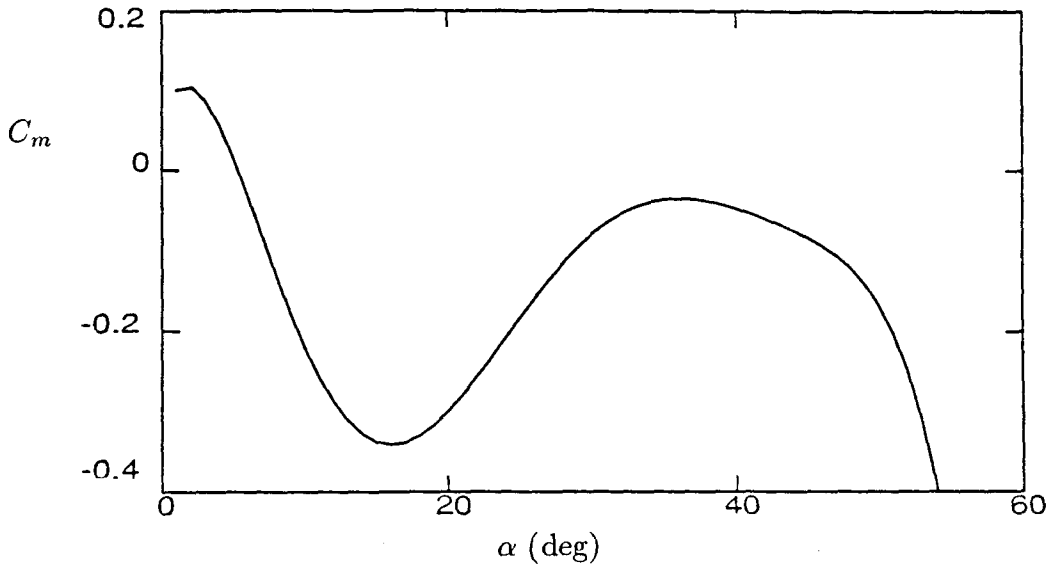

(a) Pitching Moment Coefficient

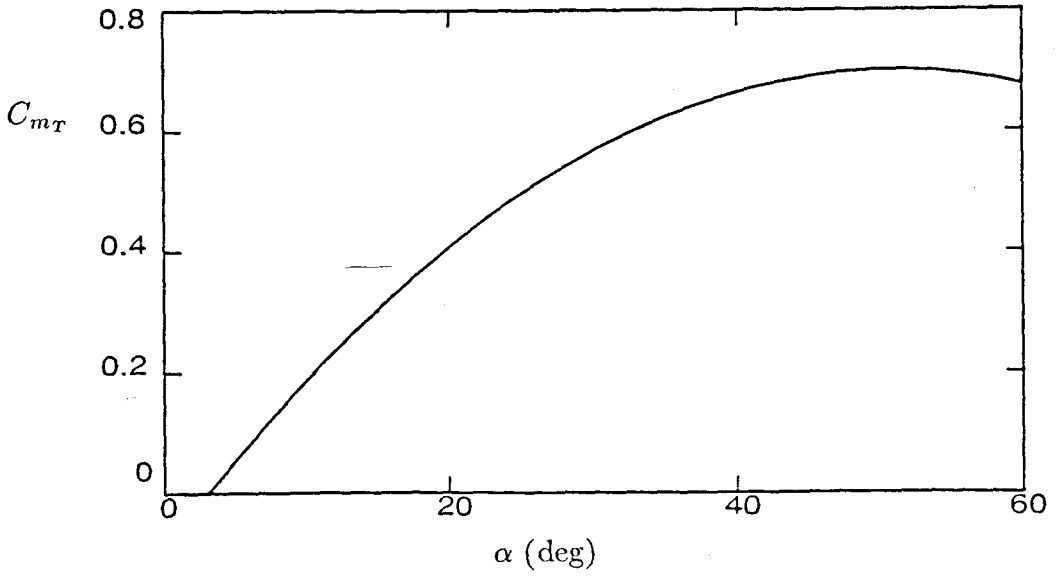

(b) Pitching Moment Due To Thrust

Figure 3.2.1: Aerodynamic coefficients for general aviation aircraft.

negative 10 to positive 90 degrees. The aerodynamic model has the form,

$$C_X = C_X(\alpha) + \delta e C_{X_{\delta e}}(\alpha)$$

$$C_Y = \beta C_{Y_\beta}(\alpha) + \delta a C_{Y_{\delta a}}(\alpha) + \delta r C_{Y_{\delta r}}(\alpha) + \frac{b}{2V}(pC_{Y_p}(\alpha) + rC_{Y_r}(\alpha))$$

$$C_Z = C_Z(\alpha) + \delta e C_{Z_{\delta e}}(\alpha)$$

$$C_\ell = \beta C_{\ell_\beta}(\alpha) + \delta a C_{\ell_{\delta a}}(\alpha) + \delta r C_{\ell_{\delta r}}(\alpha) + \frac{b}{2V}(pC_{\ell_p}(\alpha) + rC_{\ell_r}(\alpha))$$

$$C_m = C_m(\alpha) + \delta e C_{m_{\delta e}}(\alpha) + \frac{c}{2V} q C_{m_q}(\alpha)$$

$$C_n = \beta C_{n_\beta}(\alpha) + \delta a C_{n_{\delta a}}(\alpha) + \delta r C_{n_{\delta r}}(\alpha) + \frac{b}{2V}(pC_{n_p}(\alpha) + rC_{n_r}(\alpha)).$$

The data were fitted with cubic splines with tension. Several coefficients are shown in Figure 3.2.2.

3.2.3 F-14 Aerodynamic Model

An aerodynamic model for the F-14 was supplied by NASA Ames Dryden Flight Research Center. The model is used in flight simulators at Dryden Flight Research Center and has been verified by comparisons with flight tests. Four aerodynamic data bases are included in the model: low angle of attack, high angle of attack, high speed, and rotary balance data. High speed data was not used in the course of this research, which required flight speeds to be limited to Mach numbers below 0.60. This was done for simplicity, and because high angle of attack flight, the major interest of this thesis, normally occurs in pratice at subsonic speeds. Control and stability augmentation systems which are included in operational F-14's were not included in this analysis. Also, the spoilers were assumed to be retracted in the results presented here.

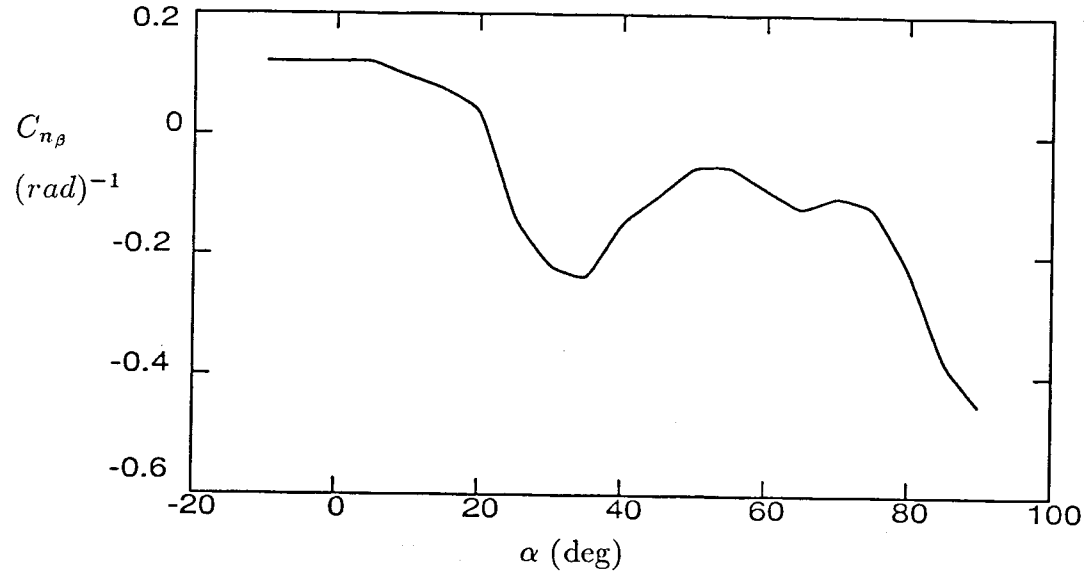

(a) Directional Stability

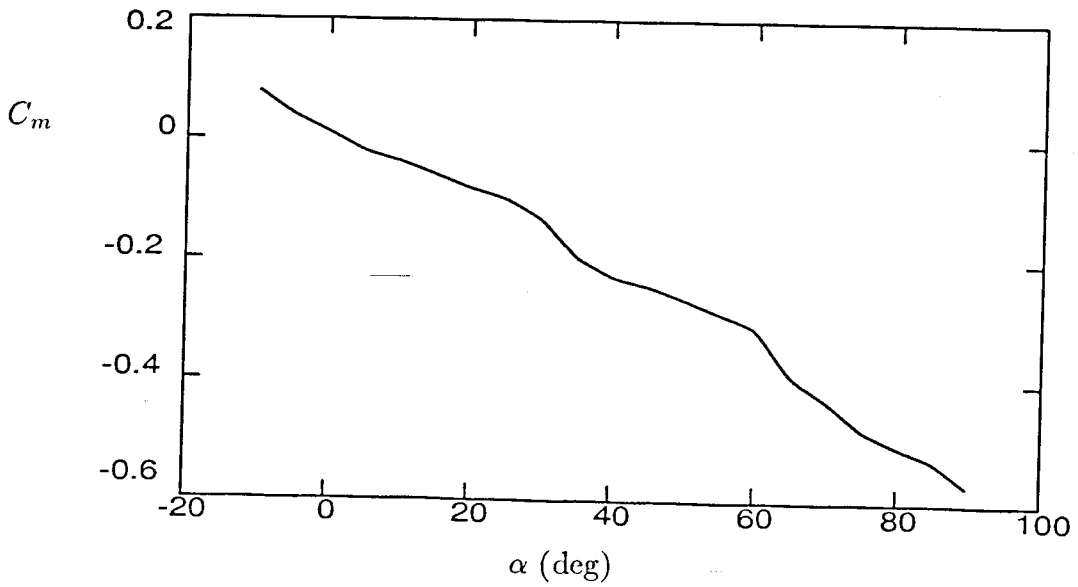

(b) Pitching Moment Coefficient

Figure 3.2.2: Aerodynamic coefficients of generic jet fighter.

The low angle of attack aerodynamic model is reported for angles of attack from zero to 55 degrees, angles of sideslip from negative 20 to positive 20 degrees, and elevator deflections from negative 30 to positive 10 degrees and has the form,

$$
\begin{aligned}
C_X =& C_X(\alpha,\beta) + \frac{c}{2V} q C_{X_q}(\alpha) \\
&+ \begin{pmatrix} C_{x_{\delta e1}}(\alpha,\beta)\delta e & ;\delta e \geq -10. \\ -10 C_{X_{\delta e1}}(\alpha,\beta) + (\delta e + 10) C_{X_{\delta e2}}(\alpha,\beta) & ;\delta e \leq -10 \end{pmatrix} \\
C_Z =& C_Z(\alpha,\beta) + \frac{c}{2V} \bar{q} C_{Z_q}(\alpha) \\
&+ \begin{pmatrix} C_{Z_{\delta e1}}(\alpha,\beta)\delta e & ;\delta e \geq -10 \\ -10 C_{Z_{\delta e1}}(\alpha,\beta) + (\delta e + 10) C_{Z_{\delta e2}}(\alpha,\beta) & ;\delta e \leq -10 \end{pmatrix} \\
C_m =& C_m(\alpha,\beta) + \frac{c}{2V} \bar{q} C_{m_q}(\alpha) \\
&+ \begin{pmatrix} C_{m_{\delta e1}}(\alpha,\beta)\delta e & ;\delta e \geq -15 \\ -15 C_{m_{\delta e1}}(\alpha,\beta) + (\delta e + 15) C_{m_{\delta e2}}(\alpha,\beta) & ;\delta e \leq -15 \end{pmatrix} \\
C_Y =& C_Y(\alpha,\beta) - \delta a C_{Y_{\delta a}}(\alpha,\beta) + \delta r C_{Y_{\delta r}}(\alpha,\beta) \\
&+ \frac{b}{2V} (\bar{r} C_{Y_r}(\alpha) + \bar{p} C_{Y_p}(\alpha)) \\
C_\ell =& C_\ell(\alpha,\beta) + D C_{\ell_{\beta 2}}(\alpha)\beta - \delta a (C_{\ell_{\delta a1}}(\alpha,\beta) + C_{\ell_{\delta a2}}(\alpha,\delta e)) \\
&+ \delta r C_{\ell_{\delta r}}(\alpha,\beta) + \frac{b}{2V} (\bar{r} C_{\ell_r}(\alpha) + \bar{p} C_{\ell_p}(\alpha)) \\
C_n =& C_n(\alpha,\beta,\delta e) - \delta a (C_{n_{\delta a1}}(\alpha,\beta) + C_{n_{\delta a2}}(\alpha,\delta e)) \\
&+ \delta r C_{n_{\delta r}}(\alpha,\beta,\delta e) + \frac{b}{2V} (\bar{r} C_{n_r}(\alpha) + \bar{p} C_{n_p}(\alpha))
\end{aligned}
$$

where,

$$
\begin{aligned}
\bar{q} =& q - \Omega \sin\beta \\
\bar{r} =& r - \Omega \sin\alpha \cos\beta \\
\bar{p} =& p - \Omega \cos\alpha \cos\beta
\end{aligned}
$$

and,

$$
\Omega = (p\cos\alpha + r\sin\alpha)\cos\beta + q\sin\beta
$$

is the rotation rate about the velocity vector.

The high angle of attack aerodynamic model is reported for angles of attack from 55 to 90 degrees, angles of sideslip from negative 20 to positive 20 degrees, and elevator deflections of zero and negative 30 degrees and has the form,

$$C_X = C_X(\alpha,\beta) + \delta e C_{X_{\delta e}}(\alpha,\beta)$$

$$C_Z = C_Z(\alpha,\beta) + \frac{c}{2V}\bar{q}C_{Z_q} + \delta e C_{Z_{\delta e}}(\alpha,\beta)$$

$$C_m = C_m(\alpha,\beta) + \frac{c}{2V}(\bar{q}C_{m_q}(\alpha) + \dot{\alpha}C_{m_{\dot{\alpha}}}(\alpha)) + \delta e C_{m_{\delta e}}(\alpha,\beta)$$

$$C_Y = C_Y(\alpha,\beta) - \delta a C_{Y_{\delta a}}(\alpha,\beta) + \frac{b}{2V}(\bar{r}C_{Y_r}(\alpha) + \bar{p}C_{Y_p}(\alpha))$$

$$C_\ell = C_\ell(\alpha,\beta) - \delta a C_{\ell_{\delta a}}(\alpha,\beta) + \frac{b}{2V}(\bar{r}C_{\ell_r}(\alpha) + \bar{p}C_{\ell_p}(\alpha))$$

$$C_n = C_n(\alpha,\beta,\delta e) - \delta a C_{n_{\delta a}}(\alpha,\beta) + \frac{b}{2V}(\bar{r}C_{n_r}(\alpha) + \bar{p}C_{n_p}(\alpha)).$$

An important aspect of the high angle of attack aerodyamic model is that the rudder has no effect on the aerodynamic forces or moments. This is common in high angle of attack flight because the wing and horizontal tail shield the flow over the rudder. Yaw control will be ineffective or nonexistent at angles of attack above 55 degrees, and could cause difficulty recovering from a spin. This will be discussed in detail in Section 6.3.

Rotary balance data is reported for angles of attack from 0 to 90 degrees, angles of sideslip from negative 20 to positive 20 degrees, elevator deflections from negative 30 to postive 10 degrees, and nondimensional rotation rates about the velocity vector from negative 0.54 to positive 0.54, where the nondimensional rotation rate is defined as,

$$\bar{\Omega} = \frac{b}{2V}\Omega.$$

The rotary balance aerodynamic model has the form,

$$
\begin{aligned}
C_X =& 0.0 \\
C_Z =& -\mathrm{DCNORM}(\alpha, \bar{\Omega}) \\
C_m =& \mathrm{DCMR}(\alpha, \bar{\Omega}) + \mathrm{DCMRB}(\alpha, \bar{\Omega}\mathrm{sign}(\beta))|\beta| \\
C_Y =& \mathrm{DCYR}(\alpha, \bar{\Omega}) + \mathrm{DCYRIS}(\alpha, \bar{\Omega})\mathrm{AKCYIS}(\bar{\Omega}, \delta e) \\
C_\ell =& \mathrm{DCLR}(\alpha, \bar{\Omega}) + \mathrm{DCLRIS}(\alpha, \bar{\Omega})\mathrm{AKCL1}(\delta e) \\
& + \mathrm{DCLRDD}(\alpha, \bar{\Omega}\mathrm{sign}(\delta a))|\frac{\delta a}{7}| \\
C_n =& \mathrm{DCNR}(\alpha, \bar{\Omega}) + \mathrm{DCNRIS}(\alpha, \bar{\Omega})\mathrm{AKCNIS}(\bar{\Omega}, \delta e) \\
& + \mathrm{AKCNB}(\alpha, \beta)\mathrm{DCNRB}(\alpha, \bar{\Omega}, \beta) \\
& + \mathrm{DCNRDD}(\alpha, \bar{\Omega}\mathrm{sign}(\delta a), \delta e)|\frac{\delta a}{7}|.
\end{aligned}
$$

Note that the rudder has no effect on the rotary aerodynamics. The rudder is usually blanketed by the vertical tail in highly rotational flows, making it difficult or impossible to recover from a fully developed spin. Absolute values are used in the rotary aerodyamic model. The first derivative of the absolute value is discontinuous at the origin, which could cause numerical difficulties in the continuation method. This problem was solved by replacing the absolute value function with the function,

$$
|x| = \begin{pmatrix} \frac{1}{2}x^2(3-x^2) & ;|x| \leq 1 \\ |x| & ;|x| \geq 1 \end{pmatrix}.
$$

The above aerodynamic coefficents were all approximated with bicubic functions using the algorithm of Press, Flannery, Teukolsky, and Vetterling [1988] in

the continuation method routine and linear interpolation in the simulation program. A discontinuity occurs in the aerodynamic data at an angle of attack of 55 degrees, where one goes from the low angle of attack data to the high angle of attack data, or vice versa. In the simulation program the two data sets were blended together for angles of attack from 55 to 60 degrees with the relation

$$C = C_L + (C_H - C_L)(\frac{\alpha - 55}{5})$$

where C_L represents low angle of attack data and C_H represents high angle of attack data. This fit is not smooth, as required by the continuation method, so in the continuation method program the data sets were blended together with the relation

$$C_L = C_L + (C_H - C_L)(3 - 2\bar{\alpha})\bar{\alpha}^2$$

where

$$\bar{\alpha} = \frac{\alpha - 55}{5}$$

for angles of attack from 55 to 60 degrees. Several coefficients are shown in Figure 3.2.3.

3.3 Feedback Control Theory

Aircraft control systems are usually designed with linear control theory. The equations of motion are linearized about a particular type of motion, for example the phugoid mode, and a control system is designed to give this linearized system desirable behavior, a desired damping and frequency of the mode. Dynamical

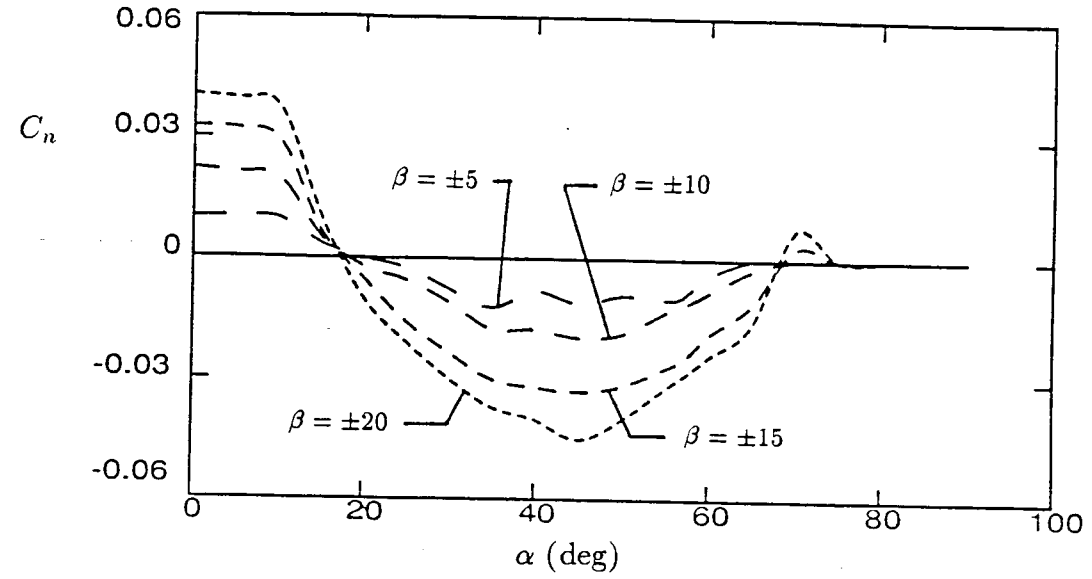

(a) Yawing Moment Coefficient

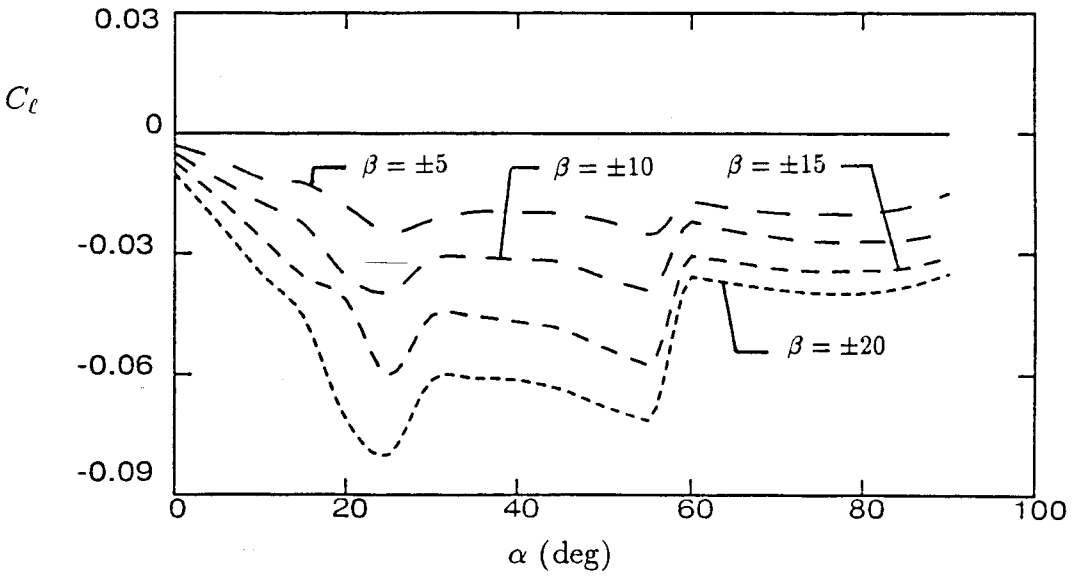

(b) Rolling Moment Coefficient

Figure 3.2.3: Aerodynamic coefficients for F-14.

systems theory proves that the stability of a steady state of a nonlinear dynamical system can be determined by calculating the eigenvalues of the linearized system at the steady state, so the above procedure should work. Indeed it has proven very effective for designing control systems.

A problem with this technique is that the linearized system used to model the various motions of the aircraft is not the exact linearized system, as determined by computing the Jacobian of the system. Variables which are secondary to the motion being analyzed are usually neglected. For example, the longitudinal modes are neglected when analyzing the lateral modes. This research will determine the effects of simple control systems on the fixed points of the full equations of motion, paying particular attention to the effects of control systems on the bifurcations of the fixed points of the equations of motion.

Control systems used in this research are simple state feedback systems as shown in Figure 3.3.1 where $F(x, \delta)$ is the aircraft model, x is the state of the aircraft, δ_p is the pilot input, and $k(x)$ is the state feedback. No actuator dynamics are included in the model, and it was assumed that the state of the aircraft was known at all times. The equations of motion with no feedback can be represented by

$$\dot{x} = F(x, \delta), \tag{3.3.1}$$

so the equations of motion with a feedback control system as shown in Figure 3.3.1 can be represented by

$$\dot{x} = F(x, \delta(\delta_p + kx)), \tag{3.3.2}$$

where

$$\delta(\delta_p, k, x) = \delta_p + k(x). \tag{3.3.3}$$

Note that the control system has not been limited to linear feedback. Nonlinear feedback is no more difficult to analyze with the continuation method than linear feedback.

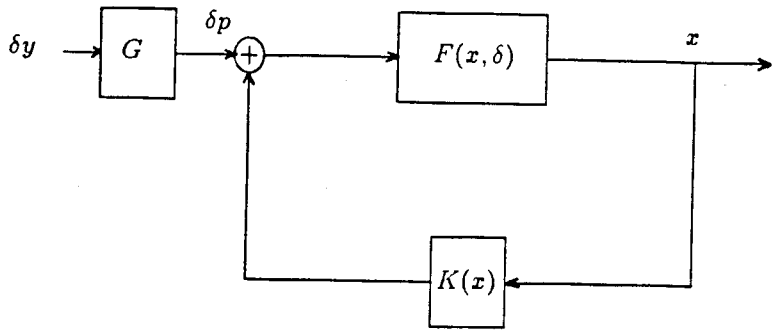

Figure 3.3.1: Schematic of feedback control system.

IV. RESULTS FOR A GENERAL AVIATION AIRCRAFT

Canard configuration aircraft are often considered more stall resistant than aircraft with an aft horizontal tail. The conventional wisdom is: since the canard is forward of the center of gravity, any loss of lift on the canard results in a nose down pitching moment giving canard configuration aircraft a natural stall resistance. Loss of lift on an aft horizontal tail on the other hand results in a nose up pitching moment which makes the stall worse. While this reasoning is correct in a general sense, this example shows that not all canard configuration aircraft have good stall behavior. This aircraft was designed with a tractor propellor (see Figure 4.1) which was directly in front of the canard. The prop wash caused the flow over the canard to stay attached at high angles of attack, with the result that the wing stalled before the canard giving the aircraft dangerous stall behavior.

Analysis of this aircraft will be restricted to longitudinal motions because complete lateral aerodynamic data were not available. This is not a severe limitation for this aircraft, as the interesting behavior is contained in the longitudinal motions. A simplified system will also allow for easier understanding of the new methods introduced in this section. This will prove helpful when analyzing the more complete aerodynamic models in Chapters V and VI. Poor design of this aircraft resulted in a pitching moment,

$$C_m = C_m(\alpha) + \delta e C_{m_{\delta e}}(\alpha) + C_T C_{m_T} + \frac{c}{2V} q C_{m_q}(\alpha),$$

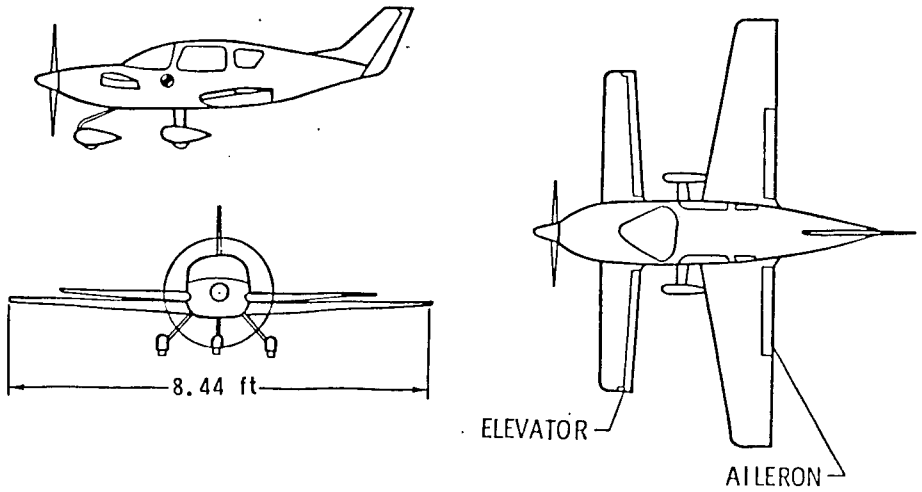

Figure 4.1: General aviation aircraft with a canard configuration; Chambers, Yip, and Moul [1983].

with several undesirable characteristics. For angles of attack between 15 and 35 degrees the pitching moment coefficent, $C_m(\alpha)$, has a positive slope (see Figure 3.2.1), which causes a local maximum in $C_m(\alpha)$ at an angle of attack of 35 degrees. This could lead to the development of a high angle of attack stall as nose up elevator deflection is applied. The thrust also has a detrimental effect on the pitch stability of the aircraft, as applying thrust results in a nose up pitching moment (see Figure 3.2.1). Specific effects of these aerodynamic characteristics can be determined by studying the fixed points of the system.

4.1 Fixed Points

Restricting the motion of the aircraft to purely longitudinal motions, ($p = r = \beta = \phi = 0$), results in the four-dimensional system,

$$\begin{aligned}
\dot{\alpha} =& q - \frac{QS}{MV}(C_Z \cos\alpha - C_X \sin\alpha) - \frac{T\sin\alpha}{MV} \\
&+ \frac{g}{V}(\sin\alpha\sin\theta + \cos\alpha\cos\theta\cos\phi) \\
\dot{V} =& \frac{QS}{M}(C_X\cos\alpha + C_Z\sin\alpha) + \frac{T\cos\alpha}{M} \\
&+ g(\sin\alpha\cos\theta - \cos\alpha\sin\theta) \\
\dot{q} =& \frac{QSc}{I_Y}C_m \\
\dot{\theta} =& q.
\end{aligned}$$

The steady states of this system can be found by setting the time derivatives equal to zero, (i.e., $\dot{\alpha} = \dot{V} = \dot{q} = \dot{\theta} = 0$), and solving the resulting algebraic equations. It is easy to see that the pitch rate, q, is zero for all steady states, so it will not be included in plots of steady states for this aircraft. Recall that in general (see

Section 3.1.1)

$$\dot{\theta} = q\cos\phi - r\sin\phi$$

so the pitch rate is not necessarily zero for steady states in which the lateral motions are nonzero.

Figure 4.2 shows the steady states as a function of elevator deflection for zero thrust. Elevator travel in the real airplane was from negative 20 to positive 35 degrees, but plots in this thesis will have elevator deflections from negative 20 to positive 40 degrees for ease of plotting. Note that positive elevator deflection produces a nose up pitching moment for a canard configuration aircraft. For a given elevator deflection, the steady states of the aircraft can be determined by drawing a vertical line representing that elevator deflection on each plot in Figure 4.2. Intersections with curves of steady states give the steady states of the aircraft for the given elevator deflection.

For physical reasons, and ease of discussion, the steady states in Figure 4.2 will be broken into three types: low angle of attack labelled 'L', intermediate angle of attack labelled 'I', and high angle of attack labelled 'H'. They represent different flight regimes but are all part of the same curve of steady states. The low and intermediate angle of attack steady states join at a saddle-node bifurcation for an elevator deflection of 48 degrees and the intermediate and high angle of attack steady states join at a saddle-node bifurcation for an elevator deflection of 10 degrees. These saddle-node bifurcations have the same properties as the one-dimensionl examples discussed in Section 2.1.5. Two fixed points exist for

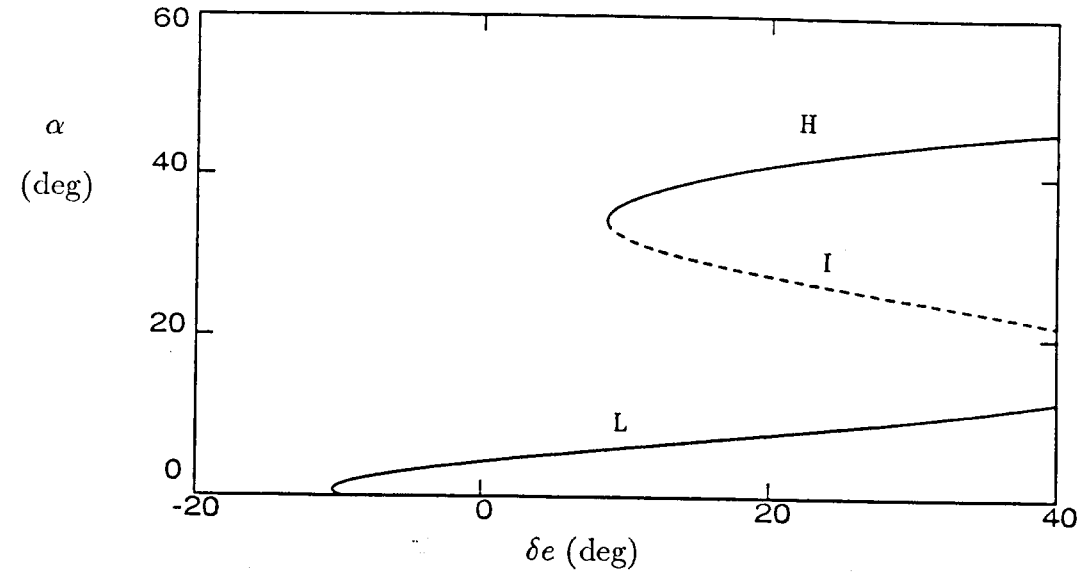

(a) Angle of Attack

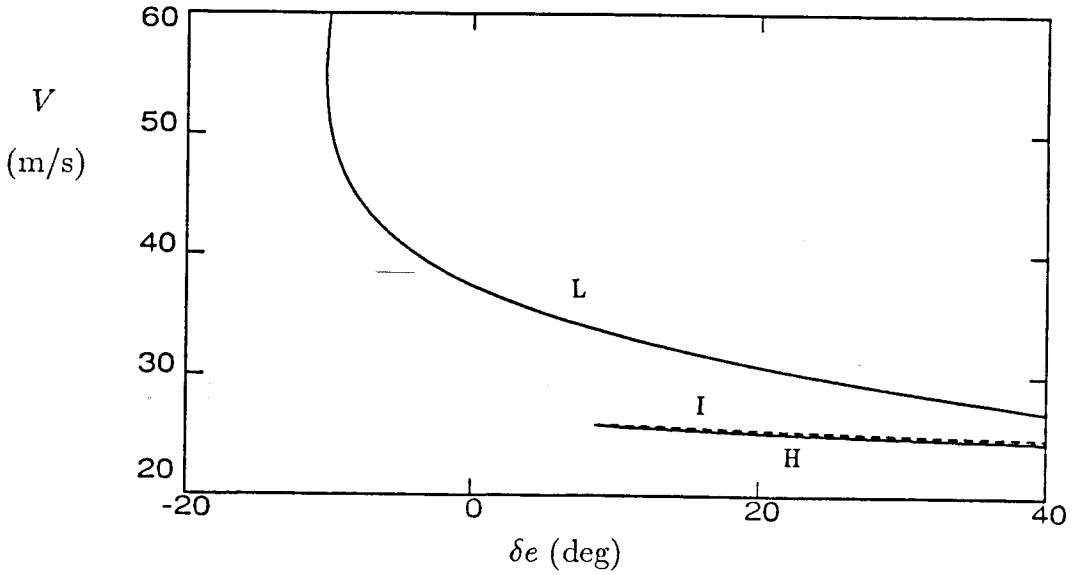

(b) Speed

Figure 4.2: Steady States for the general aviation aircraft at sea level, $C_T = 0$, —— stable, - - - unstable.

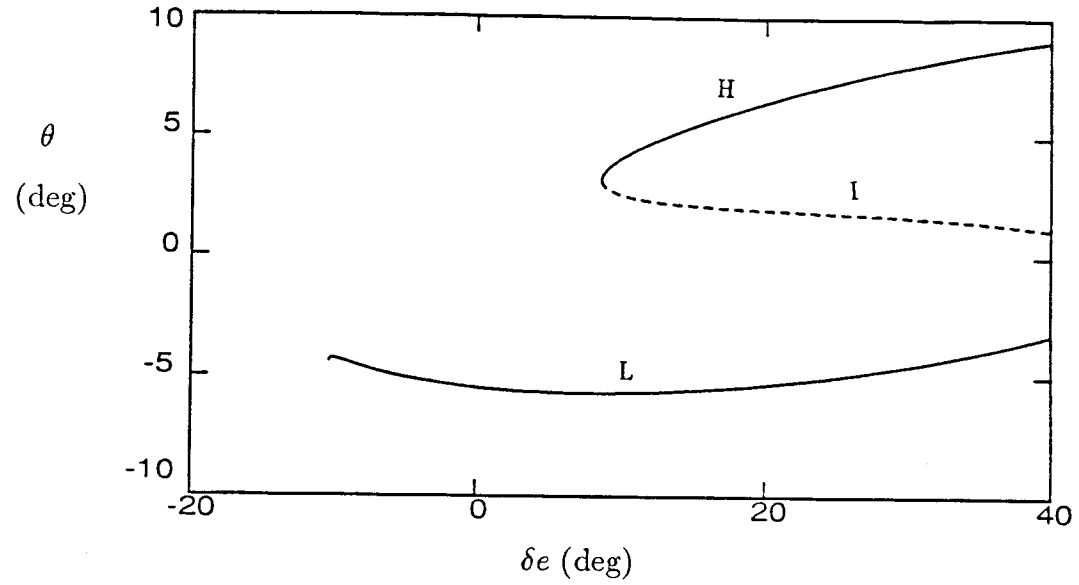

(c) Pitch Angle

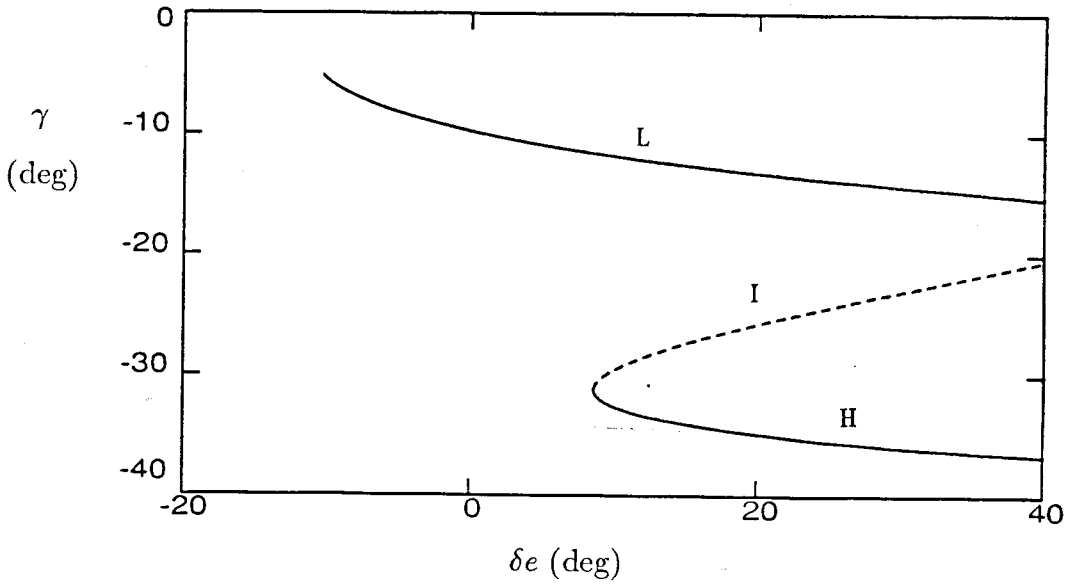

(d) Flight Path Angle

Figure 4.2: Concluded.

parameter values on one side of the bifurcation point and no fixed points exist for parameter values on the other side of the bifurcation point, and the stability of the curve of fixed points changes at the bifurcation point, because one real eigenvalue of the linearized system changes sign. These two saddle-node bifurcations will be responsible for much of the undesirable behavior of this aircraft.

The low angle of attack steady states are the desirable flight conditions; the intermediate and high angle of attack steady states represent stalled flight. While the existence of a stable high angle of attack stall is very undesirable, the low angle of attack dynamics of this aircraft at zero thrust are acceptable. Low angle of attack steady states exit for all elevator deflections (the curve stops at $\delta e = 10$ because the aerodynamic model is limited to positive angles of attack) and are always stable. Figure 4.3 shows the eigenvalues of the low angle of attack steady states. Phugoid and short period modes are present, but both are well damped and have acceptable frequencies. The damping of the phugoid mode increases significantly as the elevator deflection is increased, while the damping of the short period mode decreases.

Three steady states exist for elevator deflections of more than 10 degrees because of the saddle-node bifurcation connecting the high and intermediate angle of attack steady states. The aircraft will not fly at the intermediate angle of attack steady states because they are always unstable, but it could fly at either the low or high angle of attack steady states, which are always stable. It would be possible

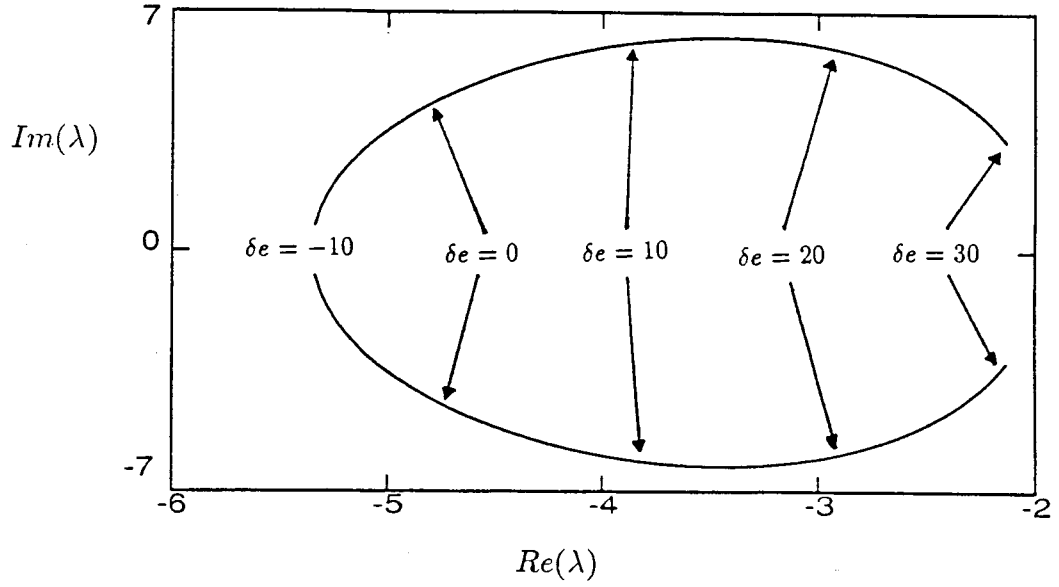

(a) Short period modes

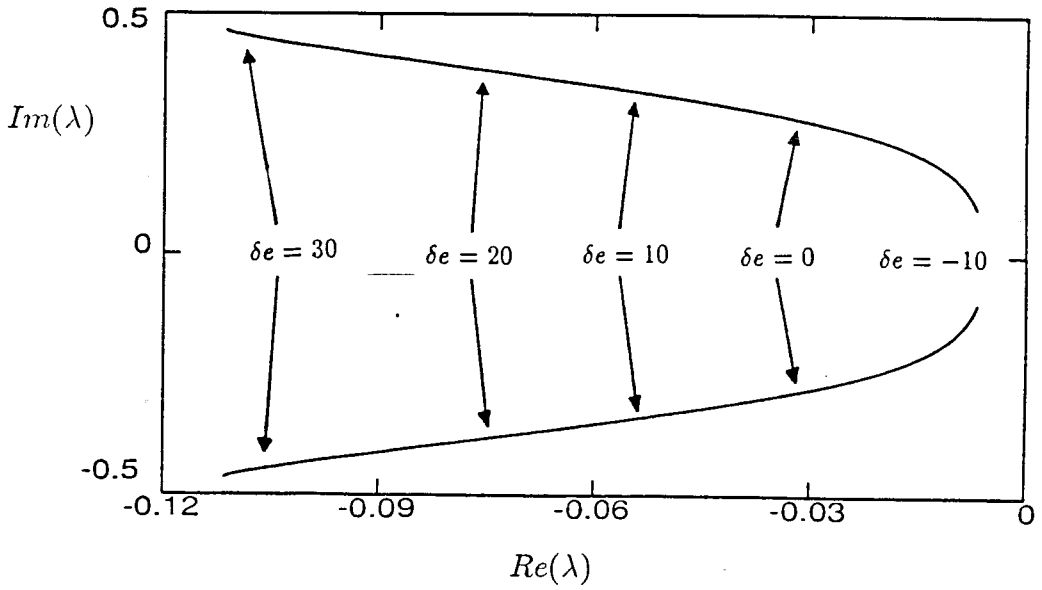

(b) Phugoid Modes

Figure 4.3: Eigenvalues of the general aviation aircraft in low angle of attack flight as a function of elevator deflection for $C_T = 0$ and $\rho = 1.2\frac{kg}{m^3}$.

for the aircraft to jump from the low angle of attack steady state to a high angle of attack steady state as a result of a gust or some other disturbance.

Recovery from a high angle of attack stall would be possible by reducing the elevator deflection to less than 10 degrees because no high angle of attack steady states exist for elevator deflections of less than 10 degrees. A simulation of recovery from a high angle of attack stall is shown in Figure 4.4. Reducing the elevator deflection puts the aircraft into a dive, which increases the velocity and decreases the angle of attack. The angle of attack is quickly reduced to the low angle of attack steady state value while the velocity and pitch angle undergo damped phugoid oscillations about their low angle of attack steady state values.

Figure 4.5 shows the steady states of the aircraft at maximum thrust (C_T=0.4). Applying thrust to the aircraft causes the saddle-node bifurcations which connect the three branches of steady states to occur at different elevator deflections. The saddle-node bifurcation which connects the high and intermediate angle of attack steady states now occurs at an elevator deflection of negative 70 degrees. This is well beyond the range of motion for the elevator, so a high angle of attack stall exists for all elevator deflections. This is a very dangerous situation and resulted in several deaths during a flight test of this aircraft. Wind-tunnel tests had not been done prior to the flight tests, so the pilot was not aware of the adverse effects of thrust on the stall behavior of the aircraft.

Recovery from a stall usually involves applying nose down elevator and maximum thrust in an attempt to increase the velocity and reduce the angle of attack.

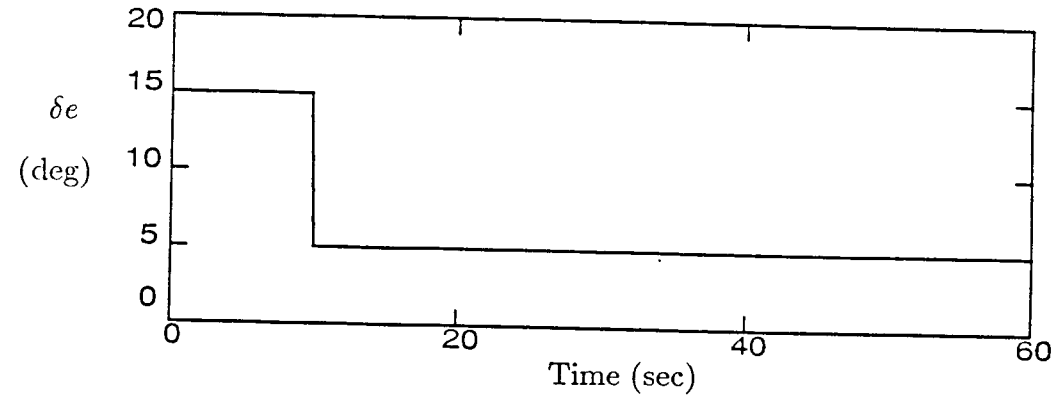

(a) Elevator Deflection

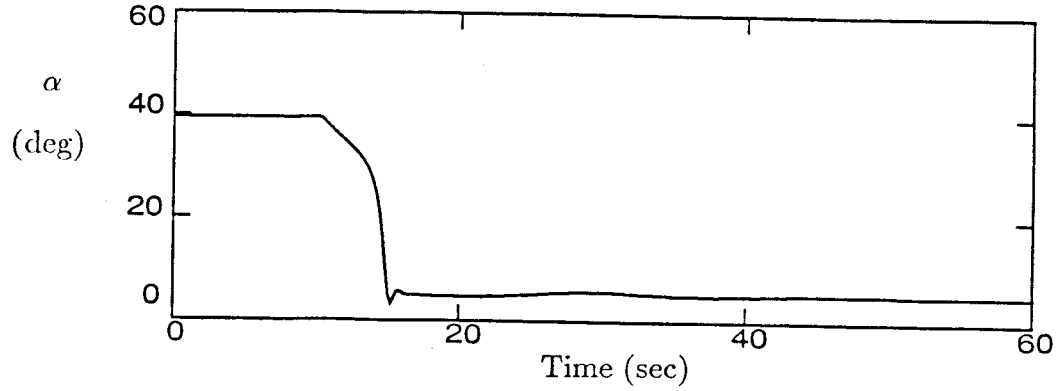

(b) Angle of Attack

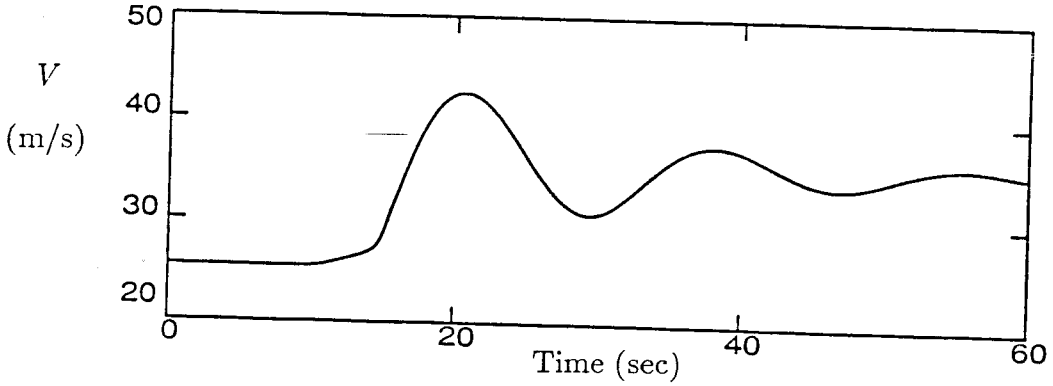

(c) Speed

Figure 4.4: Simulation of recovery from high angle of attack stall for the general aviation aircraft with $C_T = 0$ and $\rho = 1.2\frac{kg}{m^3}$.

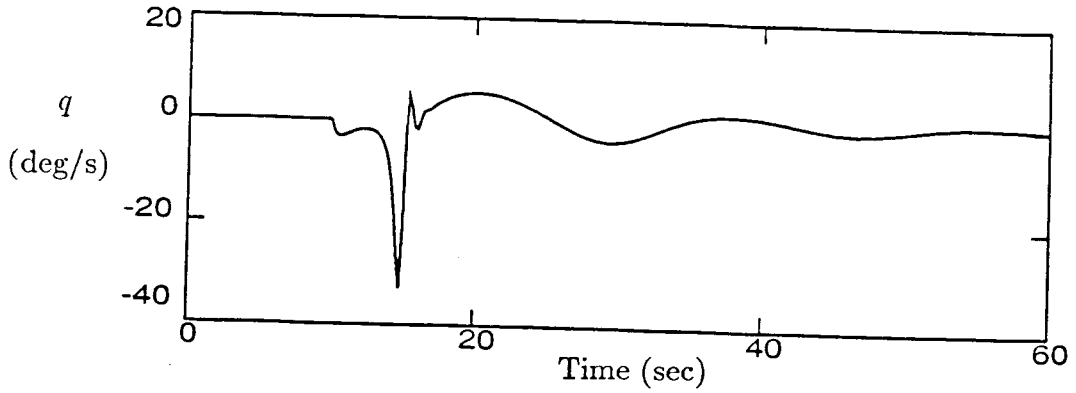

(d) Pitch Rate

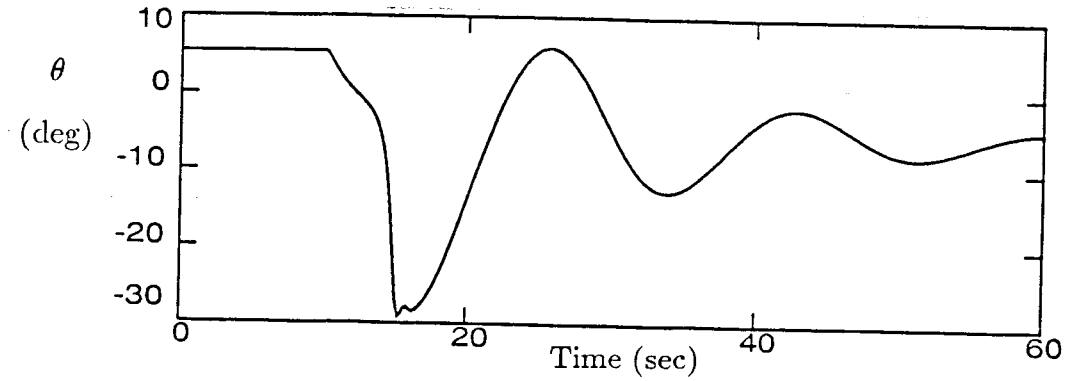

(e) Pitch Angle

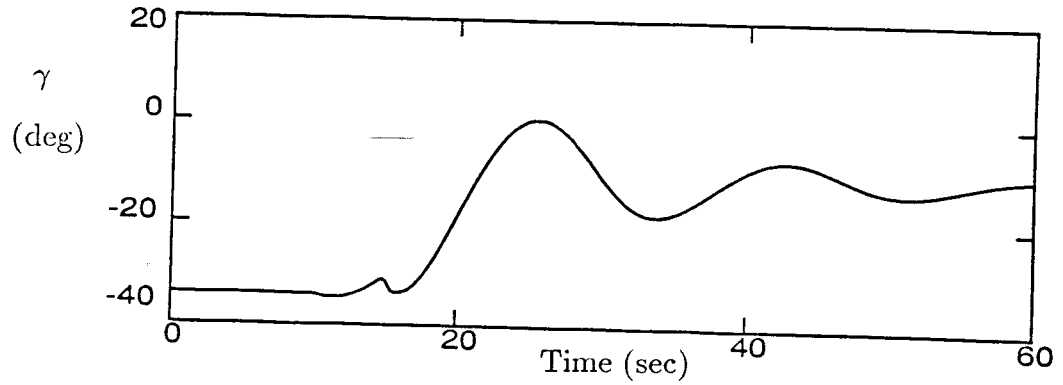

(f) Flight Path Angle

Figure 4.4: Concluded.

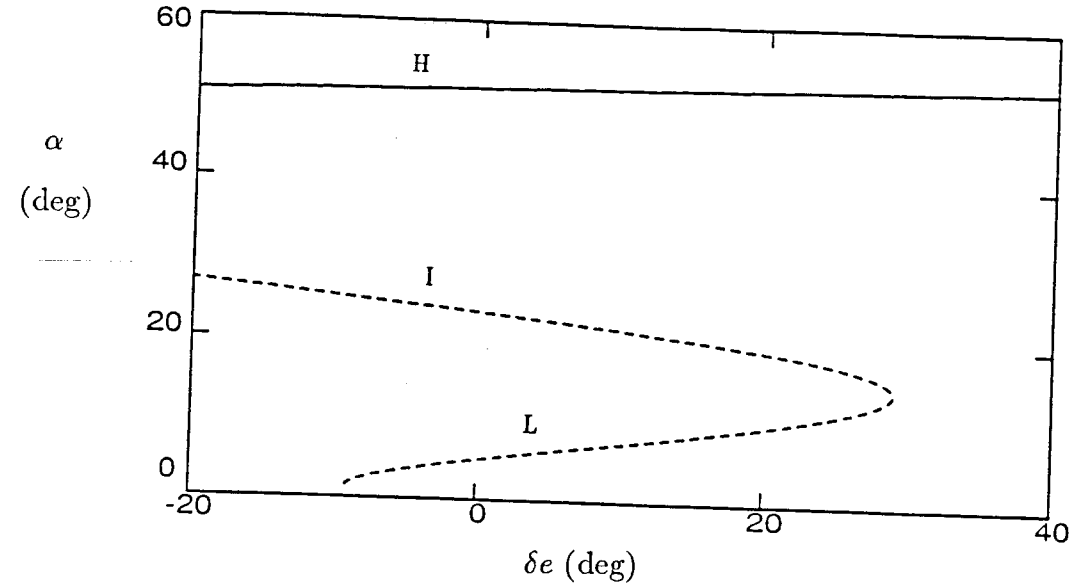

(a) Angle of Attack

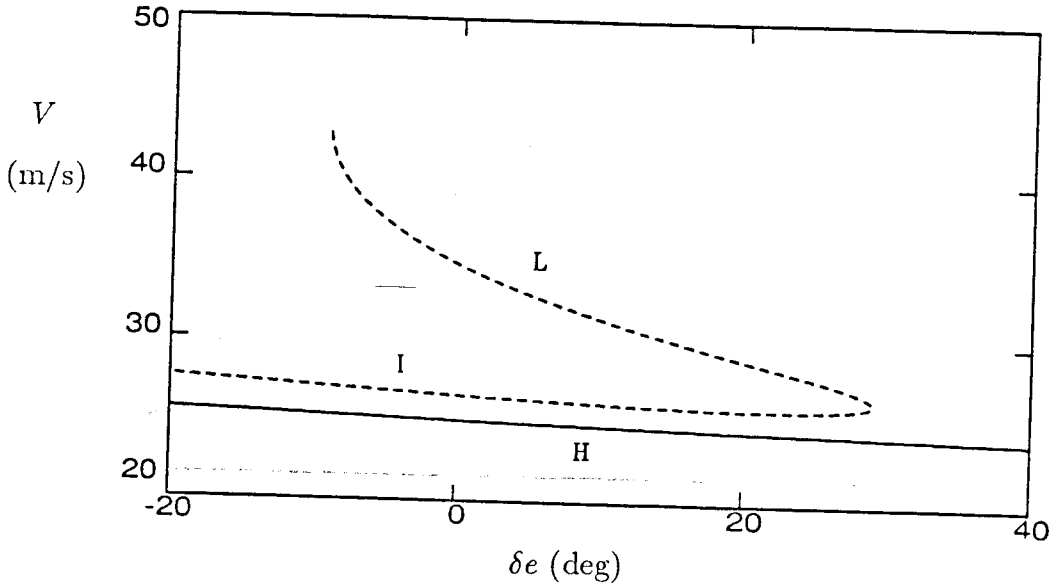

(b) Speed

Figure 4.5: Steady states for the general aviation aircraft at sea level for C_T=0.4 (maximum thrust);
—— stable, – – – unstable.

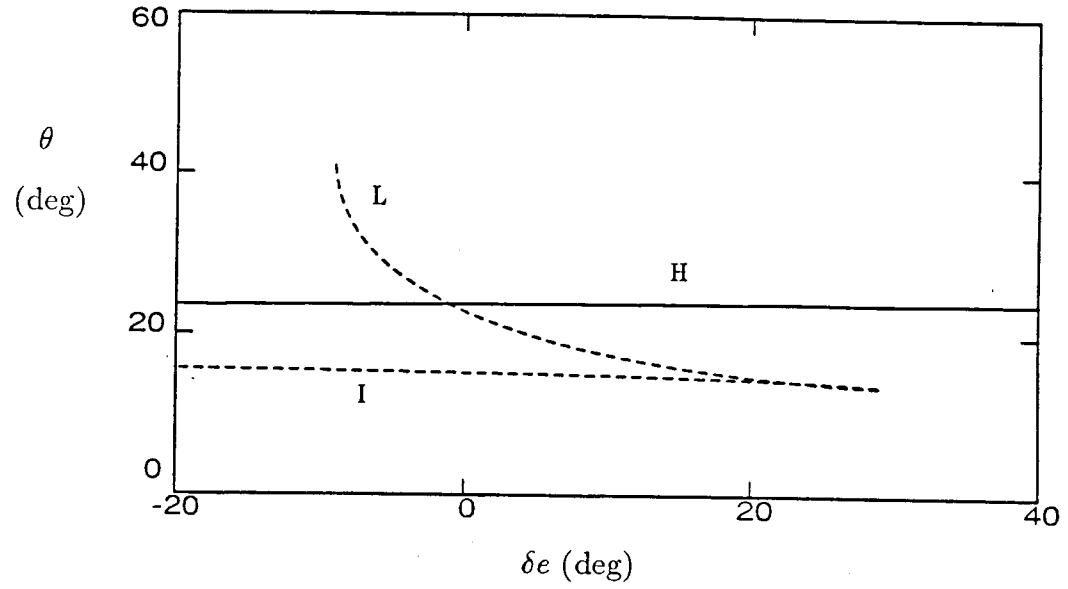

(c) Pitch Angle

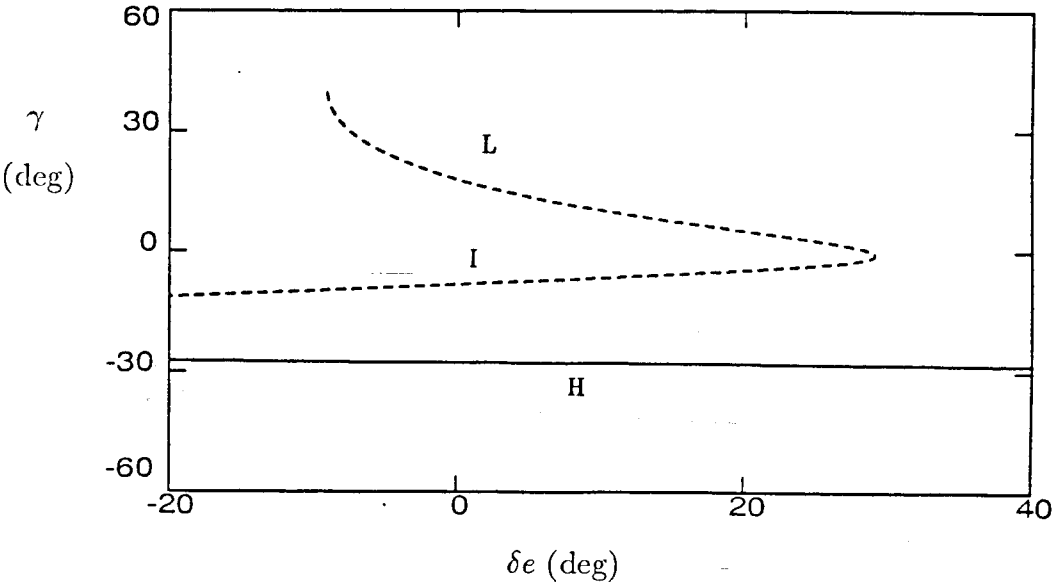

(d) Flight Path Angle

Figure 4.5: Concluded.

Applying maximum thrust during a stall in this aircraft does not bring the aircraft out of the stall, but actually increases the severity of the stall. This is caused by the effect of thrust on the pitching moment of the aircraft, $C_T(\alpha)$. Since $C_T(\alpha)$ is positive (see Figure 3.2.1), applying thrust results in a nose up pitching moment, which increases the angle of attack. A higher angle of attack will lead to a higher drag coefficient which will counteract the effect of increased thrust on the speed of the aircraft. The net result of applying maximum thrust in a stall will be an increase in the angle of attack, while the velocity stays essentially constant. A simulation of these effects is shown in Figure 4.6. Note that the velocity actually decreases as more thrust is applied in this simulation.

At maximum thrust, the saddle-node bifurcation that connects the low and intermediate angle of attack steady states occurs at an elevator deflection of 30 degrees (Figure 4.5). This is within the range of elevator deflections allowed for the aircraft, so this bifurcation point could cause problems for the pilot. Just as the aircraft recovered from a stall at zero thrust by reducing the elevator deflection past a bifurcation point (see Figure 4.4), increasing the elevator deflection past 30 degrees at maximum thrust would result in a jump to a high angle of attack stall. It would be impossible to get out of this stall without reducing the thrust.

An even more serious problem with flight at maximum thrust is that all of the low angle of attack steady states are unstable. This is clearly unacceptable and very dangerous. It may be possible for the pilot to control the airplane by actively adjusting the elevator, just as the Wright brothers did with their unstable

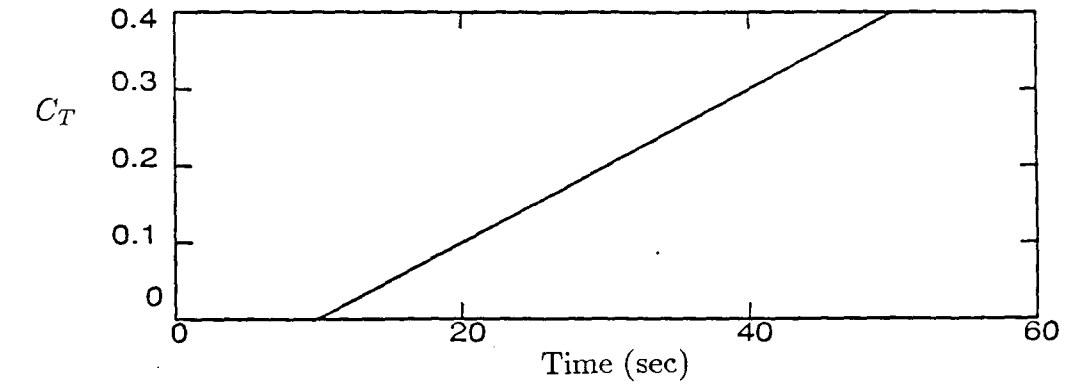

(a) Thrust Coefficient

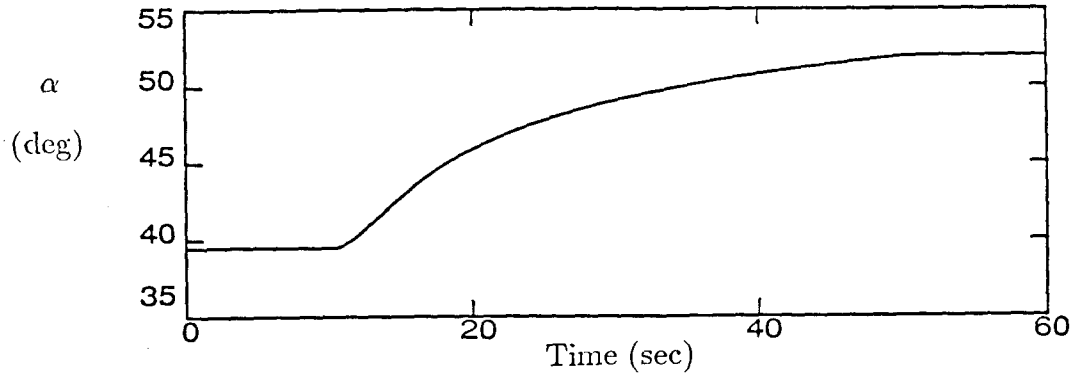

(b) Angle of Attack

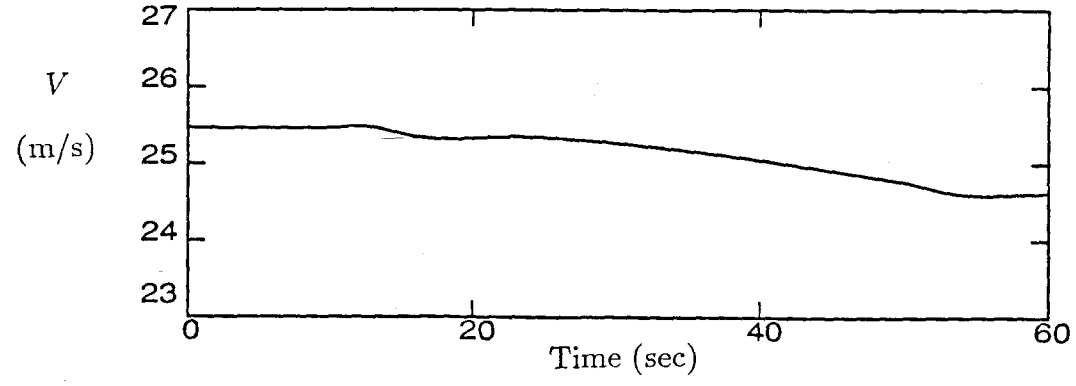

(c) Speed

Figure 4.6: Simulation of the effect of increased thrust during a stall for the general aviation aircraft with δe=15.

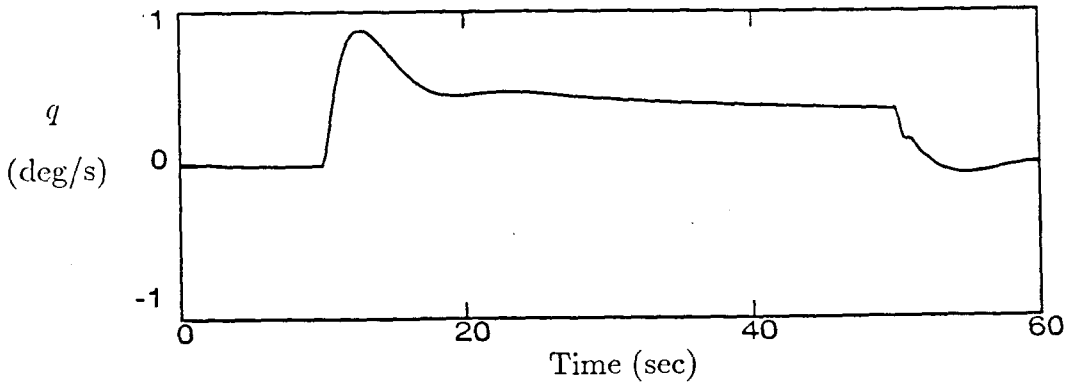

(d) Pitch Rate

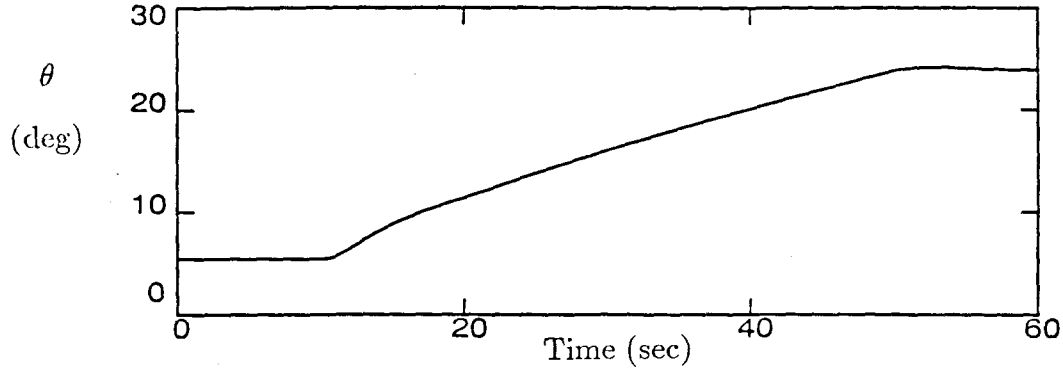

(e) Pitch Angle

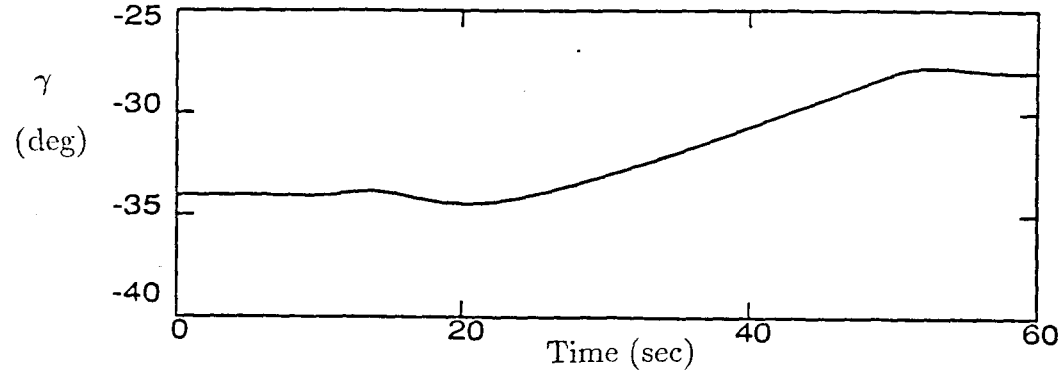

(f) Flight Path Angle

Figure 4.6: Concluded.

airplane, but this a is dangerous procedure because any lapse by the pilot could lead to a high angle of attack stall. Obviously, the best solution to this problem is to redesign the airplane, but apart from that it may be possible to solve the problem by limiting the thrust available to the pilot. The low angle of attack steady states are all stable for zero thrust, so there is probably a range of thrust setting where the low angle of attack steady states remain stable. Recall that the eigenvalues of the linearized system are continuous functions of the parameters of the system, so the stability of the low angle of attack steady states will vary continuously as the thrust is changed.

Figure 4.7 shows the steady states of the aircraft for a thrust coefficient of 0.14. A Hopf bifurcation occurs in the low angle of attack steady states at an elevator deflection of 5 degrees. This causes the low angle of attack steady states to be unstable for elevator deflections of less than 5 degrees and stable for elevator deflections greater than 5 degrees. Monitoring the eigenvalues of the low angle of attack steady states as a function of elevator deflection shows that the phugoid mode goes unstable at the Hopf bifurcation, as shown in Figure 4.8.

Hopf bifurcations related to the phugoid instability occur for a wide range of thrust coefficients and elevator deflections, as shown by the bifurcation loci in Figure 4.9. Figure 4.9 shows that a continuous curve exists in the parameter space (i.e., $\delta e - C_T$ space) along which Hopf bifurcations occur. Thus, if the pilot is flying at a condition of low angle of attack below the curve of Hopf bifurcations (the shaded region in Figure 4.9), the airplane will be stable. It will remain stable

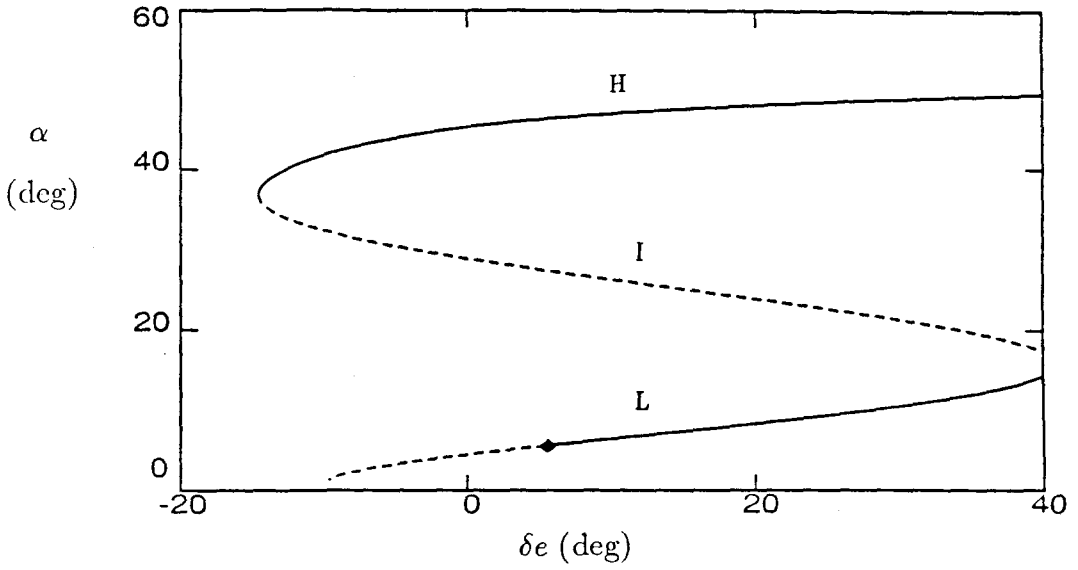

(a) Angle of Attack

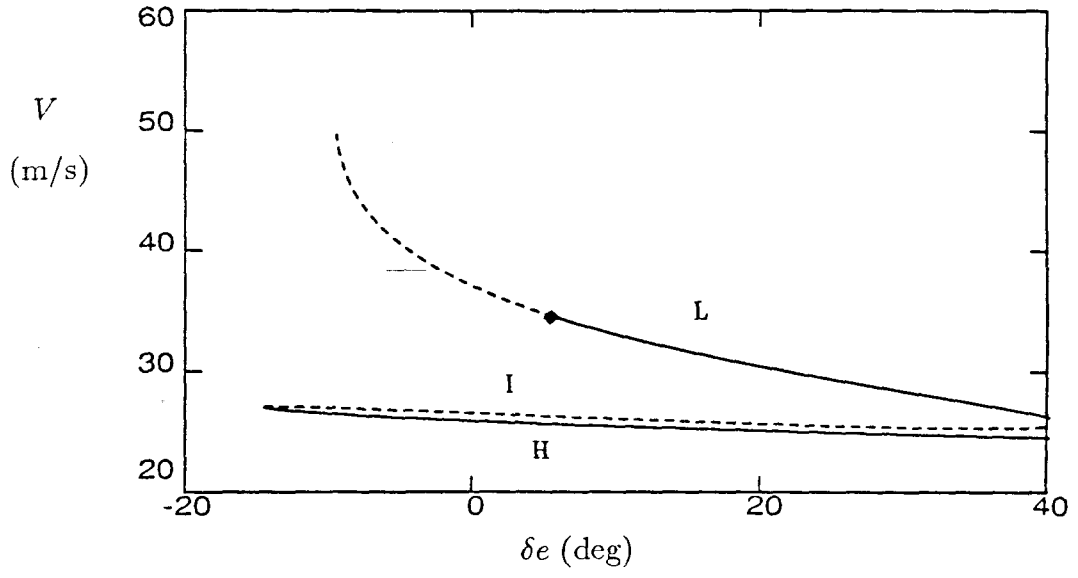

(b) Speed

Figure 4.7: Steady states for the general aviation aircraft at sea level for C_T=0.14; ◆ – Hopf bifurcation, —— stable, – – – unstable.

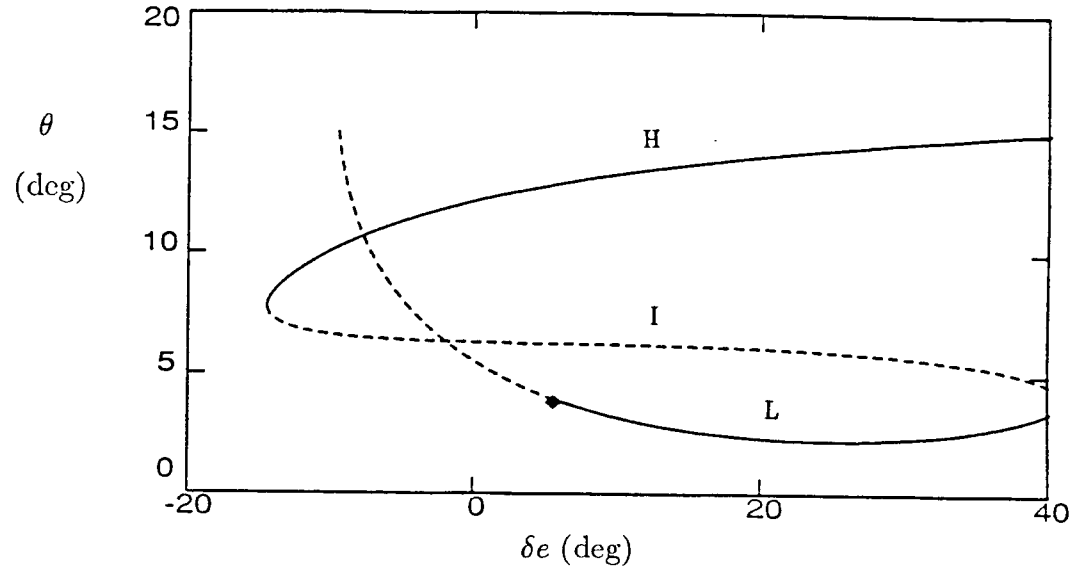

(c) Pitch Angle

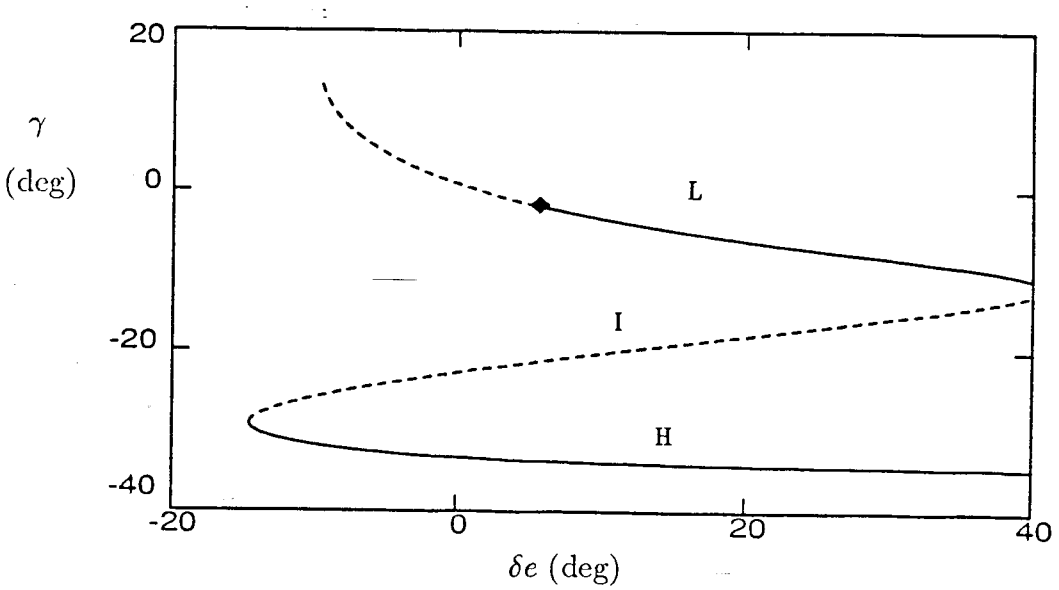

(d) Flight Path Angle

Figure 4.7: Concluded.

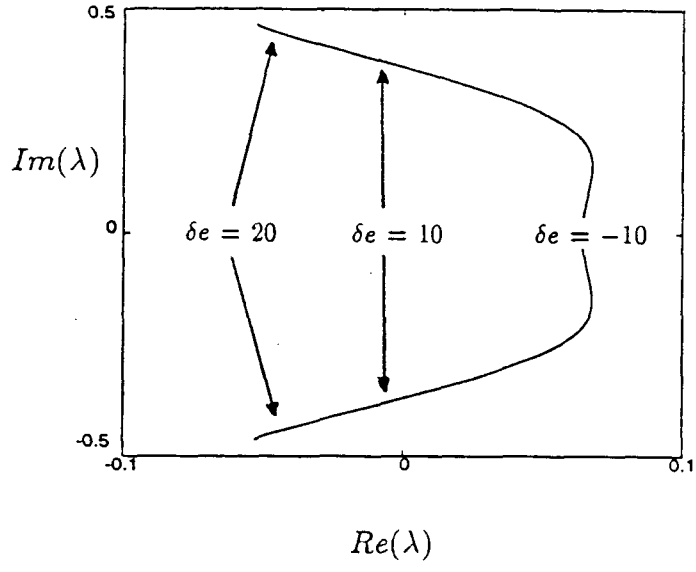

Figure 4.8: Eigenvalues of the phugoid mode of the low angle of attack steady states for $C_T = 0.14$.

as long the pilot does not apply a combination of thrust and elevator setting that is above the curve of Hopf bifurcations (neglecting any atmospheric disturbances). This curve of Hopf bifurcations could be used to put limits on the elevator deflection and thrust available to the pilot, so the pilot could never command a combination of thrust and elevator deflection which cause the phugoid mode to become unstable.

The bifurcation loci for this aircraft also contain continuous curves of saddle-node bifurcations. These curves give the combination of thrust and elevator deflection which causes a saddle-node bifurcation. The curve labelled 'H-I' represents the saddle-node bifurcation connecting the high and intermediate angle of attack steady states, and the curve labelled 'L-I' represents the saddle-node bifurcation

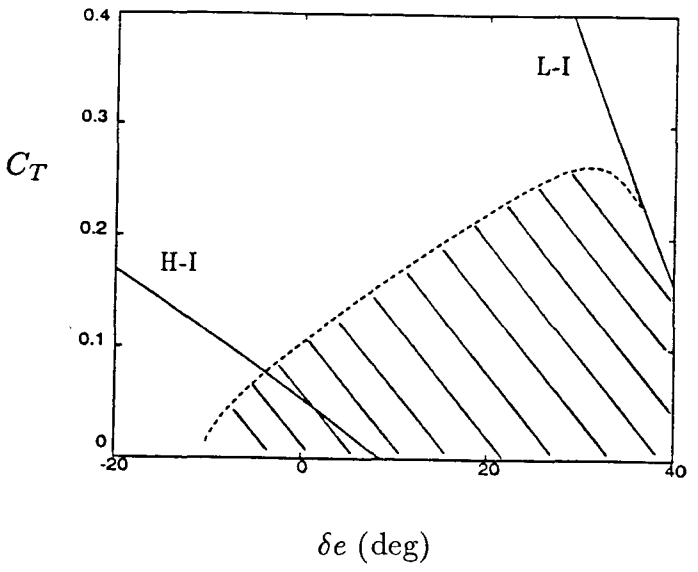

Figure 4.9: Bifurcation set of the general aviation aircraft at sea level; – – – Hopf bifurcation, —— saddle-node bifurcation.

connecting the low and intermediate angle of attack steady states. These curves can also be used to put limits on thrust and elevator deflection available to the pilot.

Knowledge of the curve of saddle-node bifucations labelled 'H-I' would be very valuable to a pilot. Recall Figure 4.4 in which recovery from a stall was obtained by decreasing the elevator deflection to a value less than that at which the saddle-node bifurcation connecting the steady states at high and intermediate angles of attack occurs. Curve H-I in Figure 4.9 shows the critical elevator and thrust settings of this saddle-node bifurcation for the entire range of thrust and elevator settings. This information could be used by the pilot to get out of the high angle of attack stall. It is especially important to have this information

for this aircraft, because the adverse effect of thrust on the stall behavior makes recovery in this aircraft much different than in most other aircraft. Note that for thrust coefficients greater than 0.15 it is impossible to get out of a stall.

Curve L-I in Figure 4.9 is also valuable to a pilot because any combination of thrust and elevator deflection above this curve will cause the aircraft to go into a stall. Even if the pilot could control the unstable phugoid mode by actively moving the elevator, any combination of elevator and thrust settings above curve L-I would result in a stall. This is because no low angle of attack steady state, stable or unstable, exists for this range of thrust and elevator settings. Thus, it would be advisable to put limits on the thrust and elevator deflections available to the pilot. Jumps in the state of the aircraft caused by saddle-node bifurcations will be central to the discussion of roll-coupling in Chapter V.

4.2 Effects of a Control System on the Steady States

Restricting the flight envelope, as discussed in the previous section, may keep the pilot out of the high angle of attack stall, but the necessary restrictions are so strict that they would make the aircraft inoperable. Take-off would be difficult, if not impossible, if the thrust was restricted to values which were low enough to keep the phugoid mode stable. Another approach to this problem would be to use a feedback control system to stabilize the phugiod mode. Phugoid instabilities result in growing oscillations in the pitch angle and airspeed, so either pitch angle or

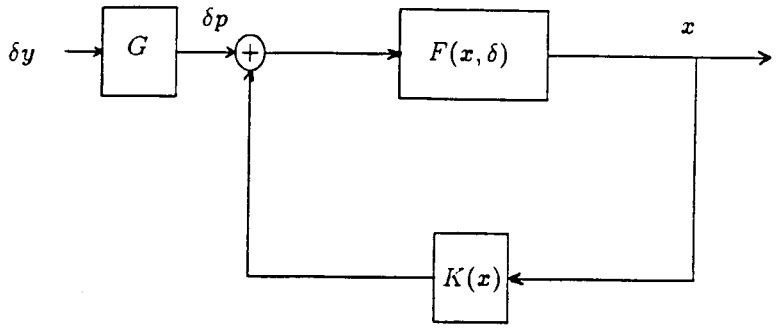

Figure 4.10: Feedback control system.

airspeed, or both, could be used as feedback variables in a feedback control system. The feedback control system used in this discussion is shown in Figure 4.10.

The feedback gain can be used as a continuation parameter to determine the effect of varying feedback gain on the steady states of the aircraft. Figure 4.11 shows the steady states as a function of the velocity feedback gain for a thrust coefficient of 0.14 and zero elevator deflection. This fixed point is unstable with no velocity feedback, as shown in Figure 4.7, but for a range of feedback gains this point becomes stable. Maximum damping of the phugoid mode occurs for a feedback gain of 0.0213, so we will use this value in our control system.

With velocity feedback to the elevator, the elevator deflection of the aircraft is given by

$$\delta e = \delta e_p + K_2 V,$$

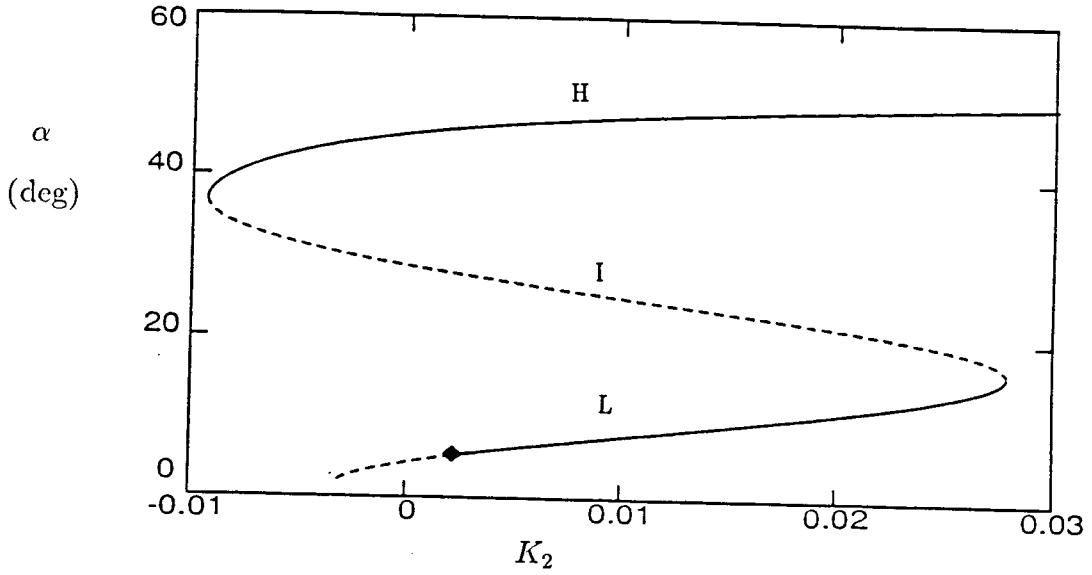

(a) Angle of Attack

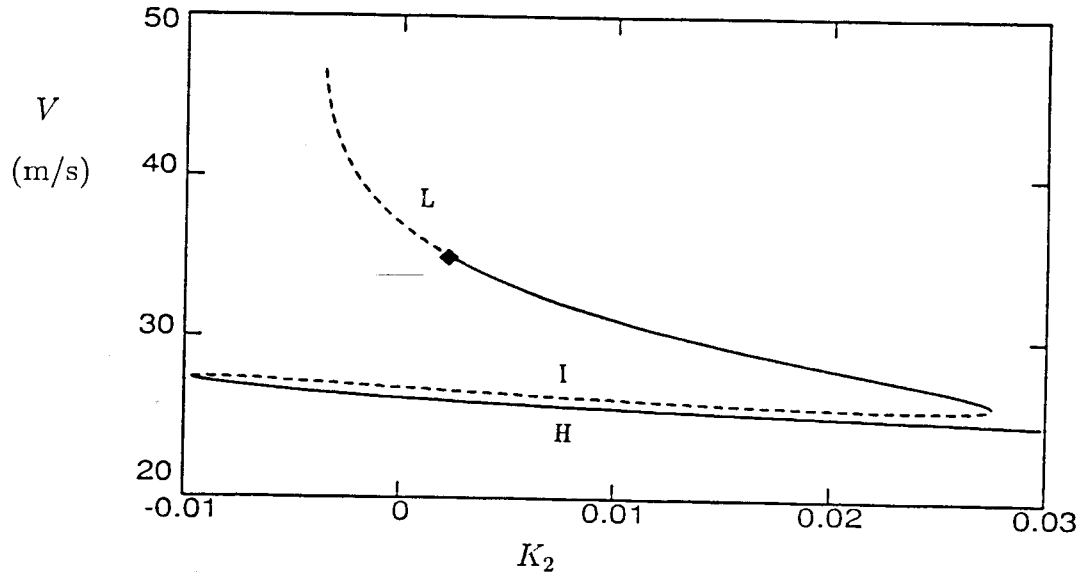

(b) Speed

Figure 4.11: Steady states of the general aviation aircraft as a function of velocity feedback gain for $C_T = 0.14$ and $\delta e = 0.0$, —— stable, – – – unstable, ◆ – Hopf bifurcation.

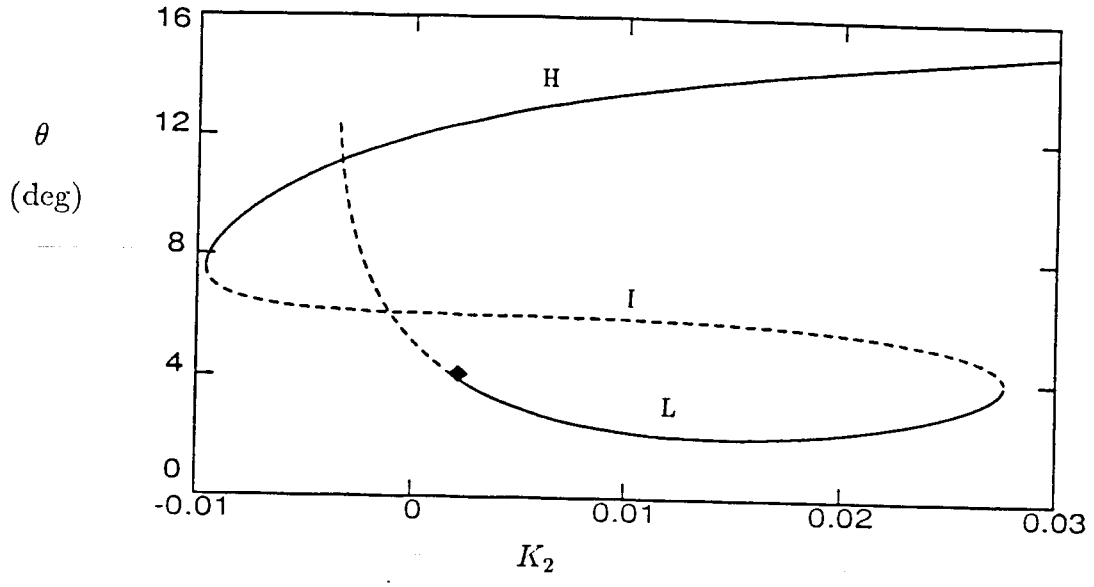

(c) Pitch angle

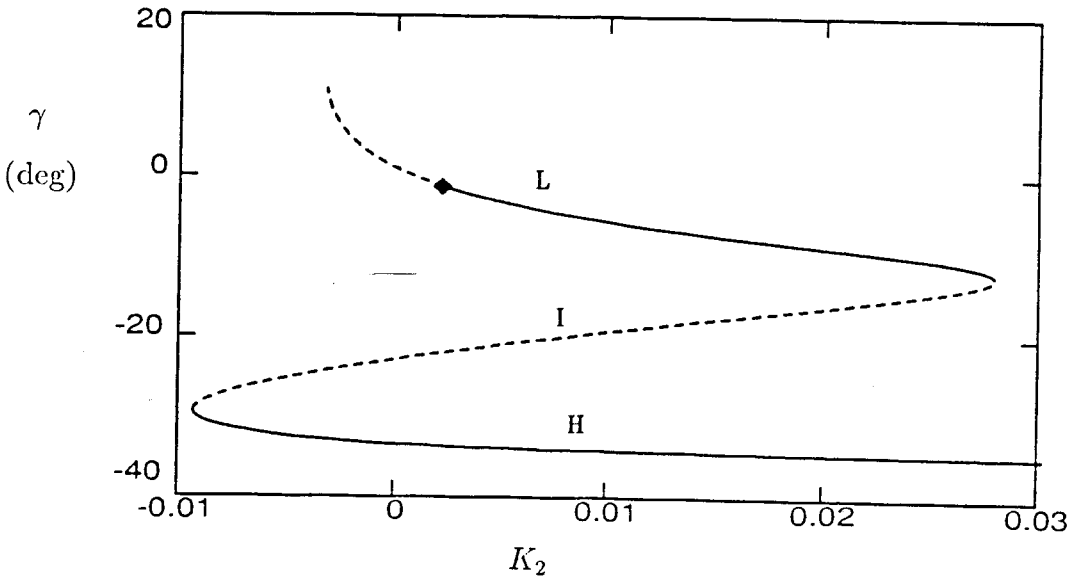

(d) Flight Path Angle

Figure 4.11: Concluded.

where δe_p is the pilot input to the elevator. Pilot input to the elevator must be scaled so maximum yoke travel is equivalent to maximum elevator travel. The scaling law can be determined by comparing the pilot input to the elevator with the actual elevator deflection at each fixed point. By calculating the fixed points as a function of elevator deflection and calculating the required pilot input at each steady state, it is possible to plot a curve relating pilot input to the elevator and elevator deflection. Figure 4.12 shows this relationship for a thrust coefficent of 0.14.

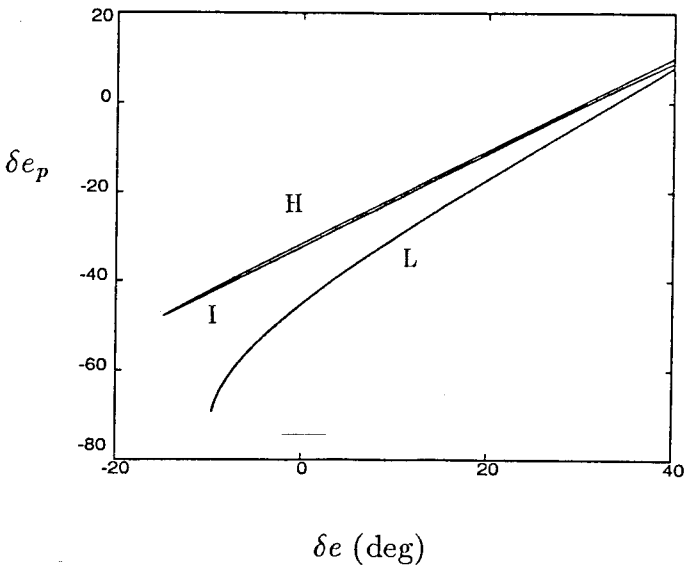

Figure 4.12: Relationship between pilot input to the elevator and actual elevator deflection for $C_T = 0.14$ and $K_2 = 0.0213$.

Figure 4.12 shows that the relationship between the pilot input to the elevator and the elevator deflection is almost linear. The relationship is different for the low and high angle of attack steady states, but we are only concerned with steady

states at low angles of attack. Fitting the low angle of attack curve with a line gives the transformation

$$\delta e_p \mapsto 1.4\delta e_y - 45$$

which will convert the yoke movement, δe_y, into the required pilot input to the elevator, δe_p. Movement of the yoke will now produce an equivalent movement of the elevator. This can be seen in Figure 4.13, which shows the steady states of the aircraft with velocity feedback to the elevator.

Figure 4.13 shows that velocity feedback to the elevator has stabilized the low angle of attack steady states, while leaving their structure unchanged. Scaling the yoke input to the elevator has also been successful. Figure 4.13(d) shows that the yoke input is the same as the elevator deflection except for a tail-off at low elevator deflections. This could easily be corrected by using a nonlinear scaling law for the yoke input. The effectiveness of the velocity feedback at stabilizing the phugoid mode can easily be seen in Figure 4.14. Without velocity feedback to the elevator, the phugoid oscillations become very large and the aircraft eventually goes into a stable high angle of attack stall. When velocity feedback is used, the phugoid mode is stable and the perturbations decay. Figure 4.14(f) shows that relatively little elevator deflection is required to counteract the perturbation.

4.3 Summary of the Results for the General Aviation Aircraft

Several important results have been determined during the analysis of the general aviation aircraft. The results are important because they show the ef-

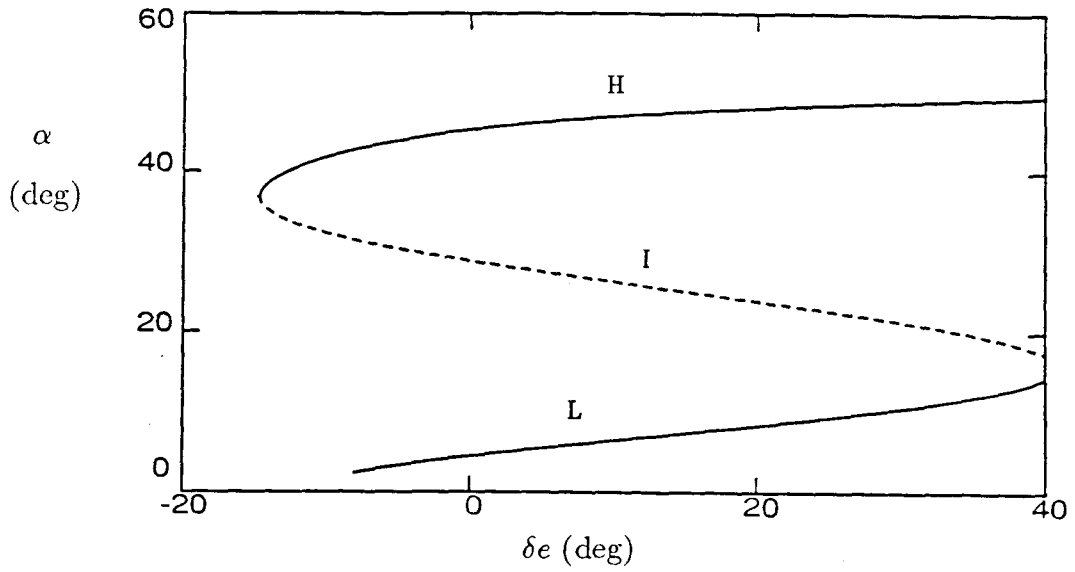

(a) Angle of Attack

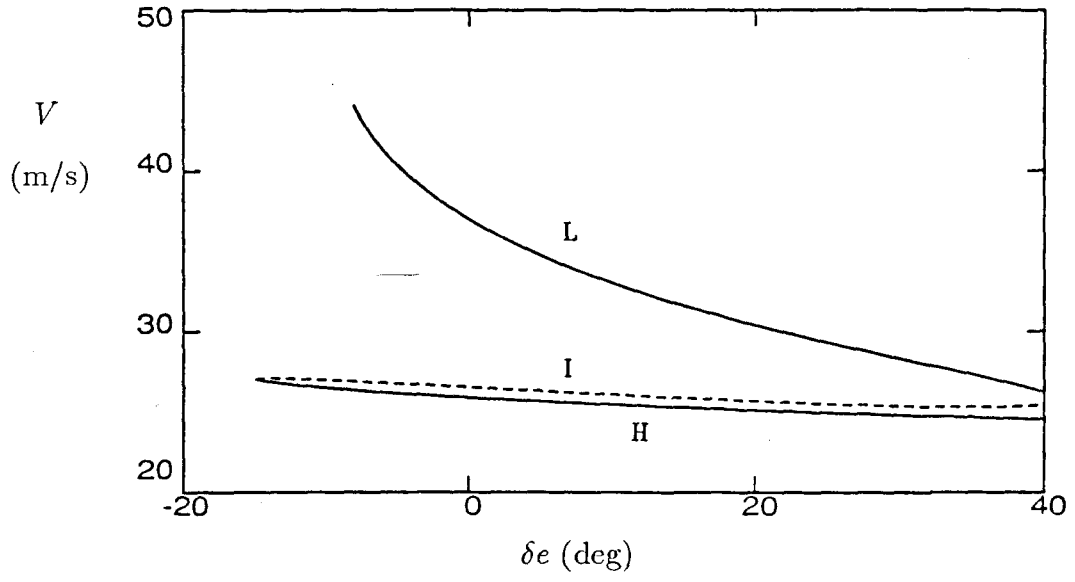

(b) Speed

Figure 4.13: Steady states of the general aviation aircraft with velocity feedback to the elevator, C_T=0.14, K_2=0.0213;
—— stable, – – – unstable.

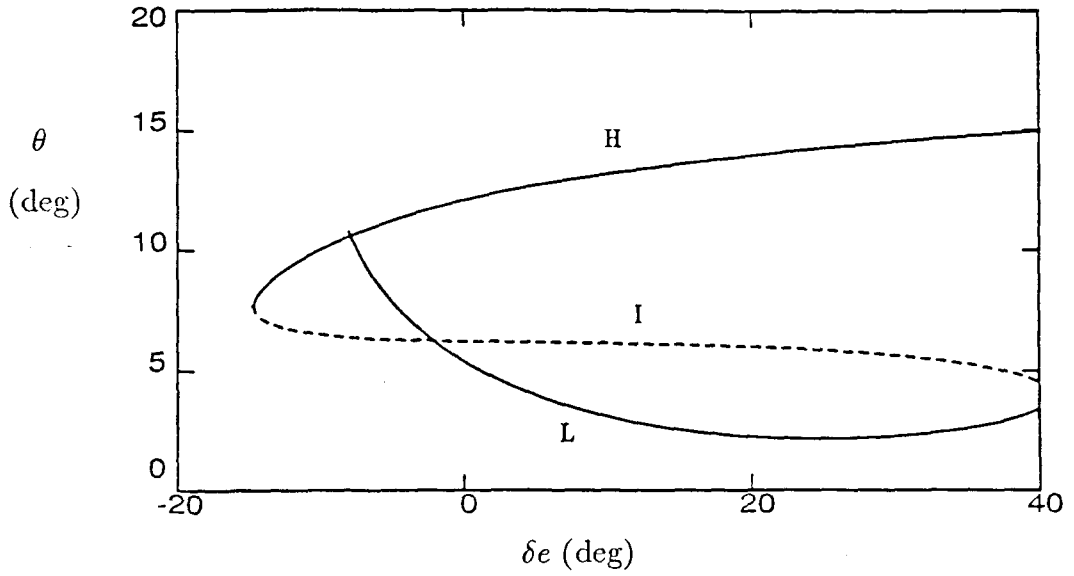

(c) Pitch Angle

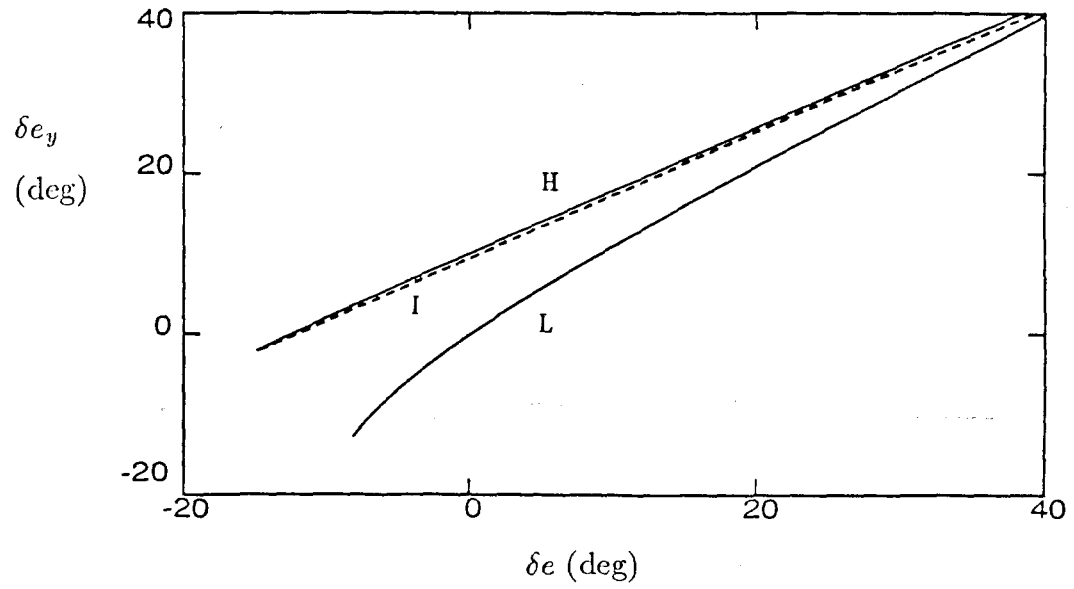

(d) Yoke Input to Elevator

Figure 4.13: Concluded.

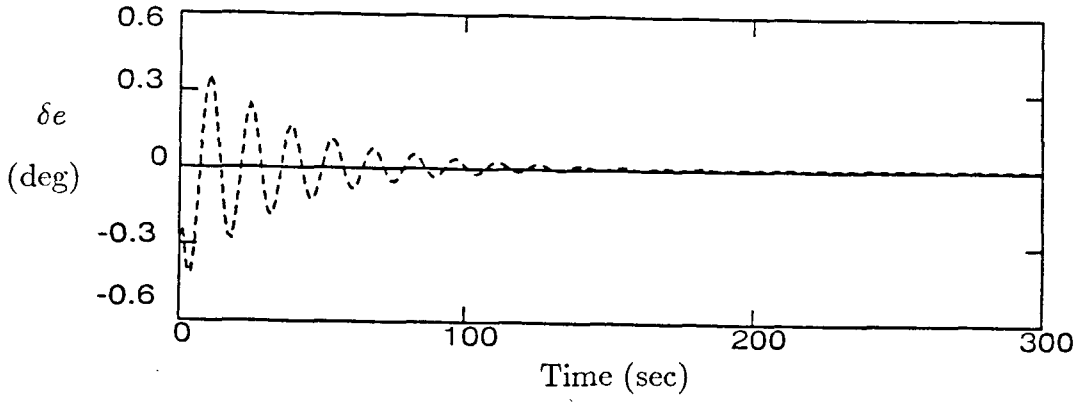

(a) Elevator Deflection

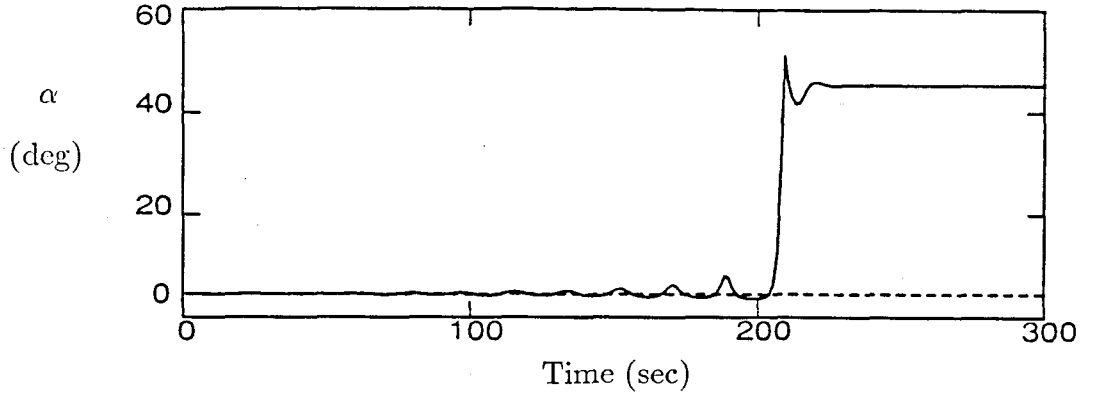

(b) Angle of Attack

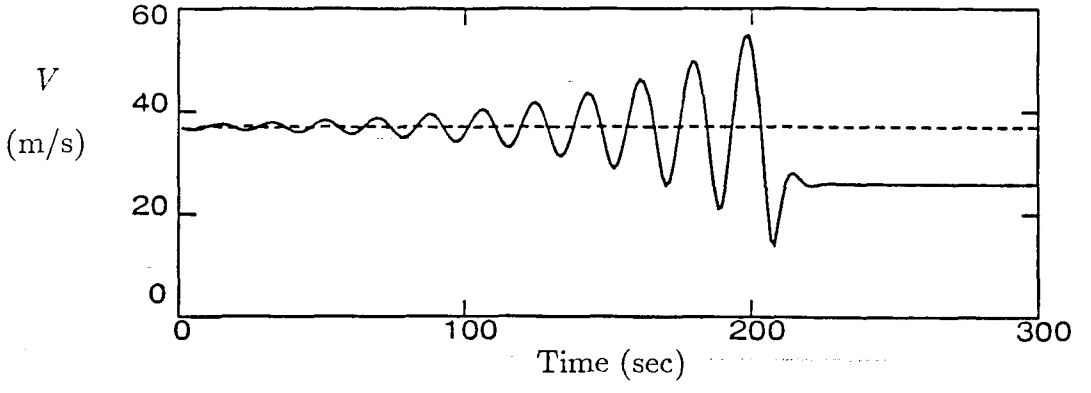

(c) Speed

Figure 4.14: Simulation of the response of the general aviation aircraft with and without velocity feedback to the elevator for C_T=0.14; – – – with feedback, —— without feedback.

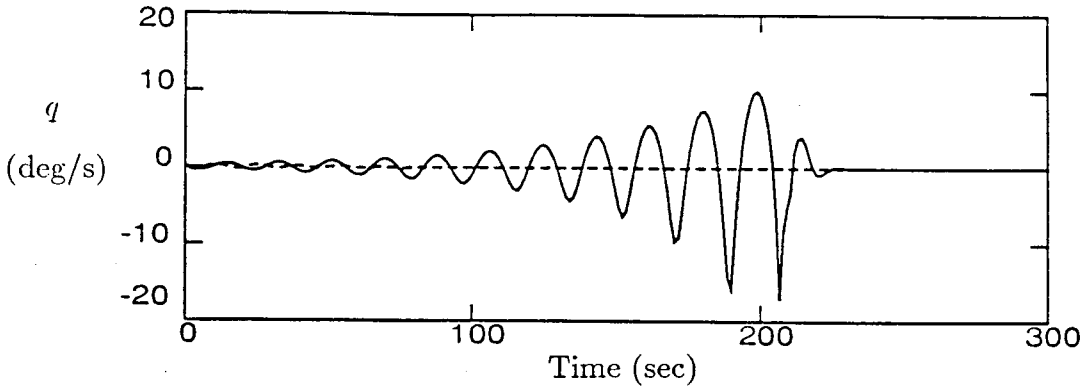

(d) Pitch Rate

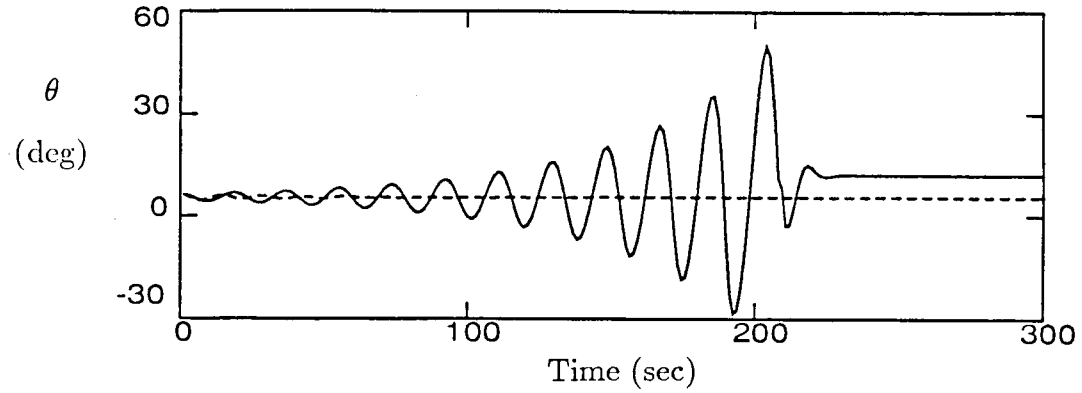

(e) Pitch Angle

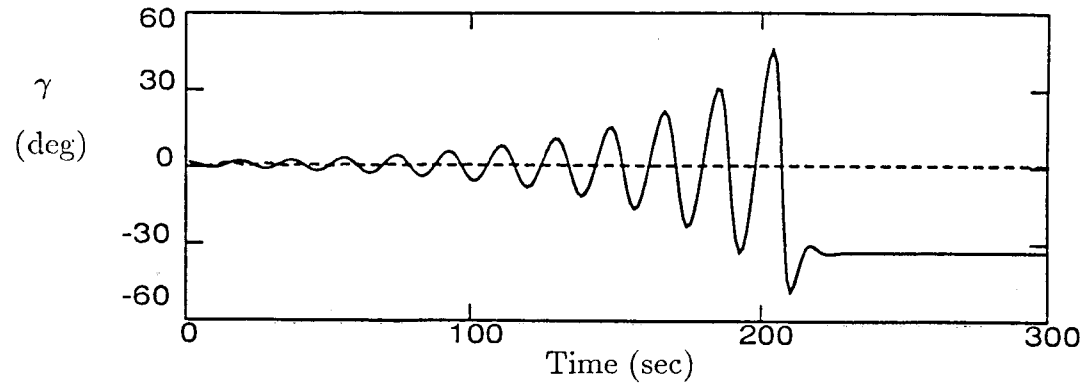

(f) Flight Path Angle

Figure 4.14: Concluded.

fectiveness of analyzing nonlinear aircraft dynamics by determining the steady states of the aircraft. Knowledge of the steady states allowed us to predict which combinations of control inputs lead to undesirable or dangerous behavior. This information could be used to put limits on the control inputs, inform pilots how to get out of undesirable flight regimes, or give designers ideas on what needs to be changed in the aircraft. It is important to note that the results are only as good as the aerodynamic model, but complex aerodynamic models can be analyzed shown in Chapters V and VI.

Several uses for this type of analysis in control system design have also been introduced. Continuation methods make it possible to determine the effects of a control system for a wide range of control surface deflections. The complete equations of motion including the control system can be analyzed to determine if nonlinear effects are important in any flight regimes. This could be especially useful for anaylzing control systems which are designed to operate at high angles of attack, where nonlinear aerodynamic effects become important. Also, the stability of each fixed point is determined by linearizing the complete equations of motion about that fixed point, as opposed to linearizing the equations of motion for a certain type of flight.

V. RESULTS FOR A GENERIC JET FIGHTER

This aerodynamic model is based on data obtained at an airspeed of 266 m/s, a density of 0.237 kg/m^3, and a Mach number of 0.80. These conditions are representative of high altitude cruising flight, but the aerodynamic model will be used to study the roll-coupling instability and high angle of attack dynamics. The results may not be quantitatively correct, but qualitative effects should be realistic. Results for the roll-coupling instability will be more reliable than the results for high angle of attack flight because roll-coupling instabilities generally occur at low angles of attack and sideslip, a flight regime modelled fairly well by these aerodynamic data. High angle of attack flight generally involves nonlinear aerodynamic effects related to large angles of sideslip which are not included in this model.

The dynamics of this aircraft will be analyzed by determining its steady states and bifurcations of these steady states. Atmospheric density will be assumed constant and equal to 0.237 kg/m^3. Steady states of the fifth, sixth, and eighth order equations of motion (see Section 3.1) will be determined to study the effects of assuming constant velocity and/or neglecting the influence of gravity on the steady states of the aircraft. Particular attention will be paid to the effects of these simplifications on the roll-coupling instability because it has been studied in the past by assuming constant speed and neglecting the influence of gravity (see Section 1.2).

This aerodynamic model was analyzed by Young, Schy, and Johnson [1980] by determining the steady states of the fifth order equations of motion with the assumption of small angles of sideslip. Jump phenomena related to roll-coupling instabilities were predicted and verified. The present work extends the results of Young, Schy, and Johnson by analyzing the roll-coupling instabilities of this aircraft with the complete equations of motion. Several new results have been obtained regarding the roll-coupling instabilities of this aircraft. By studying the steady state moment balance of the aircraft, a possible mechanism for the roll-coupling instability has been determined. Also, by computing the steady state Euler angles, it was possible to determine the orientation of the aircraft before and after a jump caused by the roll-coupling instability. Effects of rudder deflection on the roll-coupling instability have also been included in this analysis while the results of Young, Schy, and Johnson were all for zero rudder deflection.

5.1 Results for the Fifth Order Equations of Motion

The aircraft speed will always be 266 m/s in this section to match the speed at which the aerodynamic data was obtained. This speed is reasonable for low angle of attack flight, but not for high angle of attack flight. Recall that in the fifth order equations of motion the speed is kept constant by applying the required amount of thrust. No constraints are put on the amount of thrust available in this work so physically unrealistic steady states may be determined. The amount of thrust required at each steady state will be shown along with the steady states

to determine whether or not the fixed points are realistic. Thrust to weight ratios greater than one will be considered unrealistic in this thesis.

5.1.1 Existence of Multiple Branches of Steady States

Multiple branches of steady states were shown to exist for this aerodynamic model by Young, Schy, and Johnson [1980] who used an iterative search based on the fifth order equations of motion and the assumption of small angles of sideslip. This iterative scheme was used during this research to determine starting points for the continuation method. Steady states determined with the iteration scheme are not steady states of the equations of motion used in the continuation method, due to the assumption of small sideslip in the iterative scheme, but they were close enough for the continuation method to converge to steady states of the equations of motion which did not assume small angles of sideslip because the sideslip angles were small.

An iterative search for zero aileron, elevator, and rudder deflection determined eleven steady states. One steady state is a purely longitudinal motion (i.e., $p = r = \beta = 0$) while the other ten steady states represent spins. Spins are characterized by high rotation rates (in particular by high yaw rates) and high angles of attack, and the aircraft flys in a helical path about a vertical axis. This aerodynamic model is symmetric with respect to lateral motions, so all steady states arise in symmetric pairs in which the longitudinal variables are the same and the lateral variables can be either positive or negative. These steady states were used as

starting points for the continuation method. Iterative searches were not done for all parameter values so it is possible that some isolated branches of fixed points were missed. It would be difficult if not impossible to determine whether or not all possible solutions have been determined, but for this aircraft the most important steady states are those for low angles of attack, which are easy to find.

Figure 5.1 shows the steady states of this aircraft as a function of elevator deflection for zero rudder and aileron deflections. Multiple steady states exist for all elevator deflections, but most steady states are unstable. The stability of each steady state was determined by linearizing the equations of motion about the steady state and calculating the eigenvalues of the linearized equations of motion (see Section 2.1.4). All of the steady state spin modes (curves 2-6) are unstable and the purely longitudinal steady states (curve 1) are unstable for elevator deflections of greater than 15 degrees. It is not surprising that these steady states are unstable because for angles of attack greater than 20 degrees, this aircraft loses directional stability (i.e., $C_{n_\beta} < 0$; see Figure 3.2.2) and all of the unstable steady states are at angles of attack greater than 20 degrees (see Figure 5.1(d)). Loss of directional stability is certainly the cause of the loss of stability of the purely longitudinal steady states (curve 1), because when the equations of lateral motion are neglected, the longitudinal motions are stable for all elevator deflections.

Several additional factors contribute to the instability of the steady state spin modes (curves 2-6). Chambers, Bowman, and Anglin [1969] have shown that rotary balance data are important for modelling the spin behavior of an

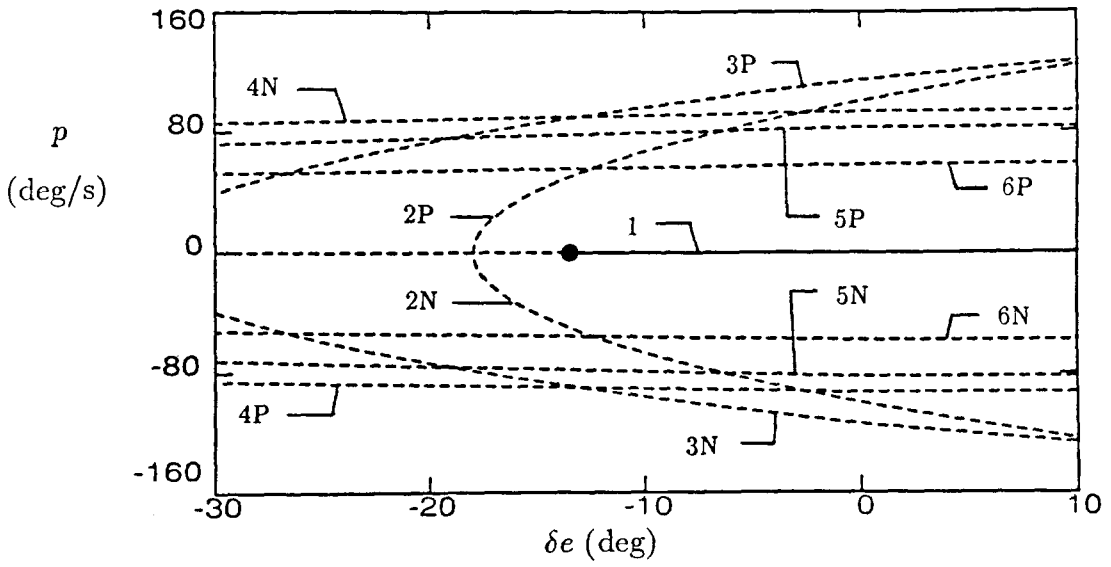

(a) Roll Rate

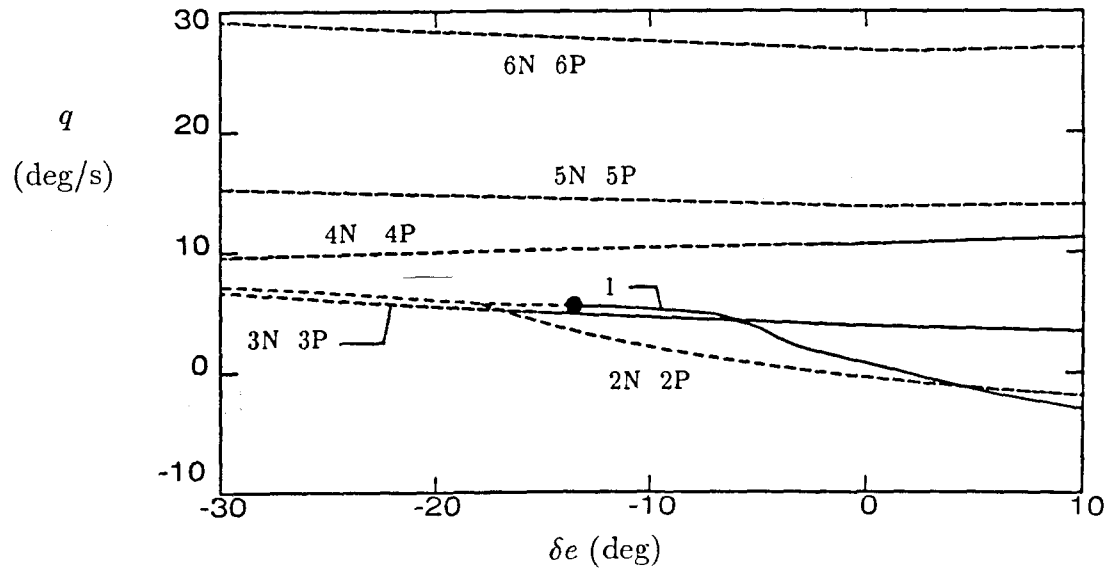

(b) Pitch Rate

Figure 5.1: Steady states for the generic jet fighter, V=266m/s, δa=0, δr=0; —— stable, - - - unstable, • - Hopf bifurcation.

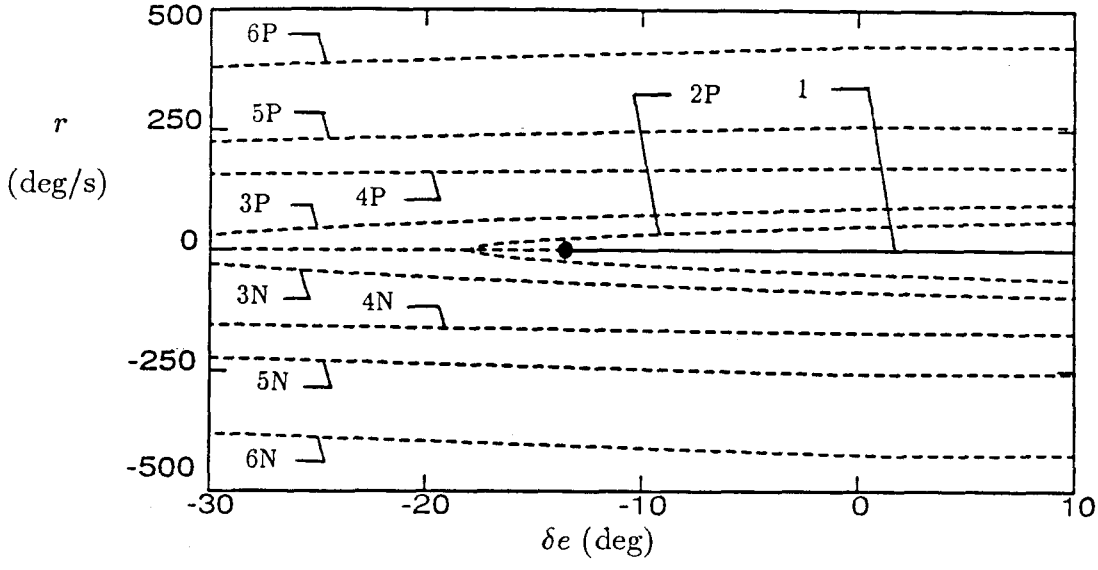

(c) Yaw Rate

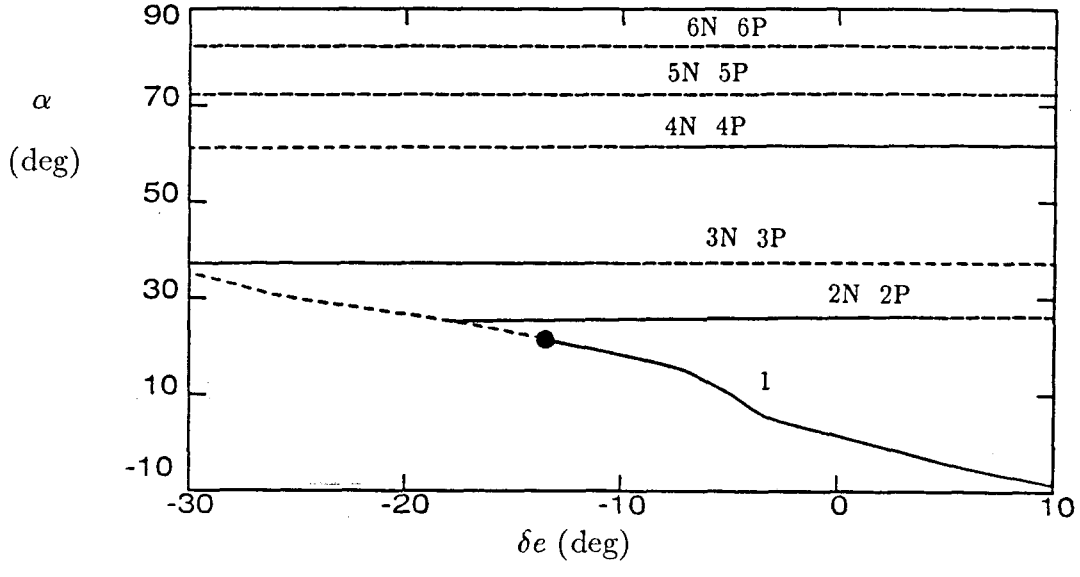

(d) Angle of Attack

Figure 5.1: Continued.

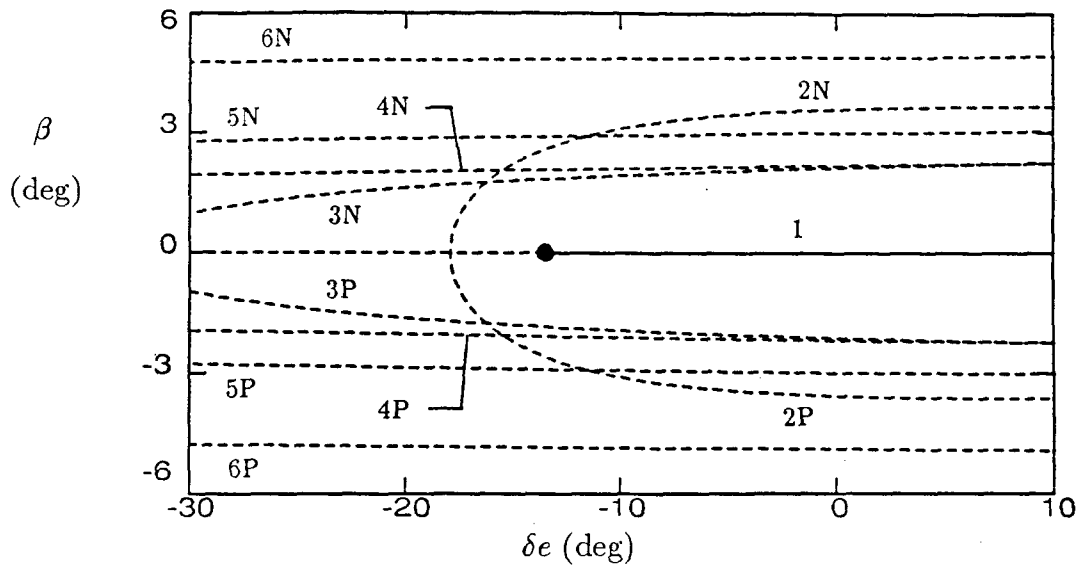

(e) Sideslip Angle

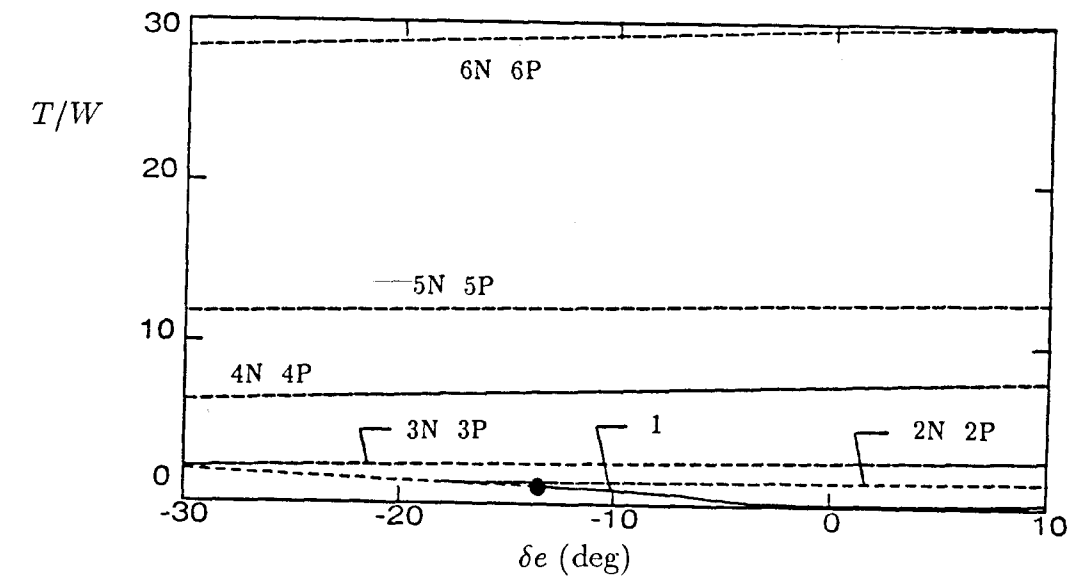

(f) Thrust to Weight Ratio

Figure 5.1: Concluded.

aircraft because the damping in yaw is a nonlinear function of the yaw rate. This aerodynamic model does not include rotary balance data so the damping in yaw is a linear function of the yaw rate, which is not valid at the high yaw rates of a spin (see Figure 5.1(c)). Requiring a velocity of 266m/s in a spin is also unrealistic. Figure 5.1(f) shows that the flat spin mode (curve 6) requires a thrust to weight ratio of almost thirty, which is impossible for a conventional aircraft.

All of the spin modes require unrealistic amounts of thrust to keep the velocity at 266m/s, so they are not physically meaningful. For this reason and because of the lack of rotary balance data, the steady state spin modes of this aircraft will not be discussed in detail. Changes in the steady state spin modes when the velocity is allowed to vary will be briefly discussed in Section 5.2. The effect of gravity on the steady state spin modes will be discussed in Section 5.3. The rest of Section 5.1 will concentrate on the steady states represented by curve 1 in Figure 5.1, the normal operating conditions of the aircraft. Two types of instabilities will be discussed: roll-coupling instabilities and high angle of attack instabilities.

5.1.2 Roll-Coupling Instabilities From Steady States with No Rudder Deflection

High rates of roll and nonzero rates of pitch or yaw cause the inertia terms in the pitching and yawing moment equations, ($\frac{I_z - I_x}{I_y} pr$, $\frac{I_x - I_y}{I_z} pq$), to become large and can lead to roll-coupling instabilities, which involve a jump in the state of the aircraft. The jump is often from one steady state to another (see Section

1.2), so the roll-coupling behavior of this aircraft will be analyzed by determining its steady states as a function of aileron deflection. Rolls will be initiated from the longitudinal steady states represented by curve 1 in Figure 5.1. Note that the steady state pitch rate is zero for purely longitudinal motions when gravity is included because of the condition for a steady pitch angle

$$\dot{\theta} = q\cos\phi - r\sin\phi = 0.$$

When gravity is not included in the equations of motion (which will be the case in this section), the equation for the pitch angle is decoupled from the force and moment equations and the steady state pitch rate is not necessarily zero for purely longitudinal steady states. Elevator deflection will produce different effects for systems which include gravity and those that neglect gravity. Elevator deflection imparts angle of attack to the aircraft in both systems, but when gravity is neglected elevator deflection imparts a pitch rate to the aircraft, whereas when gravity is included elevator deflection imparts pitch angle to aircraft. Differences caused by the assumption of zero gravity will be discussed in Section 5.3.

Figure 5.2 shows the steady states for rolls from the trim condition (i.e., $\delta e = 1.65$, $q = 0$). This aerodynamic model is symmetric in the aileron deflection so only positive roll rate solutions are shown. Lateral variables,(p, r, β), are anti-symmetric and longitudinal variables,(q, α), are symmetric in the aileron deflection along curves of steady states. Roll response of this aircraft from the trim condition is good (see Figure 5.2(a)). The steady state roll rate is almost a linear function of

aileron deflection except for a small inflection for an aileron deflection of negative 20 degrees. All the steady states are stable and high rates of roll are possible.

The steady state pitch and yaw rates are small for all aileron deflections, but they also exhibit a nonlinearity for aileron deflections near negative 20 degrees (see Figure 5.2(b)-(c)). This is probably evidence of roll-coupling, but the pitch and yaw rates are too small to produce large enough inertial moments (proportional to pq and pr) to cause an instability. Figure 5.2(d) shows that the angle of attack is negative for the trim condition and most of the steady state rolls. If gravity were included, a negative trim angle of attack would mean that the airplane was inverted, because a negative angle of attack results in a negative lift force and the lift force balances the weight in low angle of attack flight. This will be discussed in more detail in Section 5.3. Figure 5.2(e) shows that the sideslip angle is small for all steady states so the aerodynamic model should be valid. The thrust is also within reasonable limits.

Since the inertial coupling term in the yawing moment equation is proportional to the pitch rate, stronger inertial coupling might occur for rolls which are initiated from a pitch up or pitch down condition. Figure 5.3 shows the steady states for rolls from a pitch up condition (i.e., $\delta e = -1.0$, $q > 0$). For aileron deflections below 10 degrees, these steady states are similiar to the steady states for rolls from the trim condition (see Figure 5.2). The steady state roll rate increases linearly with aileron deflection while the other variables remain relatively constant. For aileron deflections greater than 10 degrees, the roll rate starts to

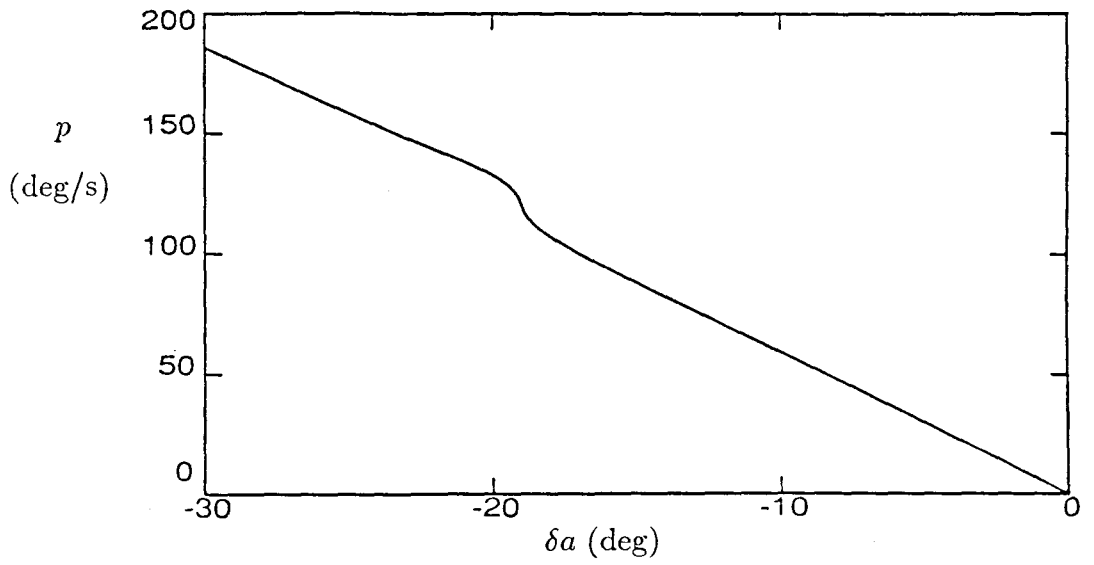

(a) Roll Rate

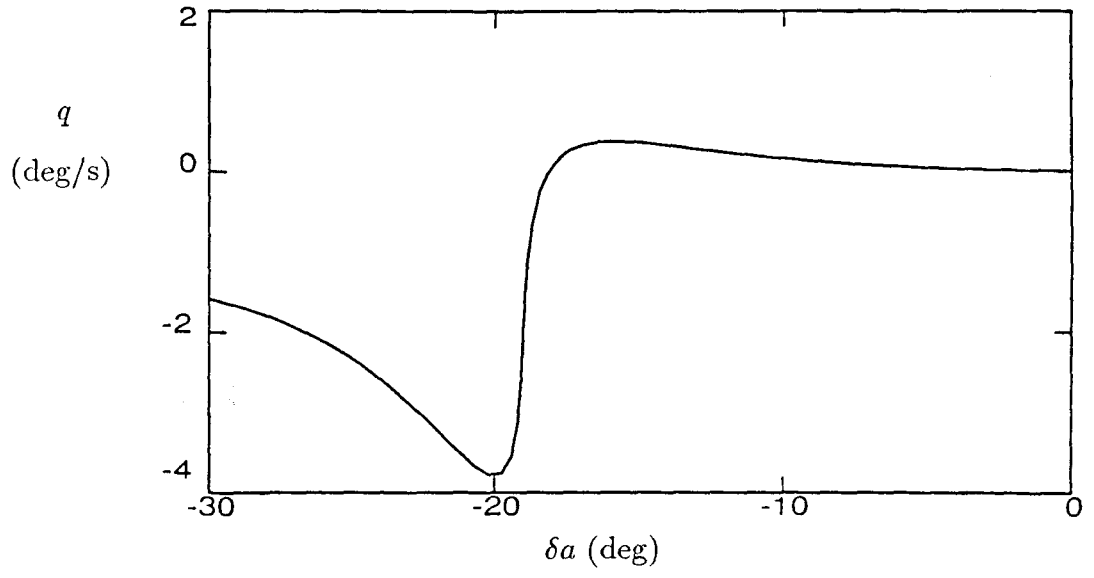

(b) Pitch Rate

Figure 5.2: Steady states for the generic jet fighter, V=266m/s, δr=0, δe=1.65; —— stable.

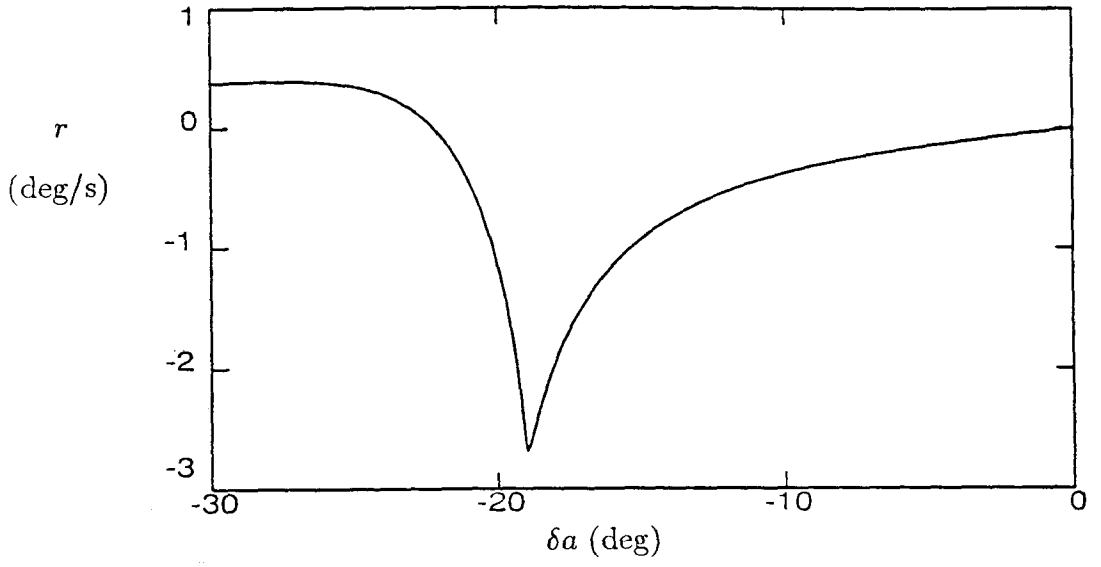

(c) Yaw Rate

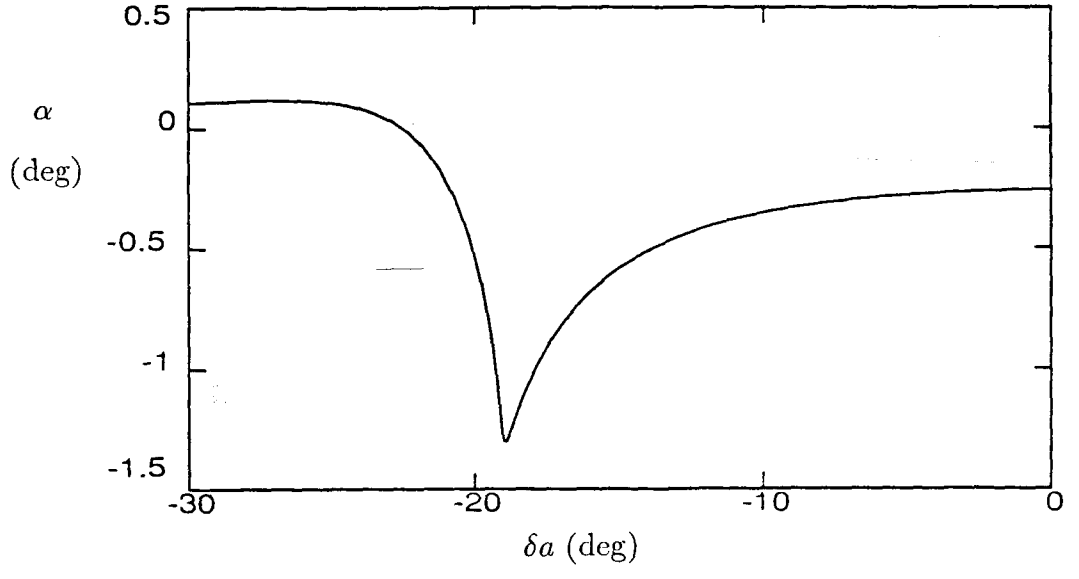

(d) Angle of Attack

Figure 5.2: Continued.

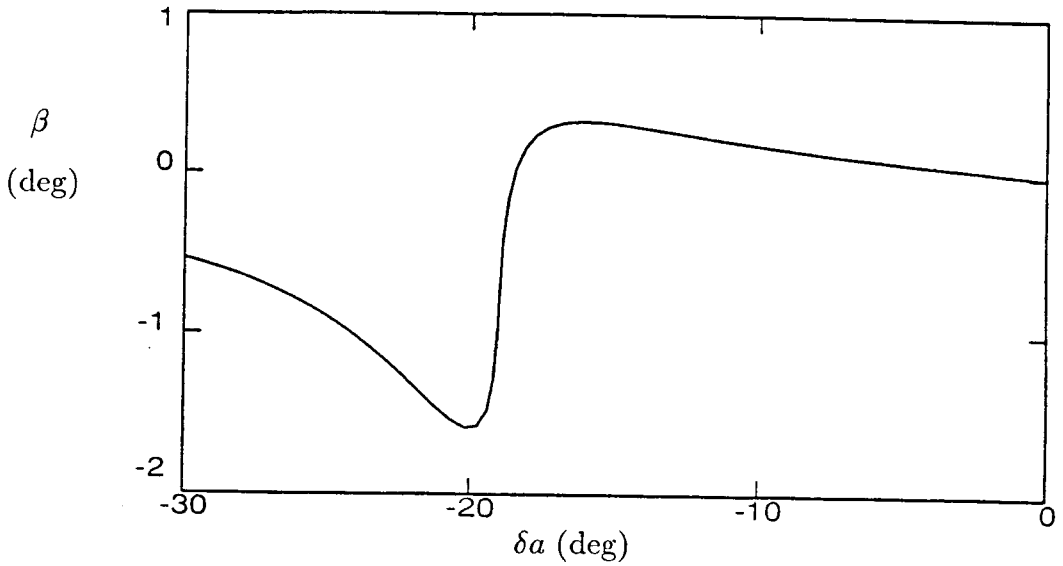

(e) Sideslip Angle

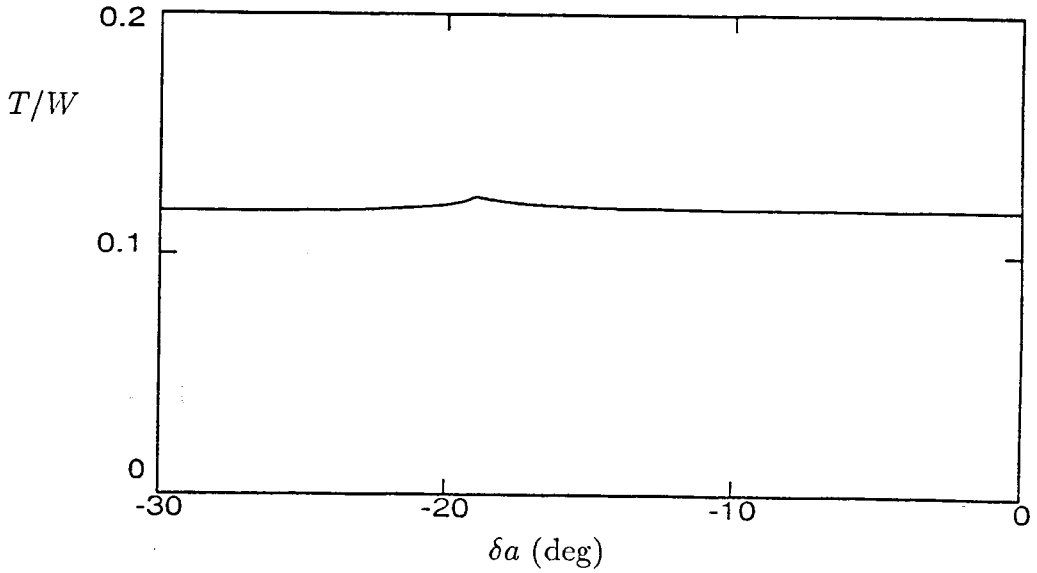

(f) Thrust to Weight Ratio

Figure 5.2: Concluded.

saturate and the pitch rate, yaw rate and sideslip angle increase rapidly. The sharp dip in the curves of steady states in Figure 5.2 at an aileron deflection of negative 20 degrees is also absent.

These changes in the steady states are caused by inertial coupling. This can be seen by studying the moment balance of the aircraft shown in Figure 5.4. Since the pitch rate is initially nonzero, the inertial yawing moment, $(\frac{I_x - I_y}{I_z} pq)$, increases rapidly as the roll rate is increased. This moment is balanced by the directional stability, (βn_β), which requires the sideslip to increase as the roll rate rate is increased as shown in Figure 5.3(e). Note that the steady state angles of attack are small and relatively constant (see Figure 5.3.(d)), so all the aerodynamic coefficients except the pitching moment coefficient, $(C_m(\alpha))$, are essentially constant. Thus for a term like directional stability $(\beta n_\beta(\alpha))$ to increase, the sideslip angle must increase.

Increasing sideslip angle causes the saturation in the steady state roll rate for large elevator deflections. Figure 5.4(a) shows that the rolling moment due to aileron deflection, $(\delta a \ell_{\delta a})$, continues to increase linearly for all aileron deflections. For small aileron deflections this moment is balanced by damping in roll, $(p\ell_p)$, but for large aileron deflections the dihedral effect, $(\beta \ell_\beta)$, increases because of the increasing sideslip angle and counters the moment due to the aileron deflection. The net result is the slower increase in the steady state roll rate as the aileron deflection is increased.

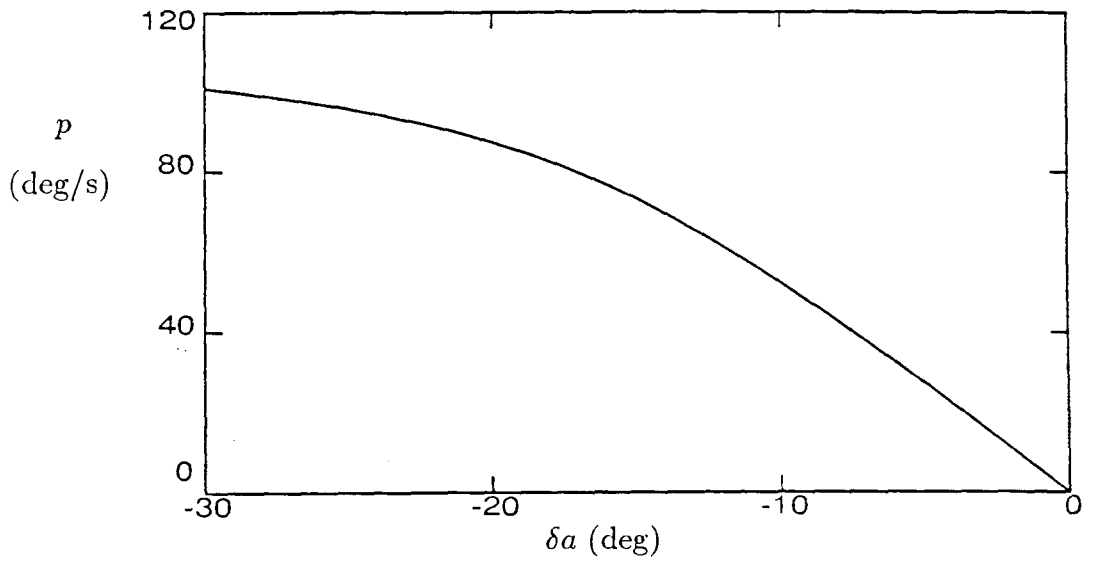

(a) Roll Rate

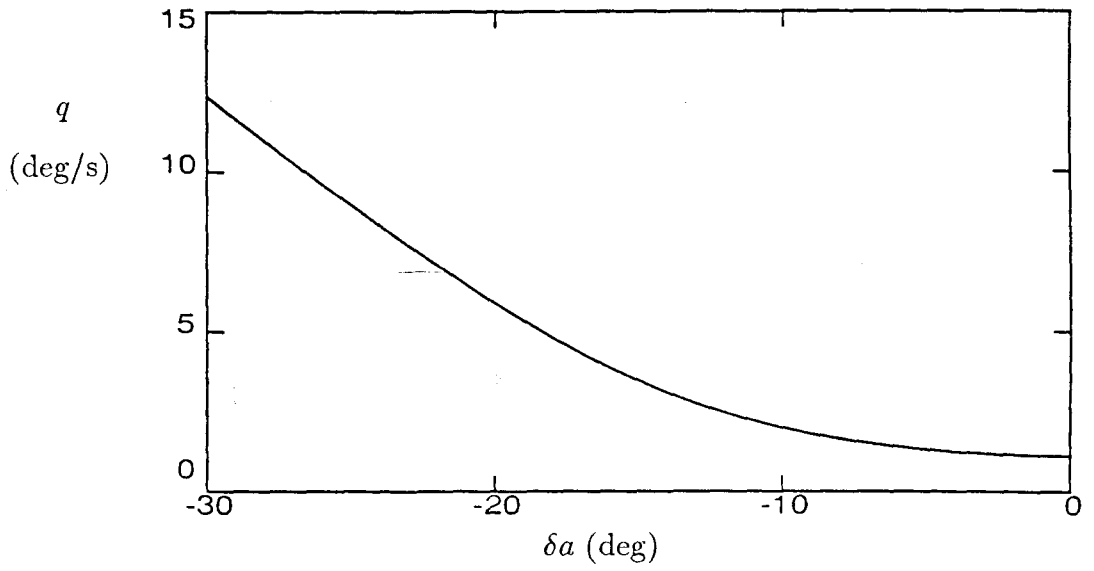

(b) Pitch Rate

Figure 5.3: Steady states for the generic jet fighter, V=266m/s, δr=0, δe=-1.0; —— stable.

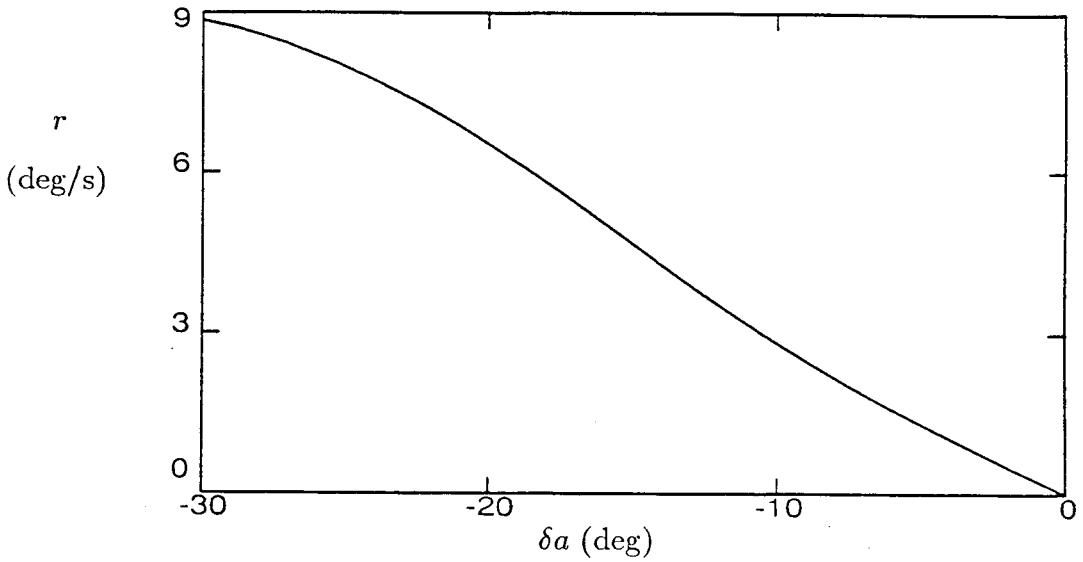

(c) Yaw Rate

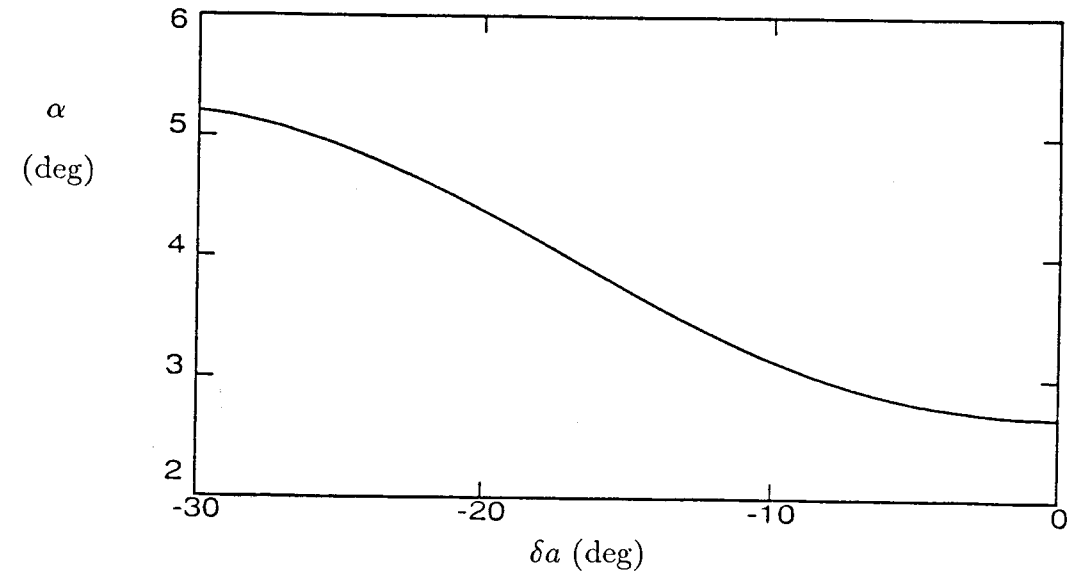

(d) Angle of Attack

Figure 5.3: Continued.

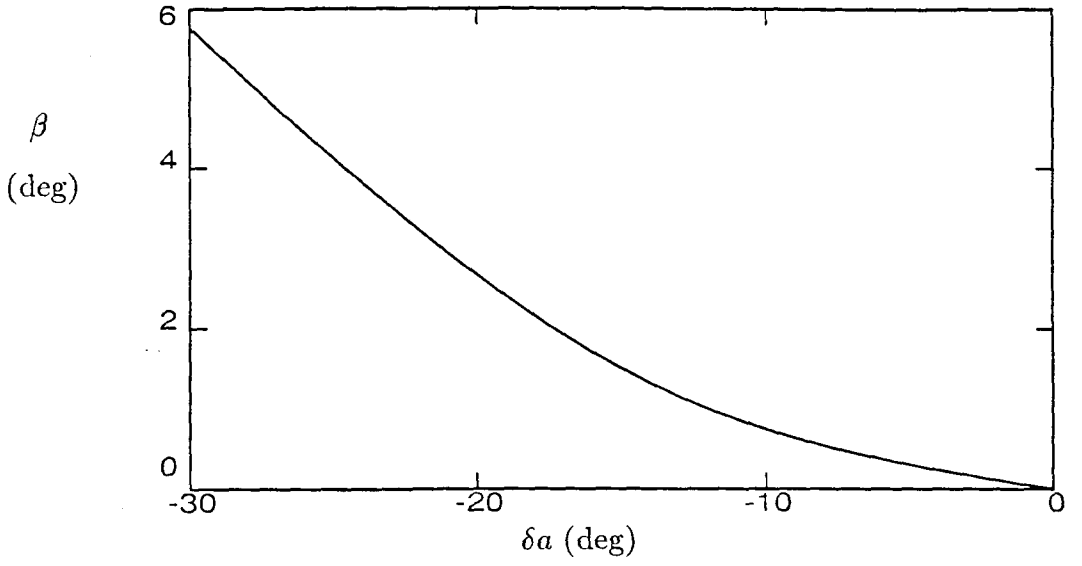

(e) Sideslip Angle

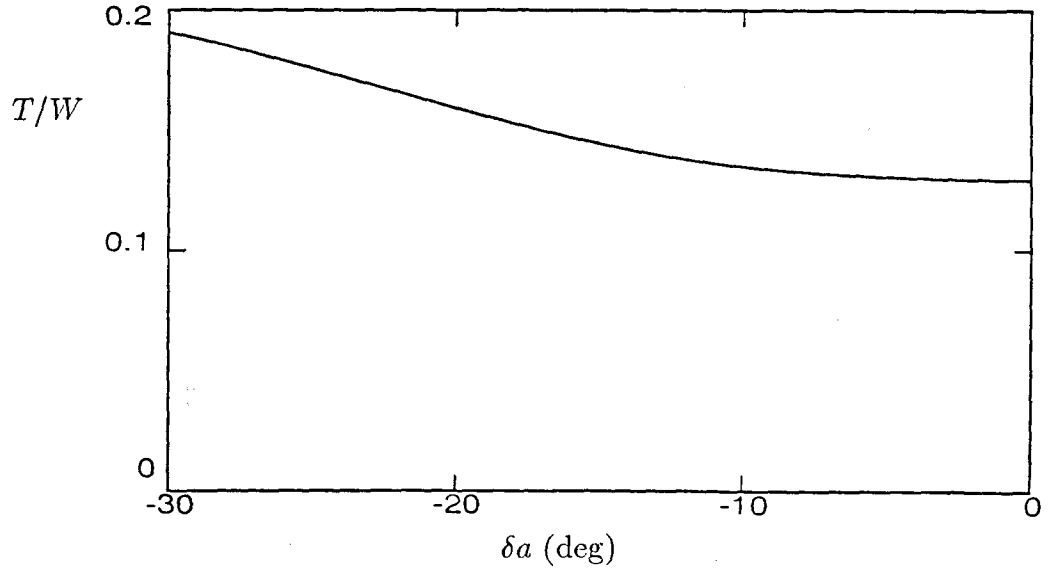

(f) Thrust to Weight Ratio

Figure 5.3: Concluded.

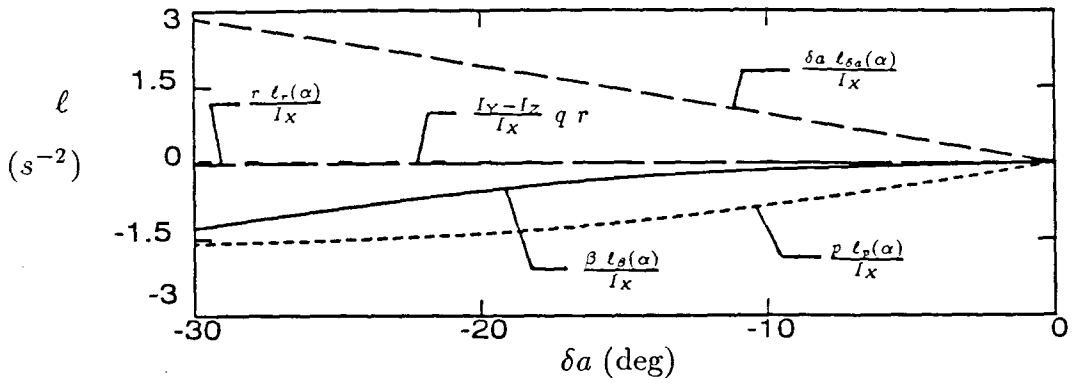

(a) Rolling Moment Balance

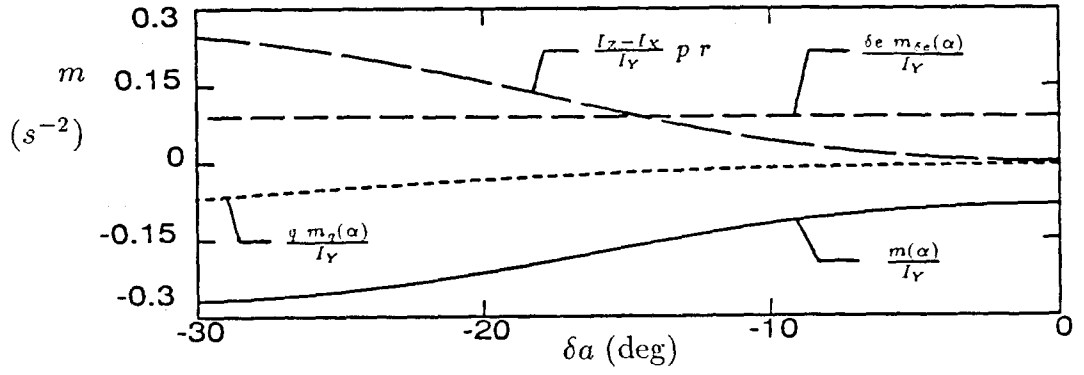

(b) Pitching Moment Balance

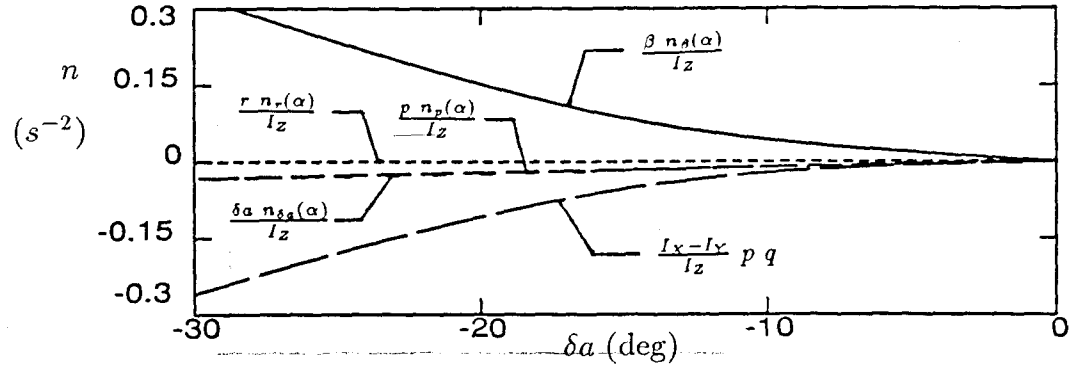

(c) Yawing Moment Balance

Figure 5.4: Moment balance for steady state rolls from a pitch up condition, δe=-1, δr=0, V=266m/s.

Effects of inertial coupling are also evident in the pitching moment balance shown in Figure 5.4(b). For small aileron deflections the moment balance is between the pitching moment coefficient, $(C_m(\alpha))$, and the moment caused by the elevator deflection, $(\delta e m_{\delta e})$, with the damping in pitch, (qm_q), having a small effect. As the airplane rolls it will typically yaw because rolling the airplane tilts the lift force,which will give the aircraft a centrifugal acceleration causing the aircraft to fly in a spiral path. (Recall that we are dealing with the steady states of the aircraft. Transient motions can be qualitatively different. For example, the adverse yaw effect causes the aircraft to yaw in a direction opposite to the direction of the roll.) If the aircraft has positive lift, the steady state roll and yaw rates will be of the same sign, which is the case in Figure 5.3. Thus as the roll rate increases the yaw rate will increase causing the inertial pitching moment, $(\frac{I_z - I_x}{I_y} pr)$, to grow. This is balanced by increasing the angle of attack which increases the pitching moment coefficient, $(C_m(\alpha))$. The damping in pitch also increases because of the growing pitch rate, but not enough to counter the inertial moment.

To summarize the above discussion, rolling the aircraft from a pitch up condition causes an inertial yawing moment which results in an increasing sideslip angle. Increasing the sideslip angle causes an increase in the dihedral effect which leads to the saturation of the steady state roll rate for large aileron deflections. The inertial pitching moment gives the aircraft a nose up moment which is balanced by increasing the angle of attack which increases the pitching moment coefficient.

It seems that the basic problem is the buildup of sideslip as the roll rate is increased. It may be possible to solve this problem by using the rudder to control the sideslip. Sideslip feedback to the rudder was used in an attempt to reduce the steady state sideslip angle, but it did not prove successful. The reason is that applying a positive yawing moment with the rudder to counteract the inertial yawing moment, intended to reduce the sideslip angle, actually produced an increased yaw rate while the sideslip angle was unchanged. Ideally one would like to be able to reduce both the sideslip angle and the yaw rate, but because both are of the same sign in this case, using the rudder to decrease one (say the sideslip angle) will increase the other (yaw rate). While rolling from a pitchup condition resulted in some undesirable inertial coupling effects, the steady states remained stable and the behavior of the aircraft was acceptable.

Since rolling from a pitch up condition reduced the steady state roll rate (relative to rolling from a trim condition), one would expect that rolling from a pitch down condition would increase the steady state roll rate. The pitch rate will be negative so the inertial yawing moment will be positive resulting in negative sideslip angles and a negative dihedral effect. Figure 5.5 shows that the steady states for rolls from a pitch down condition are similiar to the steady states for rolls from a trim condition for small and large aileron deflections but different for aileron deflections between negative 10 and negative 25 degrees. Two saddle-node bifurcations occur resulting in the existence of three steady states for aileron

deflections between negative 7 and negative 13 degrees, two of which are stable. A Hopf bifurcation, which could lead to periodic motions, also occurs.

Reasons for this behavior can be determined by examining the moment balance of the aircraft which is shown in Figure 5.6. Similiar to the balance for rolls from a pitch up condition, the inertial yawing moment is balanced by the directional stability which leads to a build-up of sideslip. For aileron deflections between negative 7 and negative 13 degrees, the steady state pitch rate is large resulting in a large inertial yawing moment. Large angles of sideslip are required to balance this moment (see Figure 5.5(e)). These large negative sideslip angles result in a significant rolling moment, due to the dihedral effect, which increases the steady state roll rate. This is clearly shown in Figure 5.6(a).

The pitching moment balance (Figure 5.6(b)) shows the difference between the two stable steady states that exist for aileron deflections between negative 7 and negative 13 degrees. For zero aileron deflection the pitching moment balance is between the pitching moment coefficient, $(C_m(\alpha))$, and the moment caused by the elevator deflection, $(\delta e m_{\delta e})$. Since the elevator deflection results in a negative pitching moment, the angle of attack must be negative to obtain a positive pitching moment coefficient. As the roll rate is increased (by increasing the aileron deflection), a negative yaw rate develops causing a negative inertial pitching moment which is balanced by a larger negative angle of attack.

For large aileron deflections the pitching moment balance is between the elevator deflection and the inertial moment as both the yaw rate and angle of

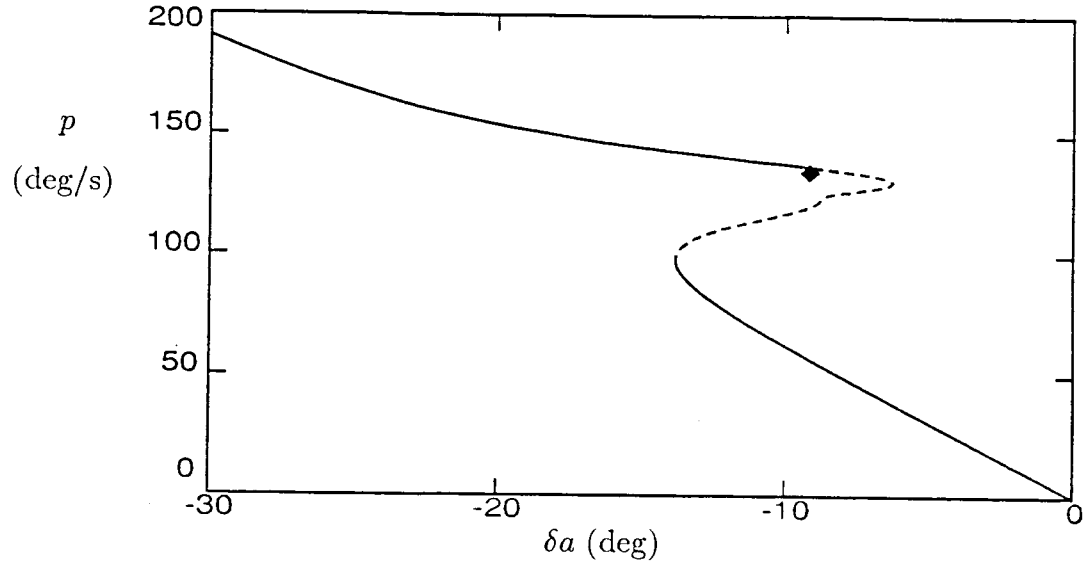

(a) Roll Rate

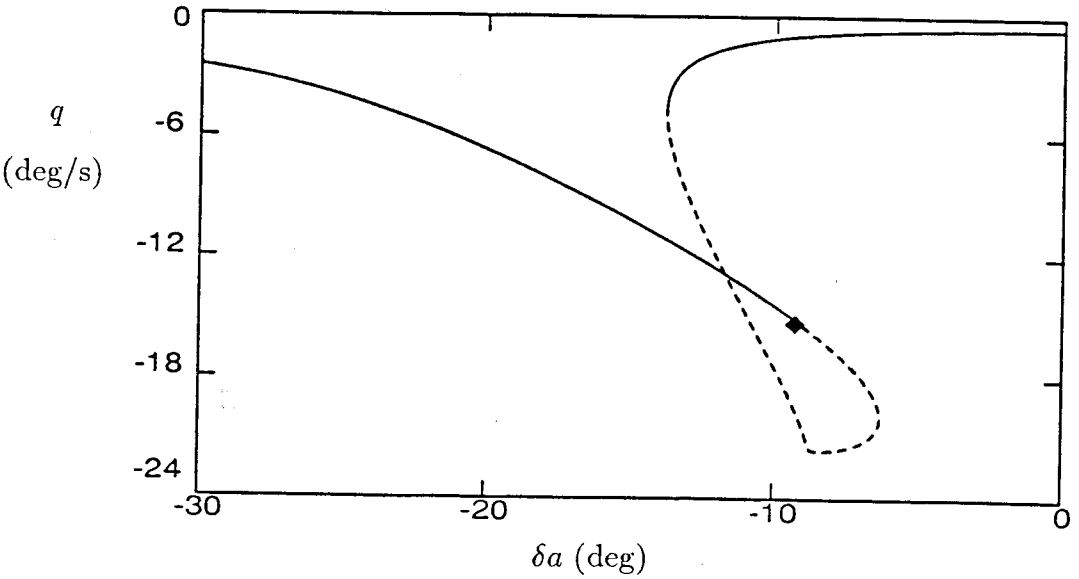

(b) Pitch Rate

Figure 5.5: Steady states for the generic jet fighter, V=266m/s, δr=0, δe=3.0; —— stable, - - - unstable, ◆ - Hopf bifurcation.

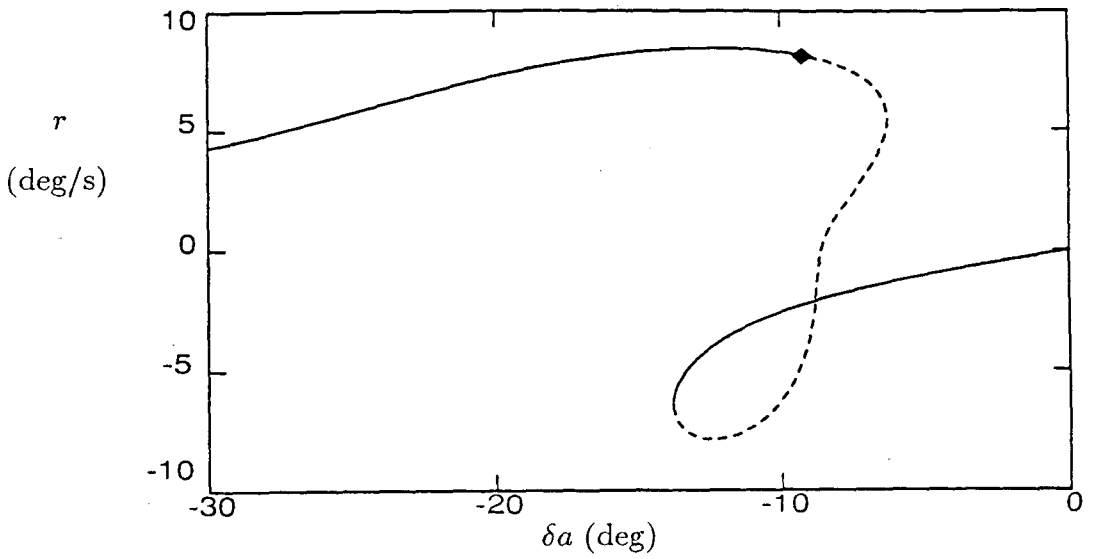

(c) Yaw Rate

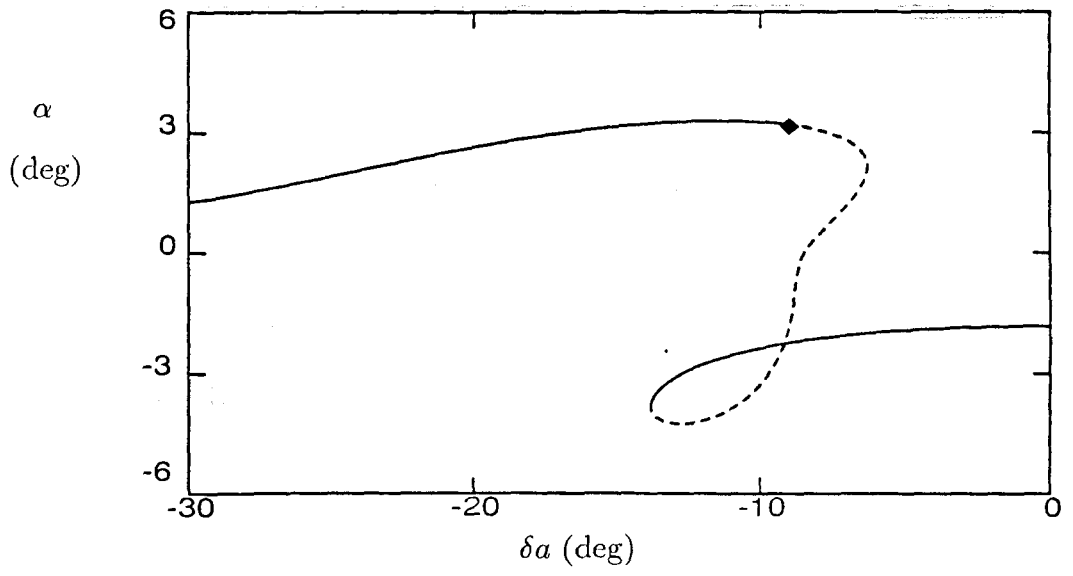

(d) Angle of Attack

Figure 5.5: Continued.

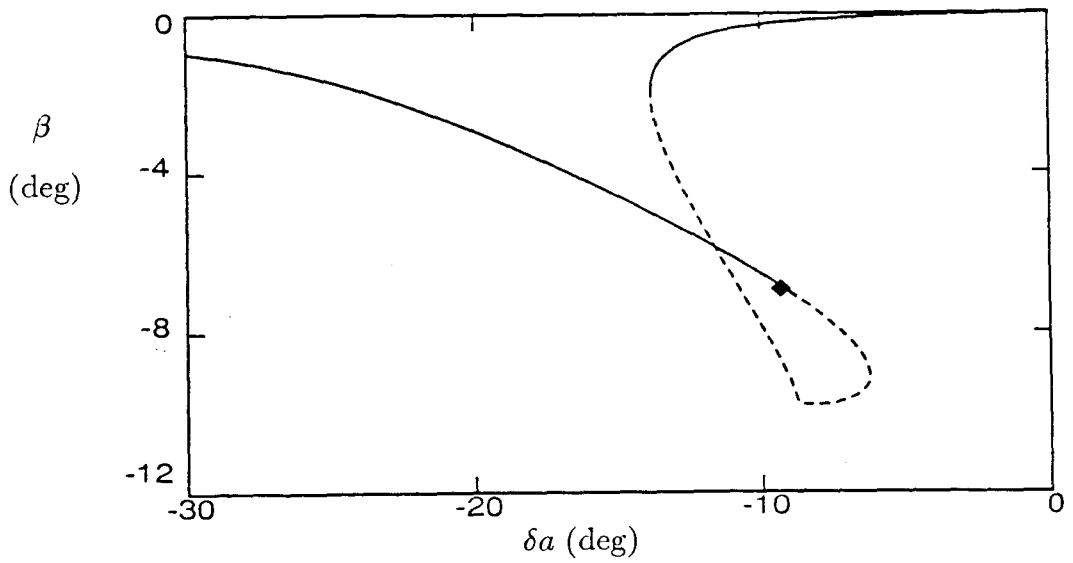

(e) Sideslip Angle

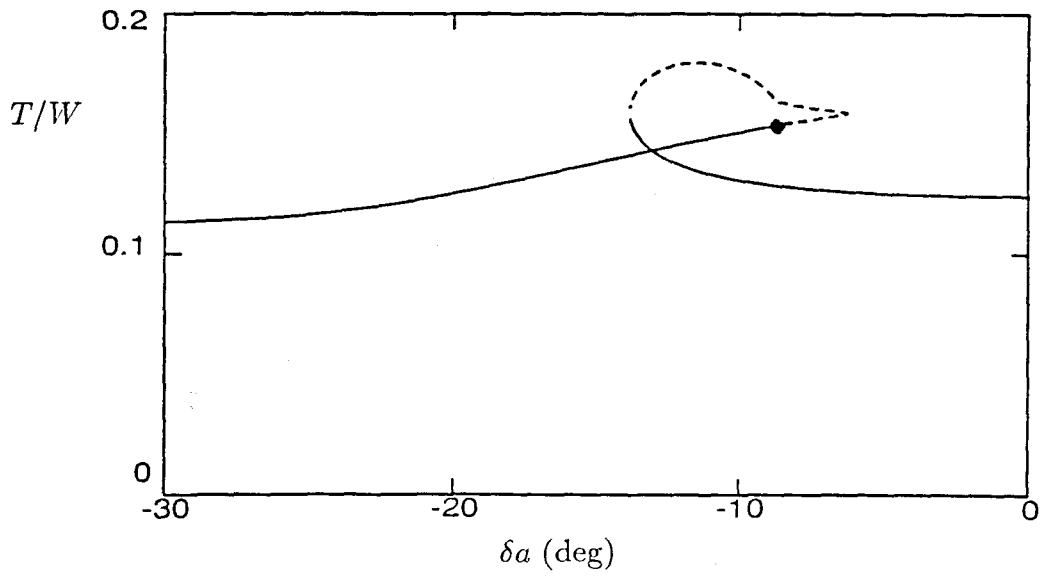

(f) Thrust to Weight Ratio

Figure 5.5: Concluded.

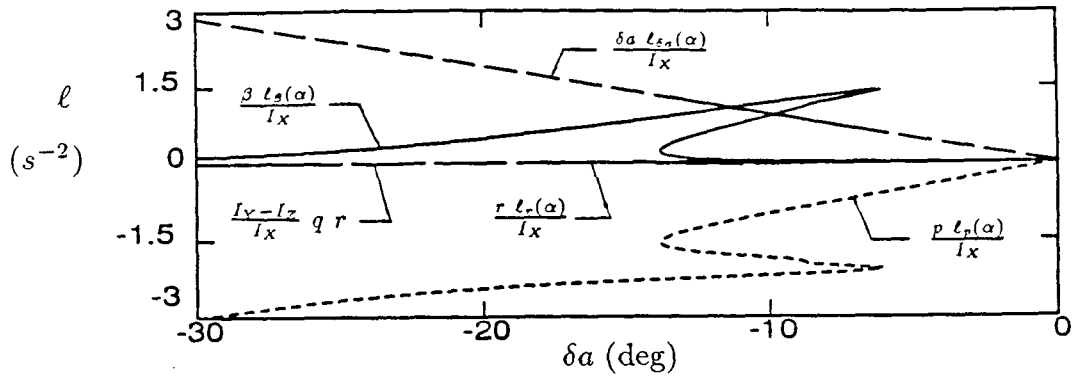

(a) Rolling Moment Balance

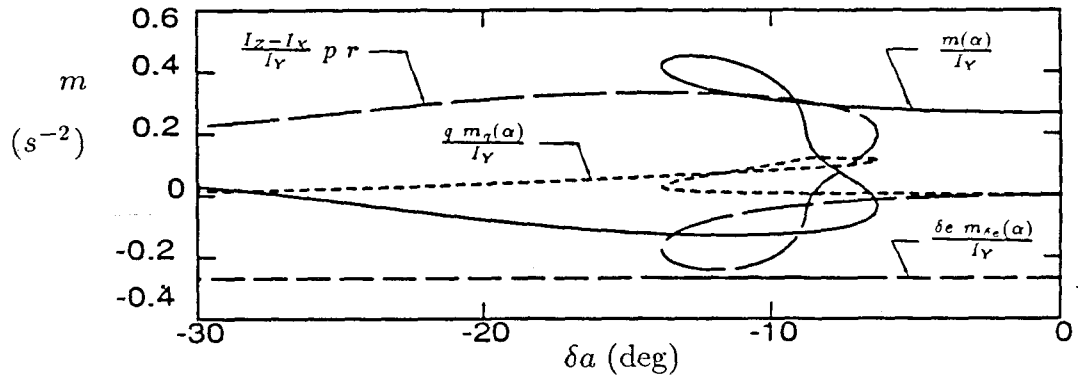

(b) Pitching Moment Balance

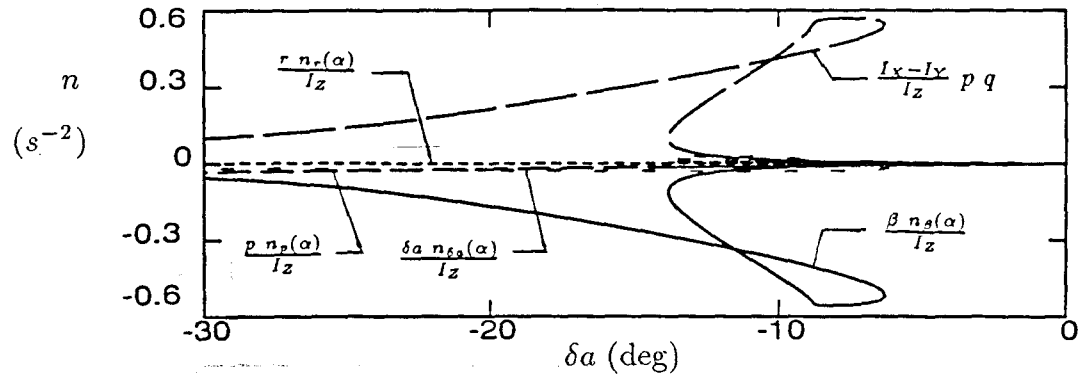

(c) Yawing Moment Balance

Figure 5.6: Moment balance for steady state rolls from a pitch down condition, δe=3, δr=0, V=266m/s.

attack are positive. The fundamental difference between the two stable steady states is the sign of the angle of attack, which causes one motion to be inverted and the other upright. The unstable steady states which connect the two curves of stable steady states bridge the gap between the upright and inverted flight regimes. Another difference between the two stable steady states is that inertial effects are minor for the low roll rate steady states, but inertial effects are the major factor in the pitching moment balance for the high roll rate steady states.

The saddle-node bifurcations in Figure 5.5 can lead to jump phenomena typical of roll-coupling instabilities. For example, assume an aircraft is in a pitch down condition with zero aileron deflection (as represented by the steady state for zero aileron deflection in Figure 5.5). As the aileron deflection is increased the steady state of the aircraft will follow the curve of stable steady states (neglecting atmospheric disturbances) as long as the aileron deflection is less than negative 13 degrees. If the aileron deflection increases past negative 13 degrees, the state of the aircraft must jump to the stable high roll rate steady states. A simulation of this is shown in Figure 5.7.

The saddle-node bifurcations also cause the hysterisis which is shown in Figure 5.7. After the aircraft jumps to the high roll rate steady states (at a time of 40 seconds) the aileron deflection is reduced to negative 10 degrees. This is less than the aileron deflection at which the jump to the high roll rate steady state occurs, but it is not low enough to get out of the high roll rate steady states (see Figure 5.5). Further reducing the aileron deflection to zero degrees is enough to

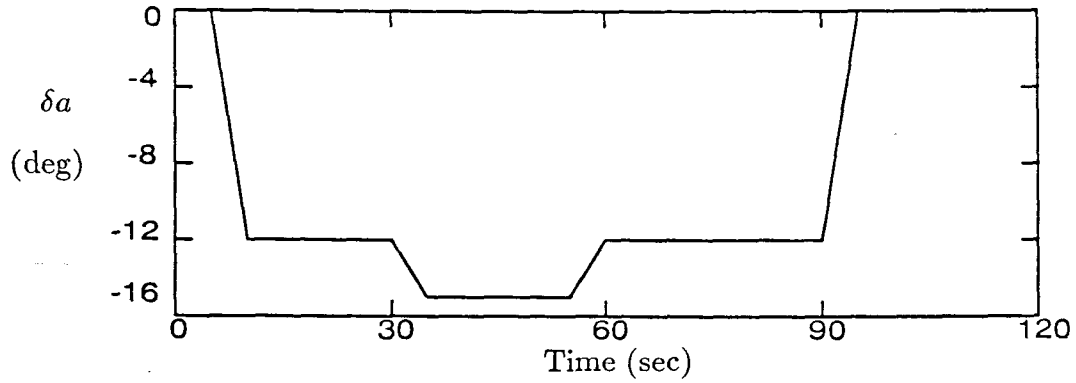

(a) Aileron Deflection

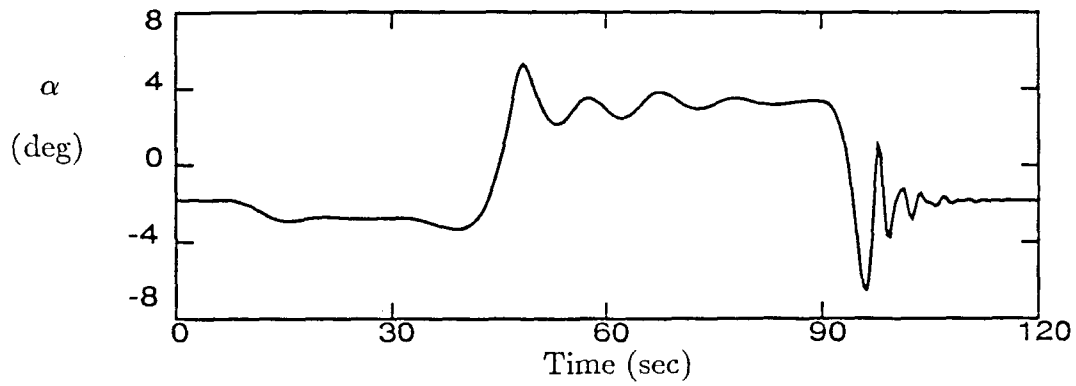

(b) Angle of Attack

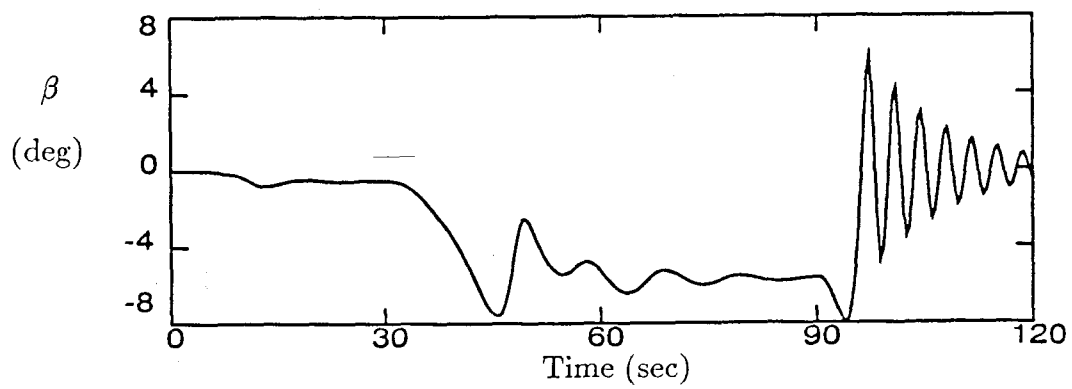

(c) Sideslip Angle

Figure 5.7: Simulation of roll-coupling instability for the generic jet fighter, δe=3, δr=0, V=266m/s.

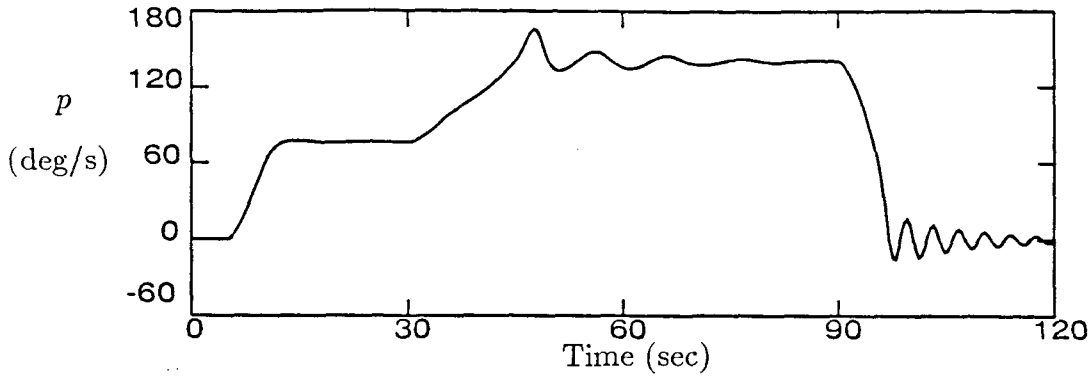

(d) Roll Rate

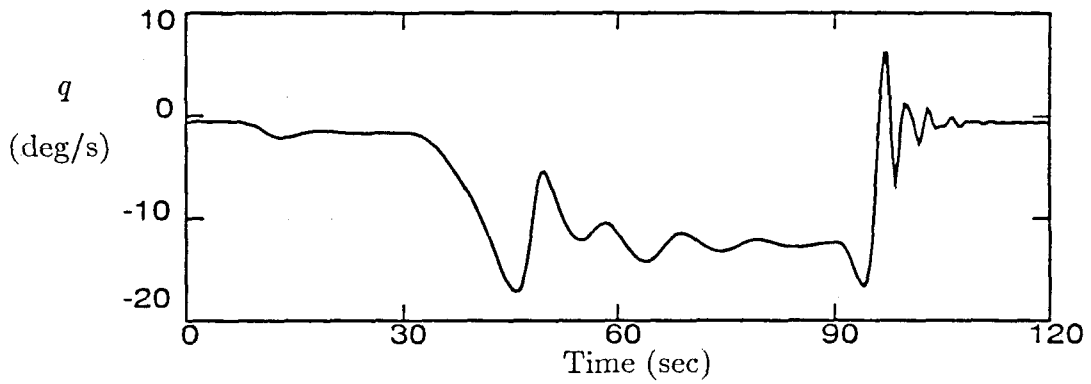

(e) Pitch Rate

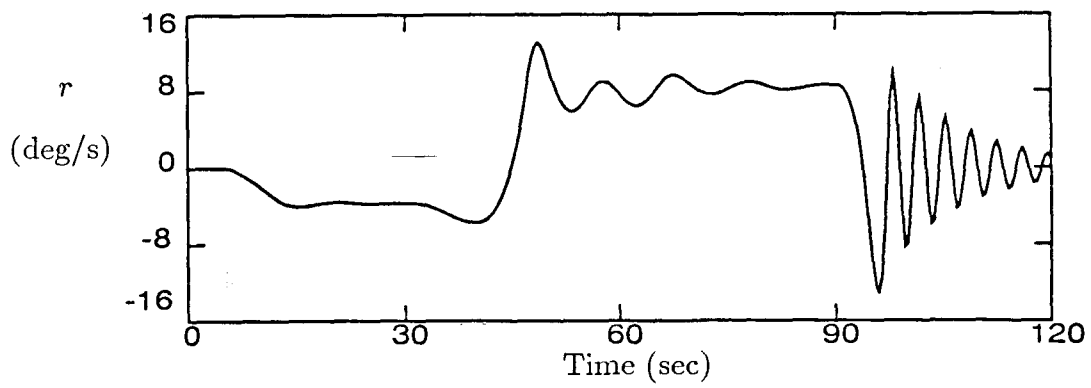

(f) Yaw Rate

Figure 5.7: Concluded.

get past the saddle-node bifurcation on the high roll rate steady states, and the aircraft jumps back to the low roll rate steady states. Information about which control surface deflections cause a jump in the state of the aircraft would be useful to pilots because it would allow them to avoid jumps or show how to get out of any undesirable state which results from a possible jump.

Saddle-node bifurcations related to roll-coupling instabilities occur for a range of control surface deflections. Figure 5.8 shows the elevator and aileron deflections which cause a jump in the state of the aircraft for zero rudder deflection. With this information it is possible to avoid jumps by staying away from the critical control surface deflections which cause jumps. One way to do this would be to program elevator and aileron deflections in such a way that the curves representing saddle-node bifurcations are never crossed.

5.1.3 Roll-Coupling Instabilities from Steady States with Rudder Deflection

The previous discussion was limited to steady states for zero rudder deflection. It may be possible to avoid roll-coupling instabilities by using the rudder to control the sideslip angle or the yaw rate. Figure 5.9 shows the steady states as a function of aileron deflection for the same elevator deflection as in Figure 5.5 and a rudder deflection of 6 degrees. The effect of rudder deflection on the steady state sideslip can be seen by comparing Figures 5.5(e) and 5.9(e). When no rudder deflection is applied (see Figure 5.5), the aircraft develops negative sideslip angles

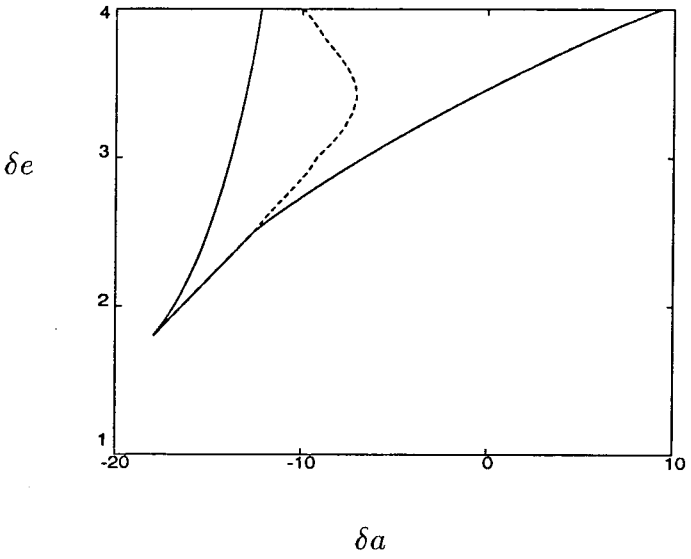

Figure 5.8: Bifurcation set of the generic jet fighter for V=266m/s, $\delta r = 0$; - - - Hopf Bifurcation, —— saddle-node bifurcation.

as the aileron deflection is increased, whereas when a 6 degree rudder deflection is applied, increasing aileron deflection results in a slight increase in the sideslip angle. Note that nonzero steady state sideslip exists for zero aileron deflection when the rudder is deflected. The positive steady state sideslip which occurs when the rudder is deflected causes a decrease in the steady state roll rate for a given aileron deflection because of the dihedral effect (see Section 5.1.2).

Applying positive rudder deflection also changes the aileron deflections at which bifurcations occur. For zero rudder deflection the maximum aileron deflection which could be applied before a jump in the state of the aircraft occurred was about negative 13 degrees (see Figures 5.5 and 5.7). When a 6 degree rudder deflection is applied, the aileron deflection can be increased to negative 20

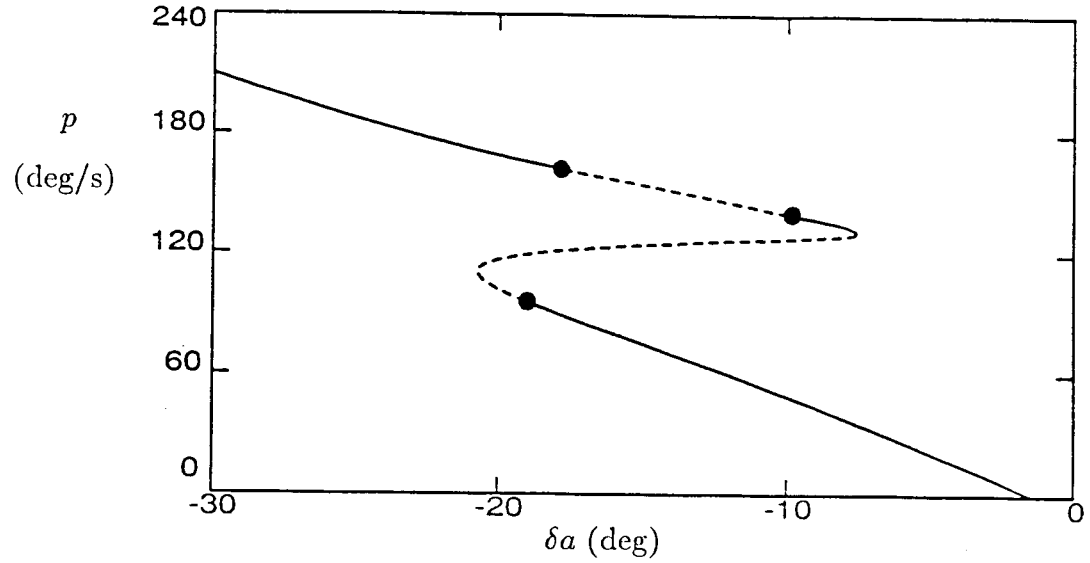

(a) Roll Rate

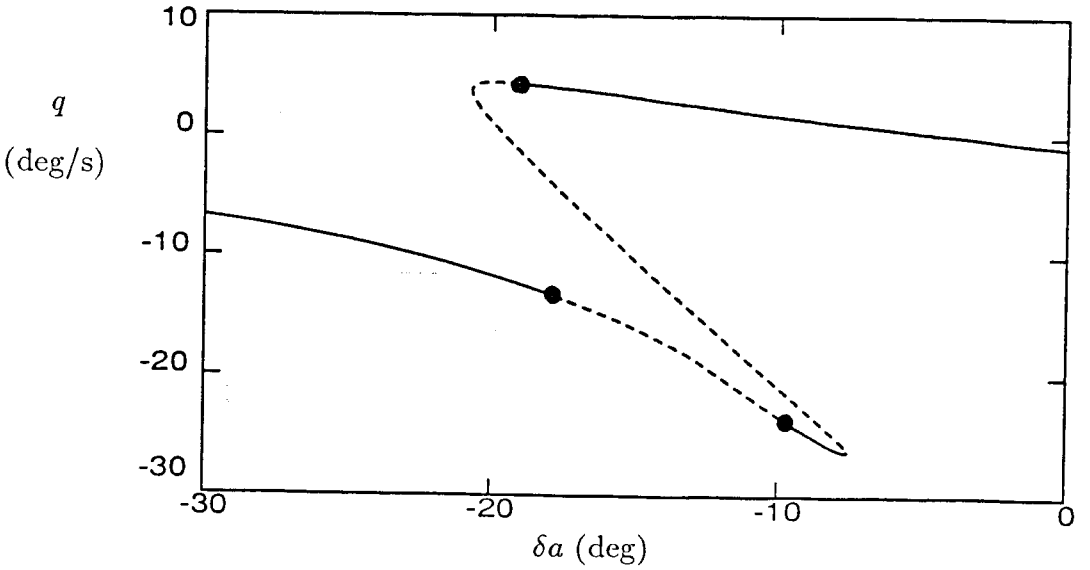

(b) Pitch Rate

Figure 5.9: Steady states for the generic jet fighter, V=266m/s, δr=6, δe=3.0; —— stable, - - - unstable, • – Hopf bifurcation.

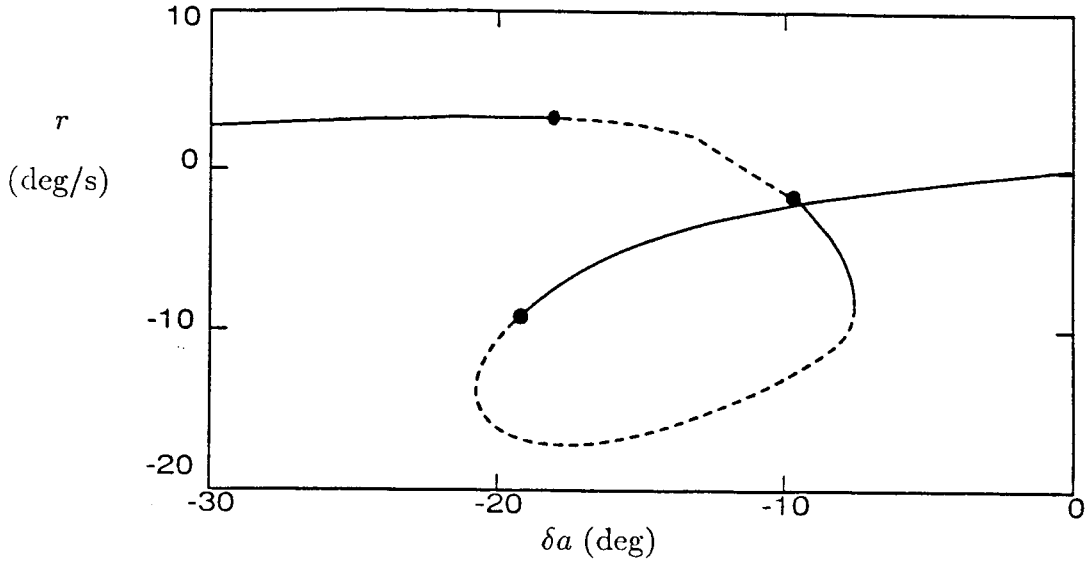

(c) Yaw Rate

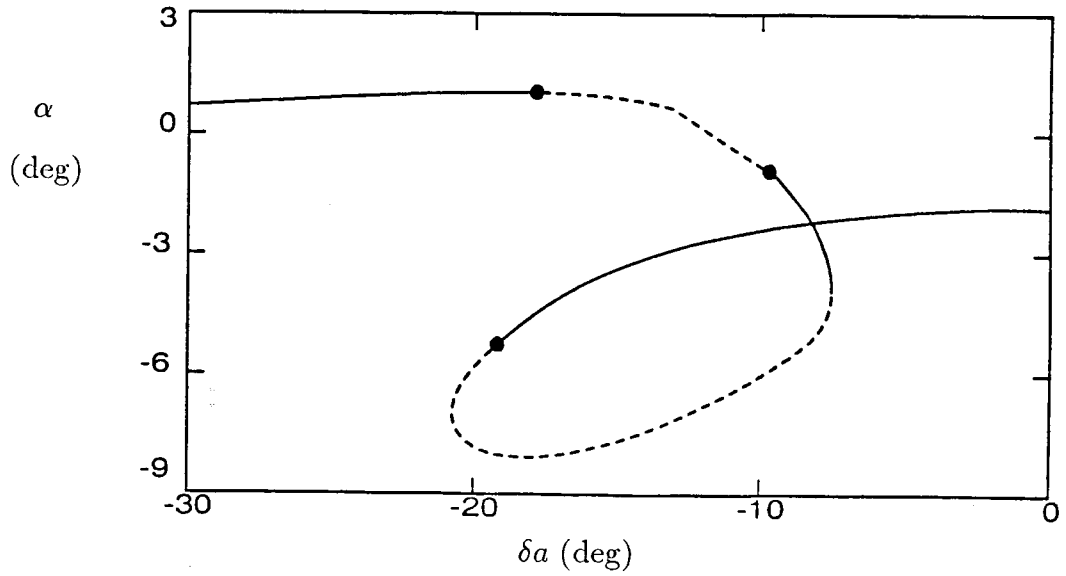

(d) Angle of Attack

Figure 5.9: Continued.

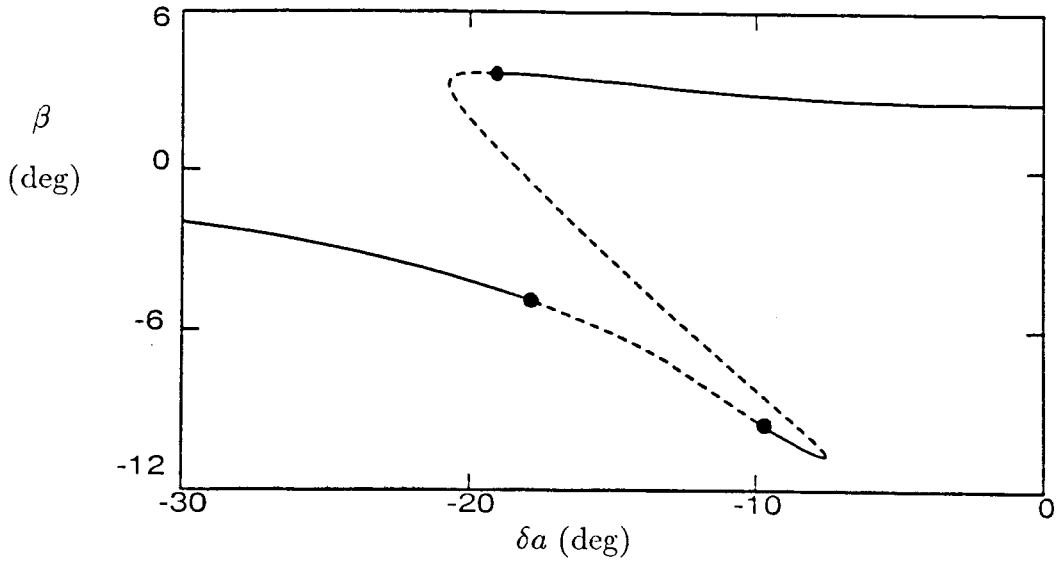

(e) Sideslip Angle

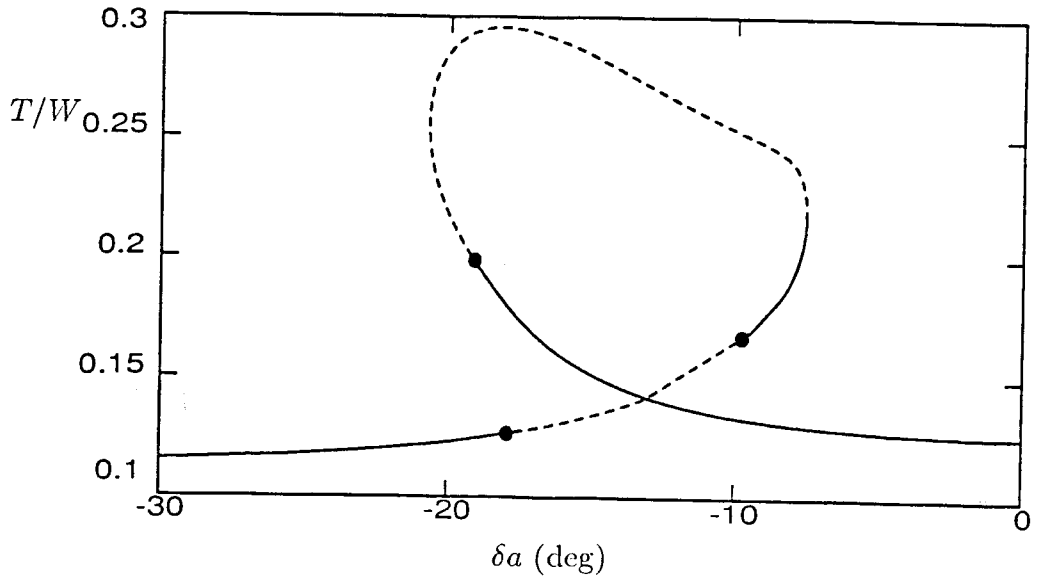

(f) Thrust to Weight Ratio

Figure 5.9: Concluded.

degrees before a jump in the state of the aircraft would occur (see Figure 5.9). Recall that the steady state of the aircraft will follow the curves in Figure 5.9 (neglecting atmospheric disturbances), so if the aileron deflection is initially zero the steady state of the aircraft will be given by the stable steady state at zero aileron deflection. As the aileron deflection is increased, the steady state of the aircraft will follow the curve of stable steady states up to an aileron deflection of negative 20 degrees. For aileron deflections slightly greater than negative 20 degrees, the steady state becomes unstable because of a Hopf bifurcation and one of two things can occur. Either a stable periodic motion will develop or the state of the aircraft will jump to the stable steady state at the higher roll rate. Aileron deflections greater than negative 22 degrees will certainly result in a jump in the state of the aircraft because of the saddle-node bifurcation which occurs at that aileron deflection.

For zero rudder deflection a saddle-node bifurcation occurs for an aileron deflection of negative 13 degrees (see Figure 5.5), but for a rudder deflection of 6 degrees, the saddle-node bifurcation did not occur until an aileron deflection of negative 22 degrees (see Figure 5.9). Figure 5.10 shows the bifurcation loci of the low roll rate steady states for an elevator deflection of 3 degrees. The figure shows that the saddle-node bifurcation occurs at larger aileron deflections as larger positive rudder is applied. For a rudder deflection of positive 12 degrees, the saddle-node bifurcation occurs at an aileron deflection of negative 30 degrees. The curve of rudder and aileron deflections at which the saddle-node bifurcations

occur could be used to design a control system for this aircraft. Rudder and aileron deflections could be programmed so that the curve on which saddle-node bifurcations occur could not be crossed.

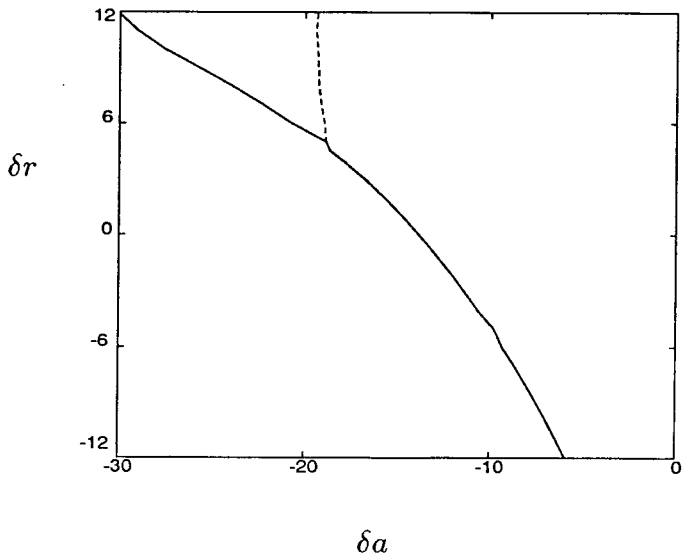

Figure 5.10: Bifurcation set of the generic jet fighter for V=266m/s, $\delta e = 3$; – – – Hopf bifurcation, —— saddle-node bifurcation.

The curve on which Hopf bifurcations occur (dashed line in Figure 5.10) would also have to be taken into account when designing a control system. Recall Figure 5.9 which shows that the low roll rate steady states become unstable because of the Hopf bifurcation. Control surface deflections would have to be further limited to stay away from the Hopf bifurcations, which could lead to periodic motions or jump phenomena. This essentially limits the maximum allowable aileron deflection to about negative 20 degrees even for large rudder deflections.

Figure 5.11 shows a simulation of the roll-coupling instability when the rudder deflection is positive 6 degrees. The aircraft behaves well when the aileron deflection is increased to negative 16 degrees. The roll rate increases substantially while the other variables change only slightly. Compare this response to the response for zero rudder deflection shown in Figure 5.7, where increasing the aileron deflection to negative 15 degrees caused a jump in the state of the aircraft. Jump phenomena also occur when positive rudder deflection is applied but at higher aileron deflections. Figure 5.11 shows that when the aileron deflection is increased to negative 24 degrees, a jump in the state of the aircraft occurs. This is caused by the saddle-node bifurcation which occurs at an aileron deflection of negative 22 degrees (see Figure 5.9).

5.1.4 Steady States at High Angles of Attack

The high angle of attack behavior of this aircraft will be analyzed by determining the steady states for aileron deflections from the longitudinal steady states represented by curve 1 in Figure 5.1. Recall that the purely longitudinal steady states represented by curve 1 become unstable because of a Hopf bifurcation at an elevator deflection of negative 14 degrees. This corresponds to an angle of attack of 20 degrees, above which the aircraft loses directional stability (i.e., $C_{n_\beta}(\alpha)$ becomes negative). Also note that curves 1 and 2 intersect at a pitchfork bifurcation for an elevator deflection of negative 18 degrees. This will not affect the dynamics

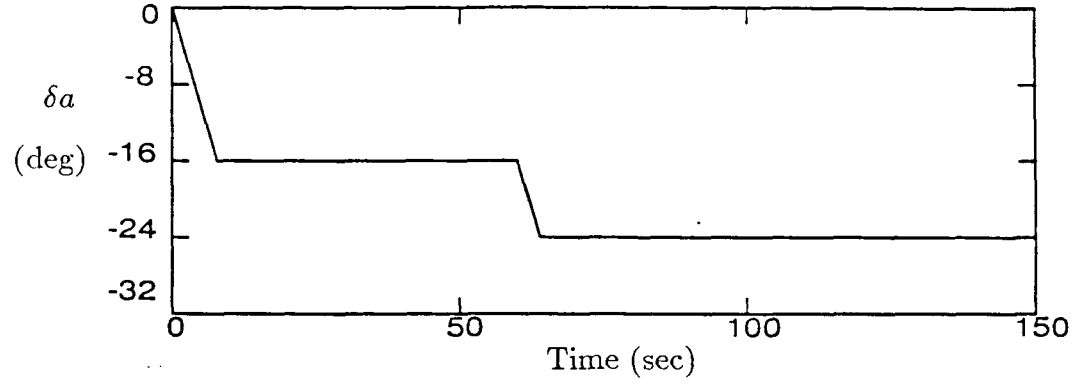

(a) Aileron Deflection

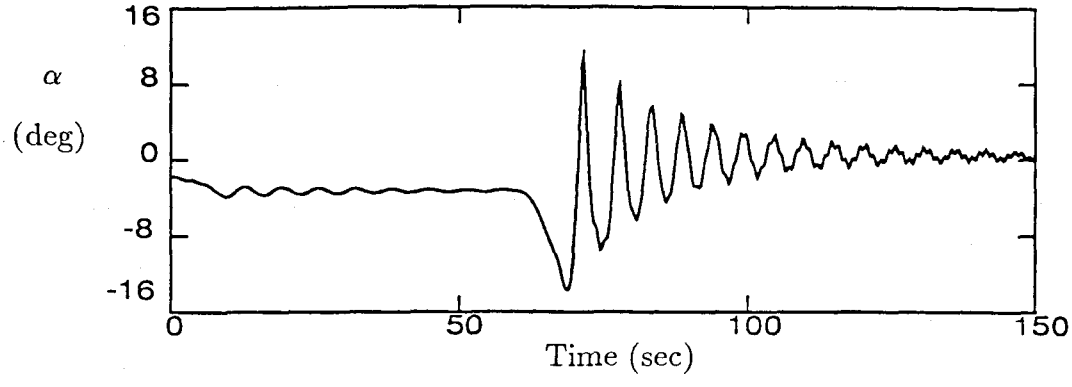

(b) Angle of Attack

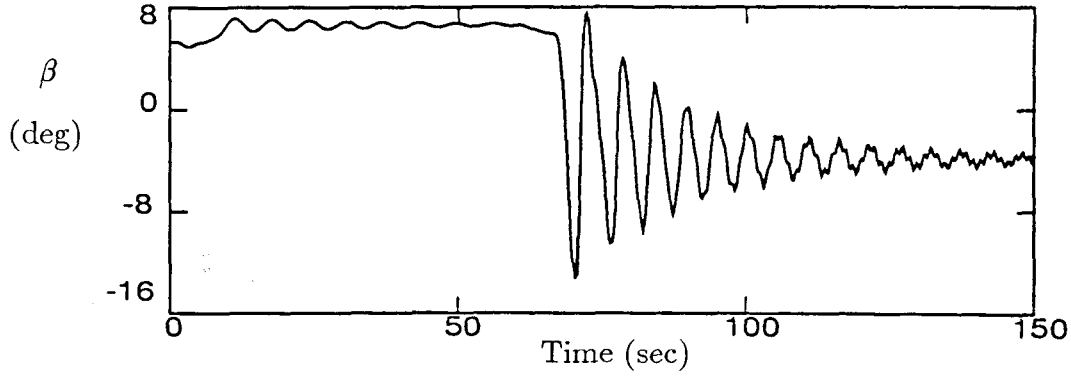

(c) Sideslip Angle

Figure 5.11: Simulation of roll-coupling instability for the generic jet fighter, δe=3, δr=6, V=266m/s.

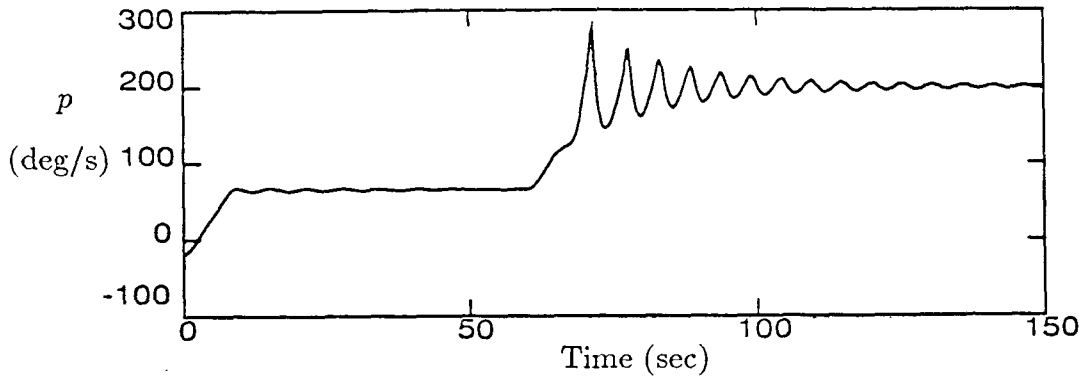

(d) Roll Rate

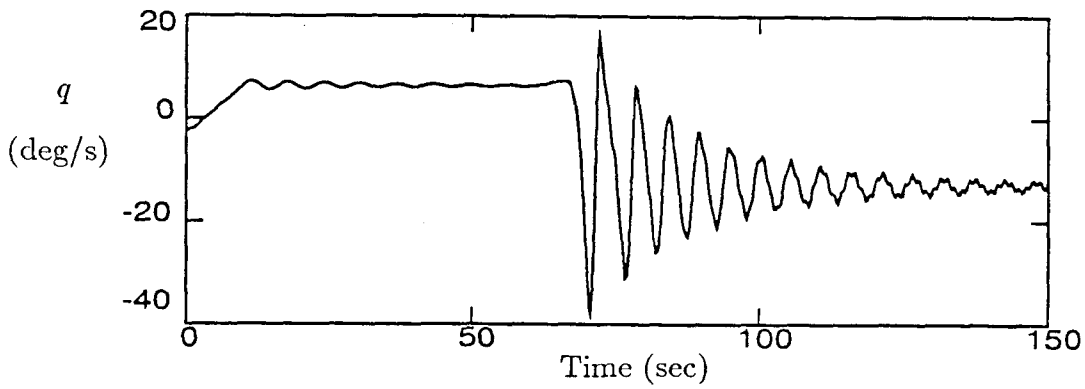

(e) Pitch Rate

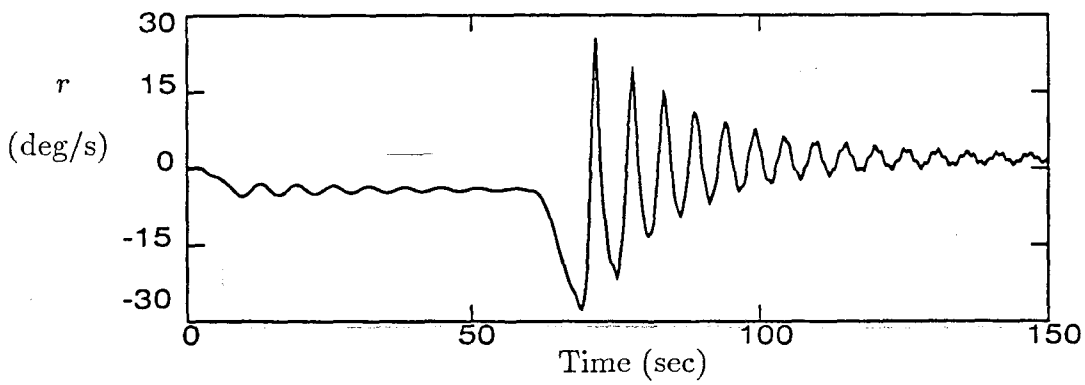

(f) Yaw Rate

Figure 5.11: Concluded.

of the aircraft because all of the steady states in the region of the bifurcation are unstable.

Figure 5.12 shows the steady states of the aircraft as a function of the aileron deflection for two elevator deflections. The ailerons have clearly lost their effectiveness for an elevator deflection of negative 12 degrees. Their only effect is to impart large sideslip angles to the aircraft (see Figure 5.12(e)). This is a result of the low directional stability (i.e., $C_{n_\beta}(\alpha)$) at high angles of attack. Since the yawing moment balance is maintained by the term βn_β, low values of n_β must be accompanied by large angles of sideslip. It should be noted that only linear sideslip effects are included in this model so steady states with large angles of sideslip may not be physically realistic.

The steady states for an elevator deflection of negative 13 degrees show that the effect of the ailerons on the roll rate has reversed. At low angles of attack, negative aileron deflections produced positive roll rates, while at the high angles of attack characterized by Figure 5.12, positive aileron deflection imparts positive roll rates to the aircraft. Aileron deflections for an elevator deflection of negative 13 degrees mainly produce large angles of sideslip similiar to the case for an elevator deflection of negative 12 degrees.

The aircraft will exhibit qualitatively different behavior for an elevator deflection of negative 13 degrees than it will for an elevator deflection of negative 12 degrees because of the saddle-node bifurcations that occur in the fixed points for an elevator deflection of negative 13 degrees. For an elevator deflection of

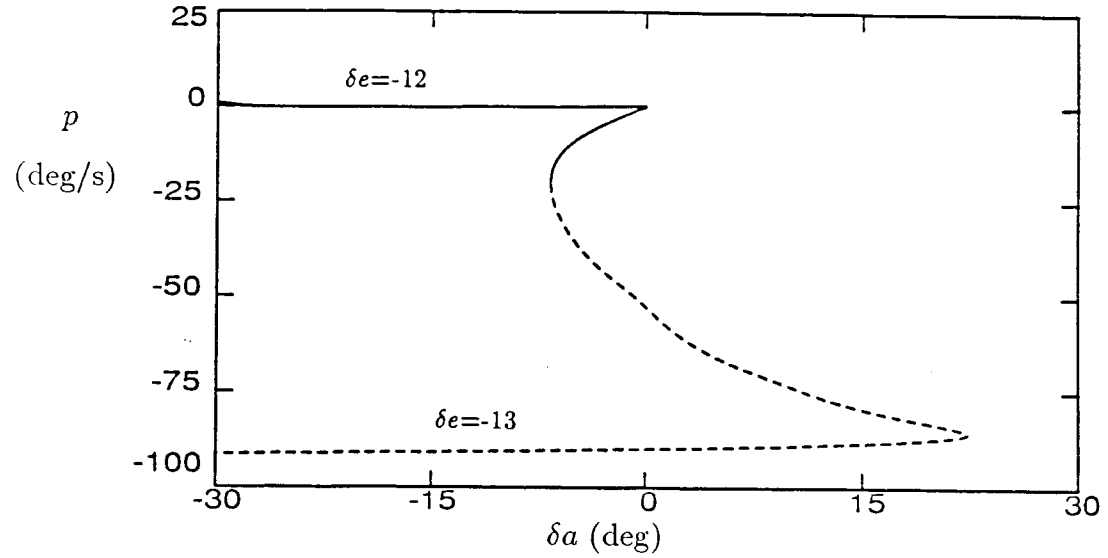

(a) Roll Rate

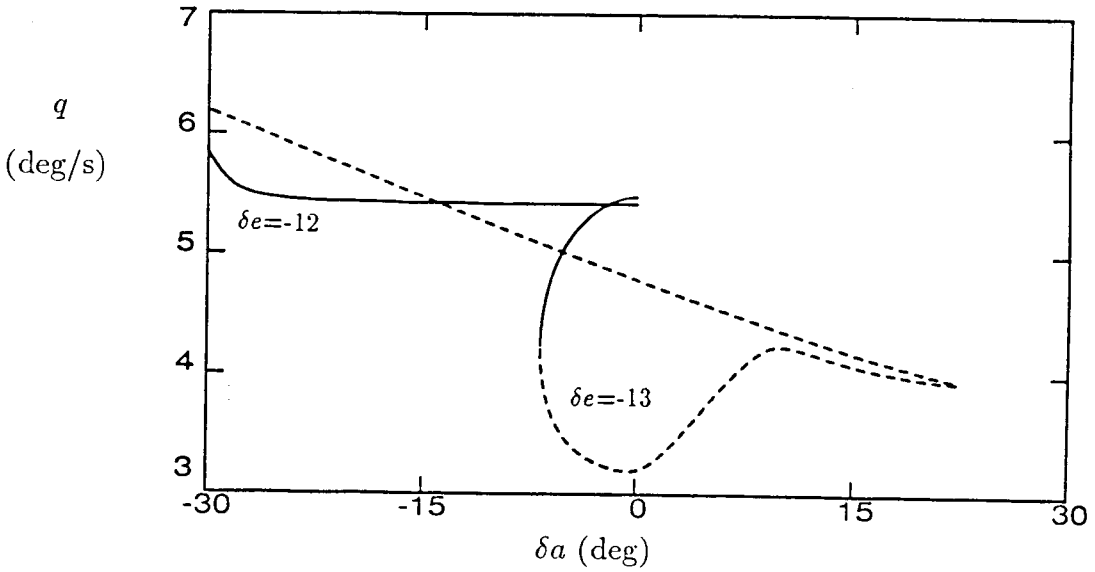

(b) Pitch Rate

Figure 5.12: Steady states for the generic jet fighter, V=266m/s, δr=0, δe=-12,-13; —— stable, - - - unstable.

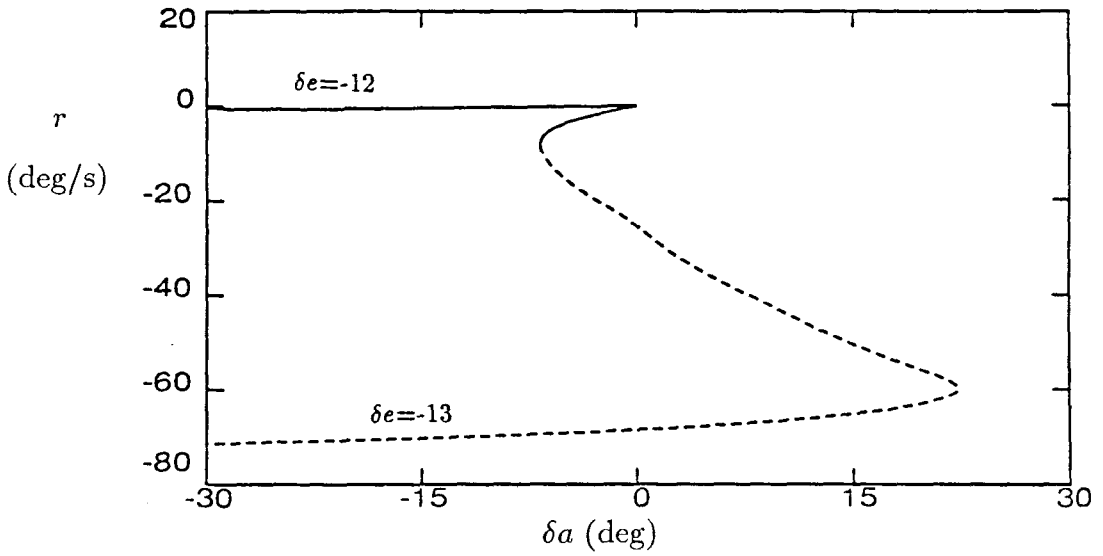

(c) Yaw Rate

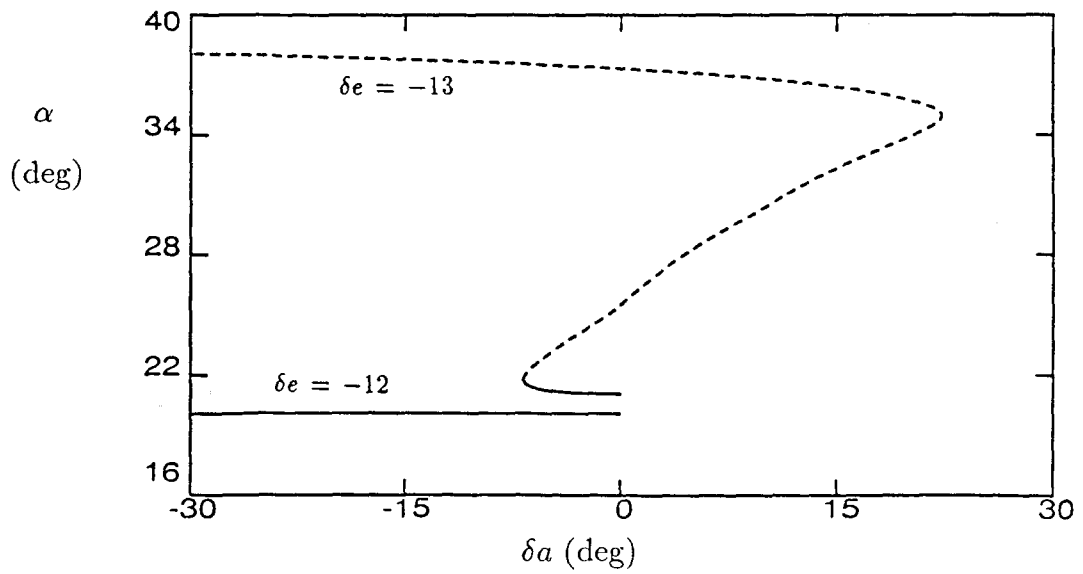

(d) Angle of Attack

Figure 5.12: Continued.

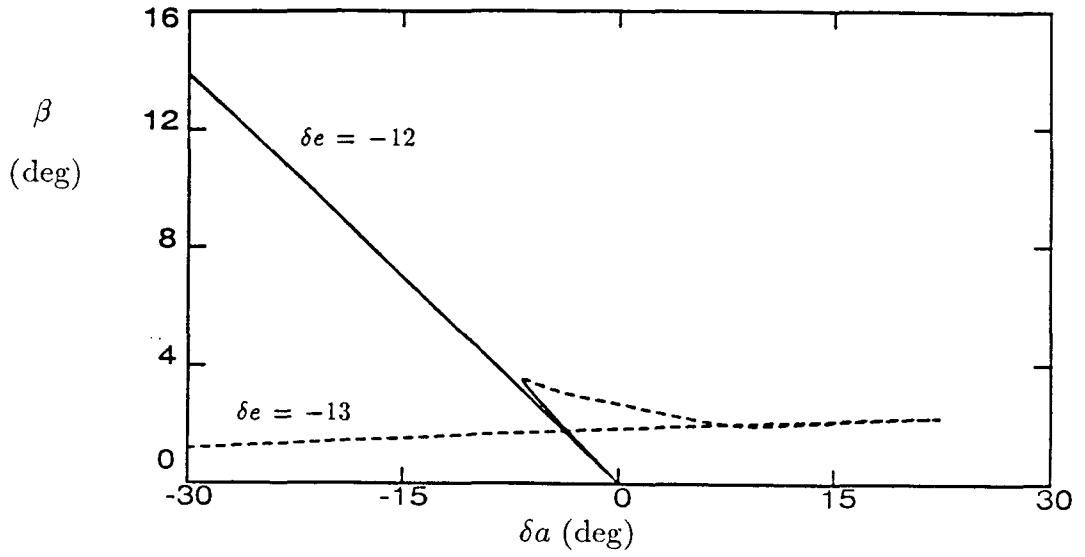

(e) Sideslip Angle

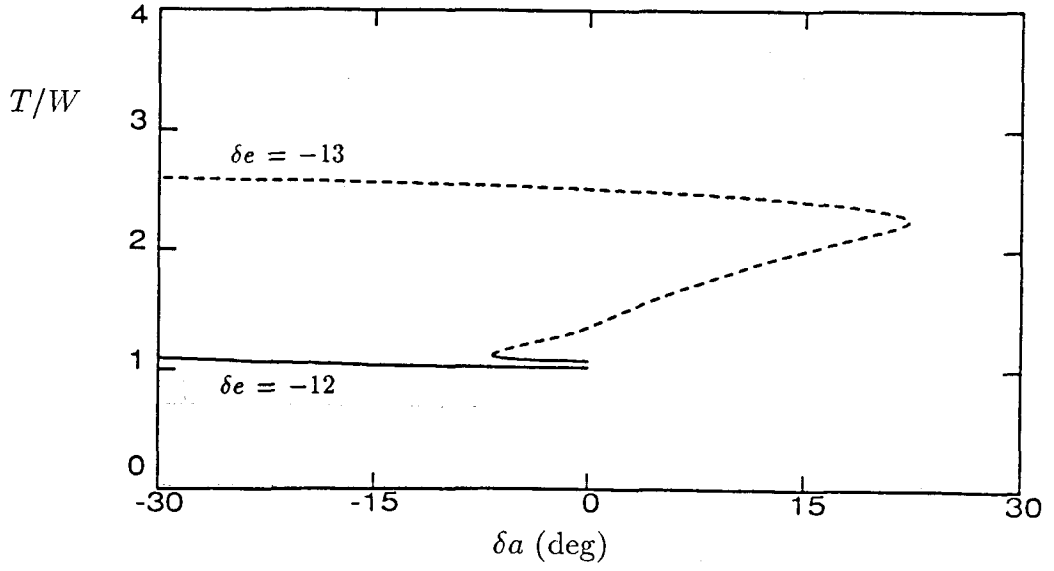

(f) Thrust to Weight Ratio

Figure 5.12: Concluded.

negative 12 degrees, stable fixed points exist for all aileron deflections and no bifurcations occur. Increasing the elevator deflection to negative 13 degrees leads to the creation of two saddle-node bifurcations, with the result that there are no stable steady states for aileron deflections greater than 8 degrees.

Since no stable fixed points exist, the aircraft must undergo some type of time dependent motion. Figure 5.13 shows a simulation in which the elevator deflection is held at negative 13 degrees as the aileron deflection is increased to a value larger than that at which the saddle-node bifurcation occurs. The aircraft undegoes large amplitude motions which seem to keep increasing. The simulation was stopped because the angle of attack became too large for the aerodynamic model. Sideslip deviations also grew well beyond the range of validity of this aerodynamic model. Rotary balance data and nonlinear sideslip dependence would have to be included in the aerodynamic model to make it valid in this flight regime. Including rotary balance data would probably cause one or more of the spin modes (curves 2-6 in Figure 5.1) to become stable and the aircraft would enter a stable spin. Requiring a velocity of 266m/s at these high angles of attack is also not very realistic. (See Sections 5.2 and 5.3 for discussions about effect of velocity on the steady states of the aircraft.)

The saddle-node bifurcation which occurs on the curve of stable fixed points for an elevator deflection of negative 13 degrees may be realistic, because the rotation rates and sideslip angle are small at the bifurcation point. Figure 5.14 shows that there is a curve of saddle-node bifurcations in the $\delta a - \delta e$ parameter

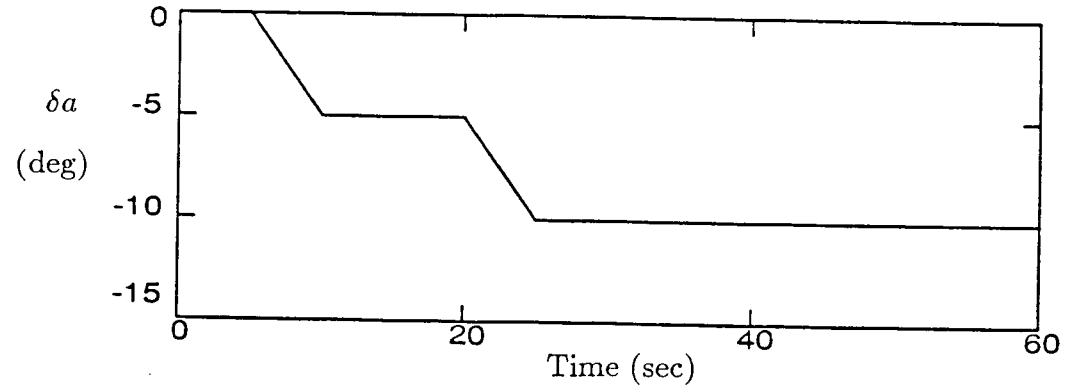

(a) Aileron Deflection

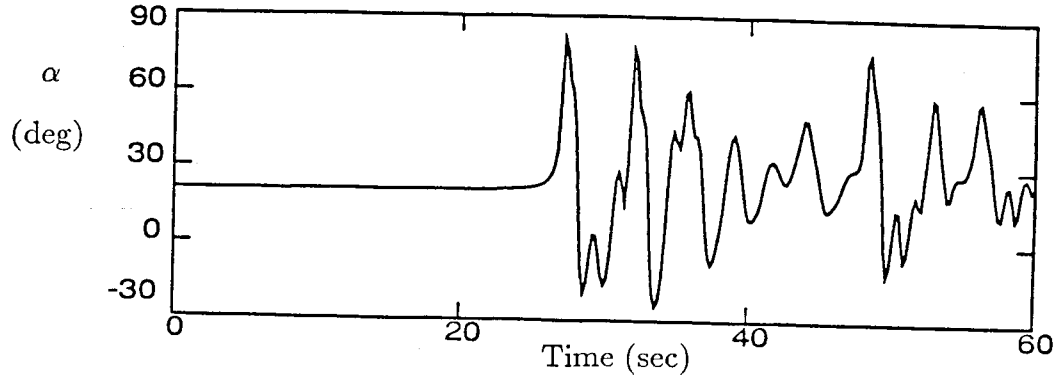

(b) Angle of Attack

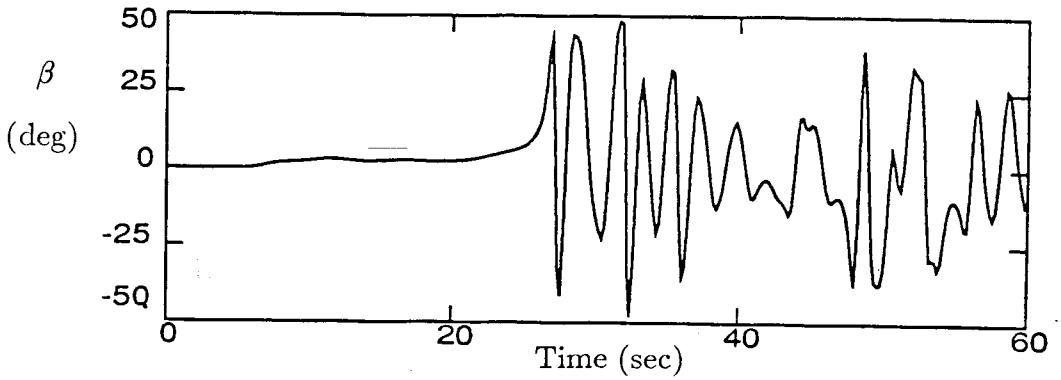

(c) Sideslip Angle

Figure 5.13: Simulation of high angle of attack instability for the generic jet fighter with variable aileron deflection, δe=-13, δr=0, V=266m/s.

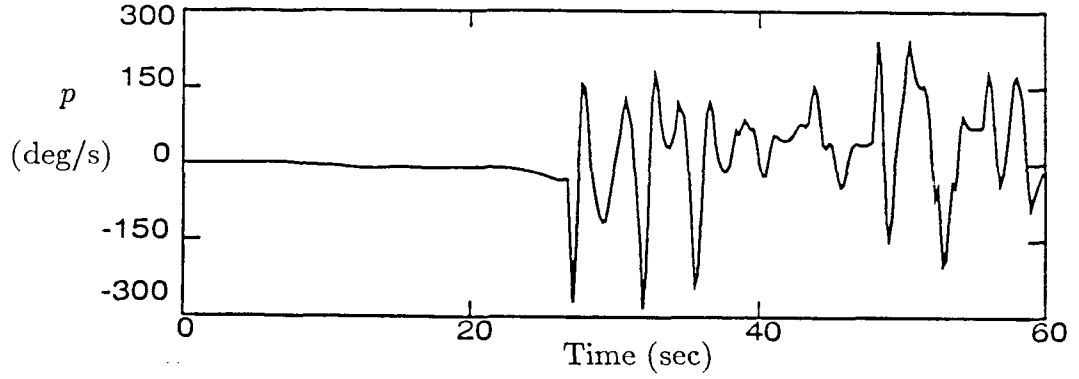

(d) Roll Rate

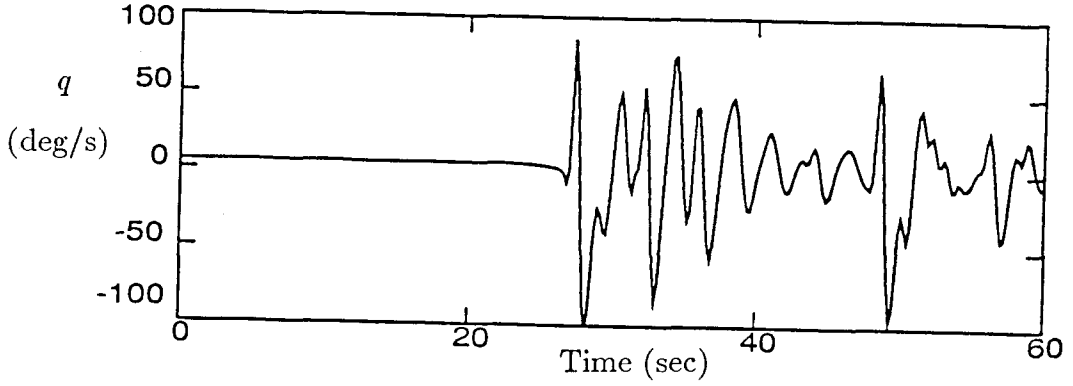

(e) Pitch Rate

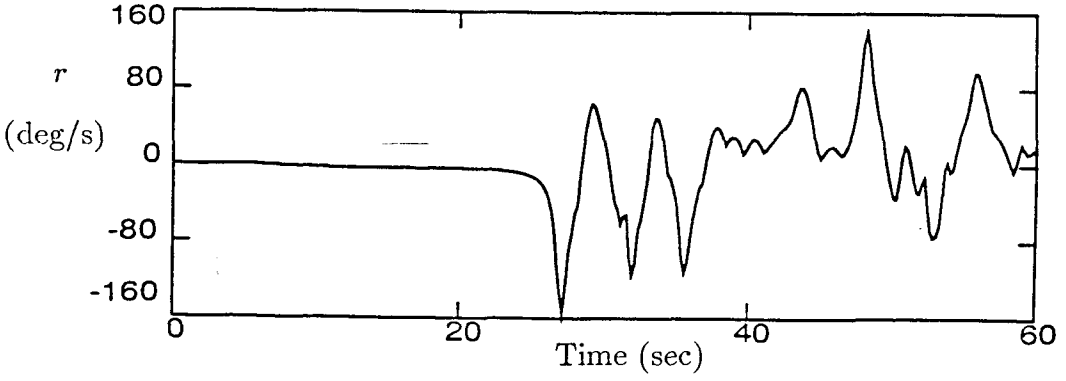

(f) Yaw Rate

Figure 5.13: Concluded.

space, beyond which no steady states exist. A curve of Hopf bifurcations also leads to the condition of no stable steady states. This could be used as guide for putting limits on the control surface deflections to keep pilots from encountering these high angle of attack instabilities.

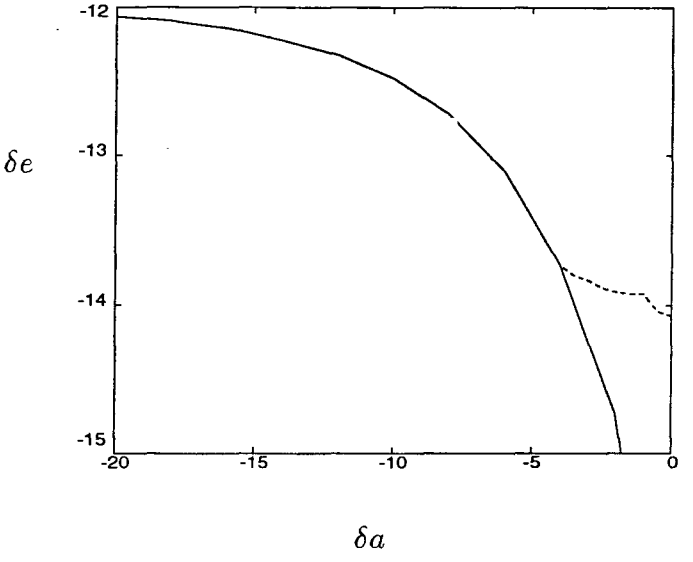

Figure 5.14: Bifurcation set for the generic jet fighter for V=266m/s and $\delta r = 0$; - - - Hopf bifurcation, —— saddle-node bifurcation.

5.1.5 Stabilization with Sideslip Feedback

Since the high angle of attack instability is related to the loss of directional stability, it might be possible to stabilize the aircraft with a feedback control system. Sideslip feedback to the rudder will increase the effective directional stability of the aircraft because the yawing moment for this aircraft is

$$C_n(\alpha) = \beta C_{n_\beta}(\alpha) + \delta a C_{n_{\delta a}}(\alpha) + \delta r C_{n_{\delta r}}(\alpha) + \frac{b}{2V}(pC_{n_p}(\alpha) + rC_{n_r}(\alpha))$$

so if δr is replaced by $K\beta$

$$C_n(\alpha) = \beta(C_{n_\beta}(\alpha) + KC_{n_{\delta r}}(\alpha)) + \delta a C_{n_{\delta a}}(\alpha) + \frac{b}{2V}(pC_{n_p}(\alpha) + rC_{n_r}(\alpha)),$$

the effective directional stability is

$$(C_{n_\beta})_{eff} = C_{n_\beta}(\alpha) + KC_{n_{\delta r}}(\alpha).$$

Figure 5.15 shows the steady states as a function of aileron deflection for a value of K of negative one. Figure 5.12 shows the equivalent picture when no feedback is used. Comparing Figures 5.12 and 5.15 shows that sideslip feedback to the rudder has a dramatic effect on the steady states of the aircraft. Roll control is maintained when feedback is used and the saddle-node bifurcations that occur for an elevator deflection of negative 13 degrees when no feedback is used have disappeared. Hopf bifurcations occur on both branches of fixed points when feedback is used (see Figure 5.15), but they occur at relatively large aileron deflections.

Figure 5.16 shows a simulation with sideslip feedback to the rudder for the same aileron and elevator deflections as were used in Figure 5.13. In Figure 5.13 large time dependent motions occurred when the aileron deflection was increased to a value greater than that at which a saddle-node biufurcation occurred causing all steady states to become unstable. Figure 5.16 shows that with sideslip feedback the behavior of the aircraft is acceptable. No instabilities occur and the transient motions are well damped.

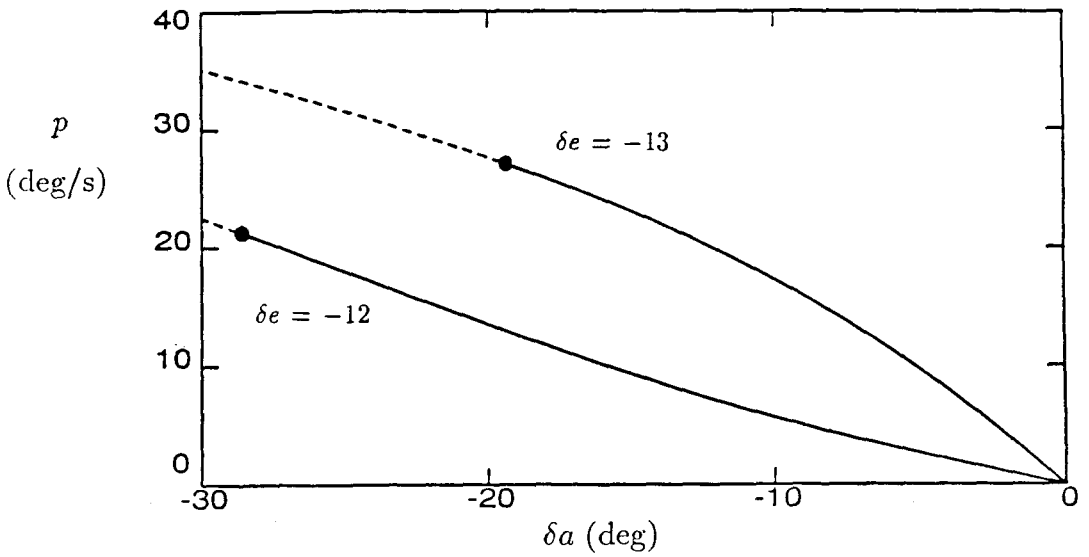

(a) Roll Rate

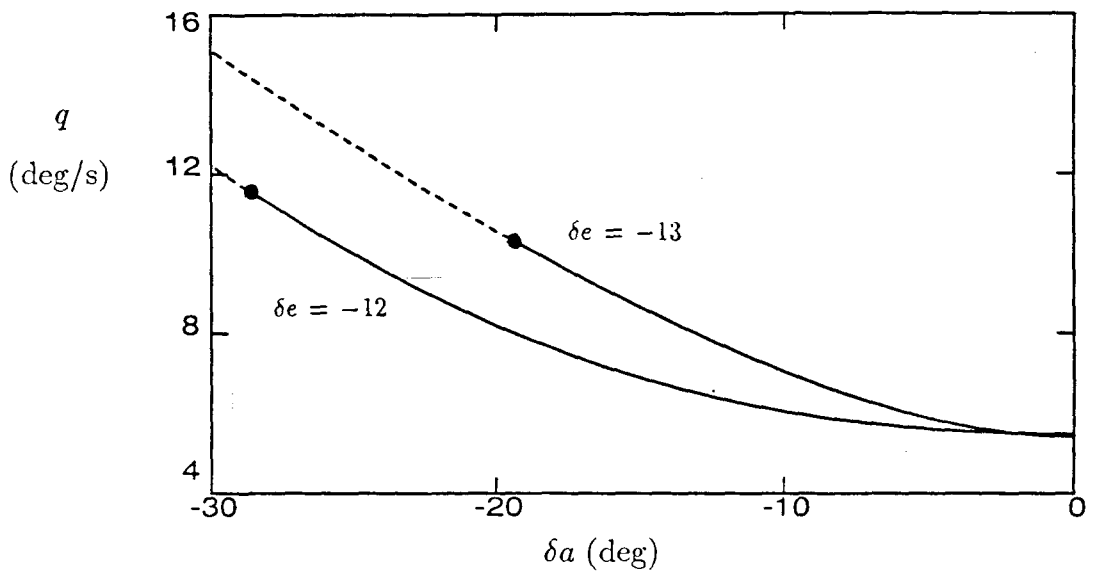

(b) Pitch Rate

Figure 5.15: Steady states for the generic jet fighter with sideslip feedback to the rudder, V=266m/s, δe=-12,-13, δr=-1β; —— stable, - - - unstable, • - Hopf bifurcation.

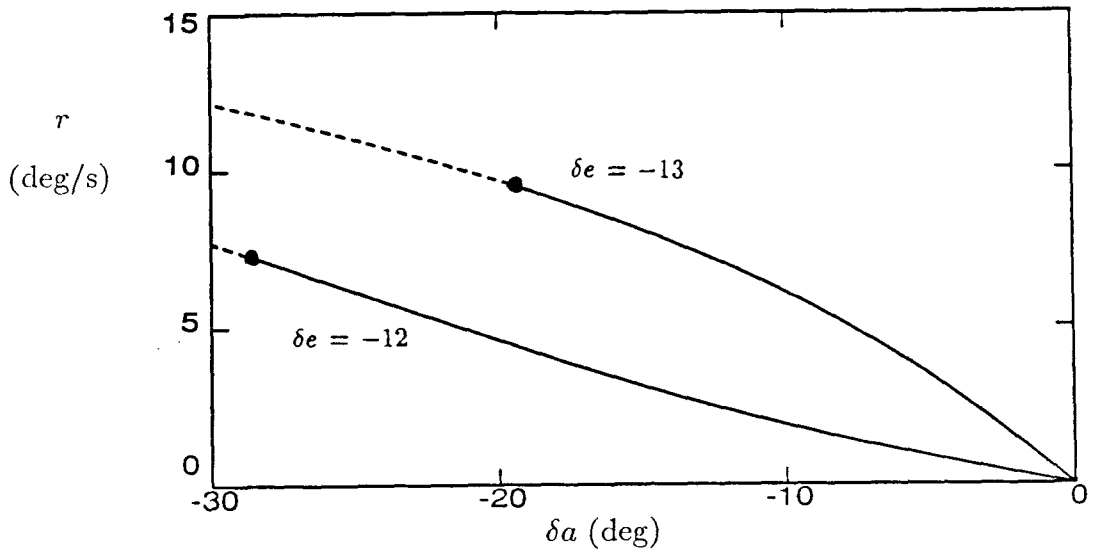

(c) Yaw Rate

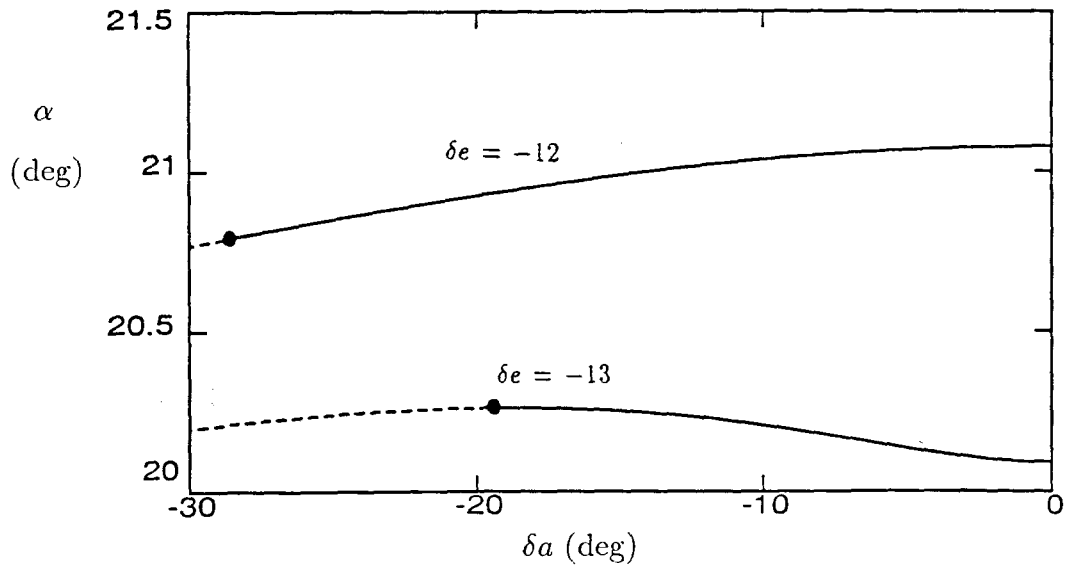

(d) Angle of Attack

Figure 5.15: Continued.

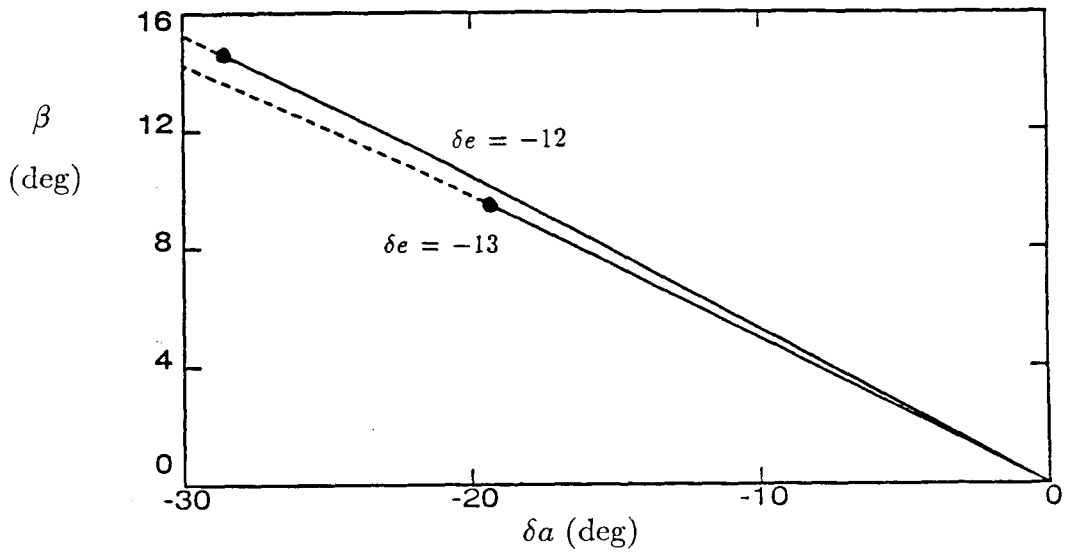

(e) Sideslip Angle

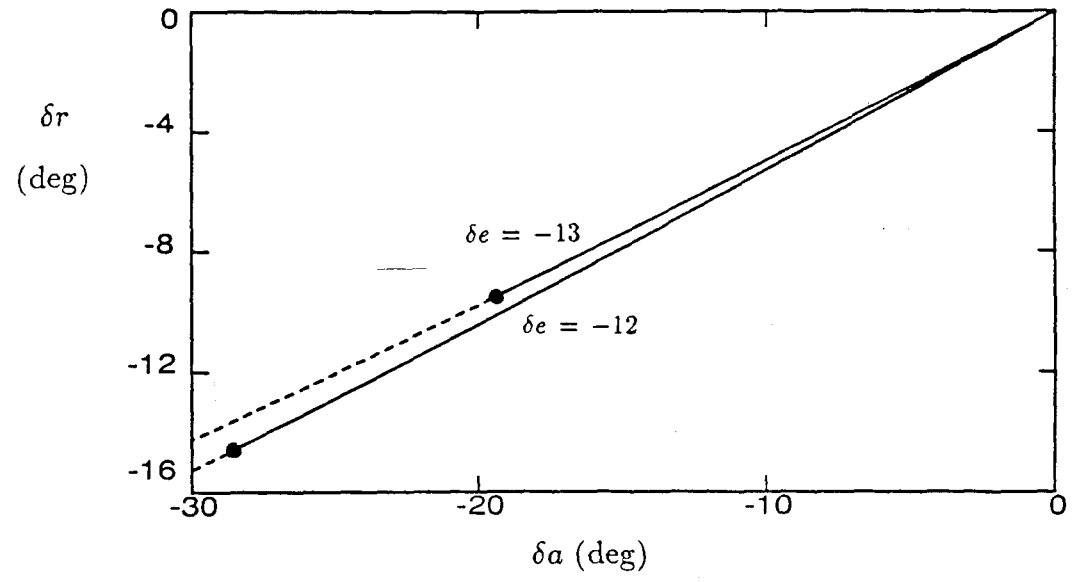

(f) Rudder Deflection

Figure 5.15: Concluded.

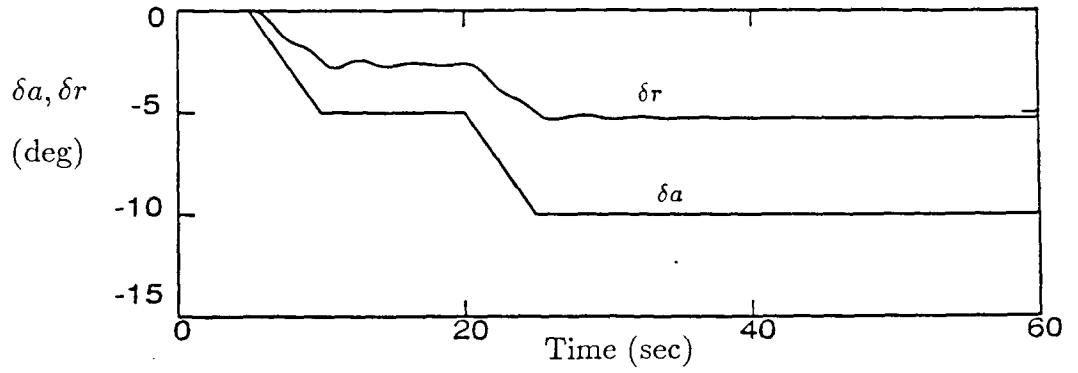

(a) Aileron and Rudder Deflections

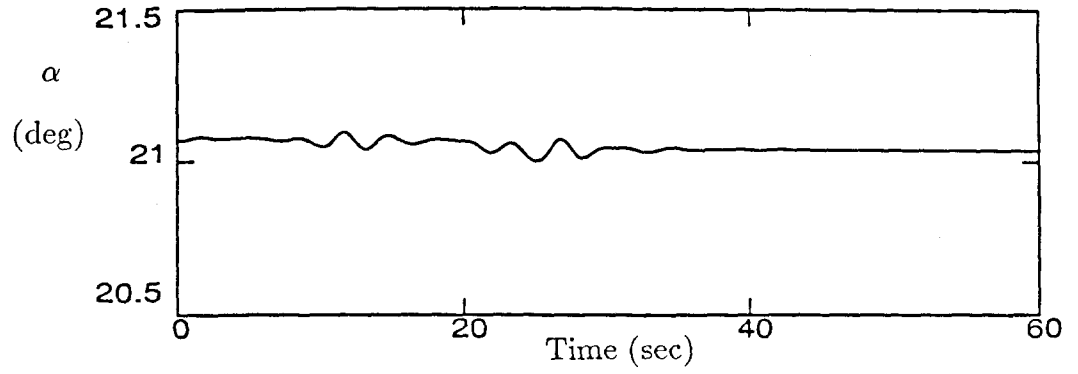

(b) Angle of Attack

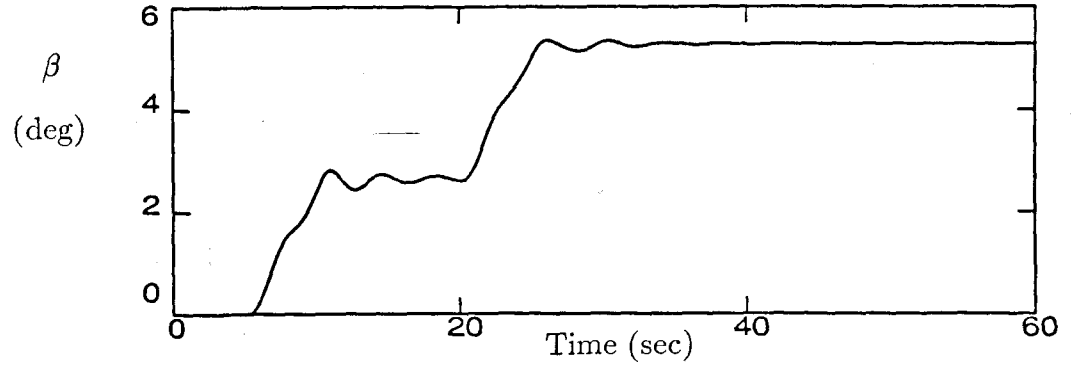

(c) Sideslip Angle

Figure 5.16: Simulation of high angle of attack instability for the generic jet fighter with sideslip feedback to the rudder, δe=-13, δr=-1β, V=266m/s.

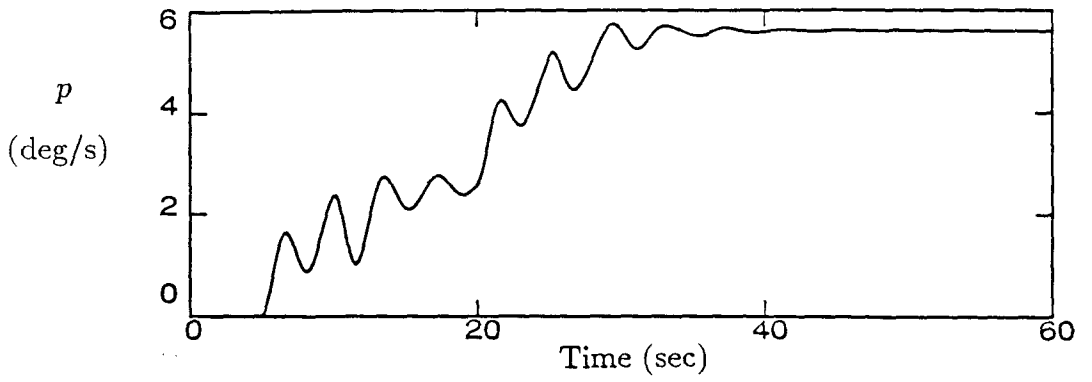

(d) Roll Rate

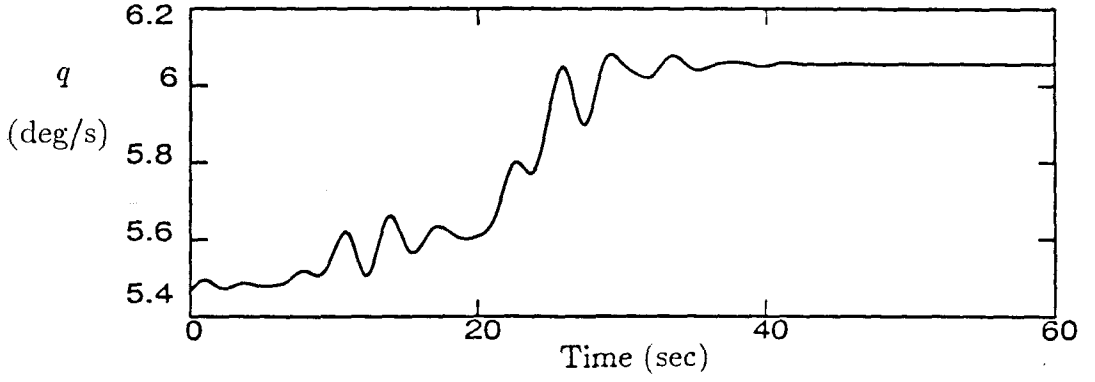

(e) Pitch Rate

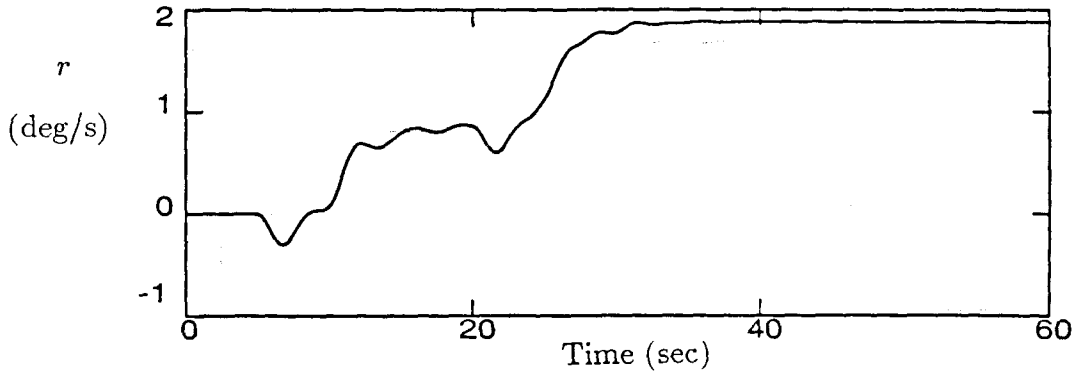

(f) Yaw Rate

Figure 5.16: Concluded.

While sideslip feedback to the rudder eliminates the saddle-node bifurcations at an elevator deflection of negative 13 degrees, saddle-node bifurcations still occur for higher elevator deflections. Figure 5.17 shows the loci of bifurcation for this aircraft when sideslip feedback is used. Comparing Figure 5.17 with Figure 5.14 (the bifurcation loci when feedback is not used) shows that the effect of feedback is to push the curve of saddle-node bifurcations to higher elevator deflections.

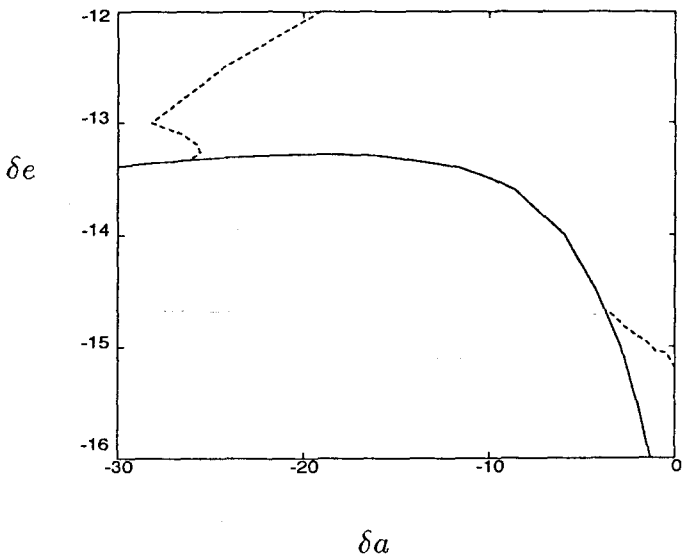

Figure 5.17: Bifurcation set for the generic jet fighter with sideslip feedback to the rudder, $\delta r = -1\beta$, V=266m/s; - - - Hopf bifurcation, —— saddle-node bifurcation.

5.2 Results for the Sixth Order Equations of Motion

The sixth order equations of motion were used to analyze the same aerodynamic model as in Section 5.1 to determine the effects of assuming constant velocity on the steady states of the aircraft. Constant velocity is often assumed in

the analysis of nonlinear aircraft dynamics, specifically the roll-coupling instability, in order to make the equations of motions more amenable to analysis. With continuation methods it is no more difficult to analyze the equations of motion including a variable velocity, which allows us to determine if and when the assumption of constant velocity is valid. A constant thrust to weight ratio of 0.12 will be used throughout this section. This thrust coefficient was chosen to match the velocity of 266m/s used in the fifth order equations of motion at the trim condition.

5.2.1 Existence of Multiple Steady States

The steady states of the fifth order equations of motion were used as starting points for the sixth order equations of motion in one of two ways. First the steady states of the fifth order equations of motion were tried with the thrust to weight ratio equal to 0.12 to see if the continuation algorithm would converge to a steady state of the sixth order system. This did not always work because the steady state spin modes of the fifth order system required large thrust to weight ratios and a thrust to weight ratio equal to 0.12 was not a close enough approximation to the true steady state of the sixth order system. The alternate approach was to use the thrust to weight ratio as the continuation parameter in the sixth order equations of motion and calculate the steady states of the sixth order system by starting at the steady states of the fifth order system.

This technique proved successful and all the steady states of the fifth order system were continued to steady states of the sixth order system. Figure 5.18 shows the steady states of the sixth order system as a function of elevator deflection for zero aileron and rudder deflections. Comparing Figures 5.18 and 5.1 shows that steady state rotation rates are much different for the fifth and sixth order systems, but the angles of attack and sideslip are essentially the same. It is clear that the velocity should be different between the two systems because of the large amounts of thrust required to keep the velocity constant in the fifth order system. This is especially true of the steady state spin modes (curves 2-6).

Different steady state velocities result in different steady state rotation rates because the velocity is a factor in the moment balance of the aircraft. For example, in a steady spin with high rotation rates the rolling and yawing moment balance for zero rudder and aileron deflection for this aerodynamic model is approximately

$$\begin{aligned} \frac{I_y - I_z}{I_x} qr &= -V \frac{\rho S b^2}{4 I_x} (p C_{\ell_p} + r C_{\ell_r}), \\ \frac{I_x - I_y}{I_z} pq &= -V \frac{\rho S b^2}{4 I_z} (p C_{n_p} + r C_{n_r}). \end{aligned} \tag{5.1}$$

The aerodynamic moments (right side of equation 5.1) are linearly proportional to the velocity so as the velocity is decreased the inertial moments must also decrease in order to maintain the moment balance. Reducing the rotation rates will further reduce the aerodynamic moments, but this is a linear effect while the inertial moments have a quadratic dependence on the rotation rates. Note that neither the fifth or sixth order equations of motion will give the correct steady

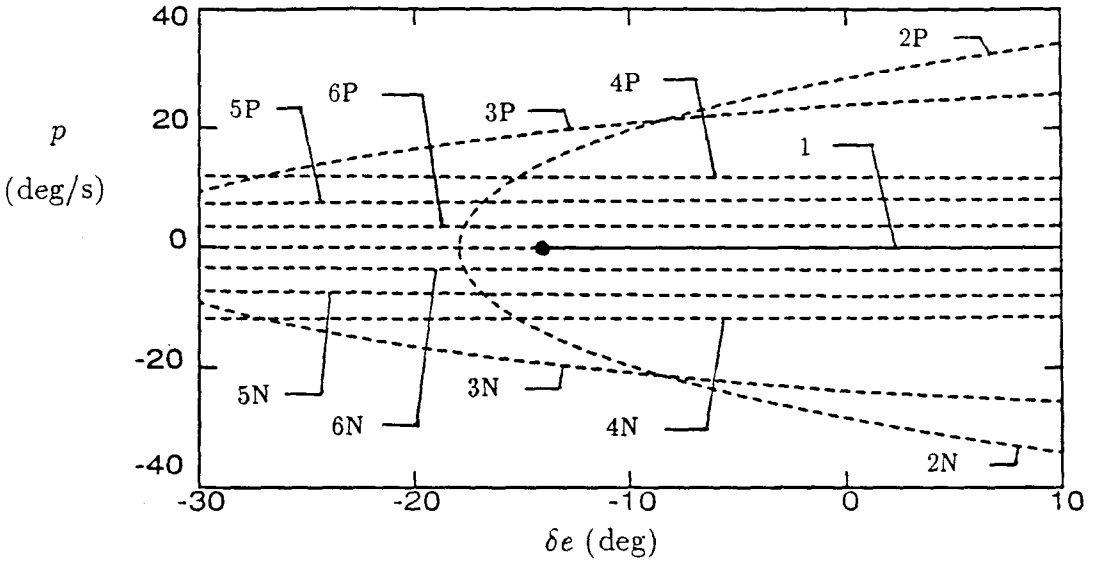

(a) Roll Rate

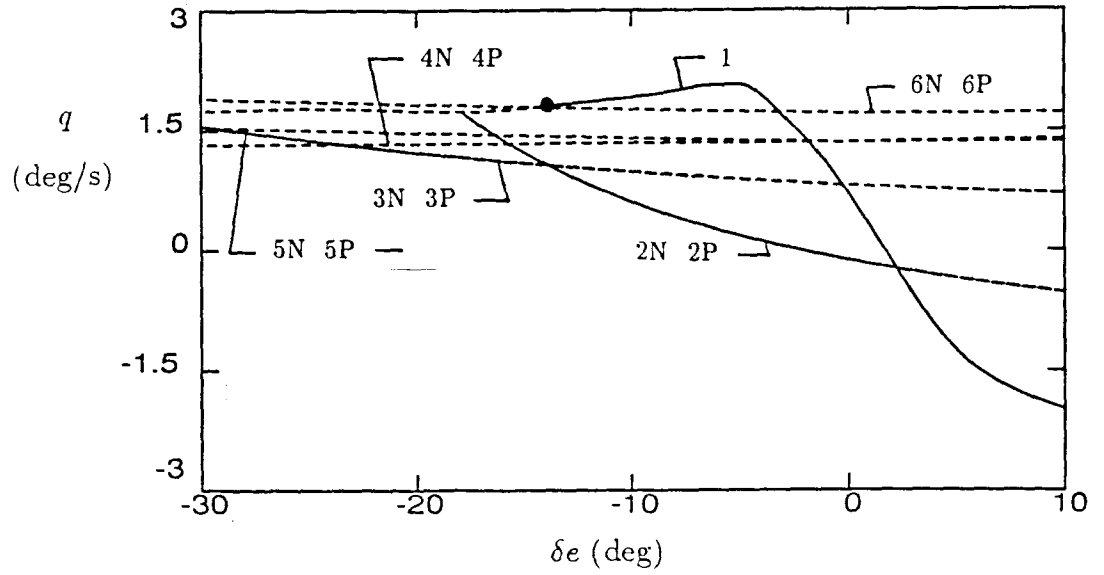

(b) Pitch Rate

Figure 5.18: Steady states for the generic jet fighter, T/W=0.12, δa=0, δr=0; —— stable, - - - unstable, • - Hopf bifurcation.

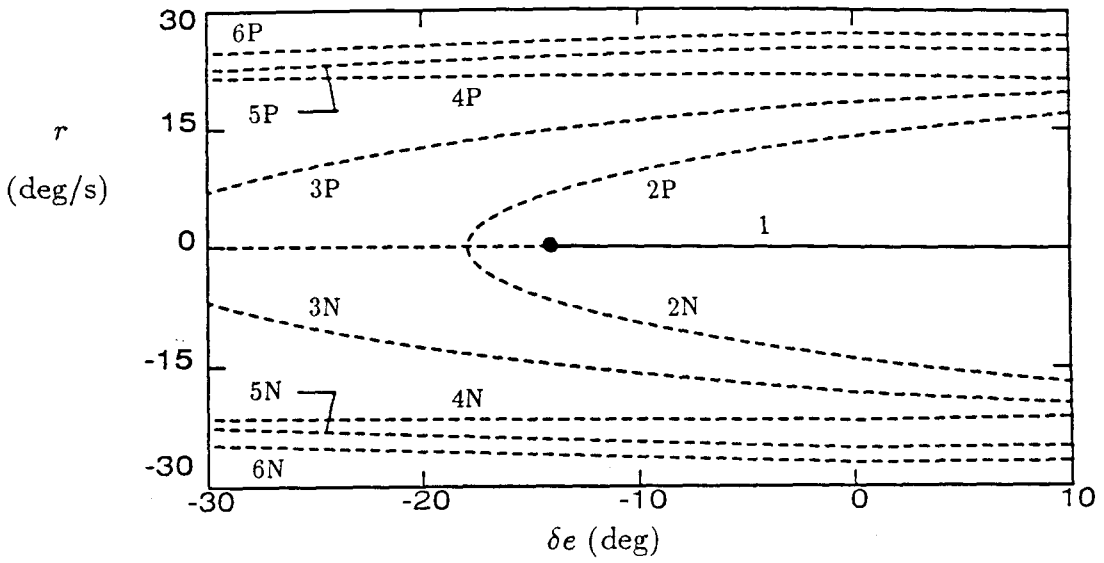

(c) Yaw Rate

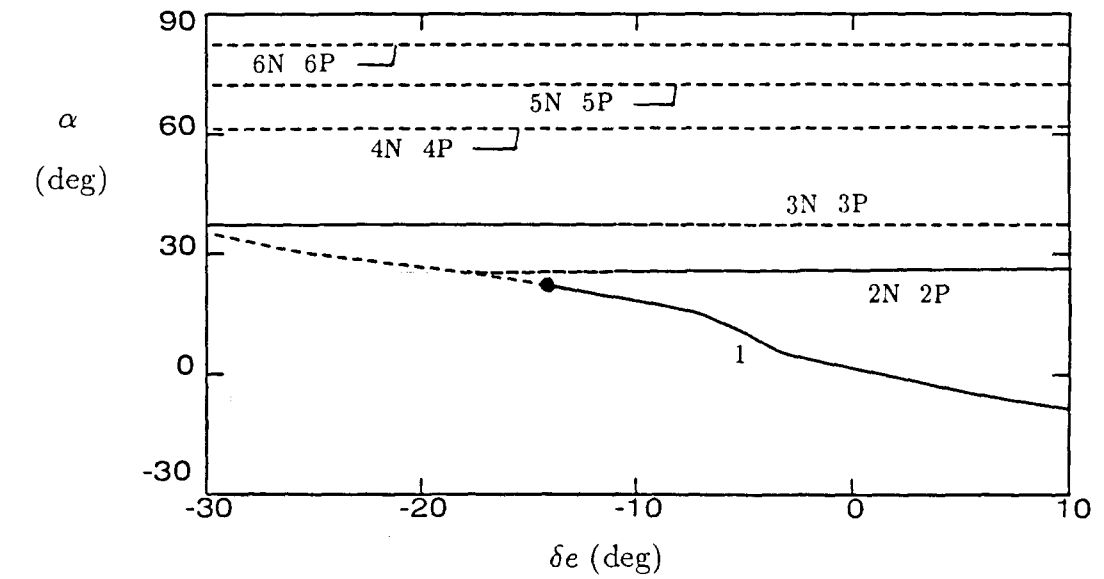

(d) Angle of Attack

Figure 5.18: Continued.

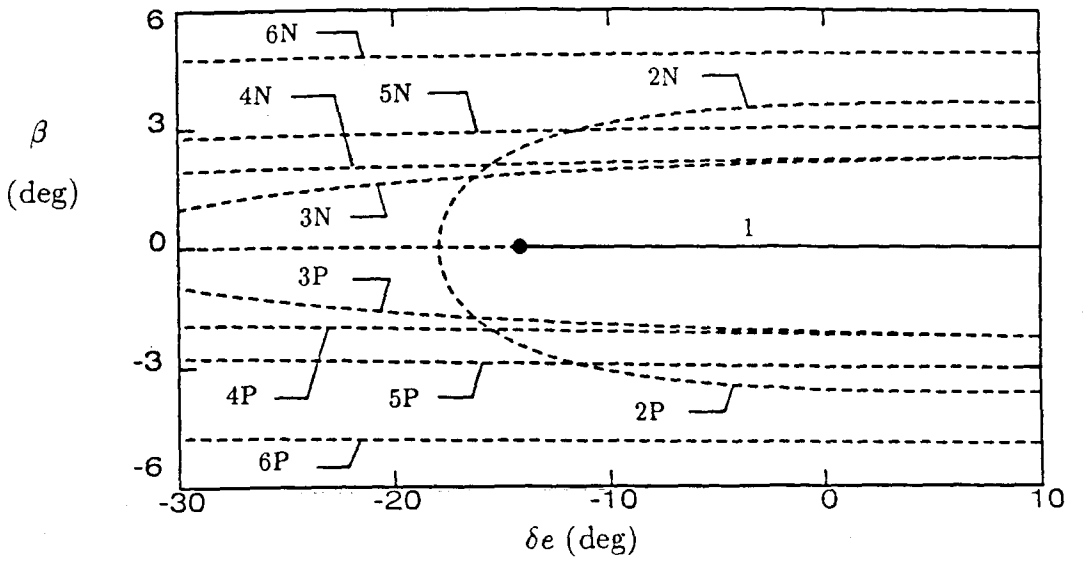

(e) Sideslip Angle

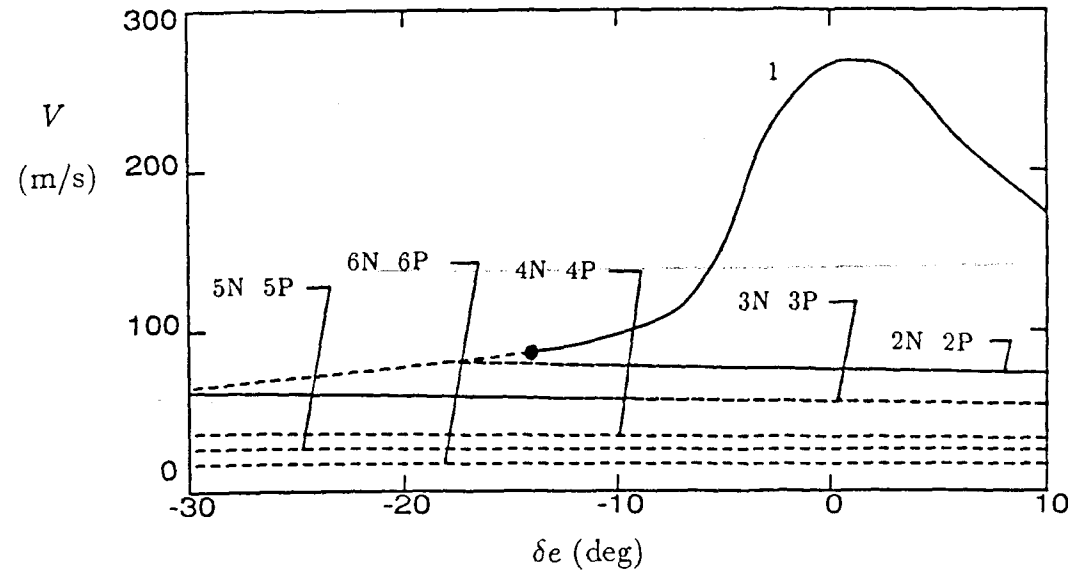

(f) Speed

Figure 5.18: Concluded.

state spin modes because gravity must be included to determine the true velocity of the aircraft (see Section 5.3).

The differences between the steady state velocity of the longitudinal motions (curve 1) of the fifth and sixth order systems are small at low angles of attack but become significant at high angles of attack. This was expected because the thrust was chosen to match the steady state speed of the fifth and sixth order systems at low angles of attack. Lower steady state velocities for the sixth order system results in lower steady state pitch rates. This can be seen for purely longitudinal motions (neglecting gravity) by examining the force balance of the aircraft. For purely longitudinal motions (i.e., $p = r = \beta = 0$) the force balance in the direction normal to the velocity is

$$q + V\frac{\rho S}{2M}(C_z(\alpha)\cos\alpha - C_x(\alpha)\sin\alpha) = 0.$$

Thus for a given angle of attack, the steady state pitch rate is proportional to the velocity. The steady angle of attack is the same for purely longitudinal steady states of the fifth and sixth order systems because it is determined by the balance of pitching moments

$$C_m(\alpha) + \delta e C_{m_{\delta e}}(\alpha) = 0,$$

which does not involve the velocity. Note that the damping in pitch, (qC_{m_q}), is generally small for longitudinal steady states and has a minor effect on the pitching moment balance.

5.2.2 Roll-Coupling Instabilities

Figure 5.19 shows the steady states of the sixth order system as a function of aileron deflection for the same elevator deflection that was used to study the roll-coupling instability for the fifth order system (see Figure 5.5). Comparing Figures 5.19 and 5.5 shows that the steady states of the fifth and sixth order systems are almost the same. This happens because the velocity does not change much as the aileron deflection is increased (see Figure 5.19(f)). Where the velocity does change, the general effect is that increases in the velocity cause increases in the rotation rates and no changes in the angles of attack and sideslip. This behavior can be explained by analyzing the force and moment balance of the aircraft.

As discussed earlier, the pitch rate is determined by the force balance in the direction normal to the velocity and is linearly proportional to the velocity. The steady state roll rate for low angle of attack flight is approximately determined by the rolling moment balance (see Figure 5.6)

$$\delta a C_{\ell_{\delta a}}(\alpha) + \frac{b}{2V} p C_{\ell_p}(\alpha) = 0,$$

so the roll rate is linearly proportional to the velocity for a given angle of attack. Also recall from Figure 5.6 that for large aileron deflections the main component of the pitching moment balance is

$$\frac{I_z - I_x}{I_y} pr + V^2 \frac{\rho S c}{2 I_y} \delta e C_{m_{\delta e}}(\alpha) = 0,$$

so if the roll rate is linearly proportional to the velocity, then the yaw rate is also linearly proportional to the velocity.

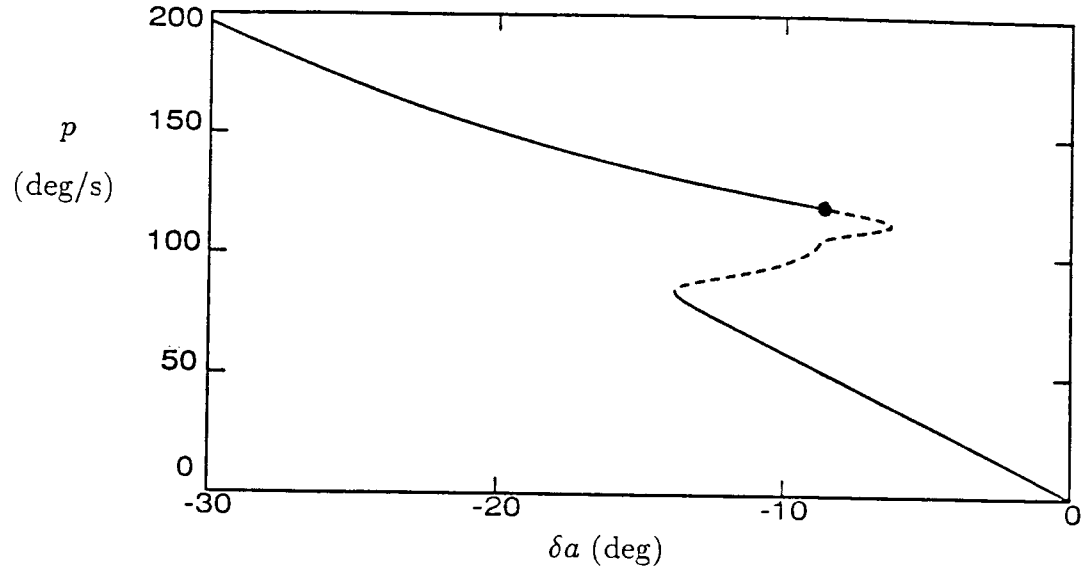

(a) Roll Rate

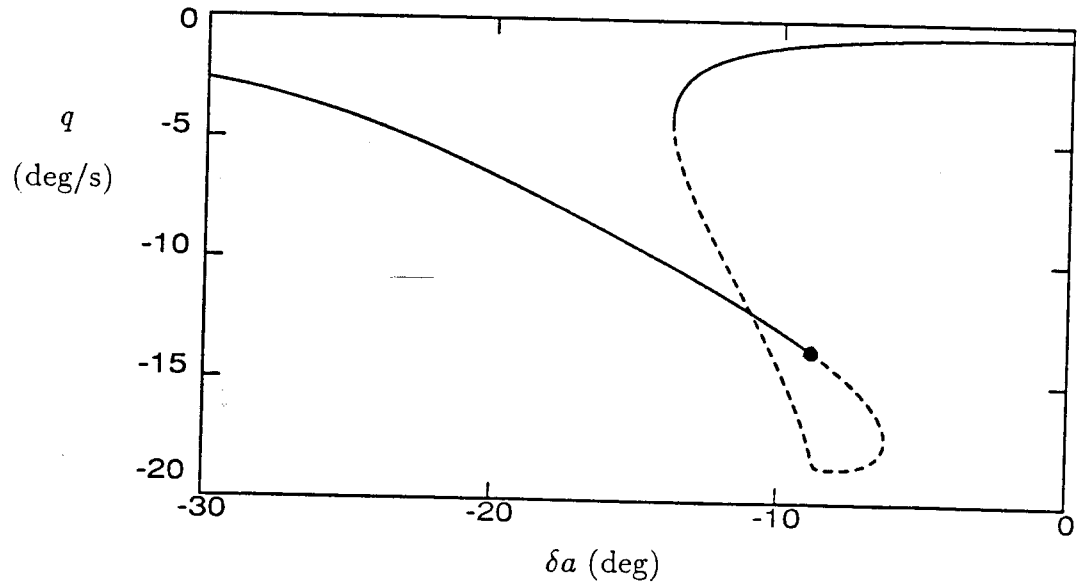

(b) Pitch Rate

Figure 5.19: Steady states for the generic jet fighter, T/W=0.12, δe=3, δr=0; —— stable, - - - unstable, • – Hopf bifurcation.

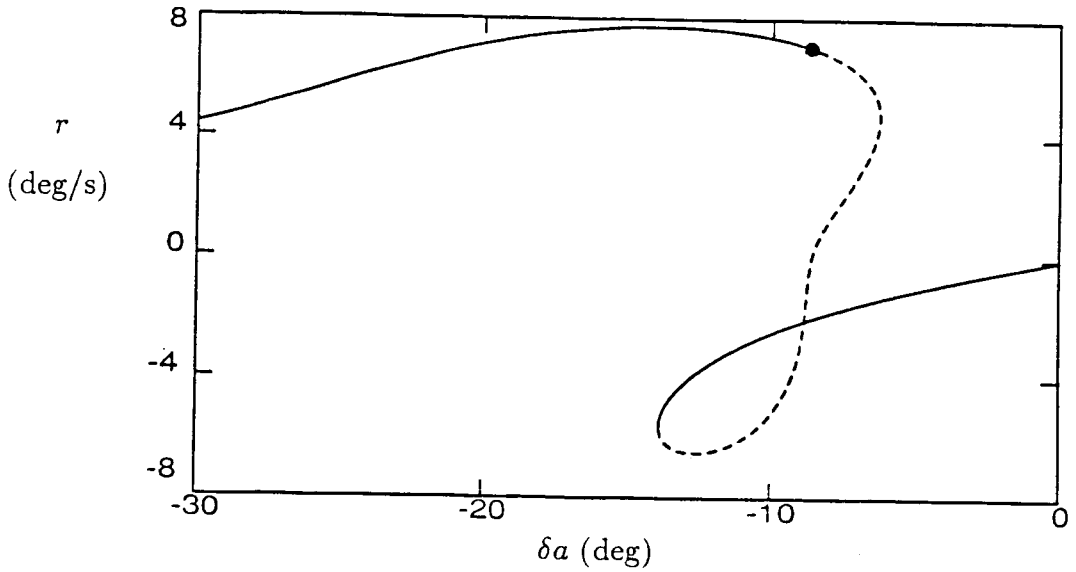

(c) Yaw Rate

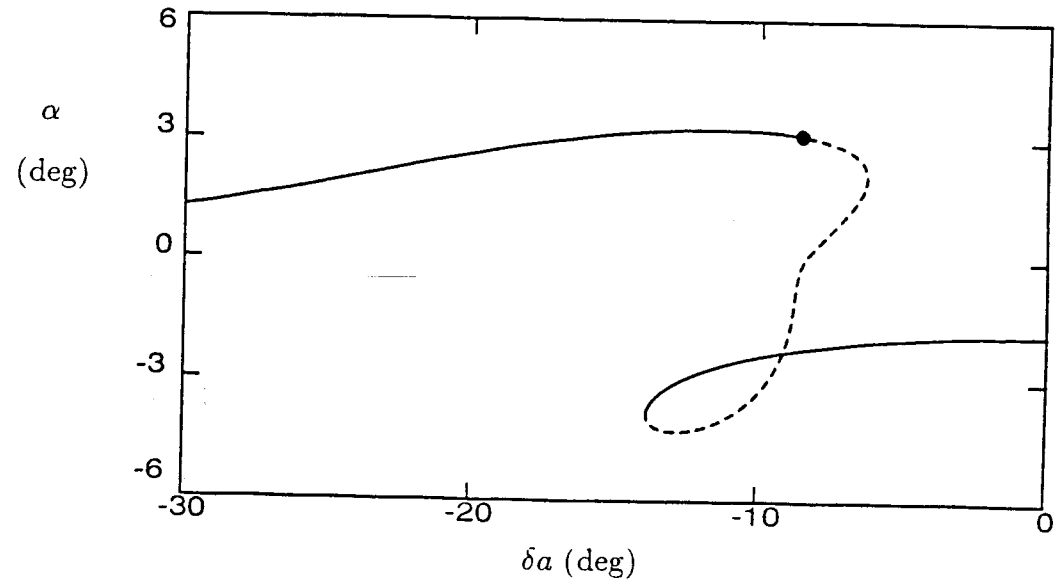

(d) Angle of Attack

Figure 5.19: Continued.

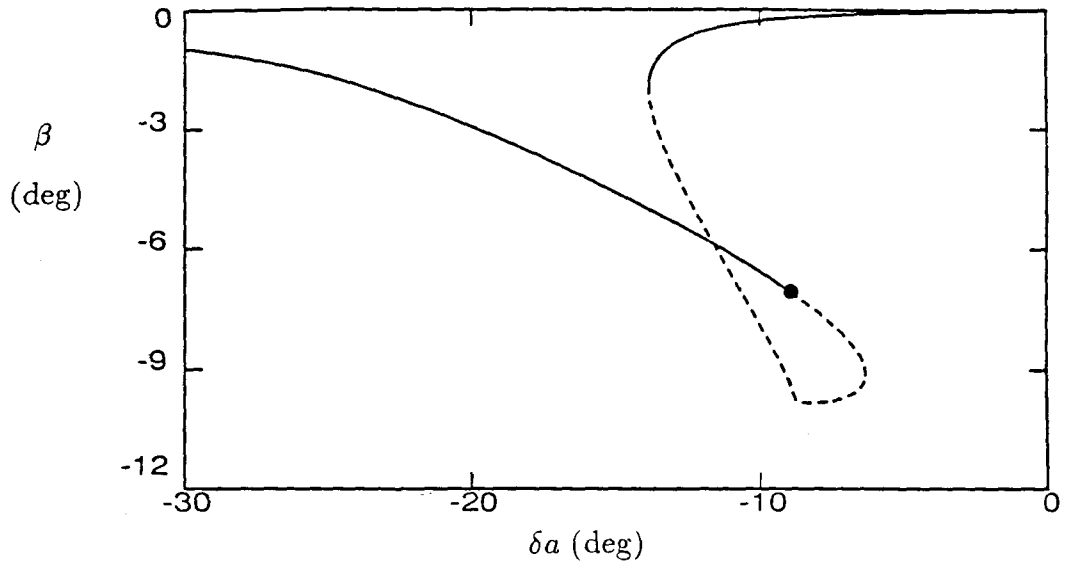

(e) Sideslip Angle

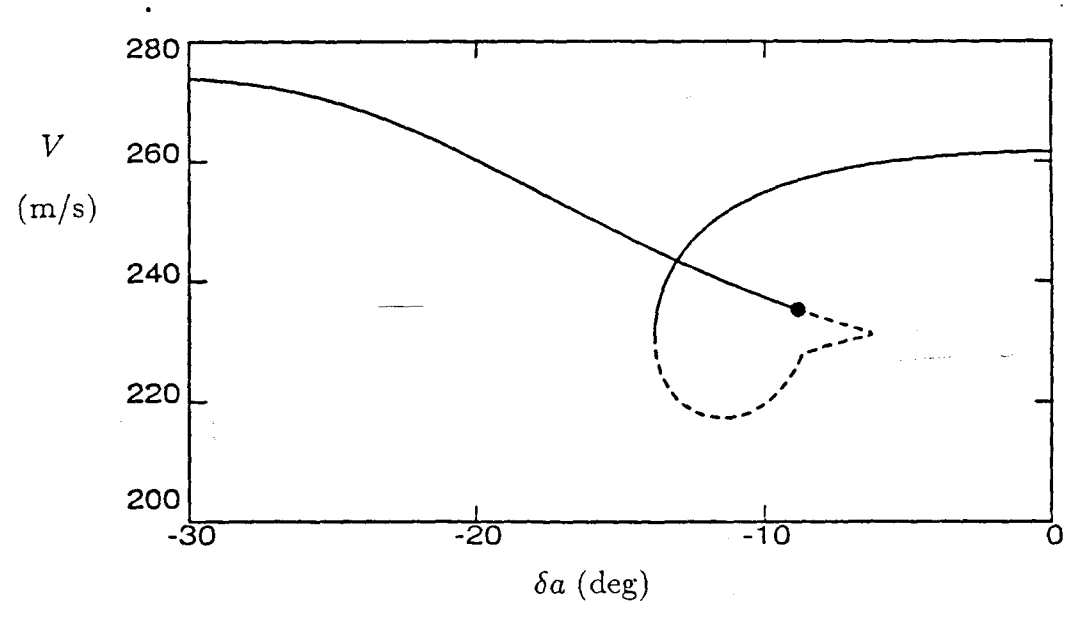

(f) Speed

Figure 5.19: Concluded.

The saddle-node and Hopf bifurcations occur at the same aileron deflections for the fifth and sixth order equations of motion. Figure 5.20 shows the elevator and aileron deflections that cause bifurcations for the sixth order system with zero rudder deflection. Figure 5.8 is the equivalent diagram for fifth order equations of motion. Comparing Figures 5.8 and 5.20 shows that the bifurcations occur for the same control surface deflections in the fifth and sixth order equations of motion. Since the steady state rotation rates are slightly different for the fifth and sixth order systems while the angles of attack and sideslip are the same, it seems that the angles of attack and sideslip are the dominant factors in determining the critical control surface deflections at which the bifurcations occur.

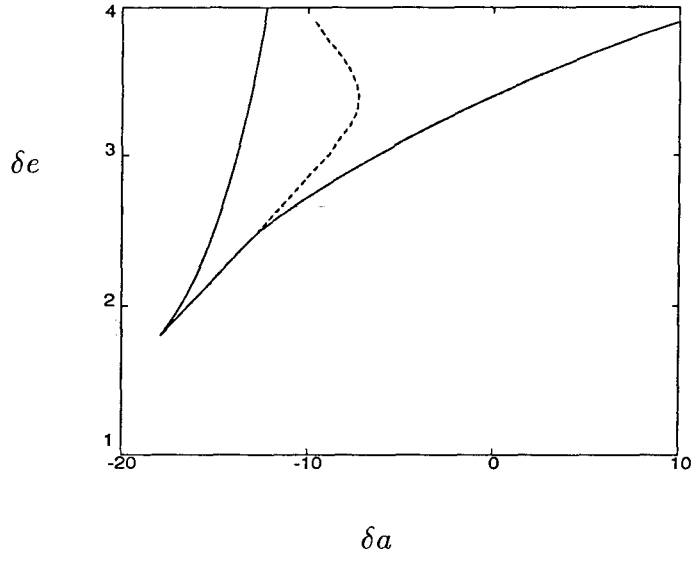

Figure 5.20: Bifurcation set for the generic jet fighter for T/W=0.12, $\delta r = 0$; – – – Hopf bifurcation, —— saddle-node bifurcation.

The angle of attack is probably the most important factor because the change in sign of the angle of attack as the aileron deflection is increased causes a fundamental change in the motion of the aircraft. For negative angles of attack the aircraft is in an inverted spin while for positive angles of attack the aircraft is in an upright spin. Also note that roll-coupling instabilities did not occur for rolls from pitch up conditions, which have positive angles of attack. These results show that analyzing the roll-coupling instability with the fifth and sixth order equations of motion gives the same critical control surface deflections. Slightly different steady states are determined for each system, but the qualitative nature of the motion is the same.

5.2.3 High Angle of Attack Dynamics

Figure 5.21 shows the steady states as a function of aileron deflection for two pitch up conditions. The same elevator deflections were used to study the high angle of attack dynamics with the fifth order equations of motion (see Figure 5.12). Comparing Figures 5.12 and 5.21 shows that the steady states are similiar for the fifth and sixth order systems even though the flight speeds are very different. This difference in flight speeds produces slightly different rotation rates, but the angles of attack and sideslip are essentially the same. Since the high angle of attack dynamics for this aircraft are dominated by the loss of directional stability, which depends on the angle attack, the saddle-node bifurcations occur at the same aileron deflections for the fifth and sixth order systems.

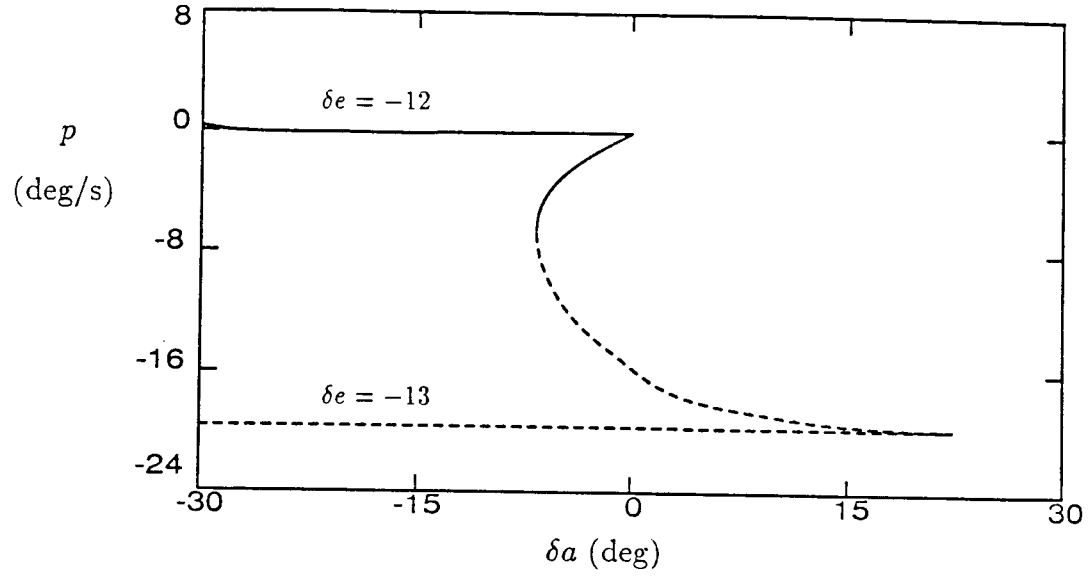

(a) Roll Rate

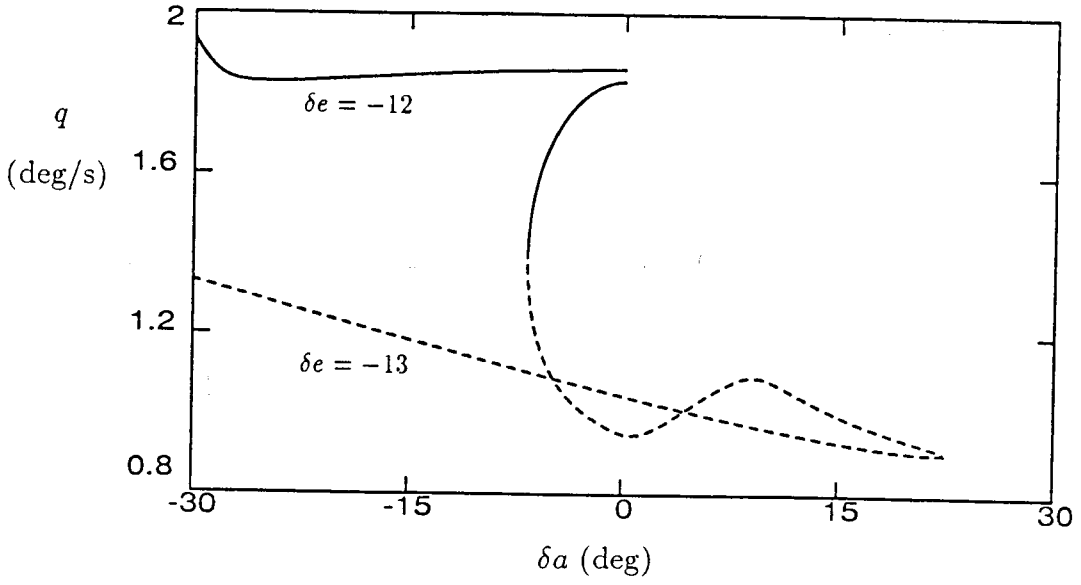

(b) Pitch Rate

Figure 5.21: Steady states for the generic jet fighter, T/W=0.12, δe=-12,-13, δr=0; —— stable, - - - unstable.

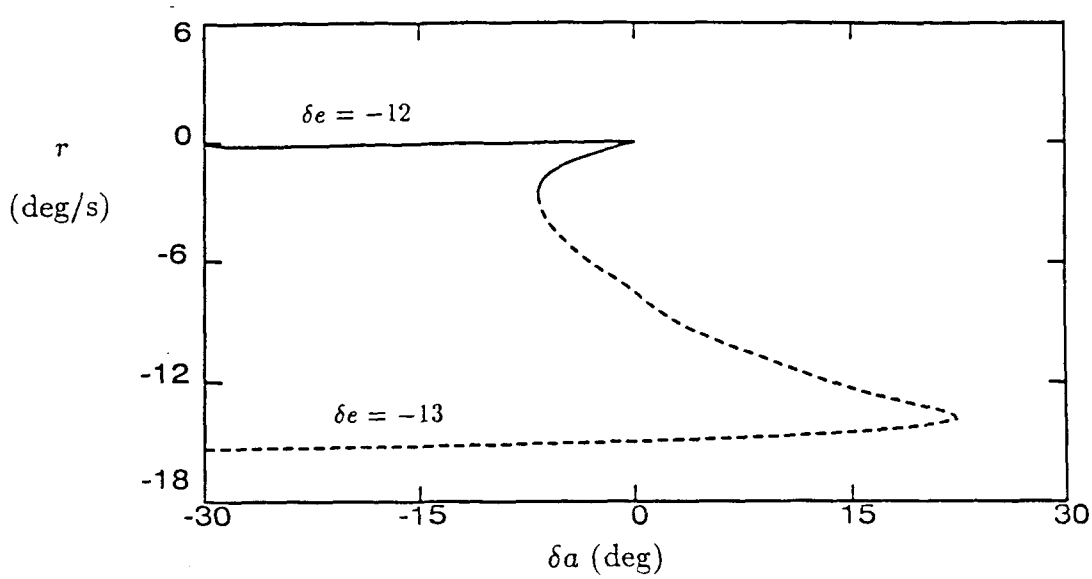

(c) Yaw Rate

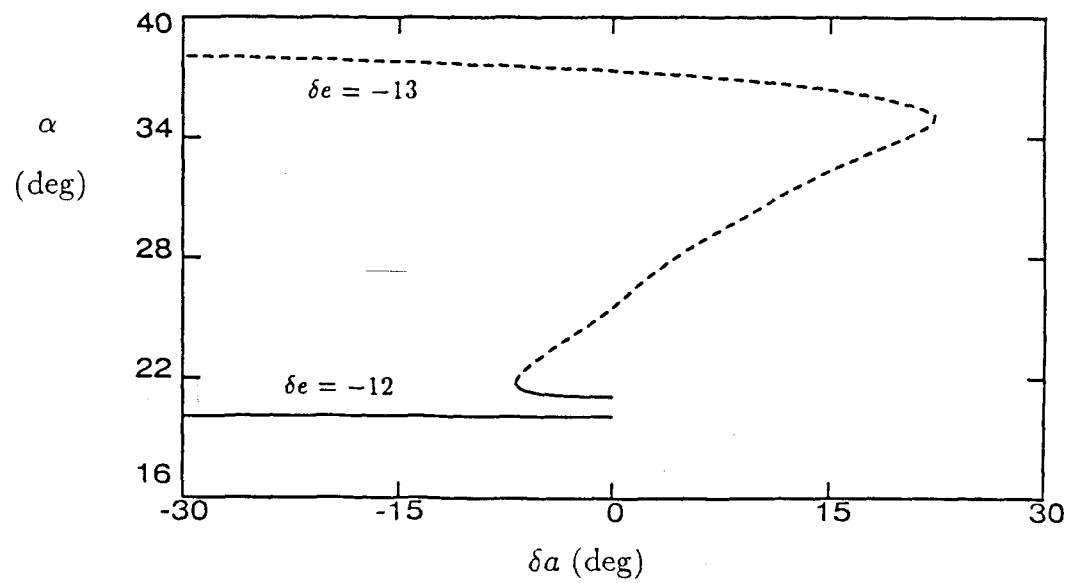

(d) Angle of Attack

Figure 5.21: Continued.

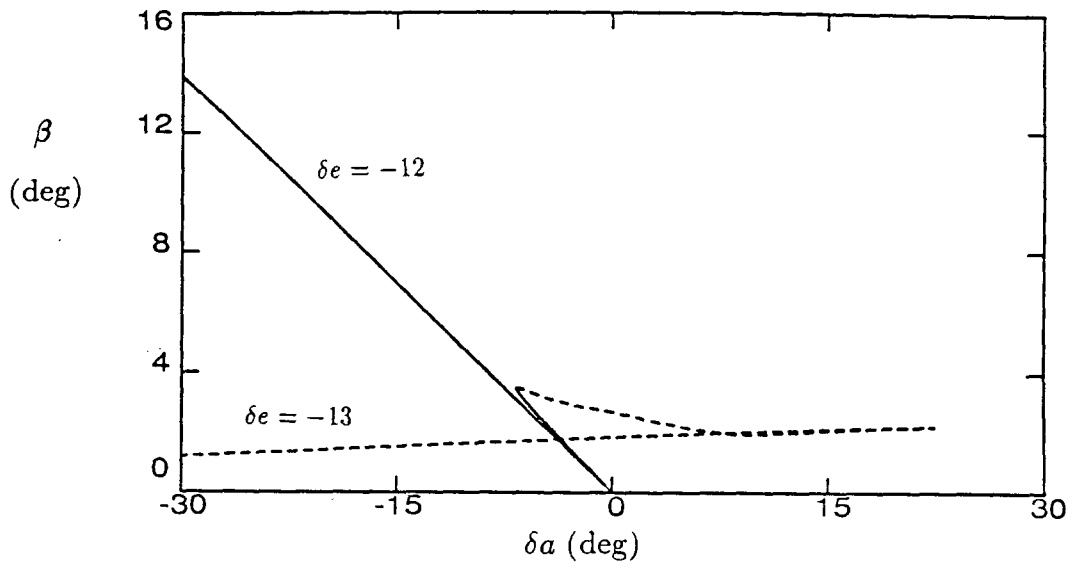

(e) Sideslip Angle

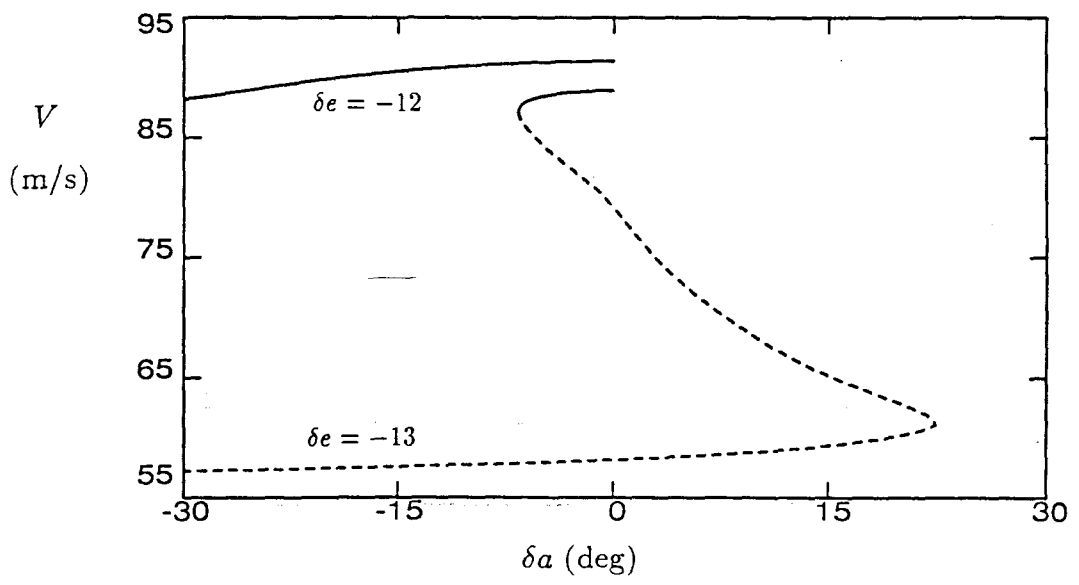

(f) Speed

Figure 5.21: Concluded.

The bifurcation loci for the sixth order system is shown in Figure 5.22. This figure is practically the same as Figure 5.8, which shows the bifurcation loci for the fifth order system. These results imply that the velocity has a minor effect on high angle of attack instabilitites and that the fifth and sixth order equations of motion give the same results. Note that Mach number effects were not included in this aerodynamic model, so any statements about the velocity only apply to low speed flight (Mach numbers less than 0.60).

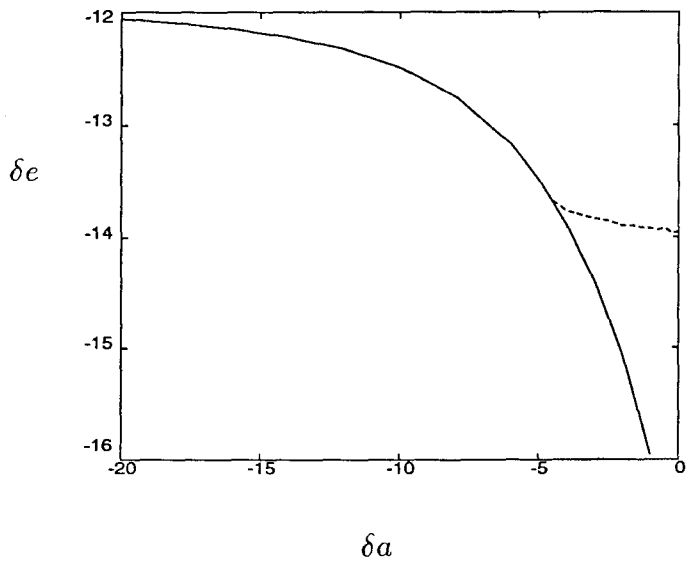

Figure 5.22: Bifurcation set for the generic jet fighter for T/W=0.12 and $\delta r = 0$; - - - Hopf bifurcation, —— saddle-node bifurcation.

5.3 Results for the Eighth Order Equations of Motion

Steady states of the eighth order equations of motion were determined to study the effect of gravity on the roll-coupling and high angle of attack instabilities.

Including gravity allows us to determine the Euler angles, so the orientation of the aircraft can be determined. The steady state velocity of the aircraft predicted with the eighth order equations will differ from the values for both the fifth and sixth order equations of motion. The thrust to weight ratio will be 0.12 for all of the following results.

5.3.1 Existence of Multiple Steady States

Starting points for the continuation method were determined by using gravity as a continuation parameter and extending the steady states of sixth order equations of motion (g=0) to steady states of the eighth order equations of motion (g=9.81m/s^2). Using this procedure, the eleven branches of steady states of the sixth order system were all extended to steady states of the eighth order system. Figure 5.23 shows the branches of steady states as a function of elevator deflection for zero aileron and rudder deflections. Several differences are evident between these steady states and the steady states of the fifth and sixth order systems (see Figures 5.1 and 5.18). Differences are particularly evident in the spin modes (curves 2-6).

Differences between the steady state spin modes of the three systems are a result of different steady state velocities. Comparing Figures 5.23, 5.18, and 5.1 shows that the velocities of the steady spin modes of the fifth order equations of motion are too large and the velocities of the steady spin modes of the sixth order equations of motion are too small (relative to the spin modes of the eighth order

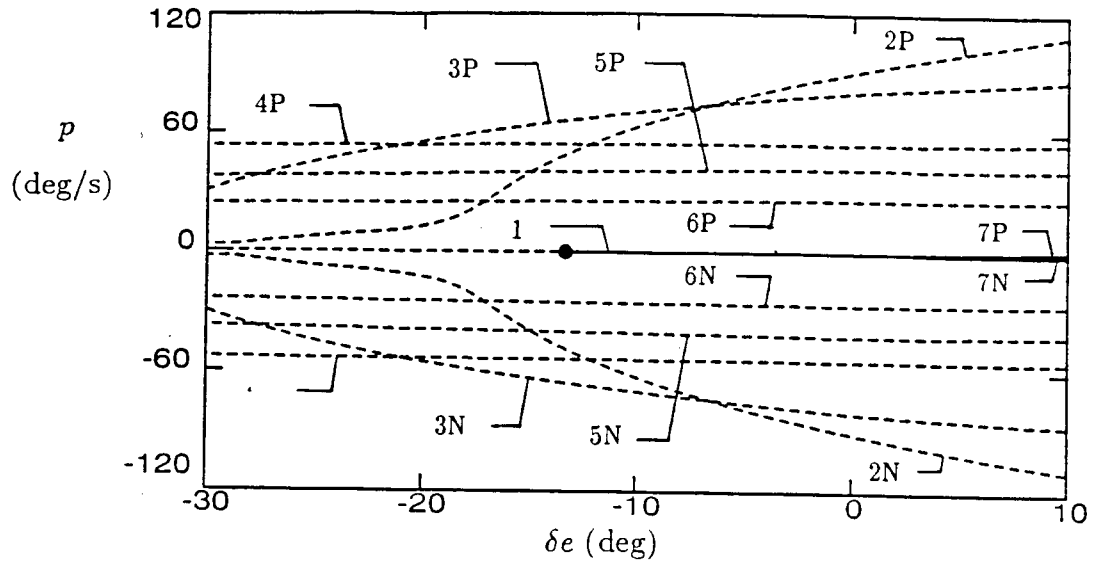

(a) Roll Rate

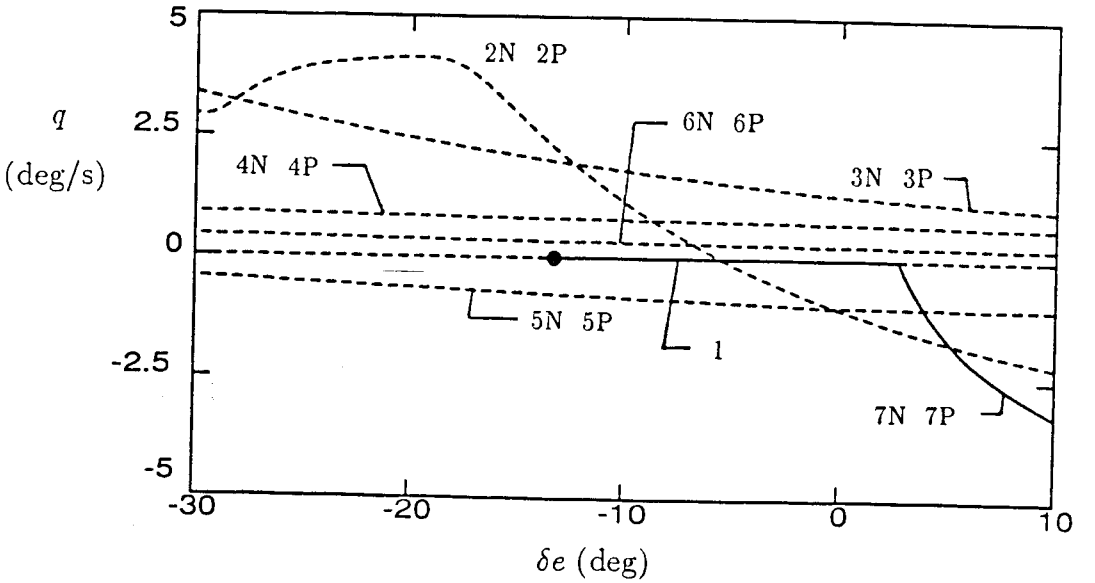

(b) Pitch Rate

Figure 5.23: Steady states for the generic jet fighter, T/W=0.12, δa=0, δr=0; —— stable, - - - unstable, • – Hopf bifurcation.

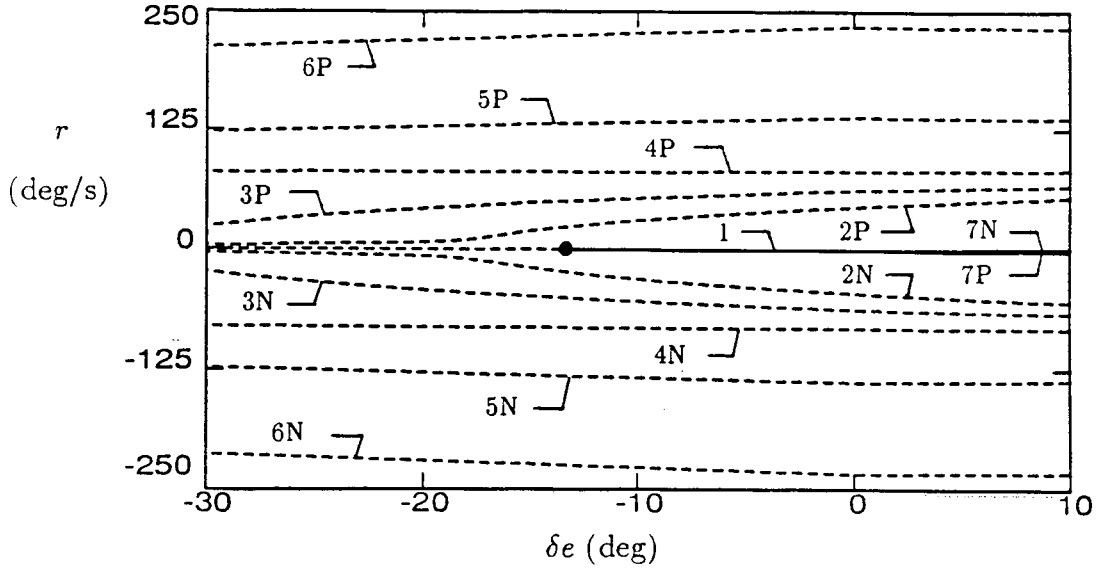

(c) Yaw Rate

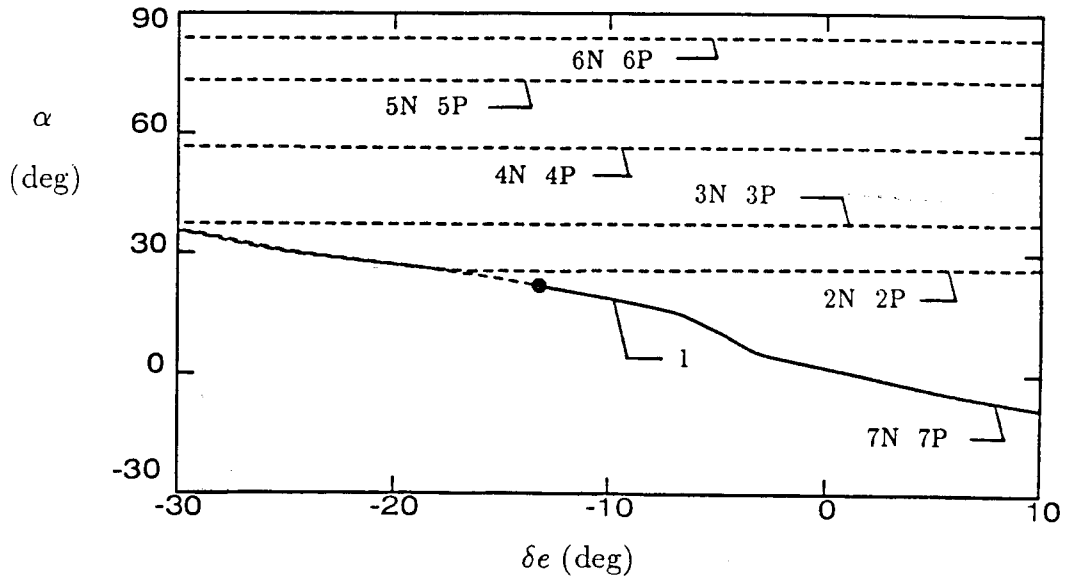

(d) Angle of Attack

Figure 5.23: Continued.

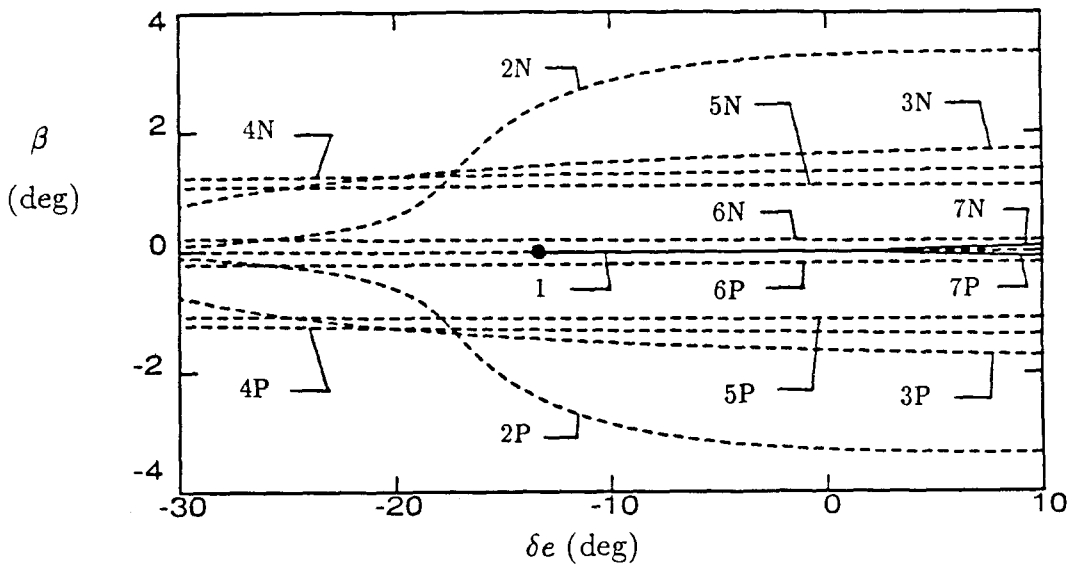

(e) Sideslip Angle

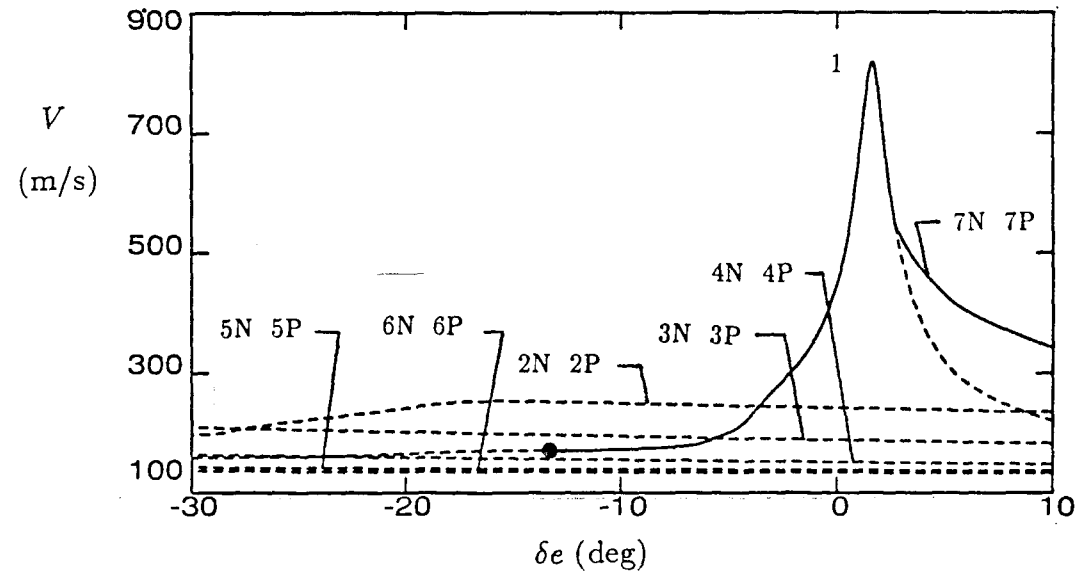

(f) Speed

Figure 5.23: Continued.

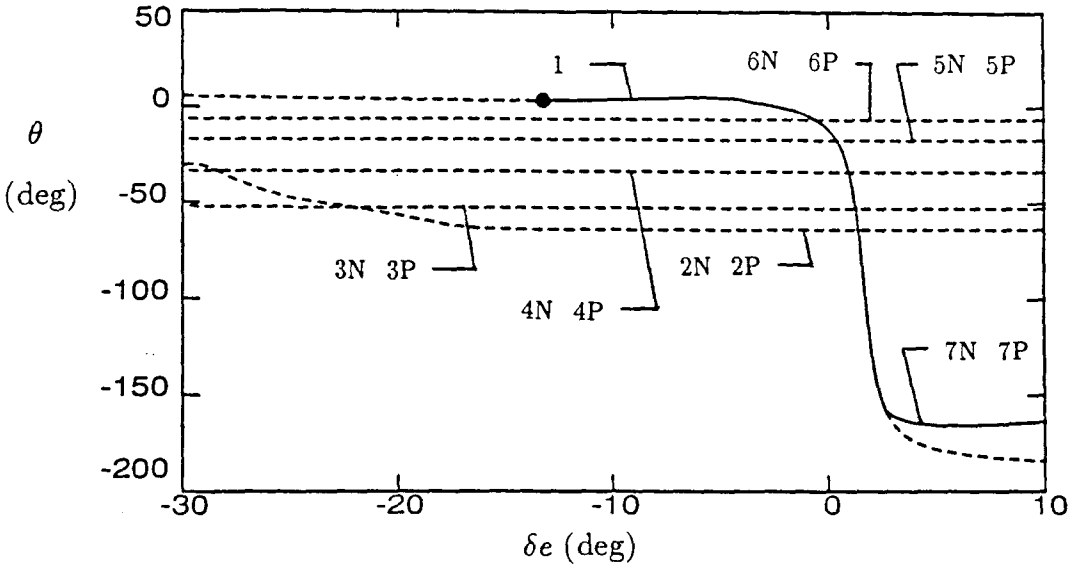

(g) Pitch Angle

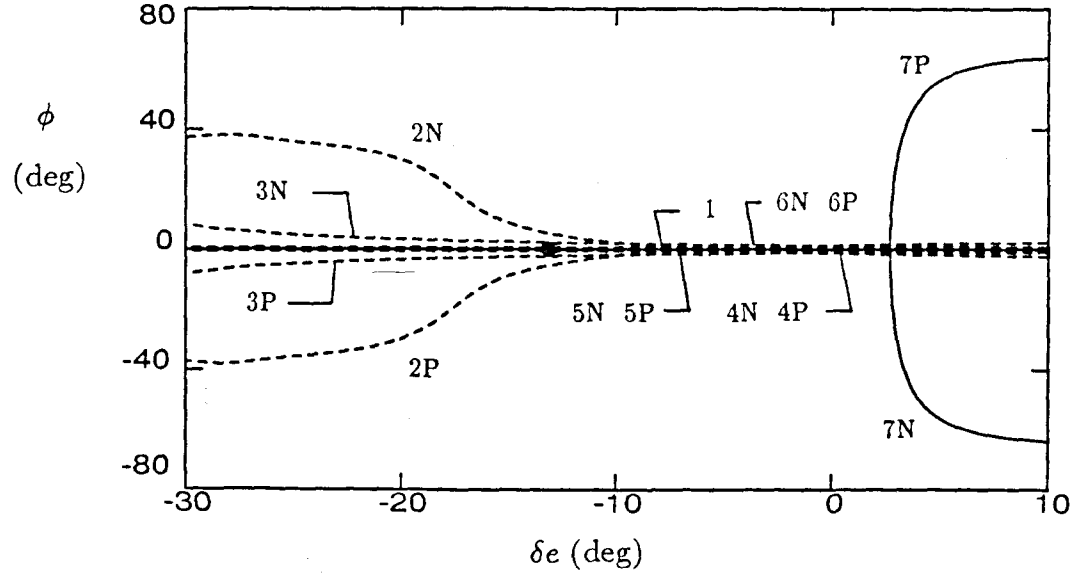

(h) Roll Angle

Figure 5.23: Concluded.

equations of motion). This results in steady state rotation rates for the fifth order system which are too large and steady state rotation rates for the sixth order system which are too small. The steady state velocity of each spin mode of the eighth order system (Figure 5.23, curves 2-6) is relatively constant, so either the fifth or sixth order equations of motion could be used to analyze the spin modes if the proper velocity or thrust coefficient were specified.

The steady state angles of attack for the spin modes of each system are essentially the same, with differences of one or two degrees for the flat spin modes (curves 5 and 6). Steady state sideslip angles are also a few degrees different for the flat spin modes of each system. Steady states of the eighth order system also include the roll and pitch angles (ϕ and θ) so the orientation of the aircraft and its flight path angle ($\gamma = \theta - \alpha$) can be determined. All of the spin modes have flight path angles of negative 90 degrees, which is typical of spins. The bank angles of all the spins modes are small.

A branch of steady states was found for the eighth order equations of motion that does not exist for the fifth or sixth order equations of motion. This branch of steady states (curve 7) intersects the branch of purely longitudinal steady states (curve 1) at a pitchfork bifurcation for an elevator deflection of positive 2.7 degrees (see Figure 5.23(h)). The pitchfork bifurcation causes the purely longitudinal steady states (curve 1) to become unstable for elevator deflections greater than positive 2.70, while the steady states represented by curve 7 are all stable. Steady states of curve 7 represent spirally divergent motions. The rotation rates are all

of the order of a few degrees per second so the aircraft will slowly diverge from a straight flight path.

5.3.2 Roll-Coupling Instabilities for the Eighth Order Equations of Motion

Several differences are evident between the purely longitudinal steady states of the eighth order equations of motion and the purely longitudinal steady states for the fifth and sixth order equations of motion (see Figures 5.1, 5.18, and 5.23) which could affect the roll-coupling behavior of the aircraft. Recall that for the fifth and sixth order equations of motion roll-coupling instabilities occurred for elevator deflections from positive 1.8 degrees to positive 4 degrees. For this range of elevator deflections, the purely longitudinal steady states of the eighth order equations of motion have very large velocities. These steady state velocities are physically unrealistic because no Mach number effects have been included in the aerodynamic model.

The steady state velocities become large for this range of elevator deflections because the aircraft goes into a steep dive. This can be seen by examining Figure 5.23(g) which shows the steady state pitch angles. For elevator deflections between negative 30 and zero degrees, the steady state pitch angles of the purely longitudinal motions (curve 1) are relatively constant and equal to about positive 5 degrees, but for elevator deflections between zero and positive 3 degrees, the steady state pitch angle goes from zero to negative 160 degrees. Thus the

aircraft goes from level flight into a steep dive and finally inverted flight. Recall that roll-coupling instabities occur at negative angles of attack (see Sections 5.1.2 and 5.2.2) which require the aircraft to be in inverted flight.

It is not clear how physically relevant this flight regime is, because pilots do not generally fly inverted and initiating high roll rate maneuvers from inverted flight is probably even less common. No known work has discussed the orientation of the aircraft during roll-coupling instabilities, because the effect of gravity is usually ignored or treated as a small perturbation, so steady state Euler angles could not be computed. We will now discuss results for the roll-coupling instability when the effects of gravity are included in the equations of motion.

Figure 5.24 shows the steady states as a function of aileron deflection for an elevator deflection of 3 degrees and zero rudder deflection. These are the same control surface deflections that were used to study the roll-coupling instability with the fifth order equations of motion (see Figure 5.5) and the sixth order equations of motion (see Figure 5.19). Comparing the steady states of the three sets of equations shows that the steady state angles of attack and sideslip are essentially the same for each set of equations even though the steady state velocity of the eighth order equations of motion is of the order of 800m/s. This large difference in the steady state velocities causes the steady state rotation rates of the eighth order equations of motion to be much larger than the steady state rotation rates of the fifth or sixth order equations of motion.

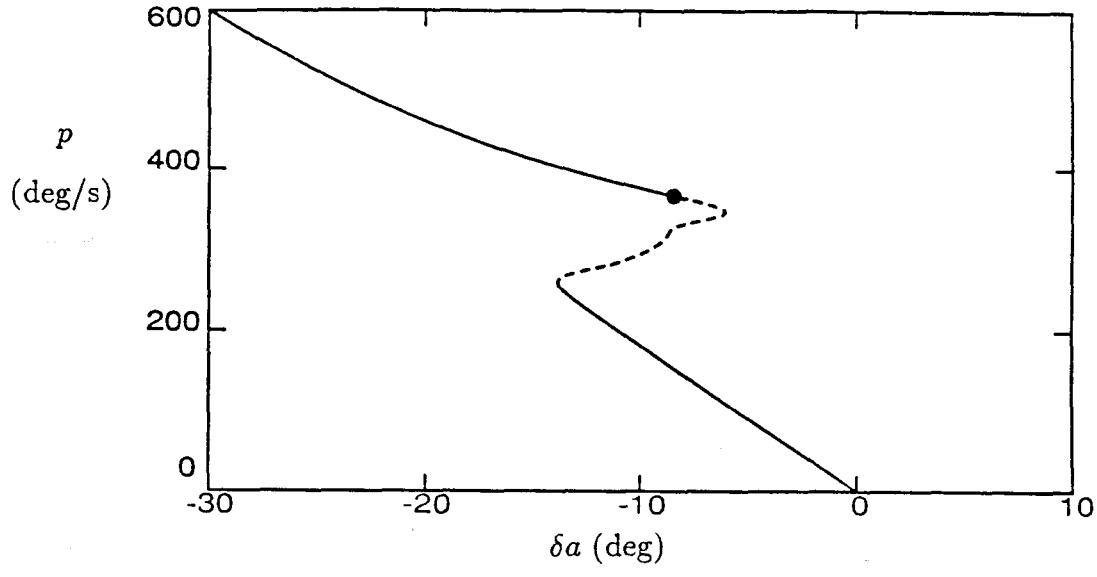

(a) Roll Rate

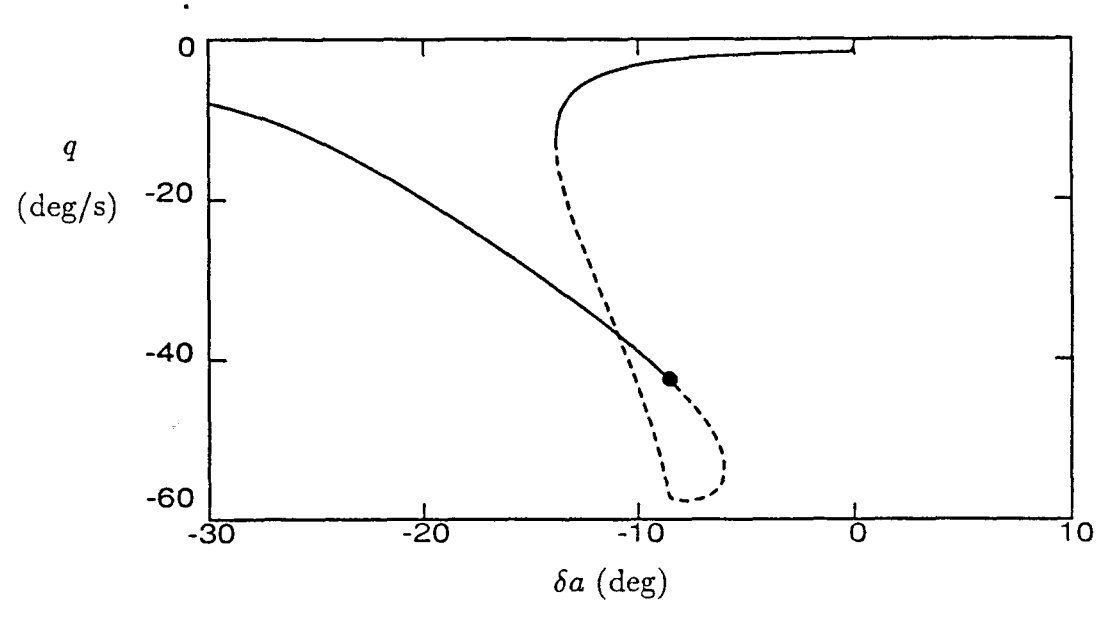

(b) Pitch Rate

Figure 5.24: Steady states for the generic jet fighter, T/W=0.12, δe=3, δr=0; —— stable, – – – unstable, • – Hopf bifurcation.

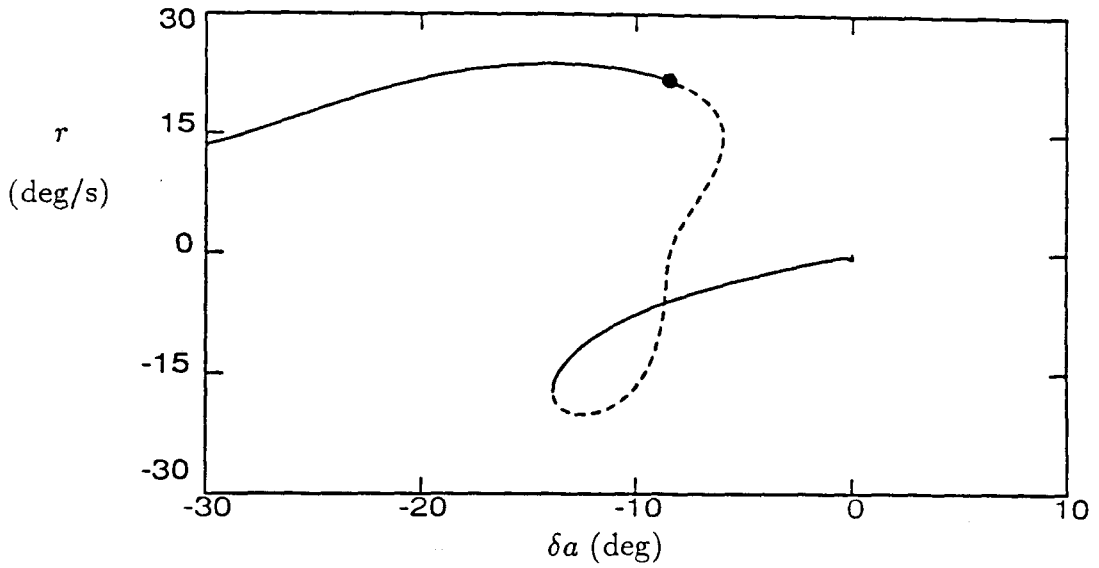

(c) Yaw Rate

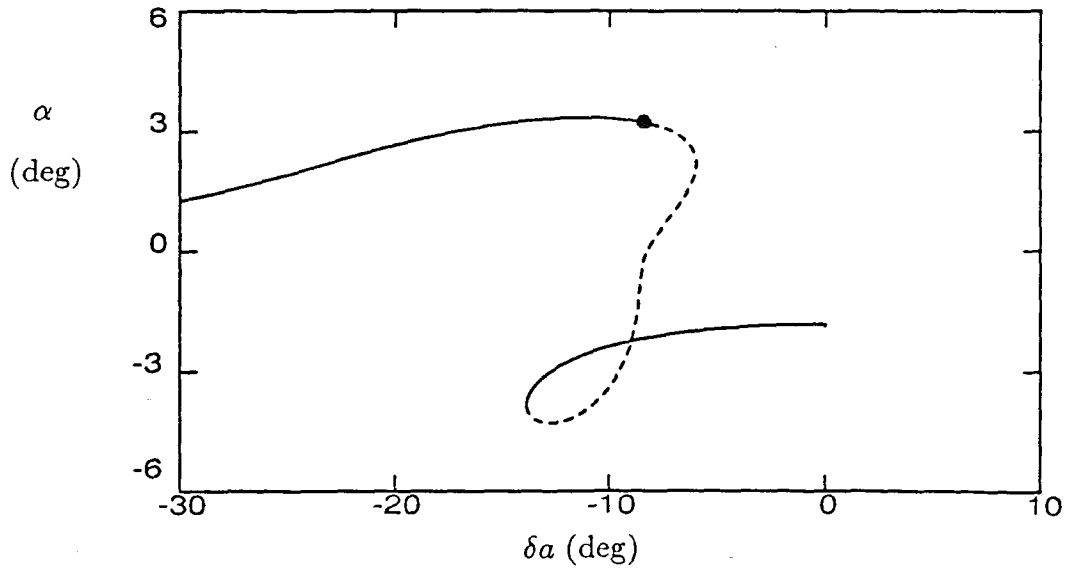

(d) Angle of Attack

Figure 5.24: Continued.

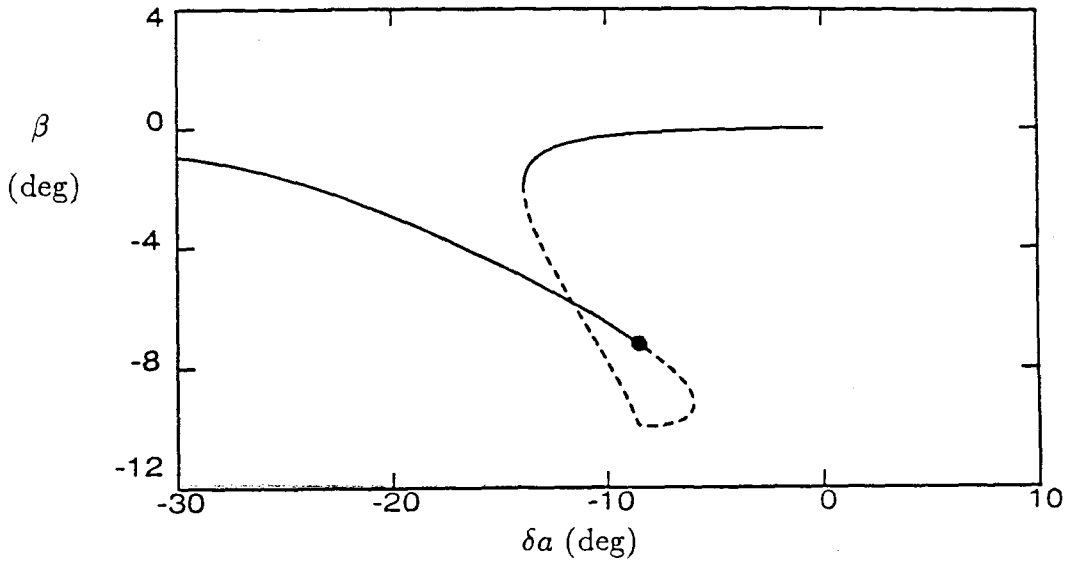

(e) Sideslip Angle

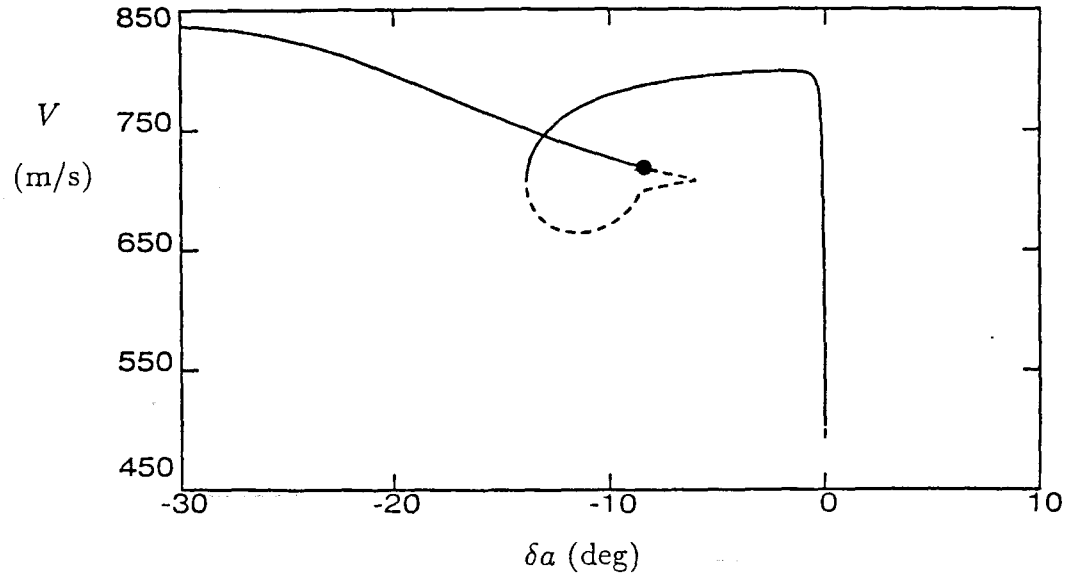

(f) Speed

Figure 5.24: Continued.

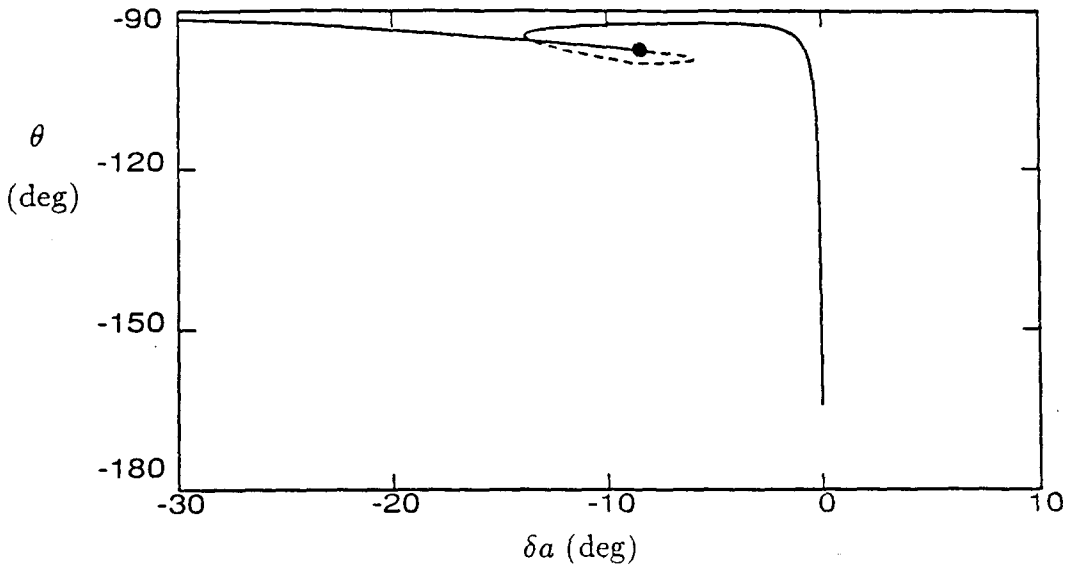

(g) Pitch Angle

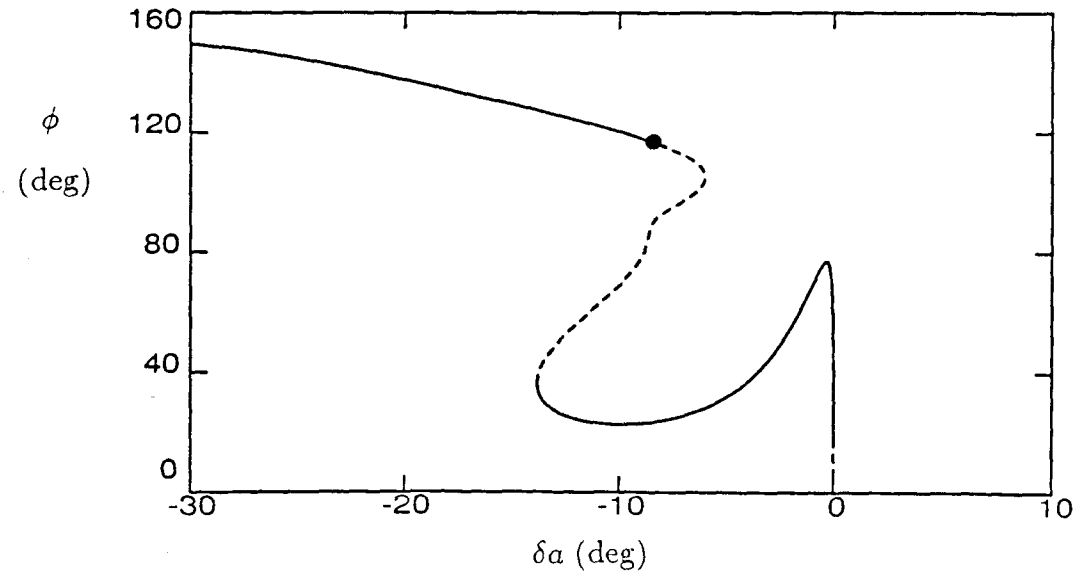

(h) Roll Angle

Figure 5.24: Concluded.

Recall that the steady state rotation rates are approximately linearly proportional to the steady state velocity (see Section 5.2.2). A quick check of this relationship can be done by comparing the steady state roll rates and velocities of the sixth and eighth order equations of motion. At an aileron deflection of negative 30 degrees, the steady state roll rate of the eighth order equations of motion is 600m/s (see Figure 5.24) and the steady state roll rate for the sixth order system (see Figure 5.19) is 200 deg/s, so the ratio of the two steady state roll rates is three. Comparing the steady state velocities of the two systems shows that the ratio is 830/275, which is also about three.

Comparing the curves of steady state rotation rates for the three systems without looking at the vertical scales, one would think that that the plots are the same. It seems that the qualitative nature of the curves of steady state rotation rates is unchanged when gravity is neglected. The saddle-node and Hopf bifurcations also occur at approximately the same aileron deflection for the three systems, so it is possible to determine the critical control surface deflections which lead to bifurcations with either the fifth, sixth, or eighth order equations of motion. Figure 5.25 shows the bifurcation loci for the eight order equations of motion for a range of elevator deflections. Equivalent diagrams for the fifth and sixth order systems are shown in Figures 5.8 and 5.20 respectively. Comparing the three diagrams shows that the three systems predict essentially the same bifurcation loci.

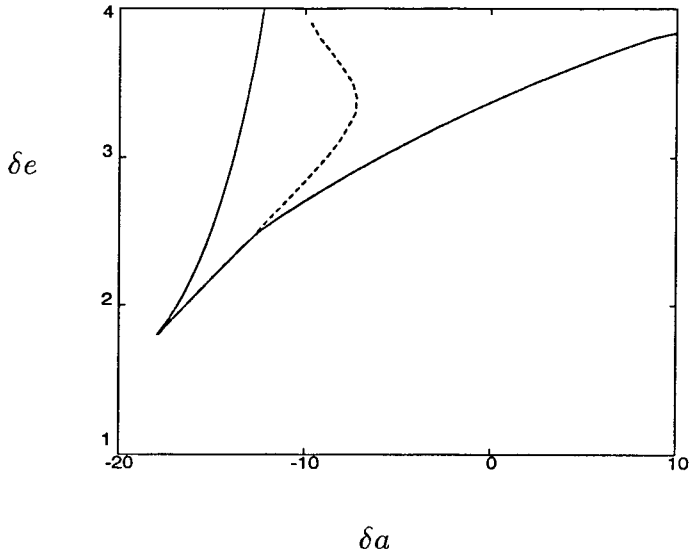

Figure 5.25: Bifurcation loci for the generic jet fighter for T/W=0.12, δr=0; - - - Hopf bifurcation, —— saddle-node bifurcation.

Recall that the pitchfork bifurcation that occurs at an elevator deflection of positive 2.7 degrees (see Figure 5.23) causes the purely longitudinal steady states (curve 1) to be unstable for nose down elevator deflections greater than 2.7 degrees. Thus, the steady state at zero aileron deflection in Figure 5.24 is unstable. This is difficult to see in the plots of steady states because a saddle-node bifurcation occurs for an aileron deflection of 0.01 degrees causing the steady states to become stable. Evidence of the saddle-node bifurcation is easiest to see in the plot of the steady state roll angle, Figure 5.24(h).

While the steady state rotation rates and angles of attack and sideslip do not change much for small aileron deflections, the steady state velocity and pitch and roll angles change significantly (see Figure 5.24). At zero aileron deflection

the steady state represents inverted flight (θ=-160 degrees) with zero roll angle. Applying a fraction of a degree of aileron deflection causes the steady state pitch angle to decrease to almost negative 90 degrees and the roll angle to increase to positive 80 degrees. This steady state represents a steep inverted dive causing the large increase in the steady state velocity.

It is interesting to note that while the steady state pitch rate stays relatively small for small aileron deflections, it undergoes a quick jump from zero to about negative 2 degrees for a small increment of aileron deflection (see Figure 5.24(b)). This is equivalent to the steady state pitch rate for the purely longitudinal steady states of the fifth and sixth order equations of motion. Thus rolls with an elevator deflection of positive 3 degrees for the eighth order equations of motion are essentially rolls from a pitch down condition.

The steady state Euler angles (Figures 5.24(g),(h)) show the change in orientation the aircraft undergoes in a jump related to the roll-coupling instability. The steady state pitch angle will stay relatively constant as the aileron deflection is increased past negative 15 degrees, but the steady state roll angle will jump about 90 degrees, from positive 30 to positive 120 degrees. Thus the aircraft jumps from an inverted dive whose orientation is given by pitching down 93 degrees and then rolling 30 degrees, to an upright dive whose orientation is given by pitching down 93 degrees and then rolling 120 degrees.

5.3.3 High Angle of Attack Instabilities for the Eighth Order Equations of Motion

The purely longitudinal steady states (curve 1) which are at high angles of attack have physically realistic steady state velocities. Comparing these steady states with the purely longitudinal steady states of the fifth and sixth order equations of motion (Figures 5.1 and 5.18) shows that the high angle of attack steady states of the three systems are similiar. Steady state roll and yaw rates are zero for all the systems and the steady state angles of attack and sideslip are essentially the same. The main difference is that the steady state pitch rate is zero for the eighth order equations of motion, but nonzero for the fifth and sixth order equations of motion.

Since the steady state angles of attack are similiar for the three systems, the Hopf bifurcation which causes the purely longitudinal steady states to become unstable occurs at similair elevator deflections for the three systems. Recall that this bifurcation is caused by the loss of directional stability, which occurs at a particular angle of attack. The pitchfork bifurcation which occurred at an elevator deflection of negative 18 degrees in the fifth and sixth order equations of motion (see Figures 5.1 and 5.18) does not occur in the eighth order equations of motion. This bifurcation occurred at the intersection of two branches of fixed points, curves 1 and 2. Examining these two curves of fixed points for the eighth order equations of motion (Figure 5.23) shows that they do not intersect because the steady state roll angles represented by curve 2 become large for elevator deflections near negative 18 degrees, while the steady roll angles of curve 1 are always zero. The disappearance of this bifurcation will not affect the dynamics of the

aircraft because the steady states are unstable, but it is important to note that neglecting gravity can change the steady states in nontrivial ways.

Figure 5.26 shows the steady states of the eighth order system as a function of aileron deflection for elevator deflections of negative 12 and 13 degrees and zero rudder deflection. Equivalent diagrams for the fifth and sixth order systems are shown in Figures 5.12 and 5.21 respectively. Comparing these three figures shows that for an elevator deflection of negative 12 degrees stable steady states exist for all aileron deflections for the fifth and sixth order systems, but a saddle-node bifurcation in the steady states of the eighth order equations of motion results in there being no stable steady states for aileron deflections greater than negative 20 degrees.

For small aileron deflections the steady of three systems are similiar except for the velocity. The steady state velocity of the sixth order equations of motion decreases slightly as the aileron deflection is increased, while the steady state velocity of the eighth order equations of motion increases rapidly. This is because the aircraft goes into a dive as aileron deflection is applied when gravity is included in the equations of motion (see Figure 5.26(g)).

Steady states for an elevator deflection of negative 13 degrees also show differences between the steady states of the three systems. For zero aileron deflection the steady state of the eighth order equations of motion are unstable, whereas this steady state is stable for the fifth and sixth order equations of motion. The difference in stability is a result of the slightly different steady state angles of attack for

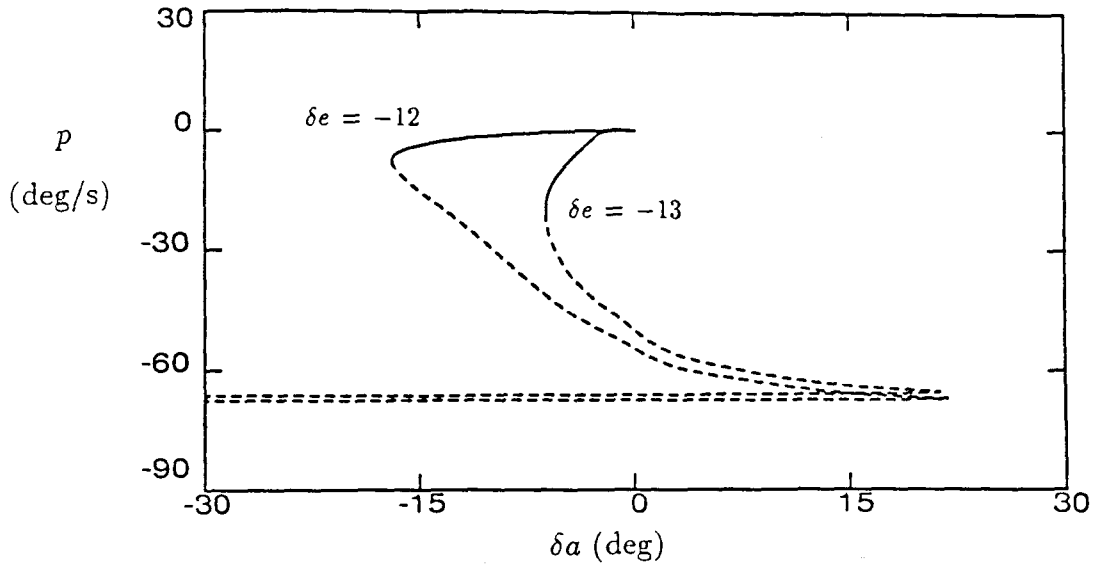

(a) Roll Rate

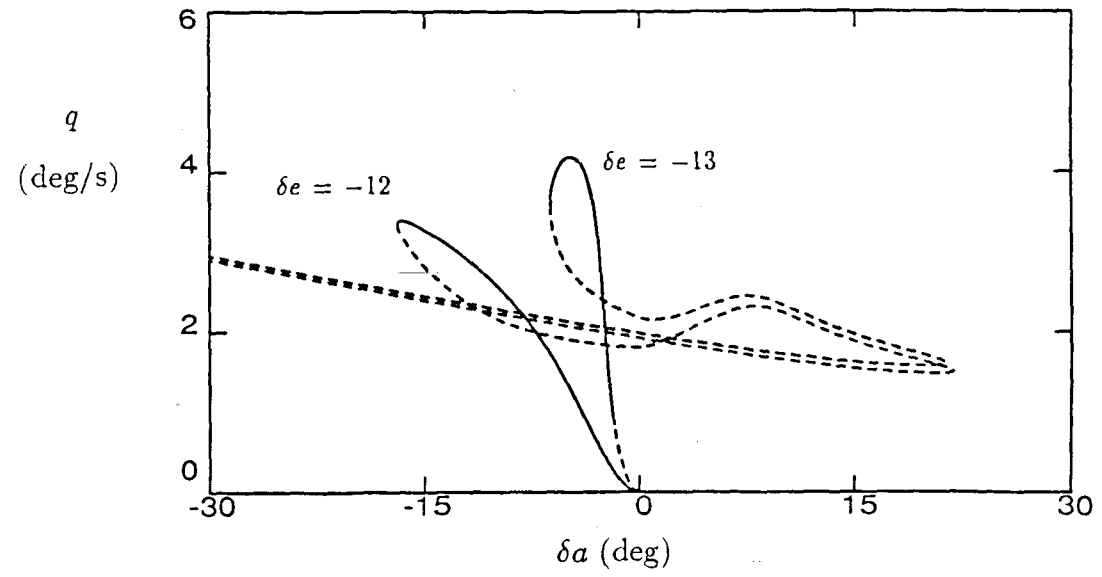

(b) Pitch Rate

Figure 5.26: Steady states for the generic jet fighter, T/W=0.12, δe=-12,-13, δr=0; —— stable, - - - unstable, • - Hopf bifurcation.

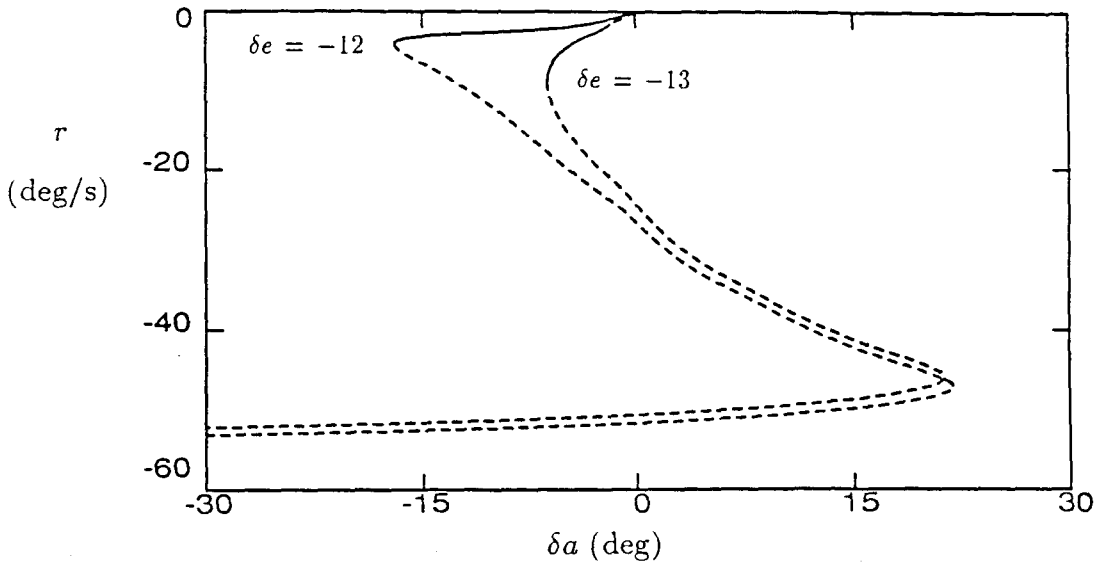

(c) Yaw Rate

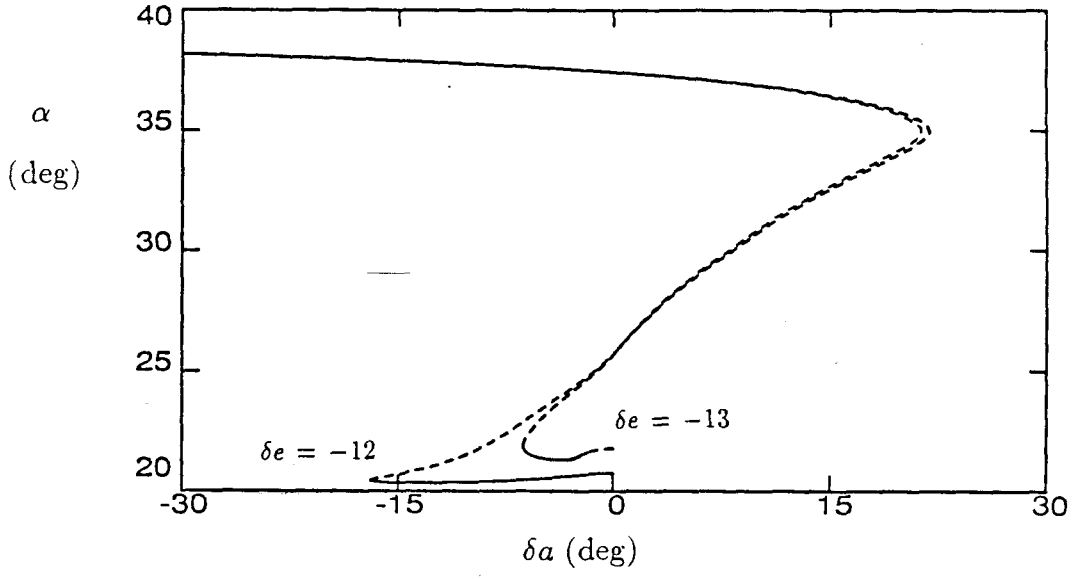

(d) Angle of Attack

Figure 5.26: Continued.

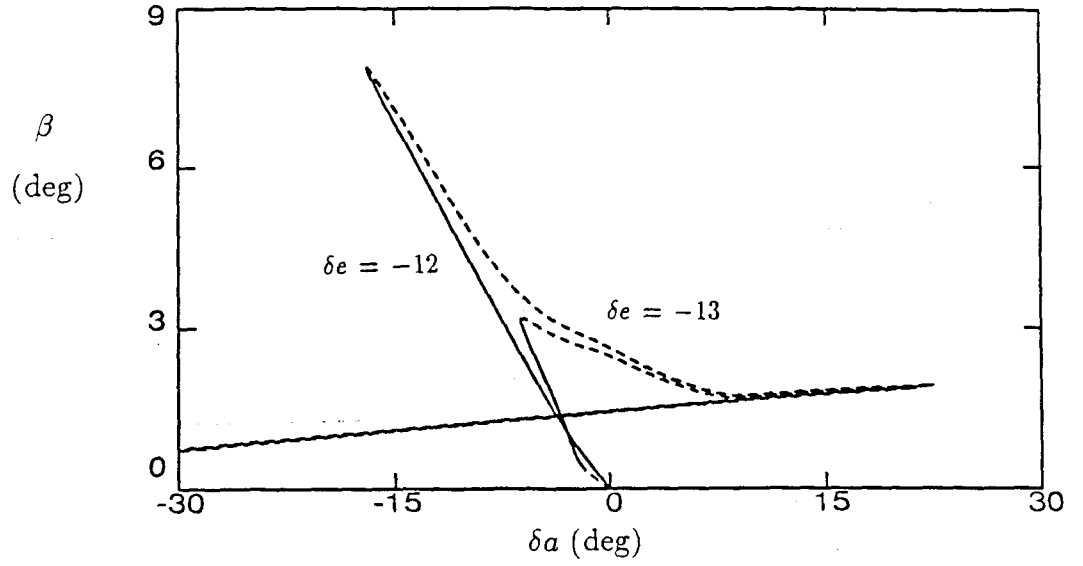

(e) Sideslip Angle

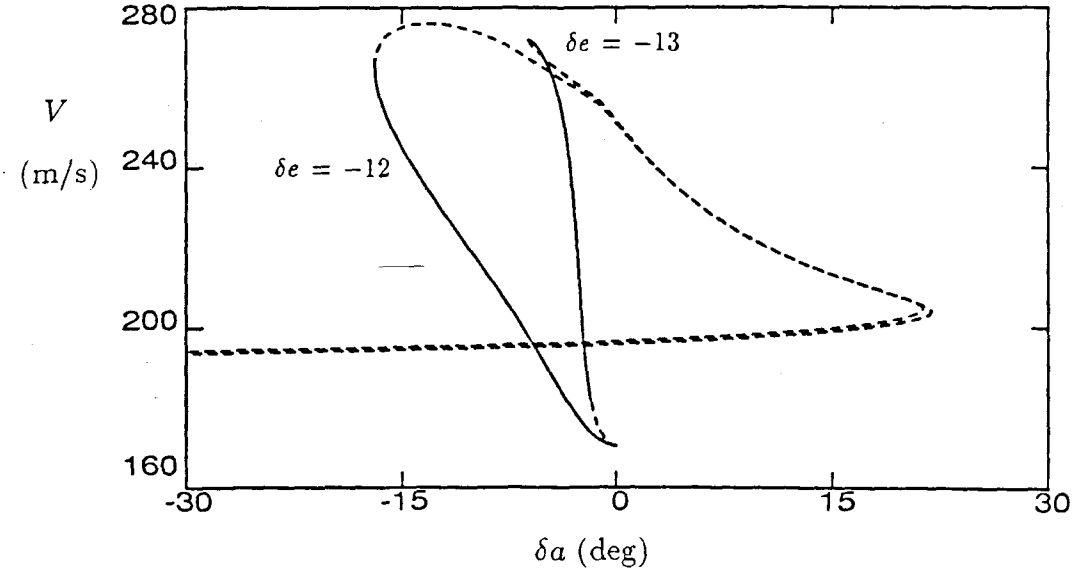

(f) Speed

Figure 5.26: Continued.

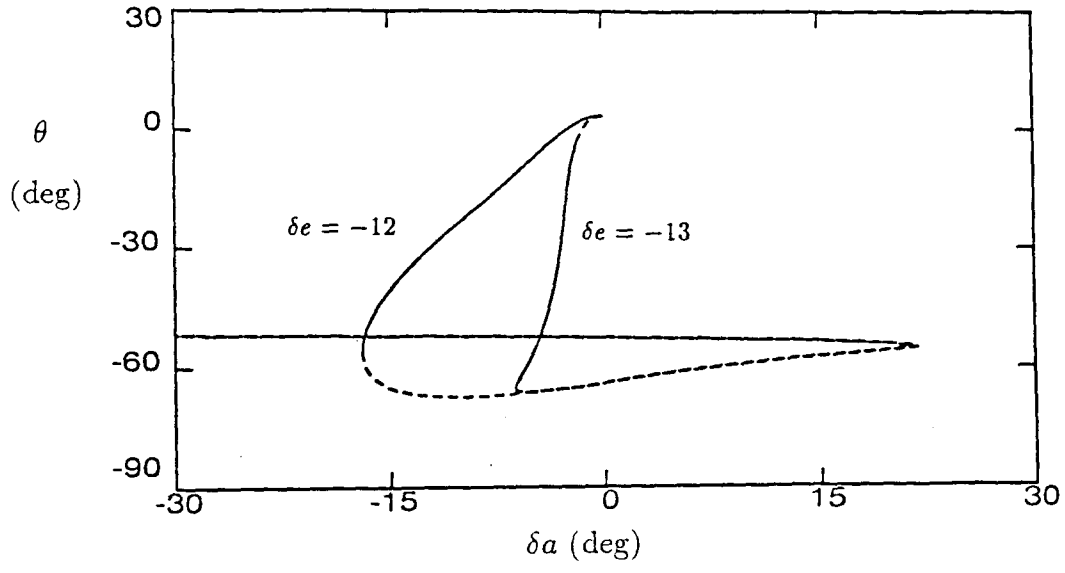

(g) Pitch Angle

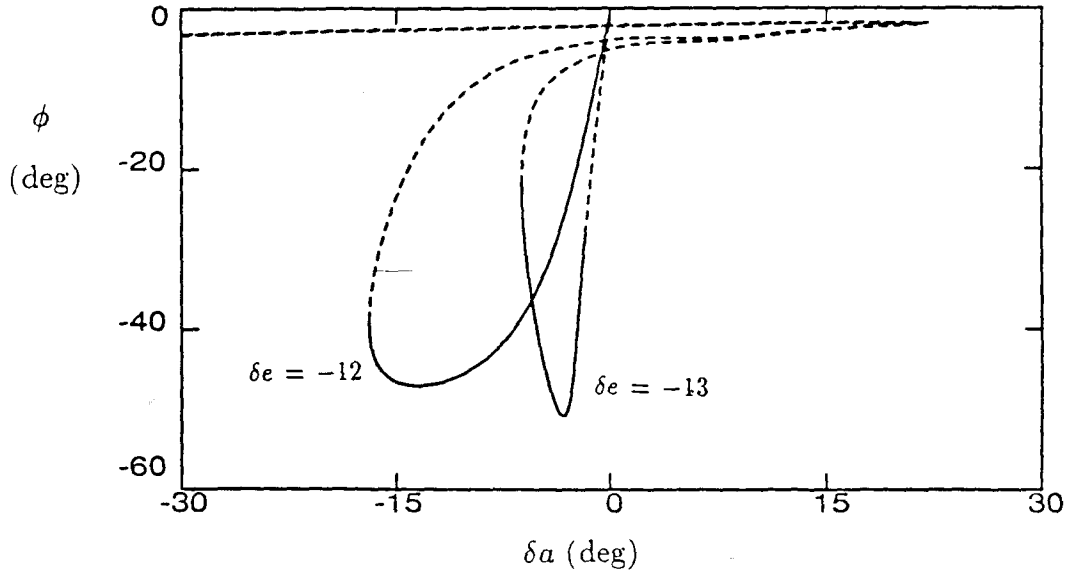

(h) Roll Angle

Figure 5.26: Concluded.

the three systems. The steady state angles of attack are about one degree higher for the eighth order system than for the fifth and sixth order system so the loss of directional stability occurs at a lower elevator deflection. This steady state is barely unstable for the eight order system, because it becomes stable when aileron deflection is applied and the angle of attack is reduced by a fraction of a degree (see Figure 5.26(d)).

The saddle-node bifurcation which leads to the condition of no stable steady states occurs for approximately the same aileron deflection for the three systems. Figure 5.27 shows the bifurcation loci for the the eighth order equations of motion. This figure is similiar to Figures 5.14 and 5.22 which show the bifurcation loci for the fifth and sixth order equations of motion respectively. Differences of one or two degrees occur in the bifurcation loci, but the qualitative nature of the loci at which bifurcations occur is the same for the three systems of equations. (Note that we are only discussing the steady states of the system, the transient motions of the three systems could be very different.)

5.4 Summary of the Results for the Generic Jet Fighter

The previous analysis has shown the effectiveness of using continuation methods for analyzing nonlinear aircraft dynamics. A nonlinear aerodynamic model was analyzed with the complete equations of motion and equations of motion which neglected the influence of gravity and assumed either constant velocity or

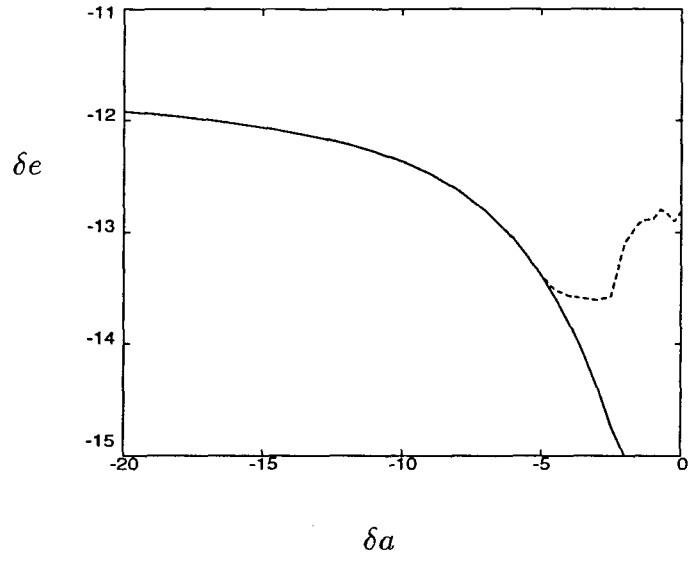

Figure 5.27: Bifurcation loci for the generic jet fighter for T/W=0.12, δr=0; - - - Hopf bifurcation, —— saddle-node bifurcation.

constant thrust (see Section 3.1). Both roll-coupling and high angle of attack instabilities were analyzed with these three equations of motion.

Several differences were observed between the steady states of the eighth order equations of motion and fifth and sixth order equations of motion. A new branch of steady states was found to exist when the influence of gravity was included in the equations of motion. The new steady states represent inverted spiral motions and cause the purely longitudinal inverted motions to become unstable. Including gravity also destroyed a pitchfork bifurcation which occurred in the high angle of attack steady states.

Results for the roll-coupling instability were similiar for the three sets of equations of motion. The bifurcation loci only varied by one or two degrees, but

the steady states for a particular set of control surface deflections did not always match. Different steady state velocities for the three systems were shown to be the source of differences in the steady states. Results from the eighth order equations of motion showed that roll-coupling instabilities occur when the aircraft is in a steep dive and the jump in the state of the aircraft is from an inverted to an upright dive. It should be noted that the roll-coupling instability for the eighth order equations of motion occurred at unrealistic velocities, so the results will not be quantitatively correct.

Larger aileron deflections were shown to be possible before a roll-coupling instability occurred if the rudder was used to control the sideslip angle. The saddle-node bifurcation could be delayed to aileron deflections greater than 30 degrees, but a Hopf bifurcation limited the range of allowable aileron deflections to 20 degrees. Rudder deflection was shown to be ineffective for controlling the large sideslip angles that resulted from roll-coupling effects for rolls from a pitch up condition.

High angle of attack instabilities were shown to occur for essentially the same control surface deflections for the fifth, sixth, and eighth order equations of motion. The instability was a result of the loss of directional stability for angles of attack greater than 20 degrees and resulted in a condition of no stable steady states. Large amplitude time dependent motions resulted from this instability. Sideslip feedback to the rudder was used to increase the directional stability of

the aircraft, but high angle of attack instabilities still occurred. Feedback did delay the instability to higher elevator deflections.

VI. RESULTS FOR THE F-14

This is the most complete aerodynamic model analyzed in this thesis. Aerodynamic coefficients are nonlinear functions of the angles of attack and sideslip, the rotation rate, and the elevator deflection. Linear rudder and aileron effects are included in the model (see Section 3.2.3). Mach number effects were not included in the aerodynamic model during this analysis, so Mach numbers are limited to 0.60. Aerodynamic data were not available for negative angles of attack so possible jump phenomena related to roll-coupling instabilities could not be determined for the F-14. (Recall that jump phenomena related to roll-coupling instabilities only occur at negative angles of attack (see Section 5.1.2). Roll-coupling effects which occur at positive angles of attack tend to produce large sideslip deviations, but no jump in the state of the aircraft.) Analysis of the F-14 will consist of determining instabilities in the normal flight regime of the aircraft and a determination of the steady spin modes of the aircraft.

Control and stability augmentation systems included in operational F-14's are not included in the aircraft model used in this analysis so results indicated here might not apply to operational F-14's. In particular, operational F-14's have variable wing sweep which is scheduled according to the Mach number, while the results presented here are for the wings fully unswept. Also, small canards are present on the F-14 just in front of the wings to provide longitudinal stability, but they are neglected in these results. F-14's also have spoilers which are retracted for

the results presented here. Atmospheric density is 0.53 kg/m^3, which corresponds to an altitude of 20,000 feet, and the applied thrust is zero.

6.1 Existence of Multiple Branches of Steady States

Six branches of steady states were found to exist for the F-14. Figure 6.1 shows the steady states as a function of elevator deflection for zero aileron and rudder deflections. Curve 1 represents steady level flight (i.e., $p = q = r = \beta = \phi = 0$), the normal operating condition of the aircraft. This branch of steady states could only be determined up to an elevator deflection of negative three degrees due to the Mach number limit of the aerodynamic model. Nose down elevator deflections beyond negative three degrees cause the aircraft to enter a steady dive resulting in a large increase in the steady state velocity. Curve 2 represents spirally divergent motions and can best be seen in Figure 6.1(h) which shows the steady state roll angles. The remaining curves represent steady spins, which are characterized by high angles of attack and large rates of rotation.

Steady states at low angles of attack (curve 1) are generally easy to find, but it can be difficult to find steady spin modes. Steady spin modes of the F-14 were determined by guessing an initial steady spin in the continuation algorithm and letting the algorithm run until either a steady spin was determined or numerical difficulties stopped the routine. Steady spins of the generic jet fighter were used as a general guide for guessing the steady spins of the F-14. This technique produced the four branches of steady spins shown in Figure 6.1 (labelled 3N,3P,4N,4P where

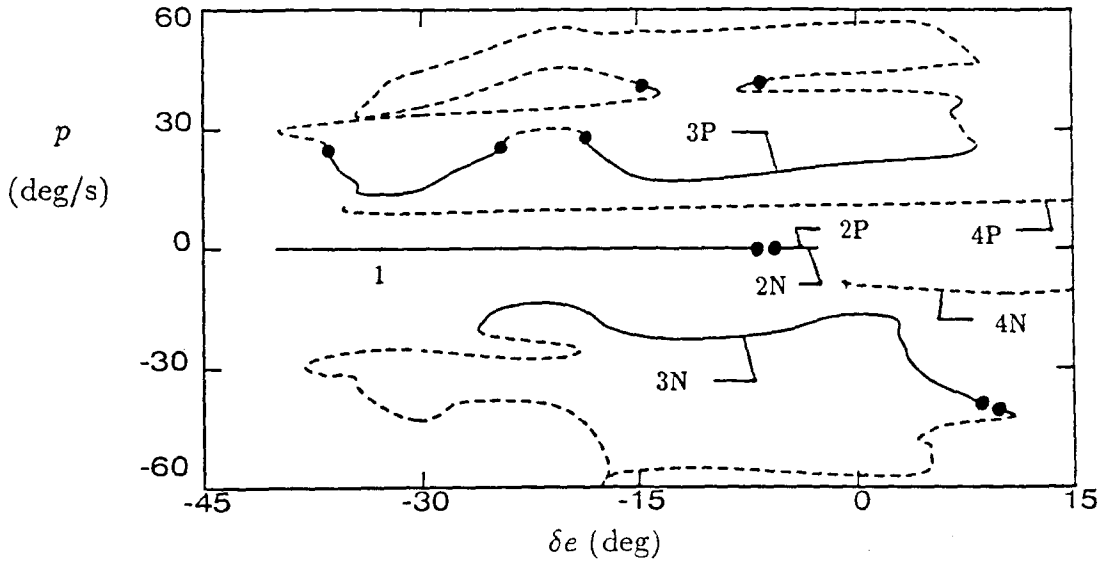

(a) Roll Rate

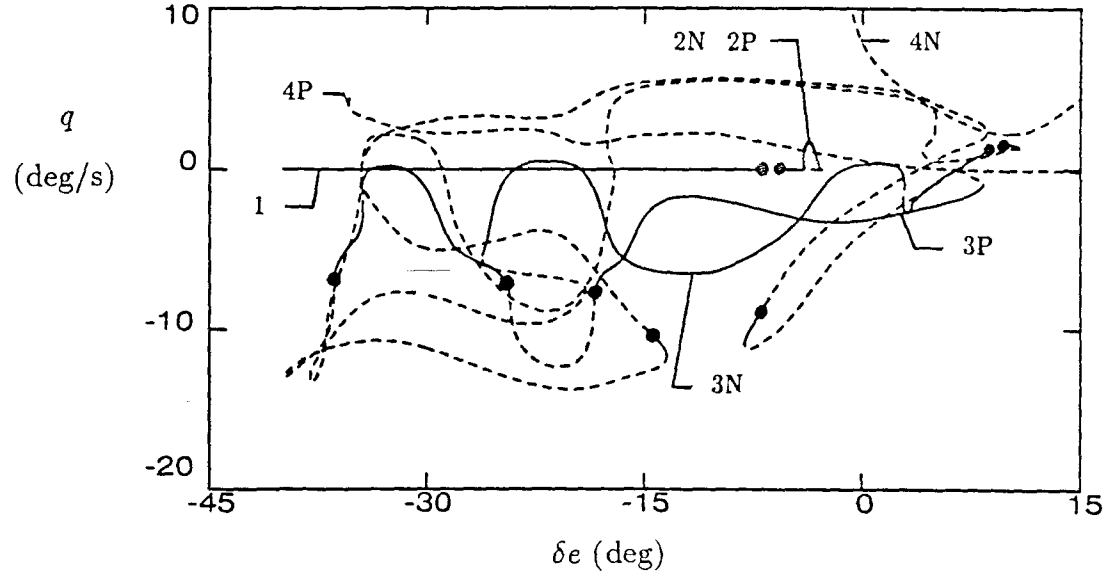

(b) Pitch Rate

Figure 6.1: Steady States for the F-14 with zero applied thrust, δa=0, δr=0; —— stable, - - - unstable, • - Hopf bifurcation.

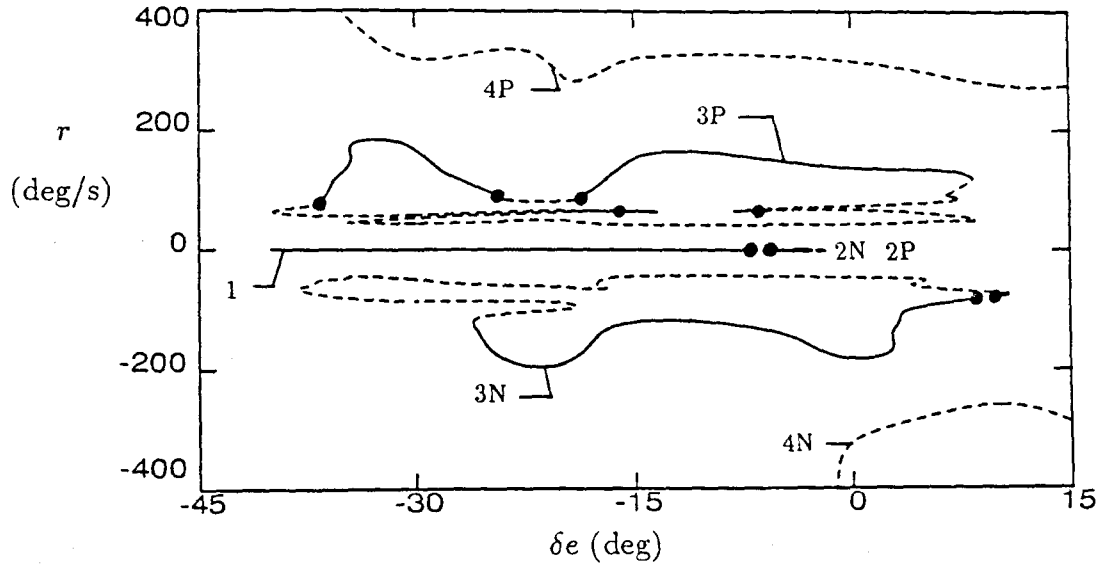

(c) Yaw Rate

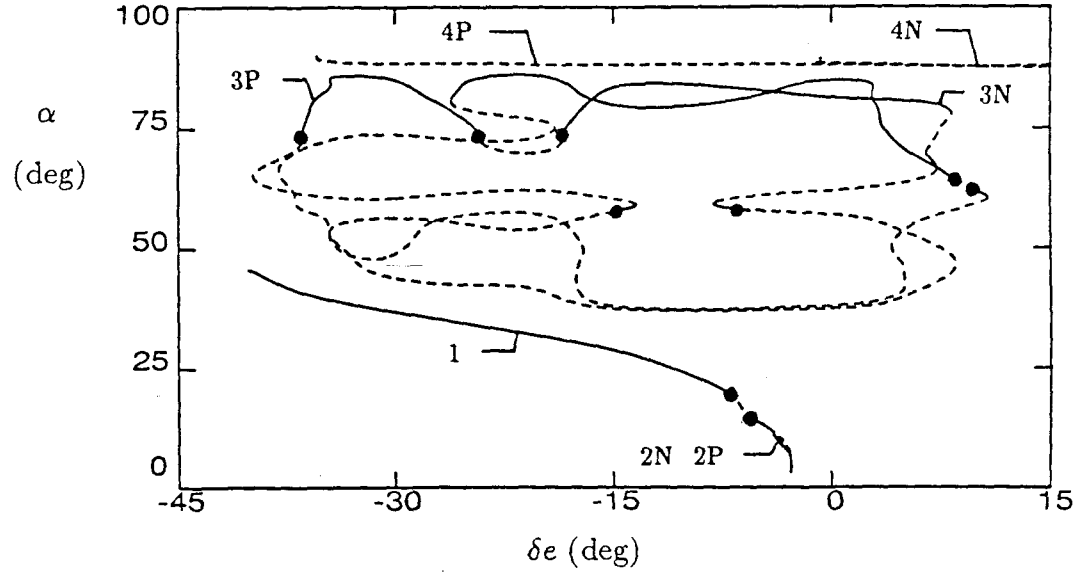

(d) Angle of Attack

Figure 6.1: Continued.

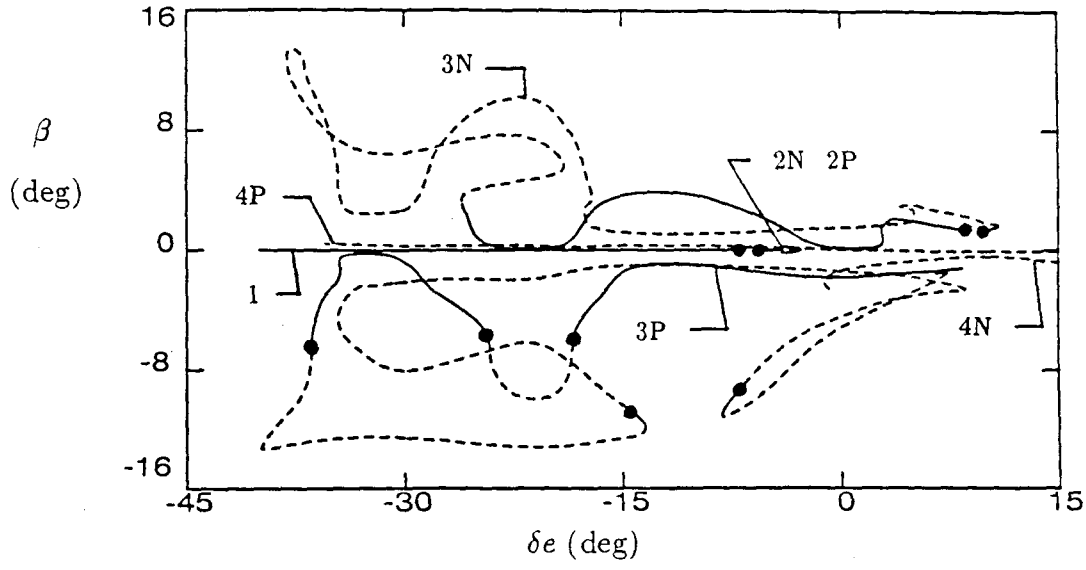

(e) Sideslip Angle

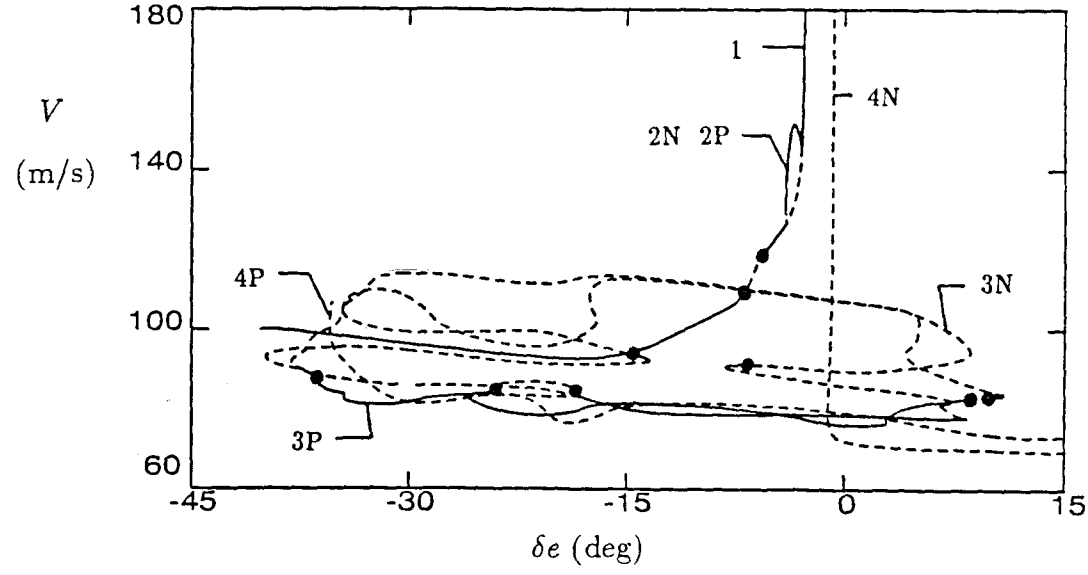

(f) Speed

Figure 6.1: Continued.

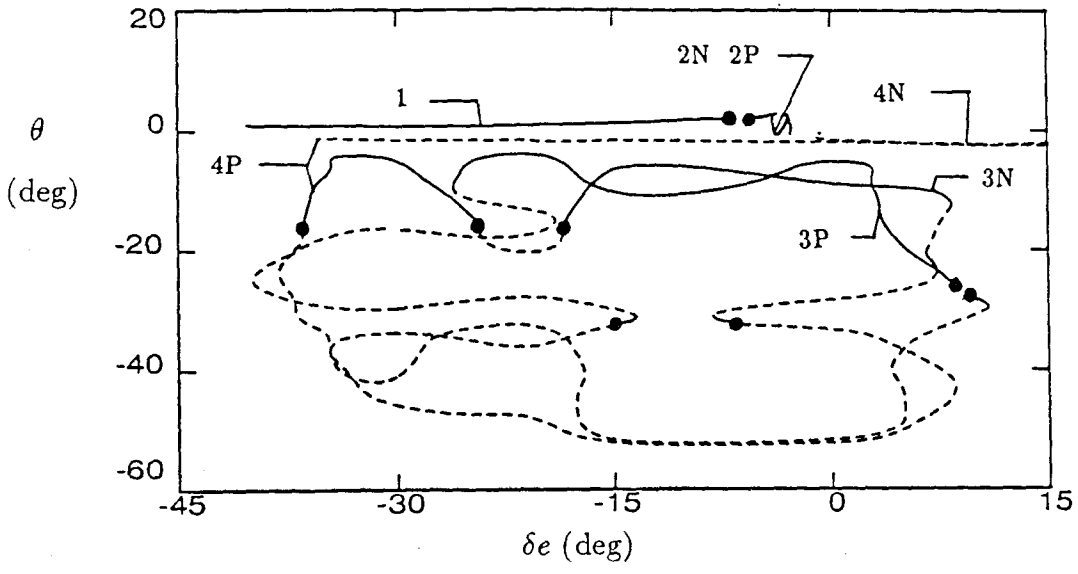

(g) Pitch Angle

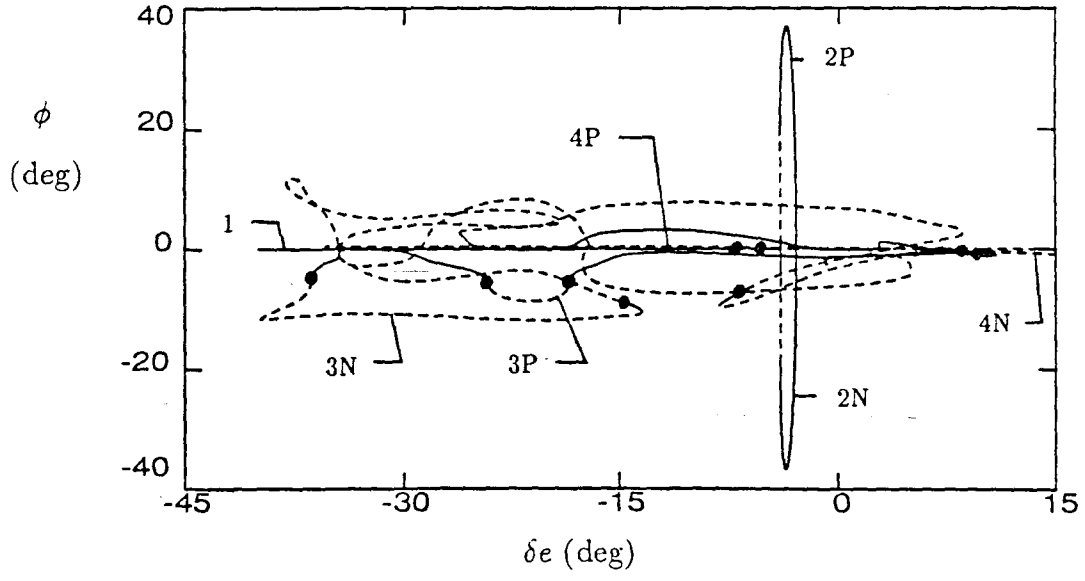

(h) Roll Angle

Figure 6.1: Concluded.

'N' and 'P' denote spins with negative and positve yaw rates respectively), but it is possible that other branches of steady spins exist. The asymmetries of the aerodynamic model are evident in the steady spins of the aircraft. If the model was symmetric the curves 3N and 3P would be symmetric as would the curves 4N and 4P (cf. Figure 5.23).

The remainder of this chapter will be divided into two parts. Instabilities which occur in the steady states represented by curve 1 (trimmed longitudinal flight) will be discussed in the following section. Several lateral instabilities will be analyzed including wing rock. Instabilities encountered during lateral maneuvers are discussed in Section 6.3. Section 6.4 contains a discussion of the steady spin modes of the aircraft. Figure 6.1 shows that stable steady spins exist for a wide range of elevator deflections, so it could be difficult to escape a spin if one is encountered. Also recall that the rudder is ineffective for angles of attack above 55 degrees so it will not be useful for recovering from a spin (recall that spins occur at high angles of attack).

6.2 Instabilities of the Longitudinal Steady States

This section will discuss the steady states represented by curve 1 in Figure 6.1, the normal operating conditions of the aircraft. Instabilitities in these steady states are important because an instability could cause the aircraft to enter a spin, which is dangerous and potentially deadly. Steady states represented by curve 1 in Figure 6.1 are stable for elevator deflections greater than negative 7 degrees,

but two Hopf and two pitchfork bifurcations occur for elevator deflections between negative 3 and negative 7 degrees.

A closer view of this region of steady states is shown in Figure 6.2. Steady spins are not included in this figure so a better picture of the Hopf and saddle-node bifurcations can be obtained. Figure 6.2 shows that for elevator deflections between negative 5.5 and negative 6.8 degrees the steady states are unstable because of two Hopf bifurcations, which could result in stable periodic motions. Figure 6.3 shows a simulation in which the elevator deflection is increased from negative 5 to negative 6 degrees, causing the aircraft to be at an unstable steady state. An aileron deflection of one-tenth of a degree is applied to excite any instabilities (see Figure 6.3(a)).

Figure 6.3 shows that the aircraft develops a steady wing rock as the initial perturbation grows. Wing rock is characterized by large oscillations in roll and sideslip (see Figures 6.3(c),(d) and (i)) while the other variables undergo small oscillations. The period of the wing rock is about 4 seconds and the instability grows very slowly (it is still not fully developed after four minutes), so it is probably not a great risk to pilots. Figure 6.3 also shows that the longitudinal variables (q, α, V, θ) are lightly damped (see Figures 6.3(b),(e),(g),(h)). The motions show evidence of a lightly damped phugoid mode, characterized by oscillations of velocity and pitch angle, with a period of about 30 seconds.

The bifurcations that occur at elevator deflections of negative 3 and 4 degrees lead to the appearance of new stable steady states (curve 2) and cause the steady

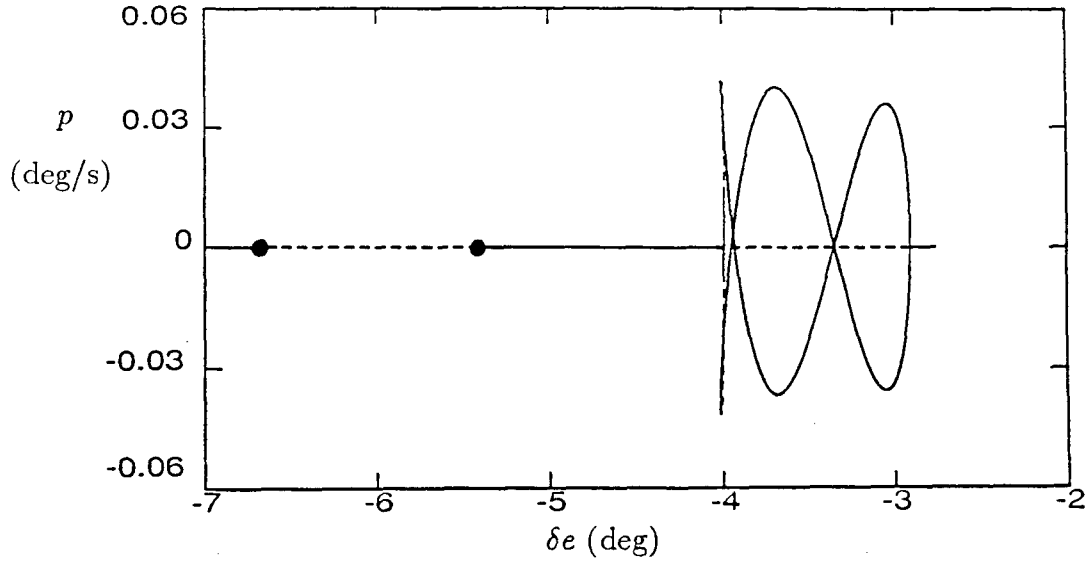

(a) Roll Rate

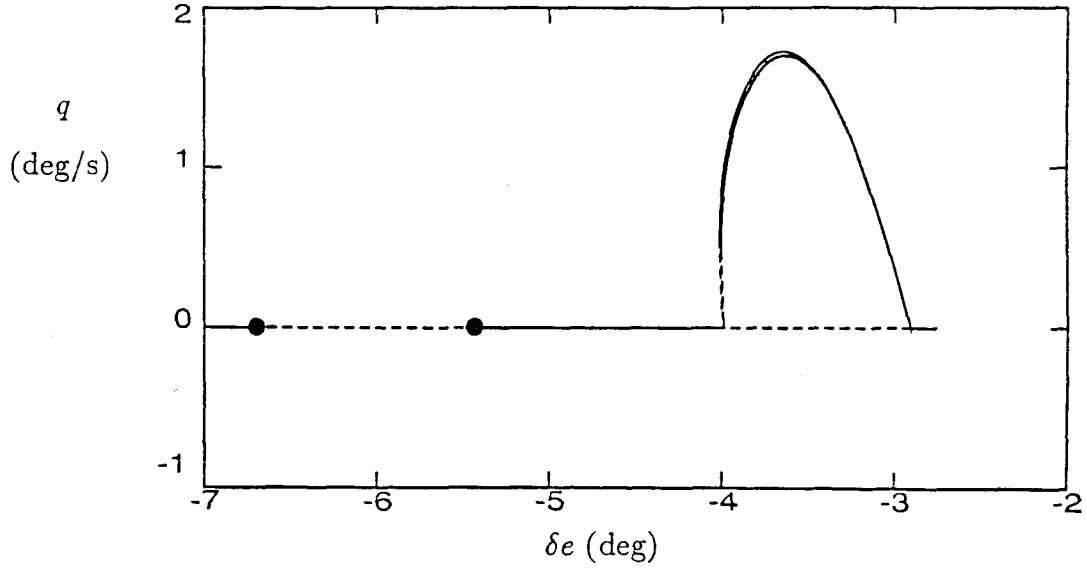

(b) Pitch Rate

Figure 6.2: Steady States for the F-14 with zero applied thrust, δa=0, δr=0; —— stable, - - - unstable, • - Hopf bifurcation.

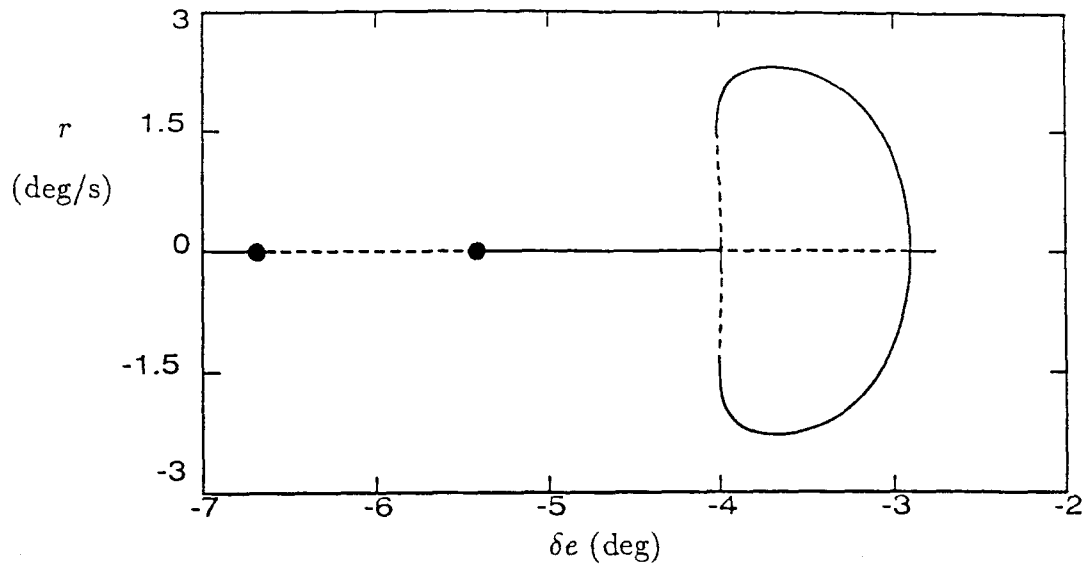

(c) Yaw Rate

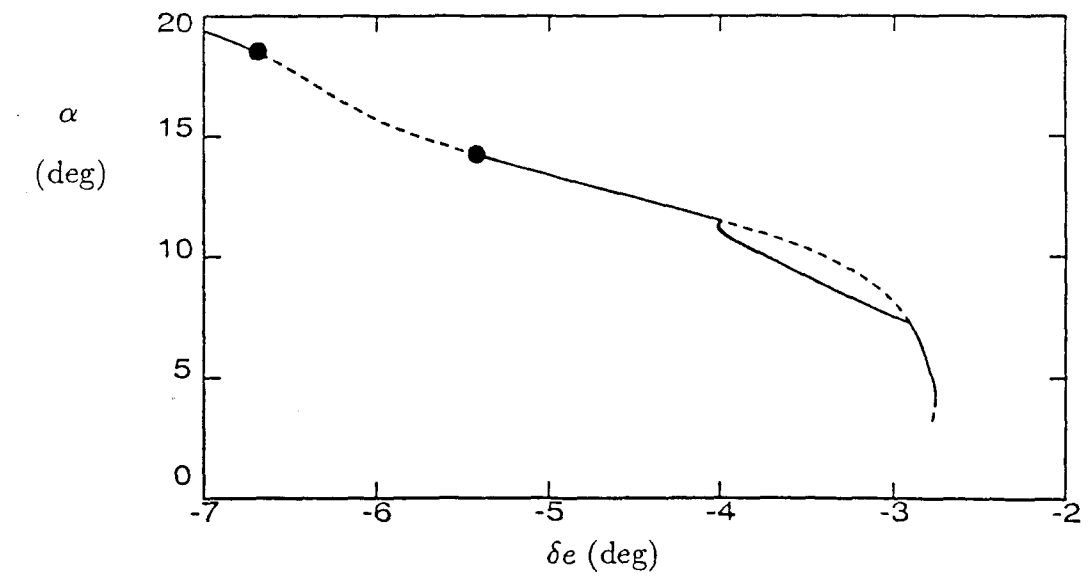

(d) Angle of Attack

Figure 6.2: Continued.

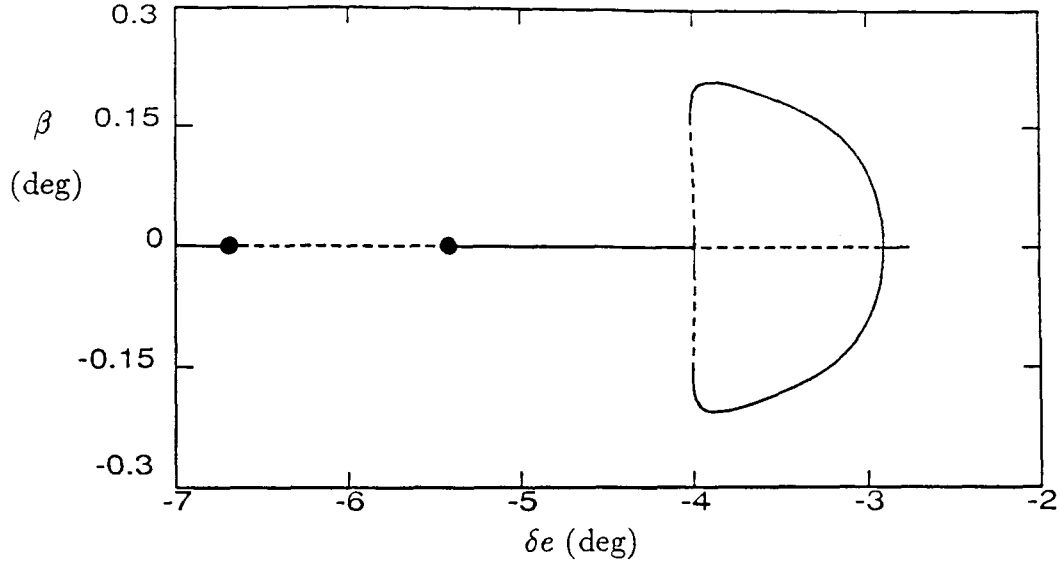

(e) Sideslip Angle

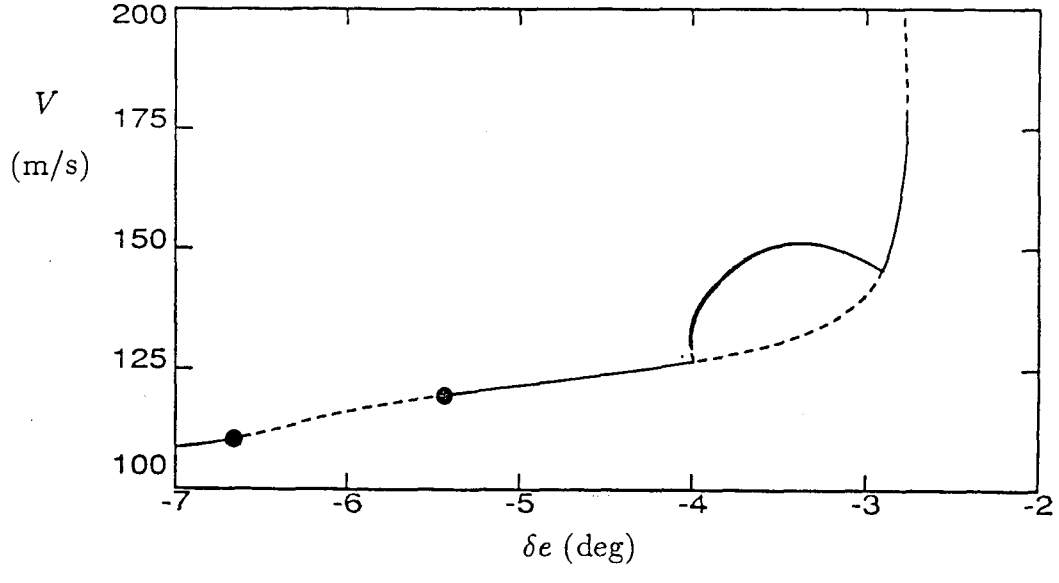

(f) Speed

Figure 6.2: Continued.

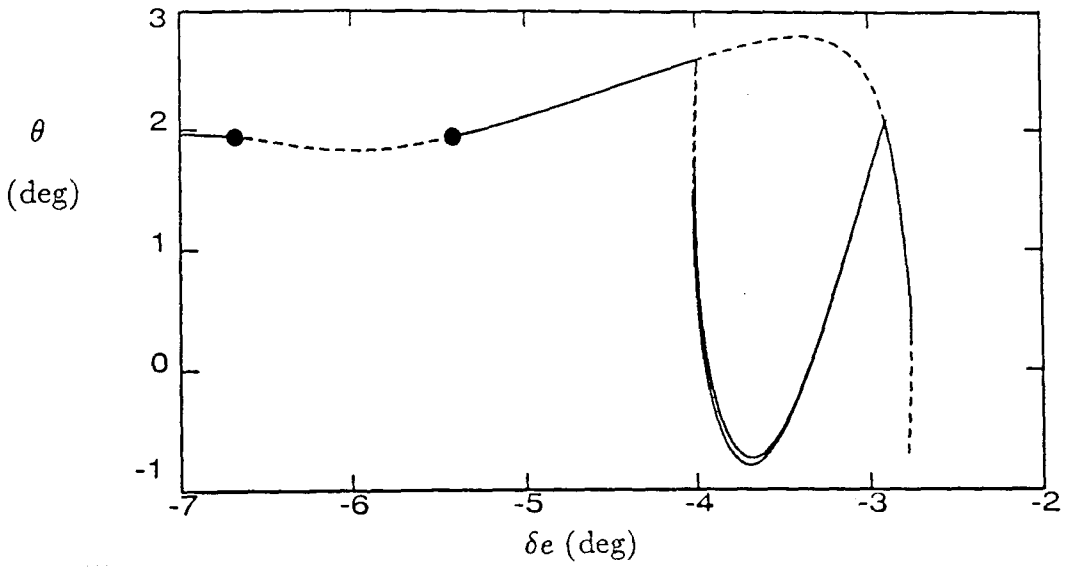

(g) Pitch Angle

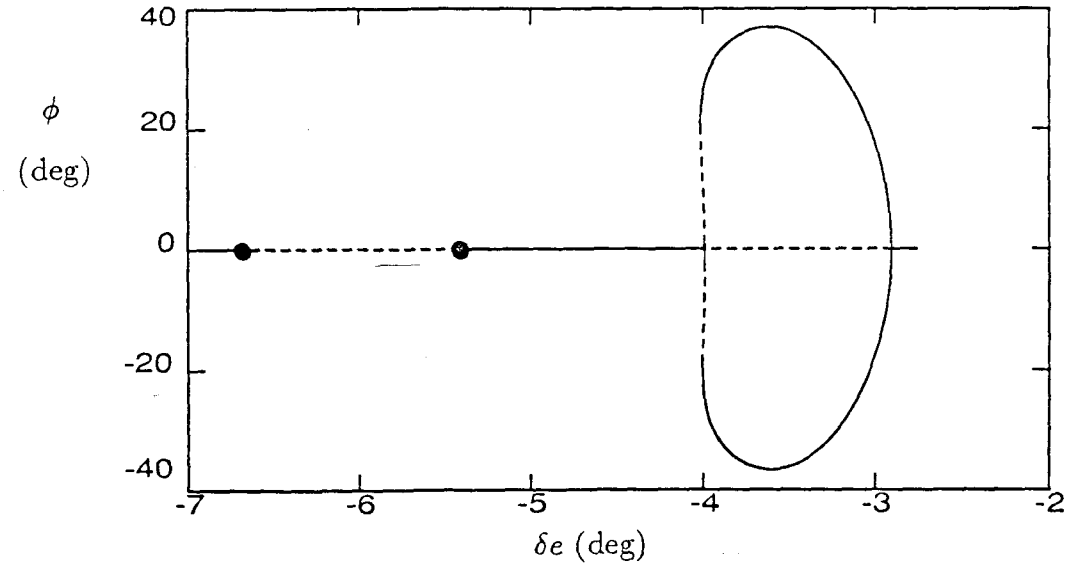

(h) Roll Angle

Figure 6.2: Concluded.

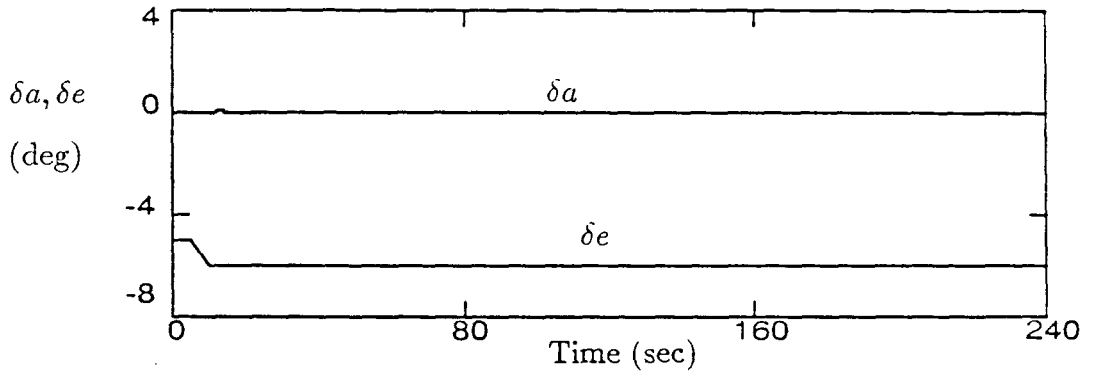

(a) Aileron and Elevator Deflections

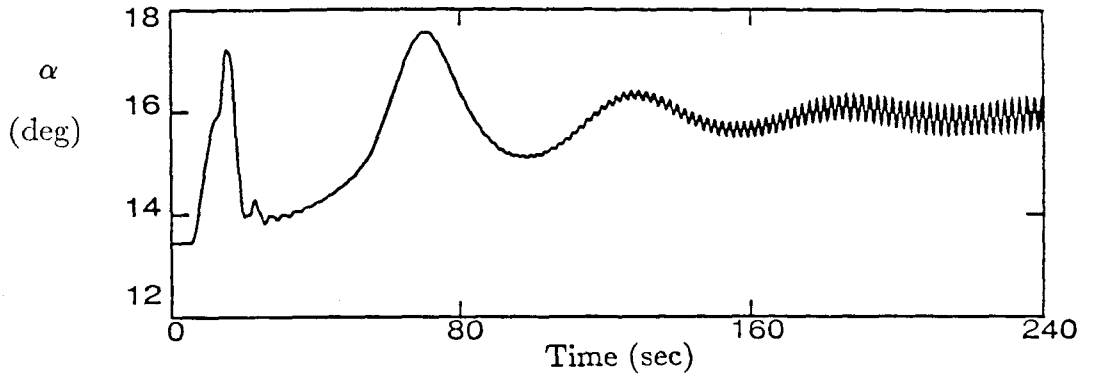

(b) Angle of Attack

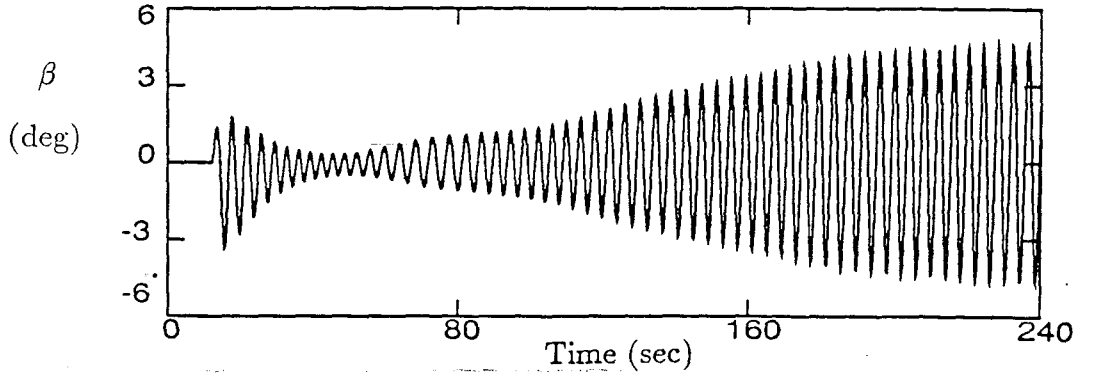

(c) Sideslip Angle

Figure 6.3: Simulation of wing rock for the F-14, T=0, δr=0.

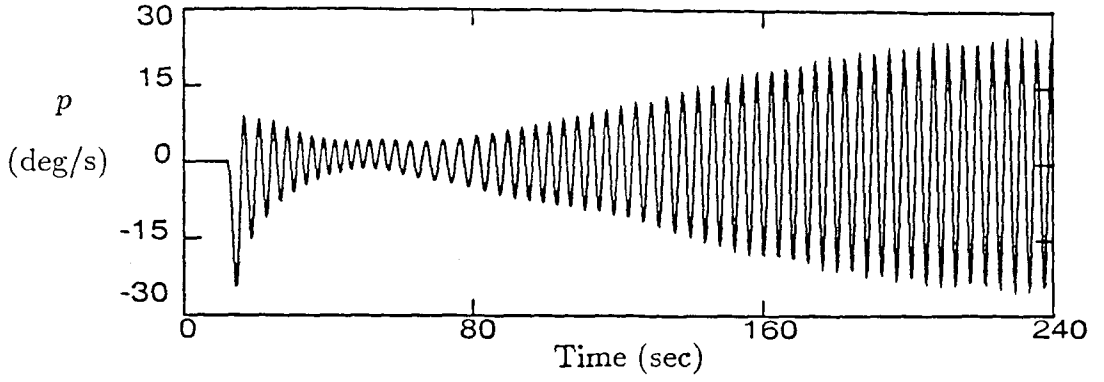

(d) Roll Rate

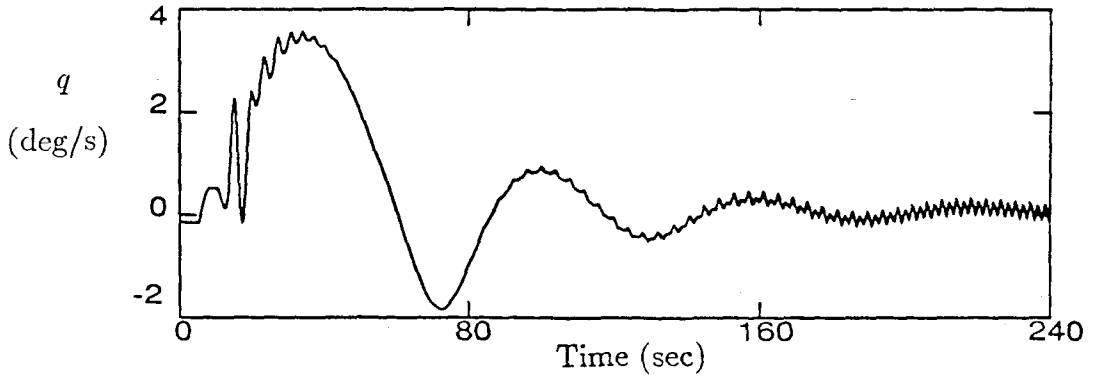

(e) Pitch Rate

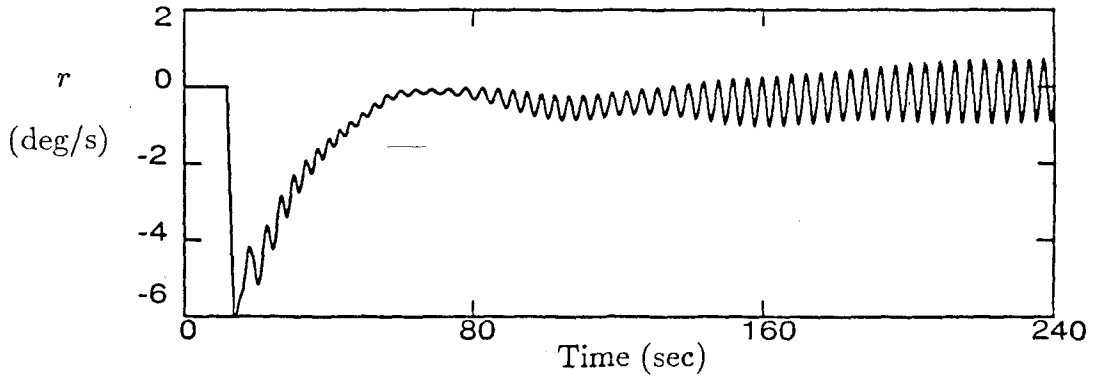

(f) Yaw Rate

Figure 6.3: Continued.

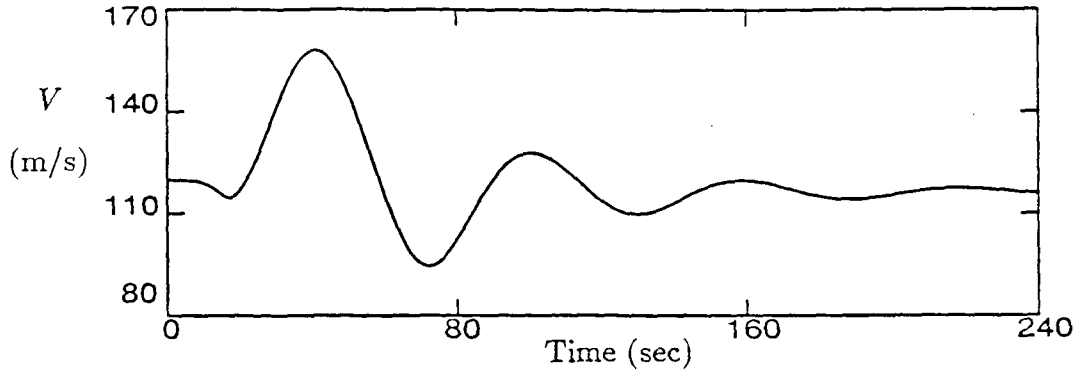

(g) Speed

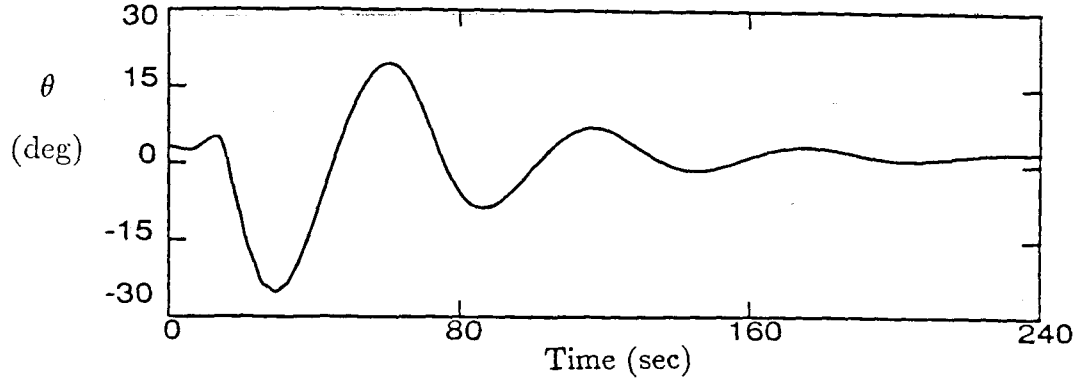

(h) Pitch Angle

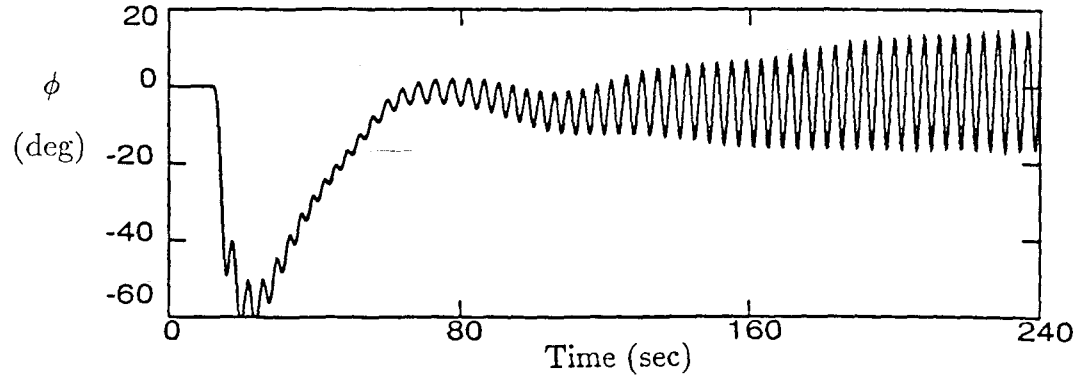

(i) Roll Angle

Figure 6.3: Concluded.

states represented by curve 1 to become unstable. Lateral motions (p, r, β, ϕ) are nonzero for the steady states represented by curve 2 so the aircraft will undergo directional divergence for elevator deflections between negative 3 and negative 4 degrees. This motion is generally classified as spiral divergence because the aircraft motion will be a slow spiral. This motion has large steady state roll angles (see Figure 6.2(h)) and the pitch angle becomes negative (see Figure 6.2(g)) which causes the velocity of the spiral motion to be larger than the velocity of the purely longitudinal steady states (curve 1). The effect of asymmetry in the aerodynamic model can be seen in the steady state pitch rates and pitch angles as the steady states are slightly different for the part of curve 2 representing positive roll rates (curve 2P) and the part representing negative roll rates (curve 2N).

A simulation of the effects of this instability on the motion of the aircraft is shown in Figure 6.4. In the simulation the elevator deflection was reduced from negative 5 to negative 3.5 degrees, followed by a one-tenth of a degree perturbation in the aileron deflection (see Figure 6.4(a)). The roll angle quickly jumps about 15 degrees in response to the aileron perturbation and then gradually increases (see Figure 6.4(i)). This instability grows slowly and after 5 minutes the roll angle is still increasing. Pilots could control this instability because only minor oscillations occur in the state of the aircraft. Lateral oscillations are small and the longitudinal oscillations (phugoid mode) have a period of about thirty seconds which can be handled by a pilot.

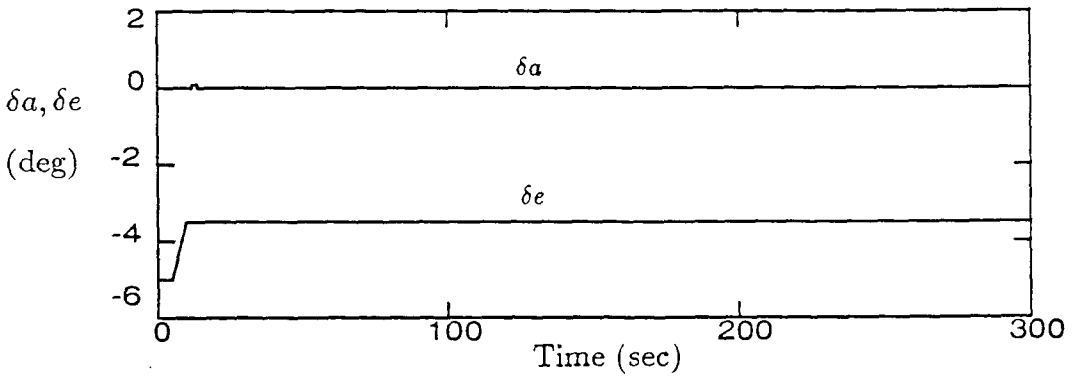

(a) Aileron and Elevator Deflections

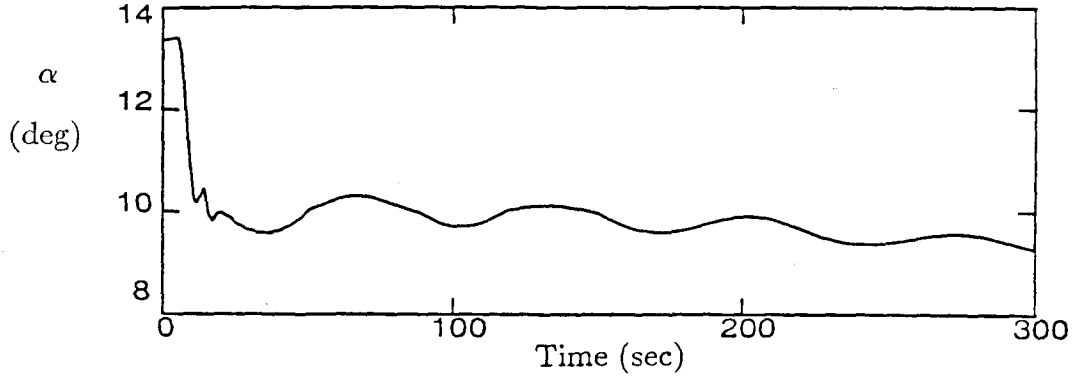

(b) Angle of Attack

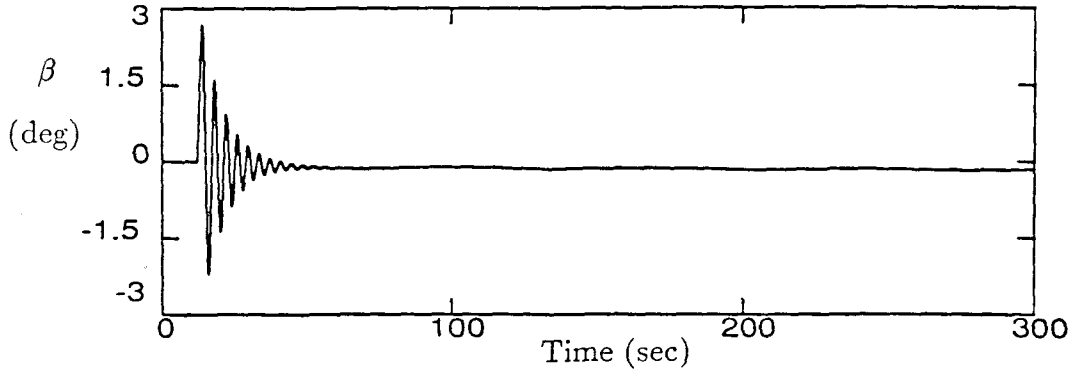

(c) Sideslip Angle

Figure 6.4: Simulation of spiral divergence for the F-14, T=0, δr=0.

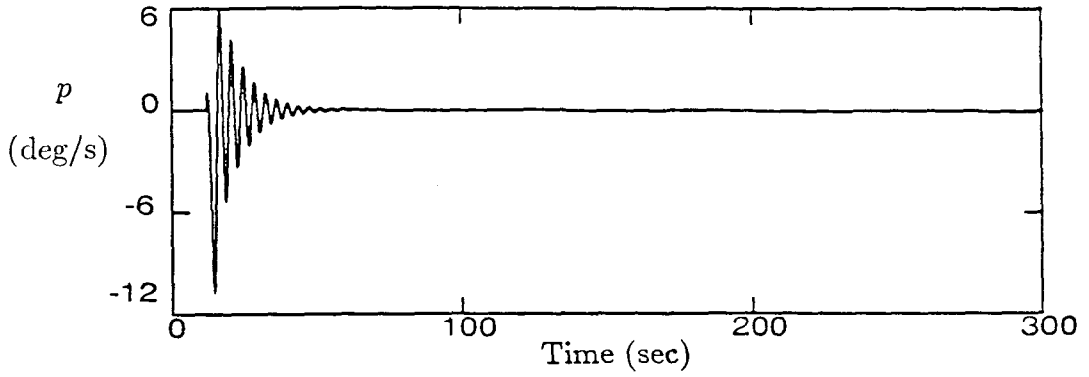

(d) Roll Rate

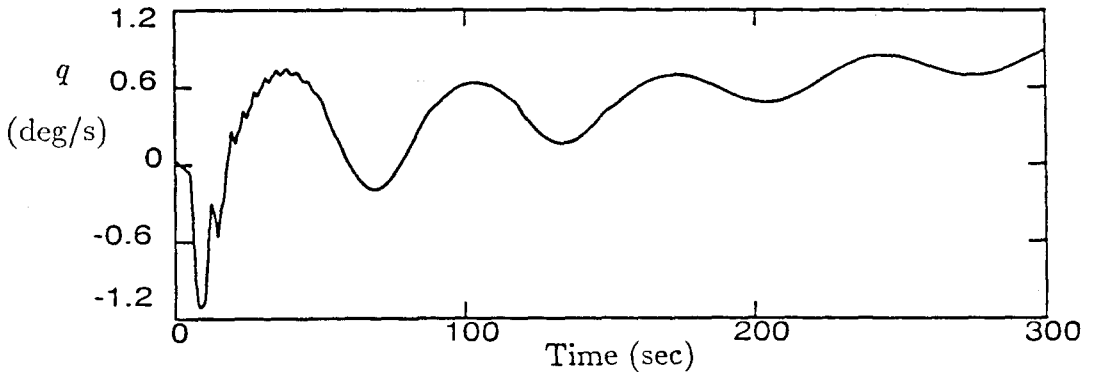

(e) Pitch Rate

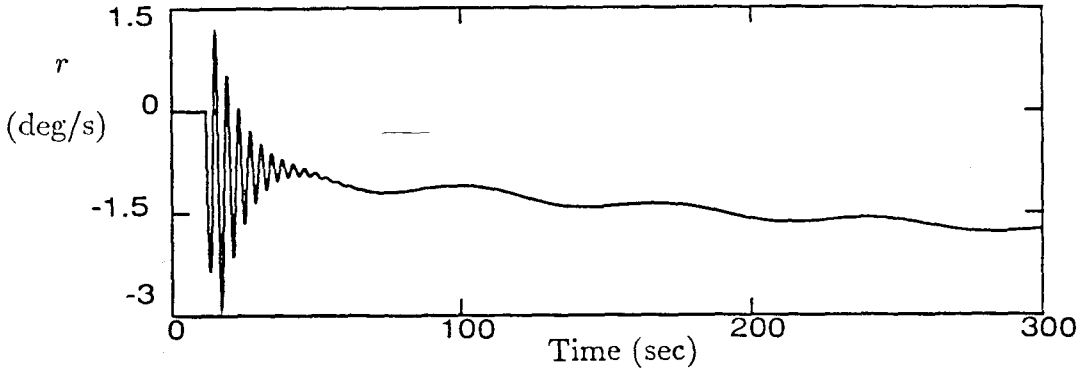

(f) Yaw Rate

Figure 6.4: Continued.

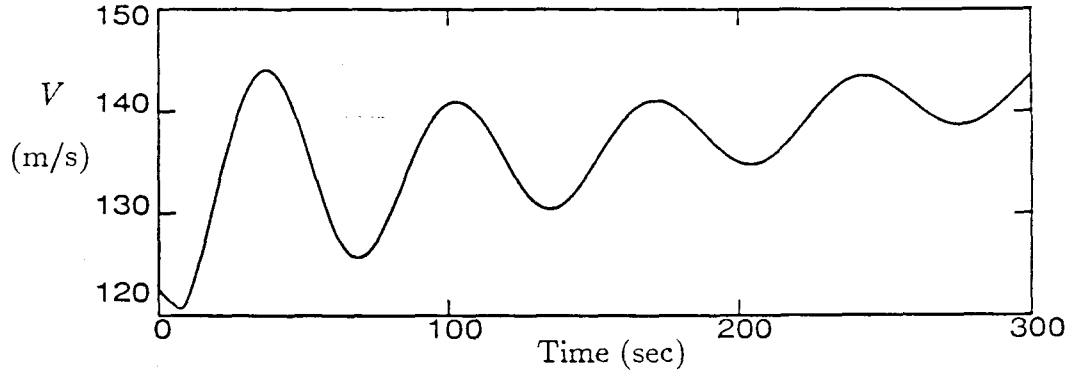

(g) Speed

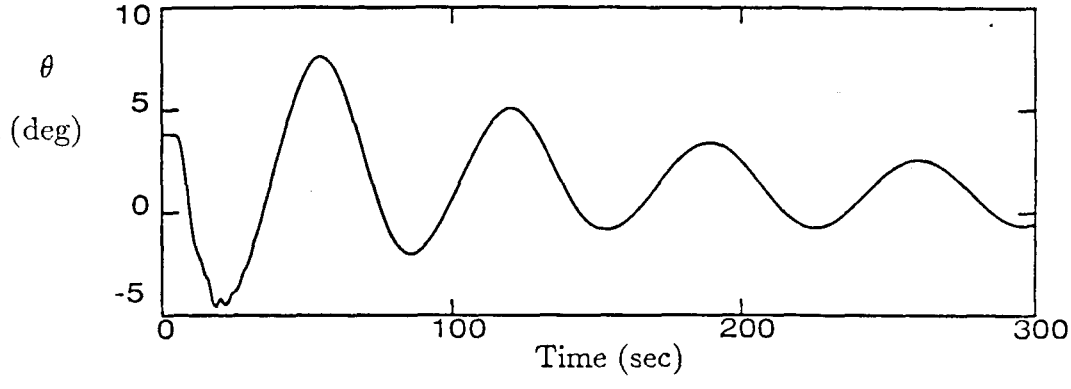

(h) Pitch Angle

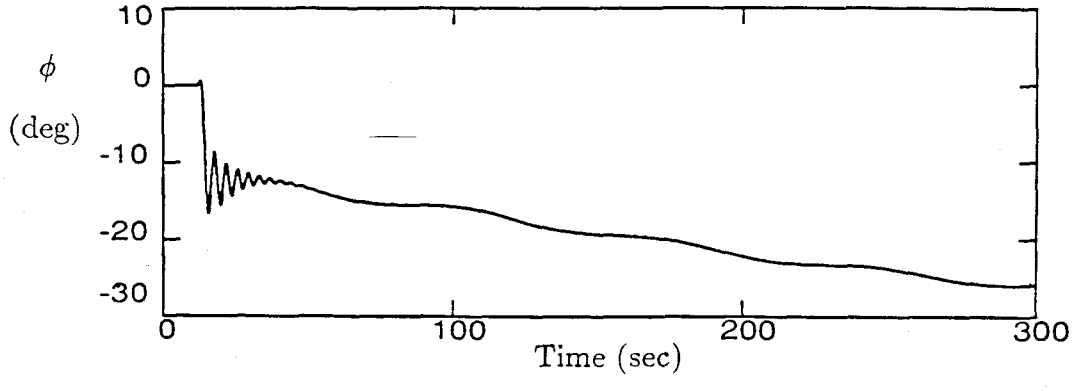

(i) Roll Angle

Figure 6.4: Concluded.

Both the wing rock and the spiral divergence can be eliminated by a simple feedback control system, as they surely are in operational F-14's. One cause of wing rock is insufficient roll damping, Ericsson [1988], which can be increased with roll rate feedback to the aileron. Spiral divergence is caused by insufficient dihedral effect, Nelson [1989], which can be augmented with sideslip feedback to the aileron. For example, if the roll rate and sideslip angle are fed back to the aileron such that

$$\delta a = K_1\beta + K_2 p,$$

then the rolling moment coefficient (neglecting rudder effects and rotary balance data) is

$$C_\ell = C_\ell(\alpha,\beta) + (K_1\beta + K_2 p)C_{\ell_{\delta a}} + \frac{b}{2V}(pC_{\ell_p} + rC_{\ell_r}),$$

and

$$C_{\ell_\beta} = \frac{dC_\ell}{d\beta} + K_1 C_{\ell_{\delta a}}$$

$$C_{\ell_p} = \frac{b}{2V}C_{\ell_p} + K_2 C_{\ell_{\delta a}}.$$

The constants K_1 and K_2 can be chosen such that the dihedral effect and roll damping are increased.

Figure 6.5 shows the purely longitudinal steady states (curve 1) when the roll rate and the sideslip angle are fed back to the aileron. The Hopf bifurcations which led to the wing rock have disappeared along with the bifurcations which led to the existence of stable steady divergent spiral motions. Comparing Figures 6.2 and 6.5 shows that the steady states represented by curve 1 are the same with

or without feedback. It should be noted that the steady states representing the spirally divergent motions could be destroyed because they only occurred for a small range of elevator deflections. The effect of the feedback was to push the two bifurcation points together causing them to destroy each other. This would not be as easy if the bifurcations occurred at vastly different elevator deflections, say ten degrees apart as opposed to one degree as in this case. Including feedback causes all the steady states represented by curve 1 to be stable.

6.3 Instabilities During Lateral Maneuvers

Figure 6.6 shows the steady states of the F-14 as a function of aileron deflection for zero rudder deflection and an elevator deflection of negative 10 degrees. For aileron deflections initiated from the purely longitudinal steady state (i.e., $\delta a = p = q = r = \beta = \phi = 0$), stable steady states exist for aileron deflections up to about 12 degrees. Increasing the aileron deflection from zero causes the aircraft to enter a spiral dive; the steady state pitch and roll angles and the velocity rapidly increase as the aileron deflection is increased (see Figures 6.6(f),(g),(h)) while the other variables change only slightly.

For aileron deflections larger than 12 degrees, the state of the aircraft will jump due to the saddle-node bifurcation which causes the curve of steady states to turn back on itself and change stability. This can be seen clearly in Figure 6.6(d) which shows the steady state angle of attack. As the aileron deflection is increased past 12 degrees (starting from zero where the angle of attack is 23 degrees), the

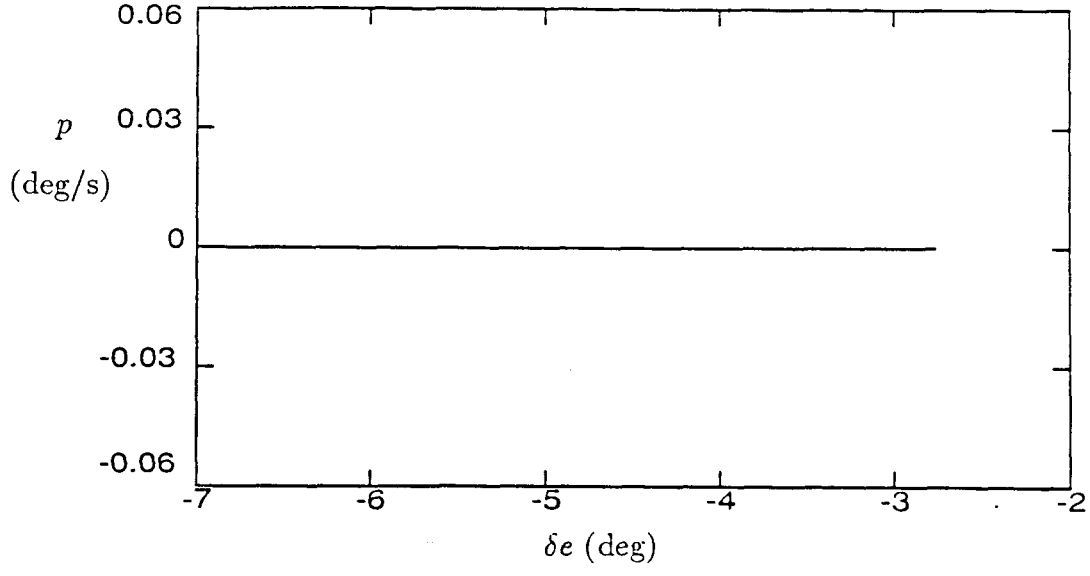

(a) Roll Rate

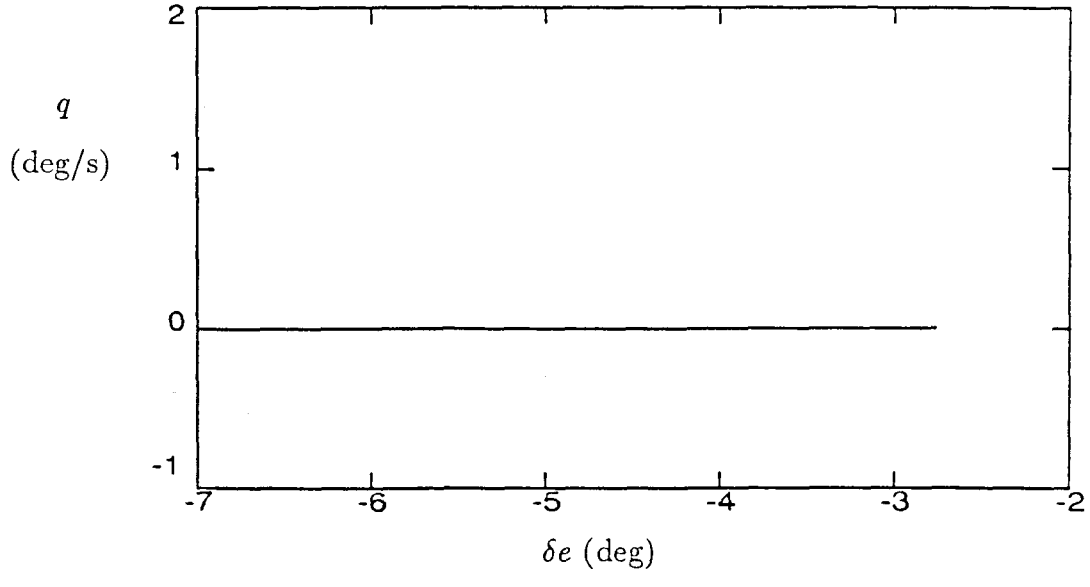

(b) Pitch Rate

Figure 6.5: Steady States for the F-14 with zero applied thrust and feedback to the ailerons, δr=0, δa=-0.1p - 0.3β; —— stable.

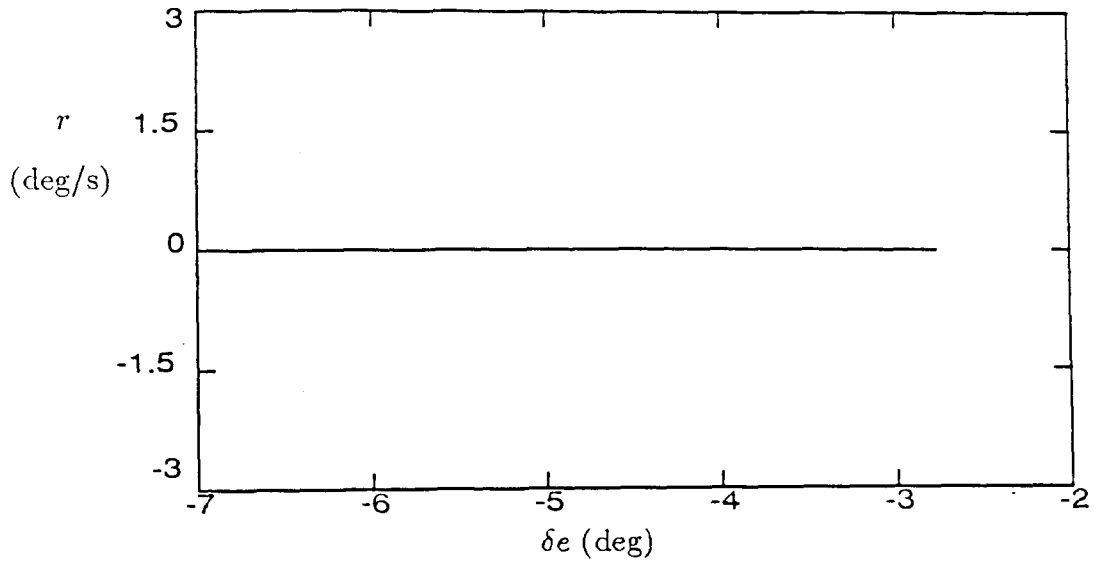

(c) Yaw Rate

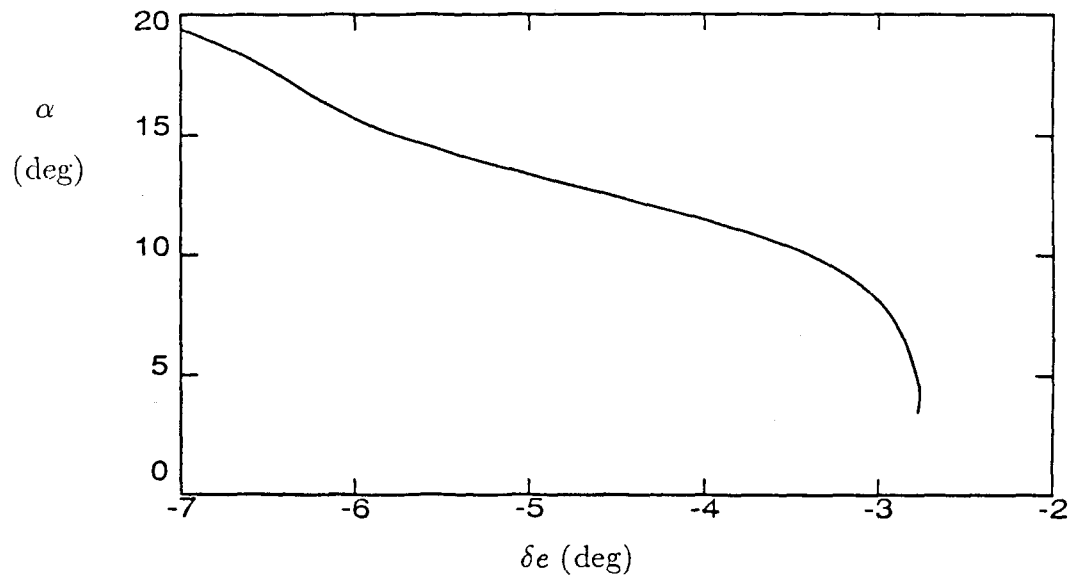

(d) Angle of Attack

Figure 6.5: Continued.

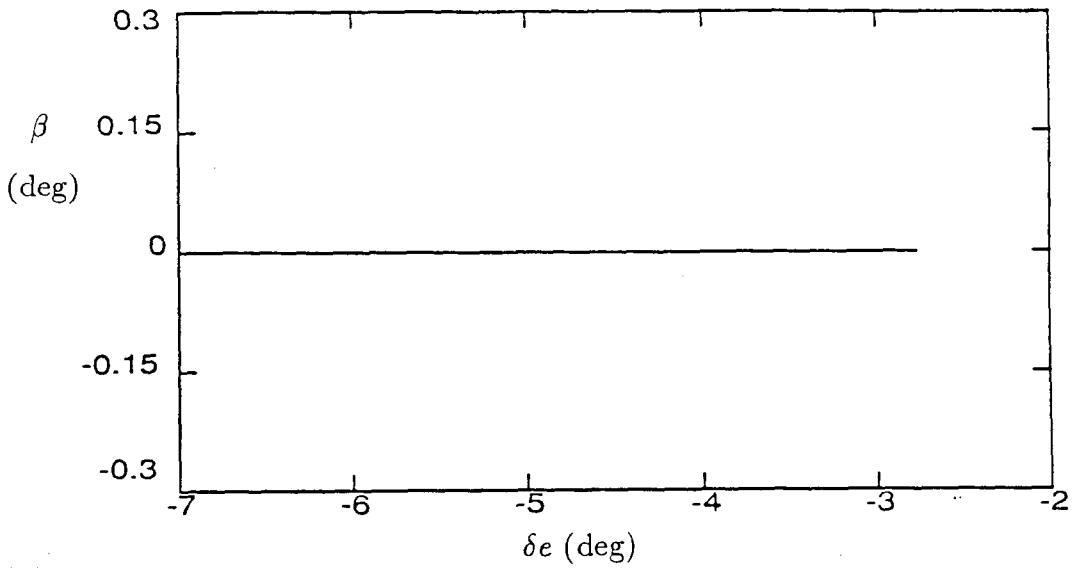

(e) Sideslip Angle

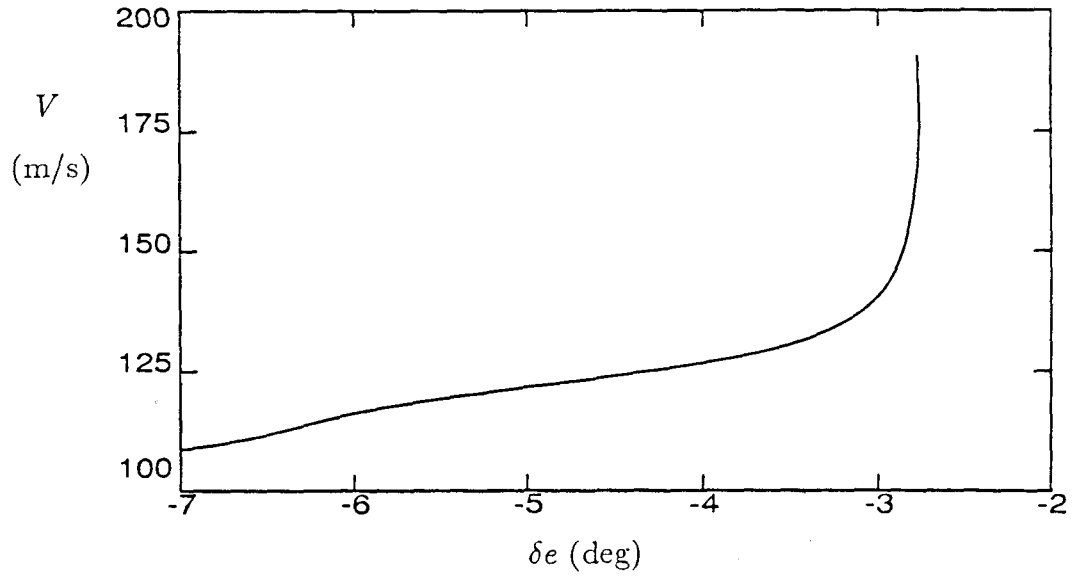

(f) Speed

Figure 6.5: Continued.

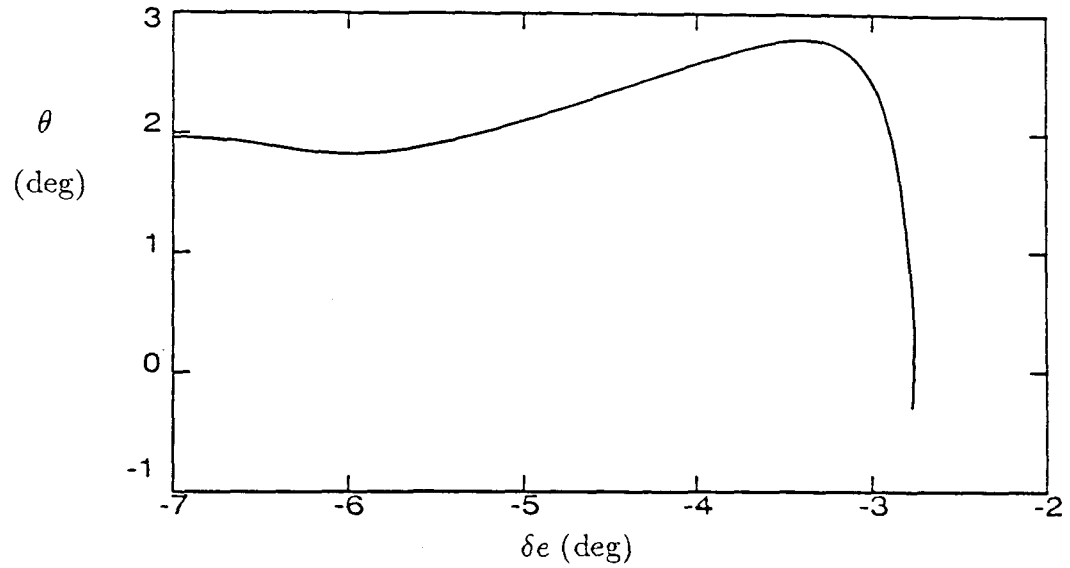

(g) Pitch Angle

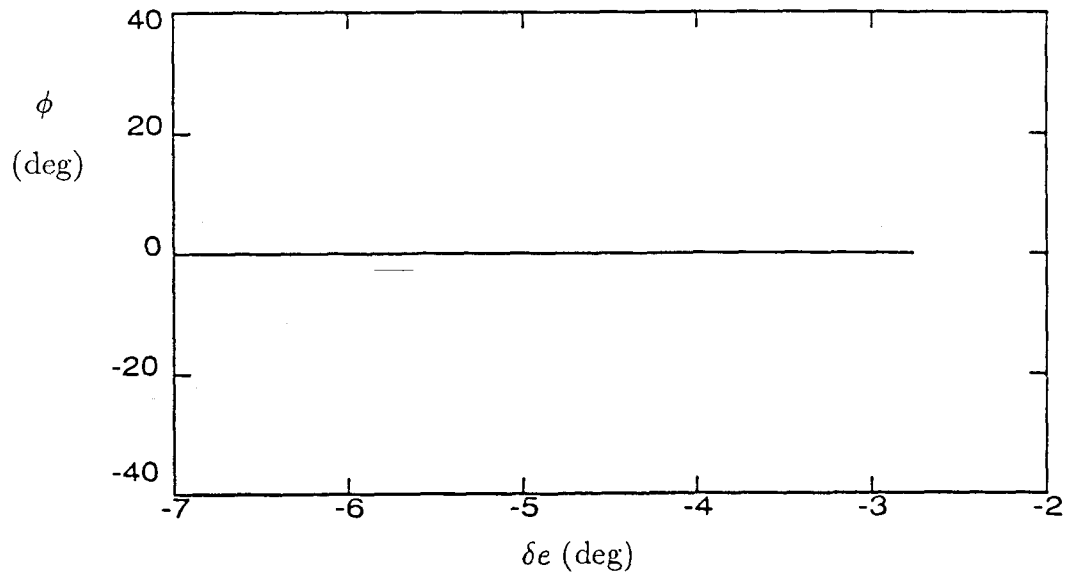

(h) Roll Angle

Figure 6.5: Concluded.

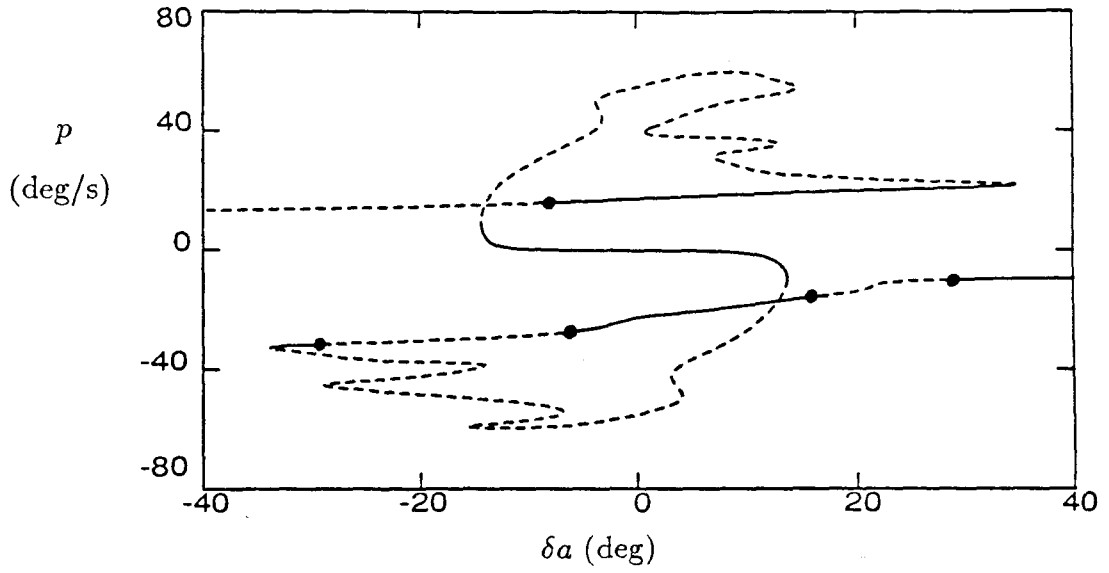

(a) Roll Rate

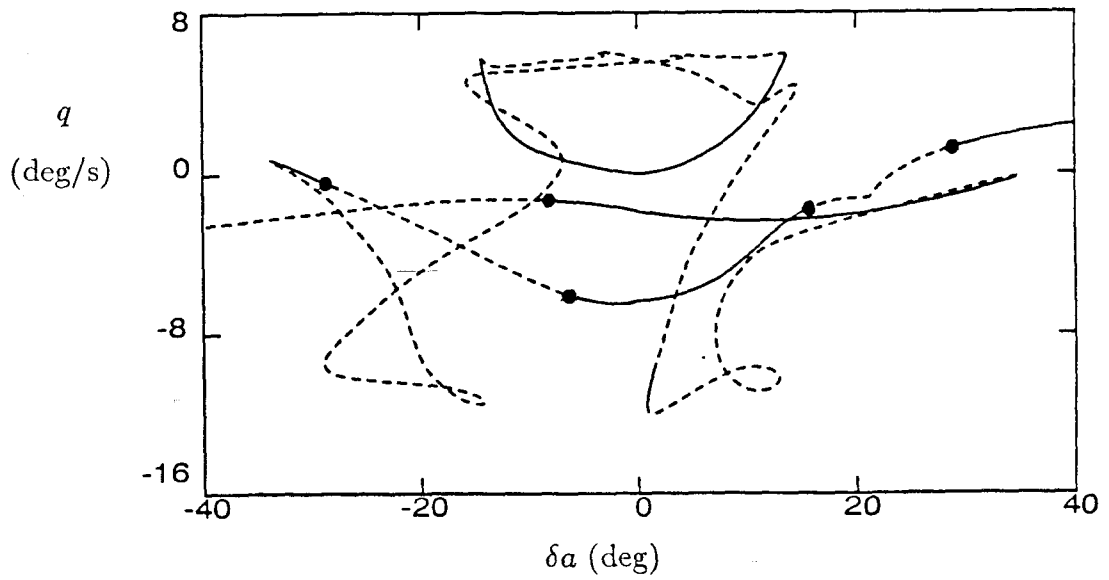

(b) Pitch Rate

Figure 6.6: Steady States for the F-14 with zero applied thrust, δr=0, δe=-10; —— stable, - - - unstable, • – Hopf bifurcation.

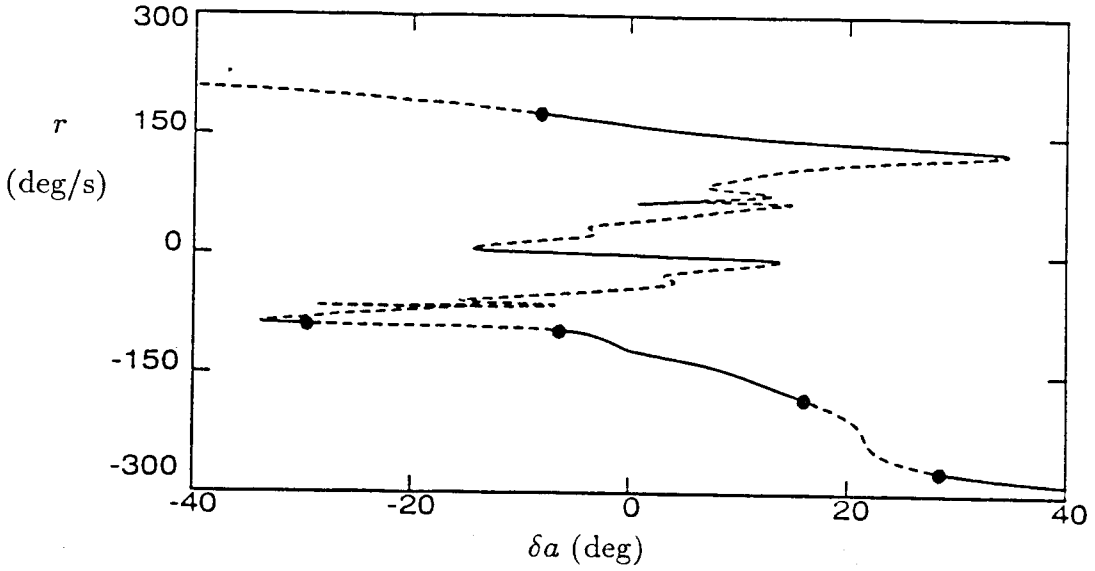

(c) Yaw Rate

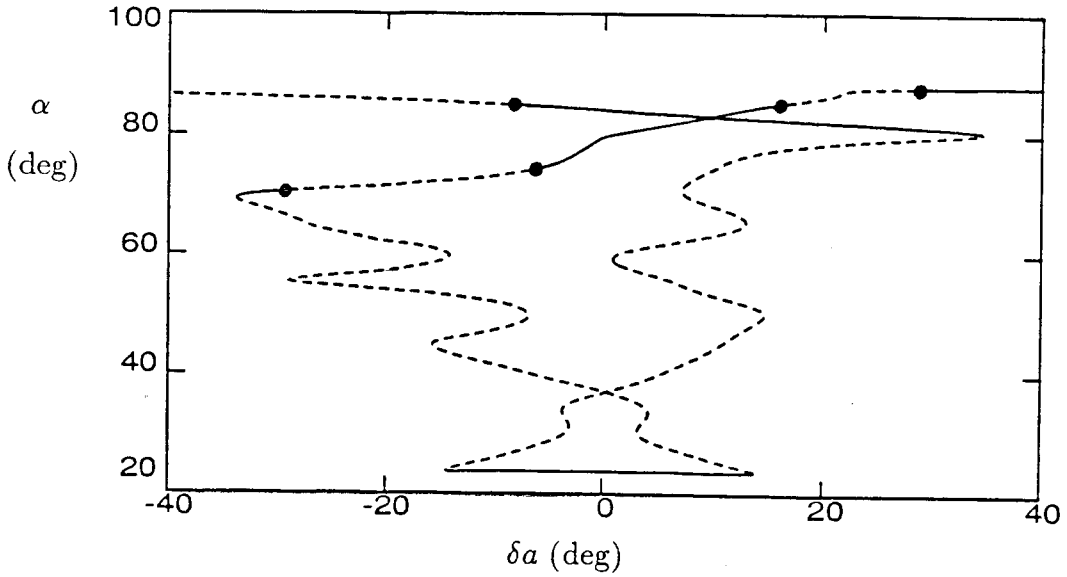

(d) Angle of Attack

Figure 6.6: Continue

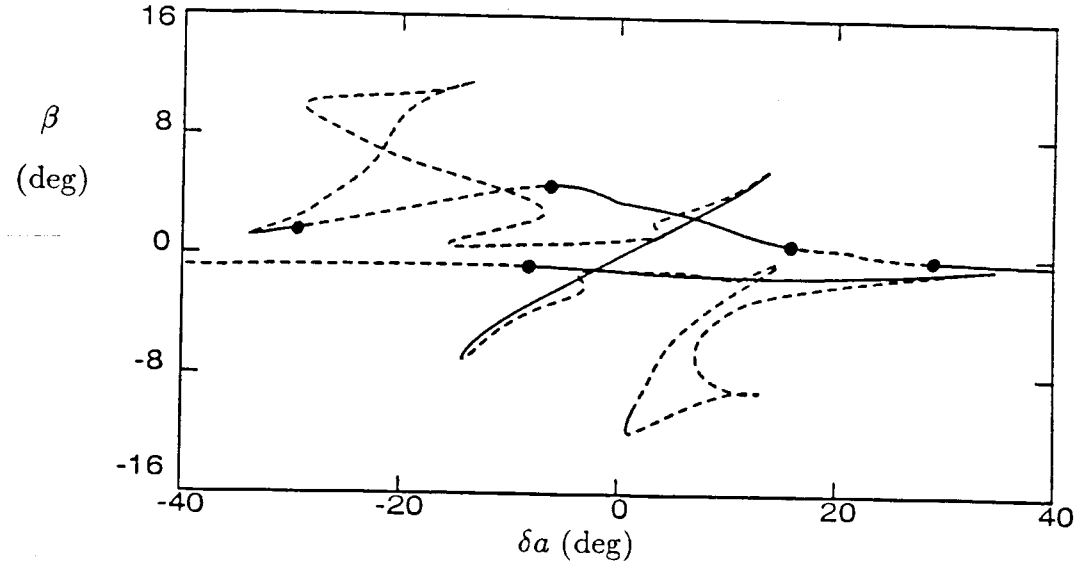

(e) Sideslip Angle

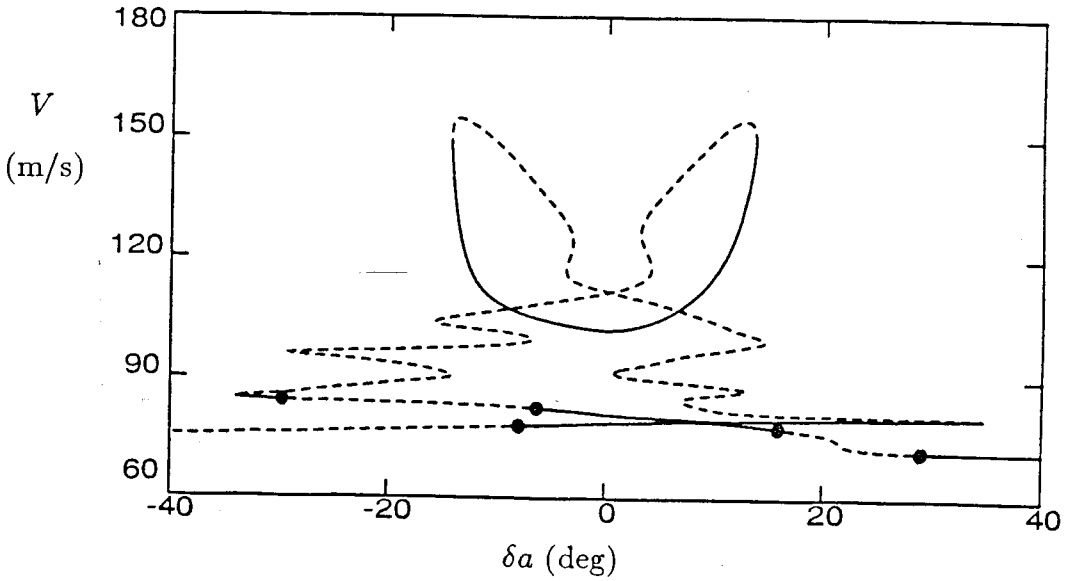

(f) Speed

Figure 6.6: Continued.

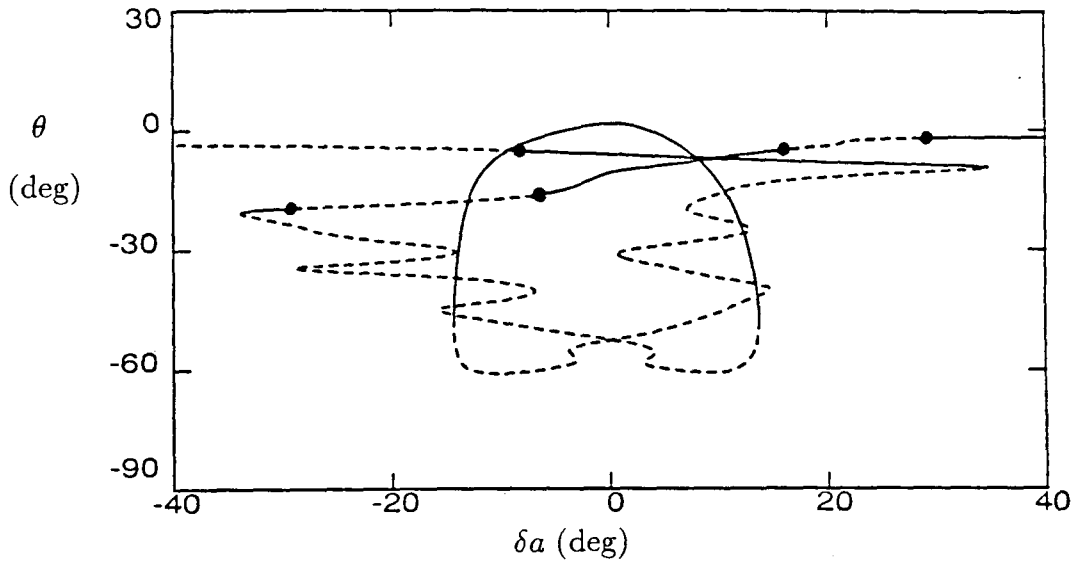

(g) Pitch Angle

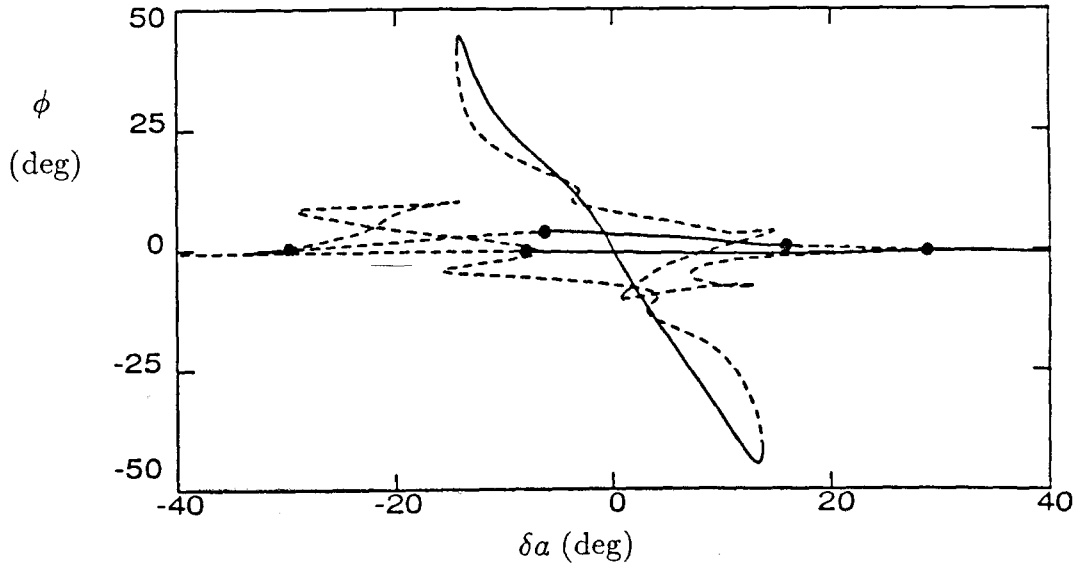

(h) Roll Angle

Figure 6.6: Concluded.

steady state angle of attack will jump to a new stable motion. Several steady states exist for an aileron deflection of, say, positive 20 degrees, some of which are stable and some unstable. It cannot be determined whether the state of the aircraft will jump to a stable steady state or some type of stable time dependent motion. Note that many Hopf bifurcations occur along the curve of steady states and each could lead to stable periodic motions.

All of the steady states except the stable segment containing the purely longitudinal steady states represent spins, which are characterized by high angles of attack and large yaw rates. It is interesting that the spin modes for an aileron deflection of zero degrees are the spin modes represented by curve 2 in Figure 6.1 at an elevator deflection of negative 10 degrees. A quick check of the flight path angles ($\gamma = \theta - \alpha$) for the steady steady spin modes shows that it is always negative 90 degrees, typical of a spin. Thus if the aileron deflection is increased past 12 degrees (positive or negative) while the elevator is held at negative 10 degrees and the rudder at zero, the aircraft will either enter a steady spin or some type of time dependent motion (most likely an oscillatory spin in which the state of the aircraft undergoes periodic oscillations). This situation is especially dangerous because it could be impossible to get out of a spin once it is entered.

For example, see Figure 6.6(c) which shows the steady state yaw rate. Assume that 15 degrees of positive aileron deflection is applied while the aircraft is in the stable purely longitudinal steady state. If the aileron deflection is changed slowly enough, the state of the aircraft will follow the curve of stable steady states until

the aileron deflection reaches 12 degrees. Beyond this point the aircraft will jump to a new stable motion. If the aircraft jumps to one of the stable steady states which have yaw rate of about 150 degrees, it could be impossible to get back to the origial steady state (i.e., r=0). One option would be to apply an aileron deflection of negative 12 degrees, which is past the Hopf bifurcations that cause these branches of steady states to become unstable, but within the range of aileron deflections for which the curve of steady states containing the purely longitudinal steady state (i.e., $r = 0$) exists. If no stable periodic motion exists as a result of the Hopf bifurcation, the state of the aircraft may jump back to the original branch of steady states.

Figure 6.7 shows a simulation of the situation discussed above. The aircraft actually goes into a spin when the aileron deflection is increased to 10 degrees (t=10 seconds), whereas the steady states predict that the jump would not occur until 12 degrees of aileron deflection had been applied. This difference could be an effect of the transient aileron deflection or of the different curve fits used in the continuation method and the simulator program. (Recall that bicubic approximations were used in the continuation routine while linear approximations were used in the simulation routine.) The aircraft seems to enter an oscillatory spin, but it is difficult to tell because the aileron deflection was changed before the oscillation could repeat itself. Decreasing the aileron deflection to negative 12 degrees decreases the yaw rate of the aircraft (see Figure 6.7(f)), but it does not bring it out of the spin.

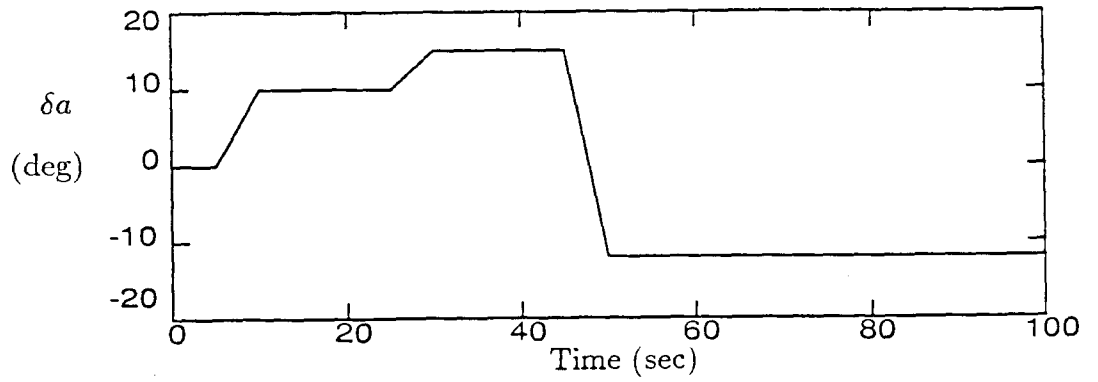

(a) Aileron Deflection

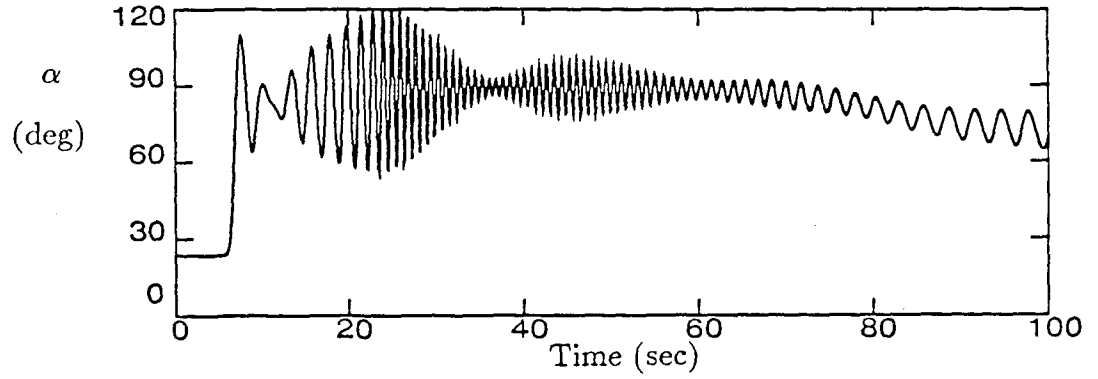

(b) Angle of Attack

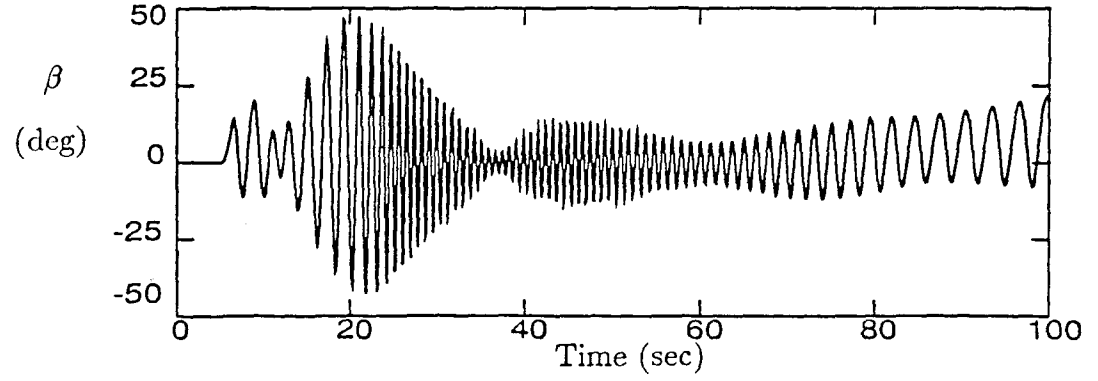

(c) Sideslip Angle

Figure 6.7: Simulation of spin entry for the F-14 with zero applied thrust, δr=0, δe=-10.

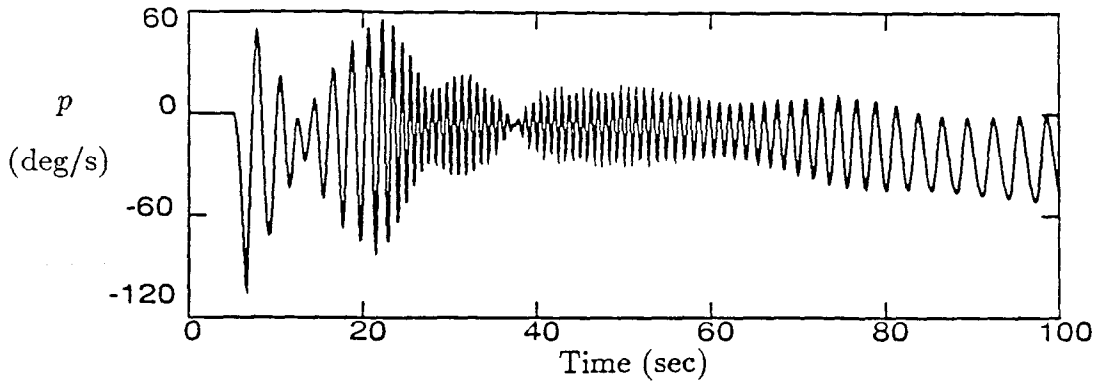

(d) Roll Rate

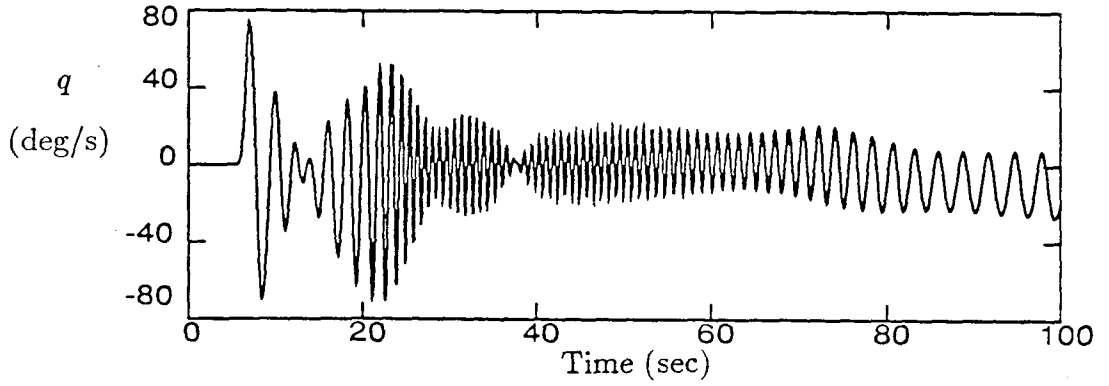

(e) Pitch Rate

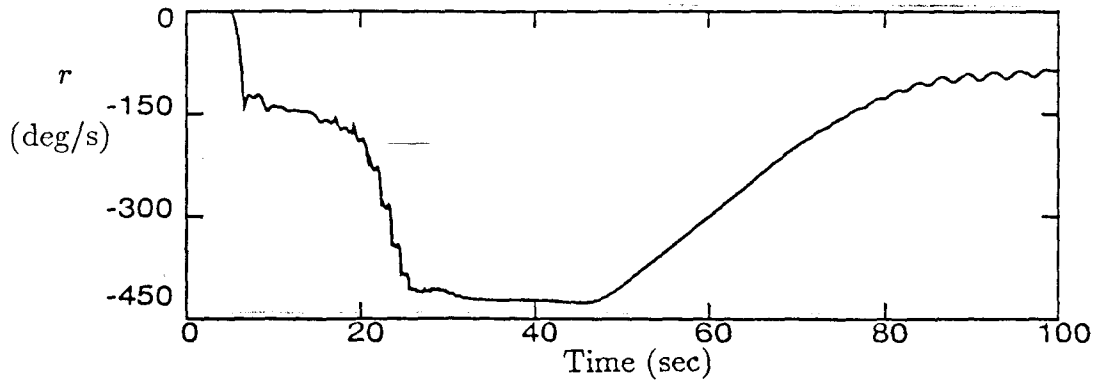

(f) Yaw Rate

Figure 6.7: Continued.

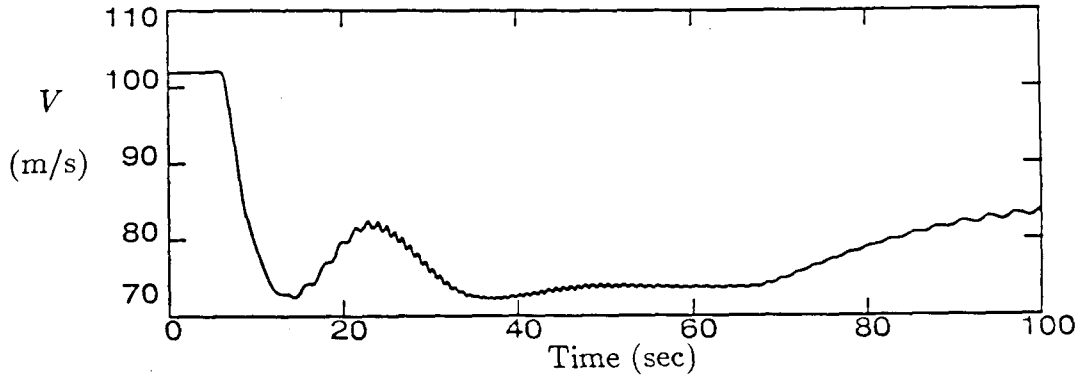

(g) Speed

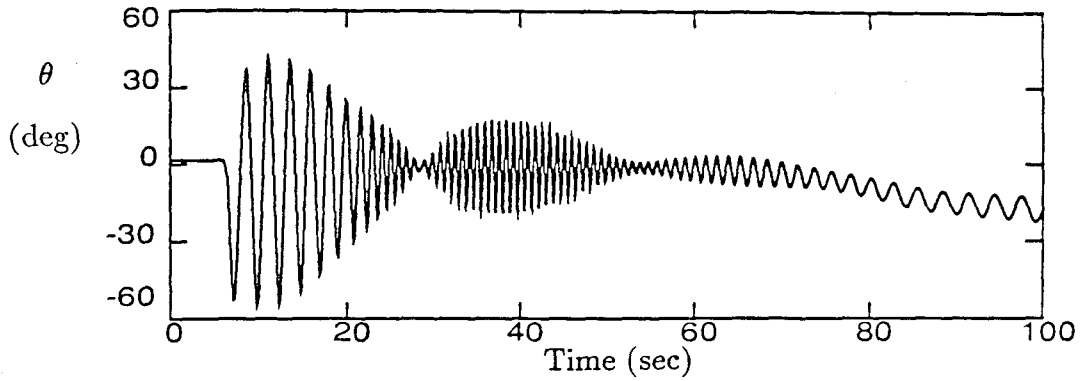

(h) Pitch Angle

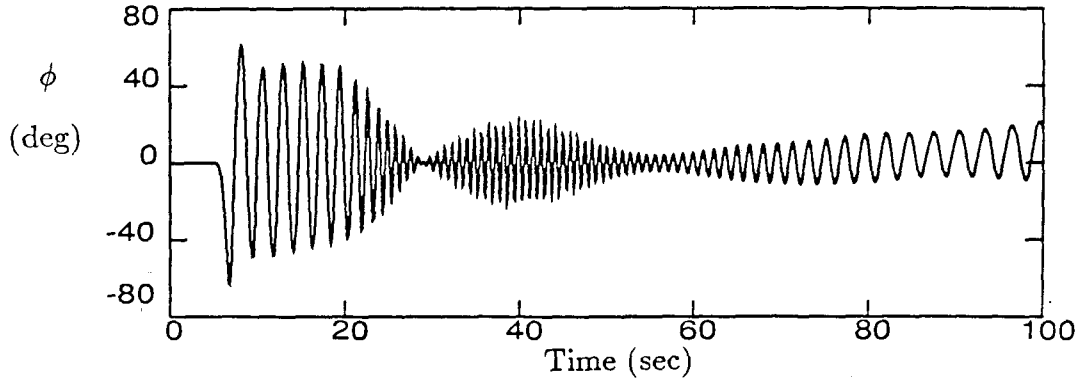

(i) Roll Angle

Figure 6.7: Concluded.

This example shows that it is impossible to get out of a spin using only ailerons when the elevator deflection is held constant at negative 10 degrees. Recall that the rudder losses effectiveness at angles of attack above 55 degrees so only the ailerons and elevator are available for attempts to recover from a spin. It would clearly be useful for pilots to know which control surface deflections cause the aircraft to enter a spin. Figure 6.8 show the aileron and elevator deflections which cause the aircraft to enter a spin for zero rudder deflection. This curve places fairly strict restrictions on the allowable aileron deflections, but these curves may change if a control system is added to the aircraft model.

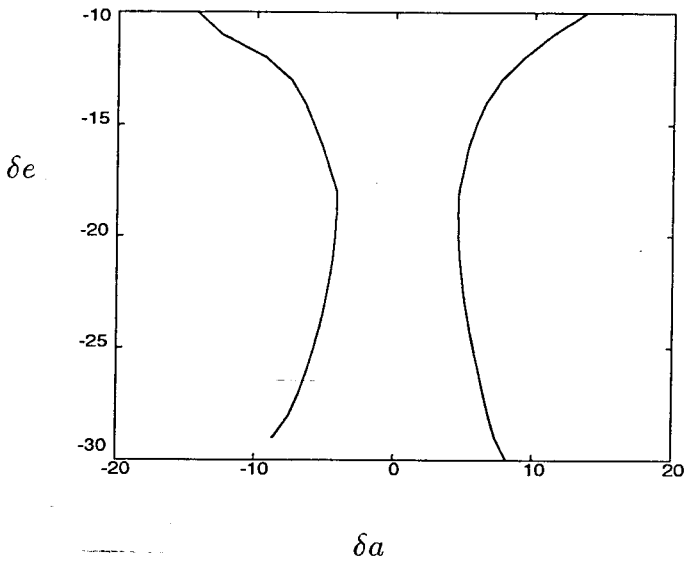

Figure 6.8: Bifurcation loci of the F-14 for zero rudder deflection.

6.4 Steady Spin Modes

The steady spin modes of the F-14 have been briefly discussed in the previous

section in relation to an instability during a lateral maneuver which caused the aircraft to enter a spin. Several additional results for the steady spin modes will be discussed in this section. Multiple spin modes exist for a broad range of control surface deflections. Figure 6.1 shows that for elevator deflections from positive 15 to negative 40 degrees with zero rudder and aileron deflections anywhere from one to nine, steady spin modes exist. It should also be recalled that more steady spin modes could exist; the search for spin modes was incomplete and there is no way to prove that all the spin modes have been found.

The steady spin modes range from steep spins with angles of attack of 45 degrees to flat spins with angles of attack of nearly 90 degrees. Steady spins labelled 4N and 4P have the highest angles of attack but these steady spins were always unstable for the range of control surface deflections used in the course of this study. The curves of steady spins labelled 3N and 3P contain both stable and unstable steady spins. Many Hopf bifurcations occur along these curves of steady states, so the existence of oscillatory spins is highly probable. (Recall the simulation in Figure 6.7 where the existence of stable oscillatory spins made it impossible to get out of a spin.)

Figure 6.1 shows that no steady spin modes (stable or unstable) exist for elevator delection greater than 40 degrees. Thus, it might be possible to recover from a spin by applying maximum nose up elevator (i.e., $\delta e = -40$). Also note that the steady states represented by curve 1 exist and are stable for an elevator

deflection of 40 degrees. Figure 6.9 shows a simulation of an attempt to recover from a spin by applying maximum nose up elevator.

The simulation was started with the aircraft trimmed at an angle of attack of 13 degrees, which corresponds to an elevator deflection of negative 5 degrees. A small perturbation in the aileron deflection causes the aircraft to enter a spin (see Figure 6.9(b)). In an attempt to recover, the elevator deflection was increased to negative 30 degrees (t=20 seconds) at which point the steady spin mode is unstable (see Figure 6.1). Instead of jumping to the stable steady states represented by curve 1, the aircraft entered an oscillatory spin (see Figure 6.9(b)). Maximum nose up elevator deflection was then applied ($\delta e = -40$). No stable or unstable steady spin modes exist for these control surface deflections, but the oscillatory spin persisted. In a final attempt to exit the spin, maximum nose down elevator was applied ($\delta e = 15$). This was not a successful spin recovery as the oscillatory spin persisted.

This example shows that knowledge of the steady spin modes of an aircraft is not always sufficient for developing a spin recovery technique. Stable oscillatory spin modes can be present when no steady states exist and can make it impossible to exit a developed spin. Continuation methods can be used to determine curves of periodic motions as a function of a parameter of the system similiar to what was done for the steady states, Doedel [1984]. These techniques were not used during the course of this study, but it would be very valuable to be able to determine the oscillatory spin modes as well as the steady spin modes of an aircraft.

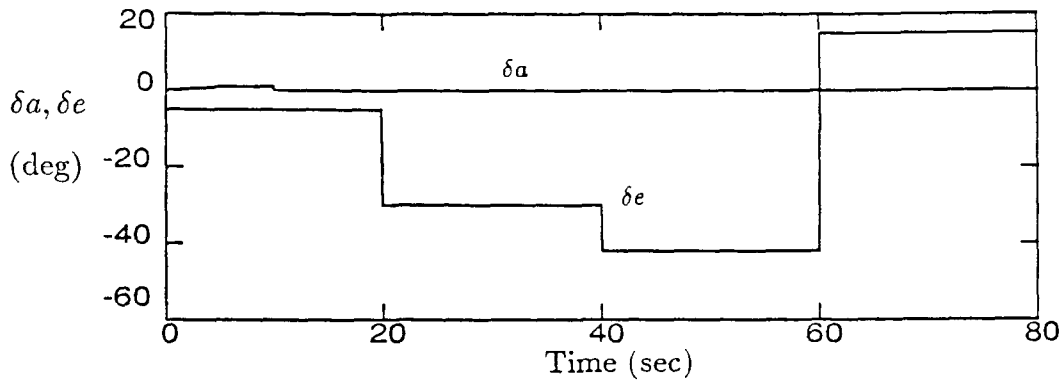

(a) Aileron and Elevator Deflections

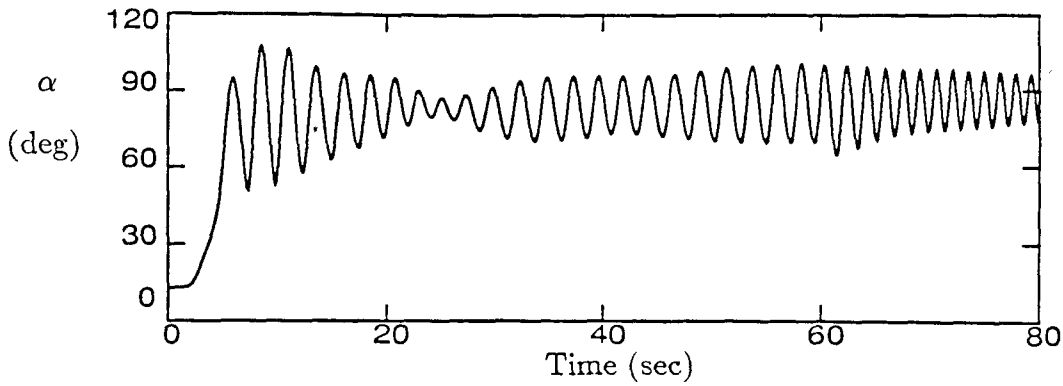

(b) Angle of Attack

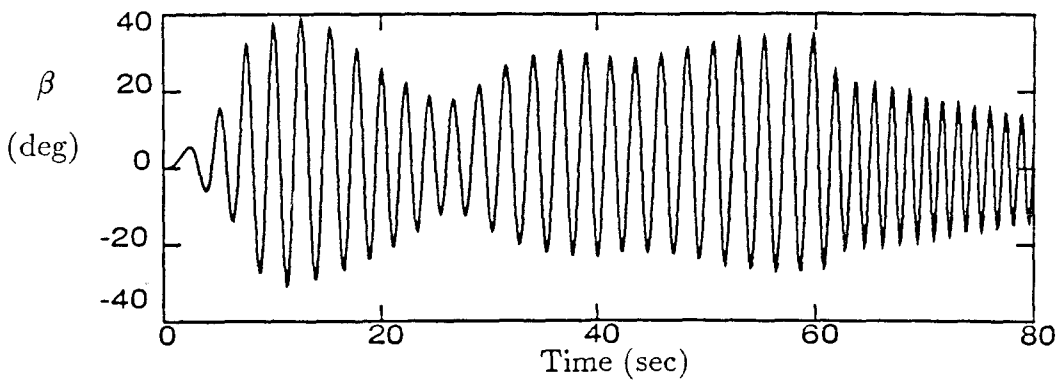

(c) Sideslip Angle

Figure 6.9: Simulation of spin entry for the F-14 with zero applied thrust, δr=0.

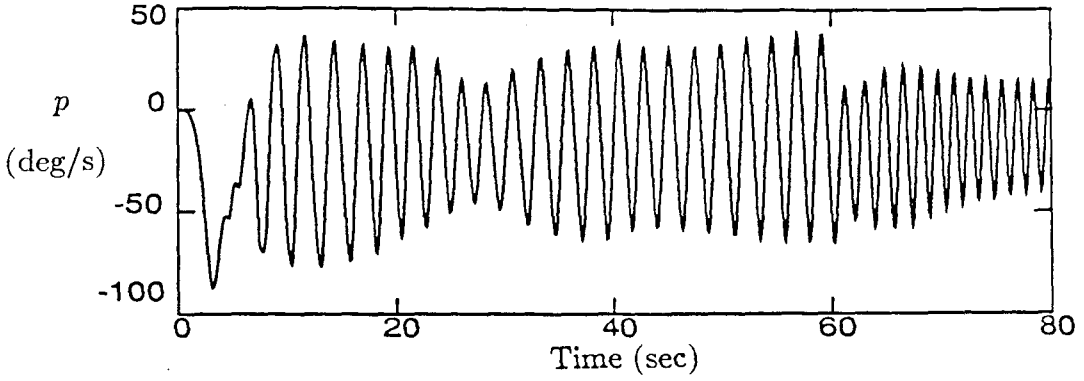

(d) Roll Rate

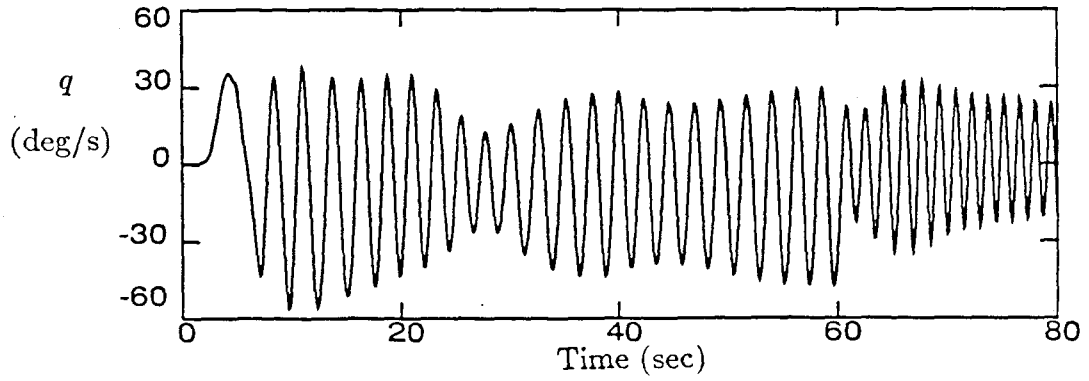

(e) Pitch Rate

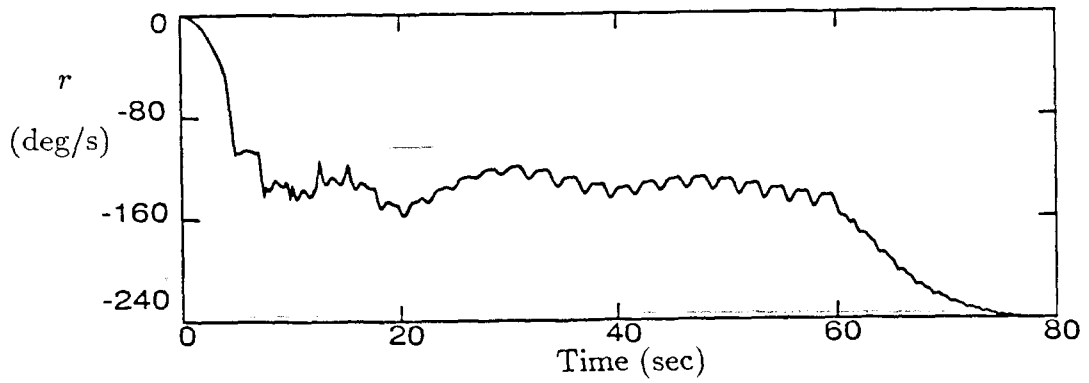

(f) Yaw Rate

Figure 6.9: Continued.

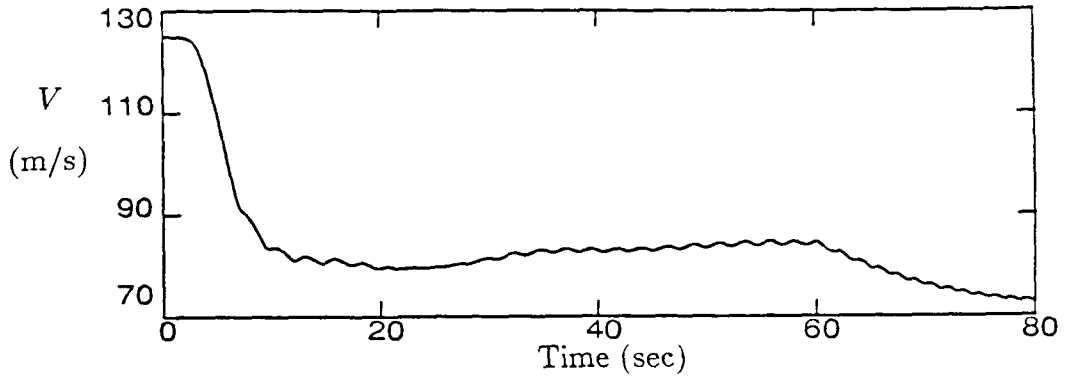

(g) Speed

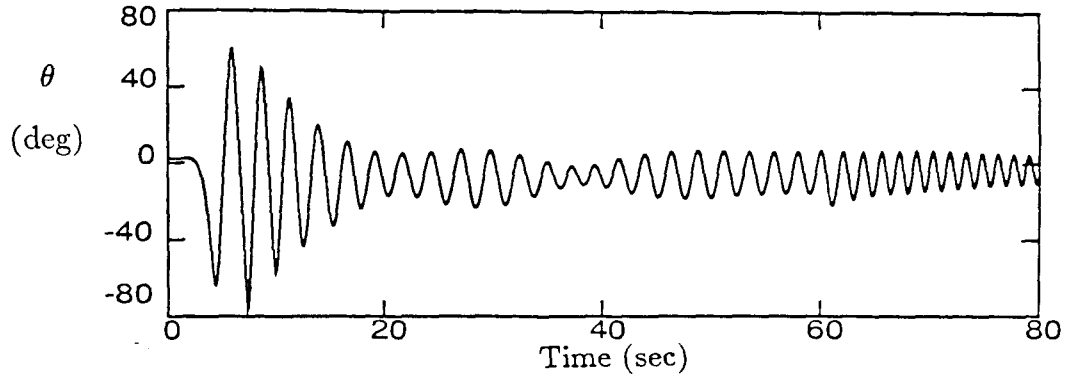

(g) Pitch Angle

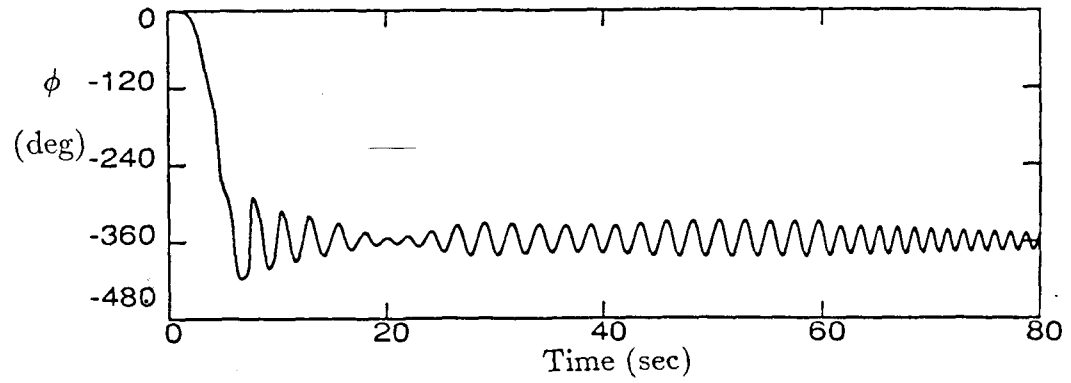

(i) Roll Angle

Figure 6.9: Concluded.

6.5 Summary of the Results for the F-14

Steady states of the F-14 were determined using the full equations of motion and a nonlinear aerodynamic model. Both wing rock and spiral divergence instabilities were found to occur in the steady state trim conditions. The wing rock instability was eliminated when roll rate feedback to the aileron was used to augment the roll damping of the aircraft. Spiral divergence was eliminated by using sideslip feedback to the aileron to augment the dihedral effect of the aircraft.

Instabilities related to saddle-node bifurcations were found to occur as the aileron deflection was increased from trimmed flight with no rudder deflection. These instabilities resulted in a jump in the state of the aircraft, causing the aircraft to enter a spin. All attempts at recovery from the spin proved futile. The existence of steady oscillatory spin modes was shown to be a major cause of the difficulty in developing successful recovery techniques for the F-14. Also, because the rudder is ineffective at angles of attack above 55 degrees, only the ailerons and elevator were available to attempt to recover from a spin.

VII. CONCLUSIONS

A continuation method has been used to determine the steady states of three nonlinear aircraft models: a general aviation canard configuration aircraft, a generic jet fighter, and the F-14. Bifurcations of these steady states have been determined and were shown to cause instabilities which resulted in qualitative changes in the state of the aircraft. Knowledge of the steady states of the aircraft was used to predict the result of an instability and to design recovery techniques. Control systems were added to the aircraft models to determine whether or not feedback could be used to eliminate the instabilities. Specific results for each aircraft are given in the following sections.

7.1 Conclusions from the Analysis of the General Aviation Aircraft with a Canard Configuration

Thrust has an adverse effect on the longitudinal stability of this aircraft, and application of thrust was shown to cause the aircraft to enter a deep stall. A recovery technique was determined by calculating the combination of thrust and elevator deflections for which the deep stall did not exist. The recovery technique was to apply nose down elevator and reduce the thrust. This aircraft also suffered from a phugoid instability at high thrust. A control system which used velocity feedback to the elevator was desiged to eliminate this instability. Feedback gain was used as the parameter in the continuation method and the gain which resulted in the maximum damping of the phugoid mode was used in the control system.

It should be noted that the nonlinear equations of motion were used to determine the feedback gain.

7.2 Conclusions from the Analysis of the Generic Jet Fighter

This aircraft model was mainly used to study the roll-coupling instability. It was shown that the jump phenomena associated with roll-coupling instabilities only occur at negative angles of attack. Roll-coupling effects at positive angles of attack lead to large sideslip deviations, but no jump in the state of the aircraft. A study of the moment balance showed that sideslip deviations are a result of the inertial yawing moment and that the jump in the state of the aircraft was a result of the change in sign of the pitching moment coefficient.

The roll-coupling instabilities of this aircraft were analyzed with the fifth, sixth and eighth order equations of motion. Steady state angles of attack and sideslip for given control surface deflections were similar for the three systems, but the steady state rotation rates and velocities were different. Bifurcations of the steady states were shown to occur at almost the same control surface deflections for each system. From these results it was concluded that the fifth or sixth order equations of motion can be used to predict control surface deflections which lead to jumps in the state of the aircraft. By determining the steady states of the eighth order equations of motion, it was shown that jumps in the state of the aircraft related to roll-coupling instabilities occur when the aircraft is in a steep dive. The

jump in the state of the aircraft causes the aircraft to go from an inverted dive to an upright dive, but the pitch angle remains near negative 90 degrees.

7.3 Conclusions from the Analysis of the F-14

Steady states of the F-14 were computed as functions of the aileron and elevator deflections for zero rudder deflection. Wing rock and spiral divergence instabilities were found to occur in the trim conditions of the aircraft. Roll rate and sideslip feedback were used to eliminate both of these instabilities. Instabilities during lateral maneuvers with no rudder deflection were found to cause the aircraft to enter a spin. Combinations of aileron and elevator deflections which caused the aircraft to enter a spin were computed. Since the rudder is ineffective for angles of attack above 55 degrees, spin recovery techniques involving only aileron and elevator deflections were attempted, but none were successful.

APPENDIX I

Calculation of the Center Manifold for a System With Parameter Dependence

Consider the Lorenz equations which are given by

$$\begin{aligned} \dot{x} &= \sigma(y - x) \\ \dot{y} &= \rho x + x - y - xz \\ \dot{z} &= -\beta z + xy \end{aligned} \tag{I.1}$$

where σ, ρ, and β are parameters. For physical reasons, σ and β are usually treated as fixed and greater than zero, while ρ is treated as a variable parameter. This convention will be used in this calculation. It is easy to see that the origin is always a fixed point of the Lorenz equations. The stability of the origin can be determined by calculating the eigenvalues of the linearized system. Linearizing about the origin gives

$$\begin{pmatrix} \dot{u} \\ \dot{v} \\ \dot{w} \end{pmatrix} = \begin{pmatrix} -\sigma & \sigma & 0 \\ \rho + 1 & -1 & 0 \\ 0 & 0 & -\beta \end{pmatrix} \begin{pmatrix} u \\ v \\ w \end{pmatrix} \tag{I.2}$$

whose eigenvalues are given by

$$\lambda = -\beta, \ -D\left(1 \pm \sqrt{1 + \rho \frac{\sigma}{D^2}}\right)$$

where

$$D = \frac{\sigma + 1}{2}.$$

One eigenvalue is zero when ρ is zero, while the other two eigenvalues have real parts less than zero, so a bifurcation will occur at the origin when ρ is zero. The

nature of the bifurcation can be determined by computing the center manifold passing through the origin for values of ρ near zero.

Before the procedures developed in Section 2.1.6 can be applied to the Lorenz equations, the linear part of the equation must be put in Jordan normal form. This can be done with the transformation

$$\vec{x} = T\vec{u} \tag{I.3}$$

where T is a matrix whose columns are composed of the eigenvectors of the linearized system. For this system

$$T = \begin{pmatrix} 1 & \sigma & 0 \\ 1 & -1 & 0 \\ 0 & 0 & 1 \end{pmatrix} \tag{I.4}$$

so the coordinate transformation is

$$\begin{aligned} x &= u + \sigma v \\ y &= u - v \\ z &= w. \end{aligned} \tag{I.5}$$

Substituting equation I.3 into the general dynamical system,

$$\dot{x} = Ax + f(x)$$

gives

$$T\dot{u} = ATu + f(Tu)$$

which can be solved for $\dot{u}$ to obtain

$$\dot{u} = T^{-1}ATu + T^{-1}f(Tu). \tag{I.6}$$

Applying this transformation to the Lorenz equations gives the system

$$\begin{pmatrix} \dot{u} \\ \dot{v} \\ \dot{w} \end{pmatrix} = \begin{pmatrix} 0 & 0 & 0 \\ 0 & -(\sigma+1) & 0 \\ 0 & 0 & -\beta \end{pmatrix} \begin{pmatrix} u \\ v \\ w \end{pmatrix} + \frac{u+\sigma v}{\sigma+1} \begin{pmatrix} \sigma(\rho-w) \\ -(\rho-w) \\ (\sigma+1)(u-v) \end{pmatrix} \qquad (I.7)$$

whose linear part is in Jordan normal form. This system has a two-dimensional stable manifold (v, w) and a two-dimensional center manifold (u, ρ). The center manifold has the form

$$W^c = ((u, v, w, \rho) | v = h_1(u, \rho), w = h_2(u, \rho), h_i(0, 0) = 0, Dh_i(0, 0) = 0)$$

so the system can be written,

$$\begin{aligned} \dot{u} &= Bu + f(u, \rho, h_1, h_2) \\ \begin{pmatrix} \dot{v} \\ \dot{w} \end{pmatrix} &= C \begin{pmatrix} v \\ w \end{pmatrix} + g(u, \rho, h_1, h_2) \end{aligned} \qquad (I.8)$$

where

$$B = 0, \quad f = \frac{\sigma}{1+\sigma}(\rho - w)(u + \sigma v)$$
$$C = \begin{pmatrix} -(1+\sigma) & 0 \\ 0 & -\beta \end{pmatrix}, \quad g = \begin{pmatrix} \frac{1}{1+\sigma}(w-\rho) \\ u - v \end{pmatrix} (u + \sigma v).$$

Using the equation for the center manifold we can write

$$\begin{aligned} \begin{pmatrix} \dot{v} \\ \dot{w} \end{pmatrix} &= D \begin{pmatrix} h_1(u, \rho) \\ h_2(u, \rho) \end{pmatrix} \dot{u} \\ &= C \begin{pmatrix} h_1(u, \rho) \\ h_2(u, \rho) \end{pmatrix} + g(u, \rho, h_1, h_2) \end{aligned} \qquad (I.9)$$

which can be written as the functional equation,

$$Dh[Bu + f(u, \rho, h)] = Ch + g(u, \rho, h). \qquad (I.10)$$

The center manifold in a neighborhood of the origin can be approximated by

$$\begin{aligned} h_1(u, \rho) &= a_1 u^2 + a_2 u\rho + a_3 \rho^3 + \cdots \\ h_2(u, \rho) &= b_1 u^2 + b_2 u\rho + b_3 \rho^2 + \cdots, \end{aligned} \qquad (I.11)$$

and substituting these relations into the functional equation for the center manifold, equation I.10, gives

$$\begin{pmatrix} 2a_1u + a_2\rho + \cdots \\ 2b_1u + b_2\rho + \cdots \end{pmatrix} \left(\tfrac{\sigma}{1+\sigma}\rho u + \cdots \right) - \begin{pmatrix} \frac{-1}{1+\sigma}(\rho u + \cdots) \\ u^2 + \cdots \end{pmatrix} \begin{pmatrix} (1+\sigma)(a_1u^2 + a_2u\rho + a_3\rho^2 + \cdots) \\ \beta(b_1u^2 + b_2u\rho + b_3\rho^2 + \cdots) \end{pmatrix} = 0. \tag{I.12}$$

Matching terms of equal powers of u and ρ in each equation,

$$\begin{aligned} u^2: &\quad a_1 = 0, \qquad \beta b_1 - 1 \to b_1 = \frac{1}{\beta} \\ u\rho: &\quad (1+\sigma)a_2 + \frac{1}{1+\sigma} = 0 \to a_2 = \frac{-1}{(1+\sigma)^2}, \qquad b_2 = 0 \\ \rho^2: &\quad a_3 = 0, \qquad b_3 = 0, \end{aligned}$$

so the equation for the center manifold is

$$\begin{aligned} v &= \frac{-1}{(1+\sigma)^2}u\rho + \cdots \\ w &= \frac{1}{\beta}u^2 + \cdots \end{aligned} \tag{I.13}$$

Substituting these relations into the differential equation for u gives

$$\dot{u} = \frac{\sigma}{1+\sigma}u\left(\rho - \frac{1}{\beta}u^2 - \frac{\sigma}{(1+\sigma)^2}\rho^2\right) + \cdots \tag{I.14}$$

which gives the dynamics of the system restricted to the center manifold. Equation I.14 is the equation for a pitchfork bifurcation occurring at the origin when ρ equals zero. For ρ less than zero, the origin is the only fixed point and it is stable, while for ρ greater than zero, the origin is unstable but two new stable fixed points appear.

APPENDIX II

Derivation of the Equations of Motion

II.1 Rotational Accelerations

The change in angular momentum of a body relative to an inertial reference frame is

$$\vec{N} = (\frac{d\vec{L}}{dt})_{in} \qquad (II.1)$$

where $\vec{N}$ is the applied moment and $\vec{L}$ is the angular momentum. We are interested in the angular accelerations of an aircraft in an axis system which is fixed to the aircraft, which is not an inertial reference frame, so we must use the transformation

$$(\frac{d\vec{L}}{dt})_{in} = (\frac{d\vec{L}}{dt})_{rot} + \vec{\omega} \times \vec{L} \qquad (II.2)$$

where $\vec{\omega}$ is the angular velocity of the aircraft and 'in' and 'rot' represent inertial and rotational reference frames.

The angular momentum of a body is given by

$$\vec{L} = I \bullet \vec{\omega} \qquad (II.3)$$

where I is the inertia tensor of the body. If the inertia of the body is constant, the change of angular momentum is

$$(\frac{d\vec{L}}{dt})_{rot} = (I \bullet \frac{d\vec{\omega}}{dt})_{rot}. \qquad (II.4)$$

Now combining equations II.1-II.4 gives

$$\vec{N} = I \bullet \frac{d\vec{\omega}}{dt} + \vec{\omega} \times (I \bullet \vec{\omega}). \qquad (II.5)$$

Defining the moment and angular velocity vectors as

$$\vec{N} = (\ell, m, n)$$

$$\vec{\omega} = (p, q, r)$$

and the inertia tensor as

$$I = \begin{pmatrix} I_{xx} & I_{yx} & I_{zx} \\ I_{xy} & I_{yy} & I_{zy} \\ I_{xz} & I_{yz} & I_{zz} \end{pmatrix}$$

allows equation II.5 to be written

$$\begin{pmatrix} \ell \\ m \\ n \end{pmatrix} = \begin{pmatrix} I_{xx} & I_{yx} & I_{zx} \\ I_{xy} & I_{yy} & I_{zy} \\ I_{xz} & I_{yz} & I_{zz} \end{pmatrix} \begin{pmatrix} \dot{p} \\ \dot{q} \\ \dot{r} \end{pmatrix} + \begin{pmatrix} p \\ q \\ r \end{pmatrix} \times \begin{pmatrix} I_{xx} & I_{yx} & I_{zx} \\ I_{xy} & I_{yy} & I_{zy} \\ I_{xz} & I_{yz} & I_{zz} \end{pmatrix} \begin{pmatrix} p \\ q \\ r \end{pmatrix}.$$

Carrying out the operations we find the system

$$\ell = I_{xx}\dot{p} + I_{xy}\dot{q} + I_{xz}\dot{r} + I_{yz}(q^2 - r^2) + I_{xz}pq - I_{xy}pr + (I_{zz} - I_{yy})qr$$

$$m = I_{xy}\dot{p} + I_{yy}\dot{q} + I_{yz}\dot{r} + I_{xz}(r^2 - p^2) + I_{xy}qr - I_{yz}pq + (I_{xx} - I_{zz})pr$$

$$n = I_{xz}\dot{p} + I_{yz}\dot{q} + I_{zz}\dot{r} + I_{xy}(p^2 - q^2) + I_{yz}pr - I_{xz}qr + (I_{yy} - I_{xx})pq.$$

If a principle axis system is used,

$$I_{xy} = I_{xz} = I_{yz} = 0$$

and the equations can be written

$$\begin{aligned} \ell &= I_{xx}\dot{p} + (I_{zz} - I_{yy})qr \\ m &= I_{yy}\dot{q} + (I_{xx} - I_{zz})pr \\ n &= I_{zz}\dot{r} + (I_{yy} - I_{xx})pq. \end{aligned} \qquad (II.6)$$

II.2 Translational Acceleration

The change in linear momentum relative to an inertial axis system is

$$(\frac{d(M\vec{v}_{in})}{dt})_{in} = \vec{F} \qquad (II.7)$$

where M is the mass, $\vec{v}_{in}$ is the translational velocity in an inertial axis system, and F is the applied force. For constant mass equation II.7 is

$$M(\frac{d\vec{v}_{in}}{dt})_{in} = \vec{F}. \qquad (II.8)$$

The acceleration in the inertial axis system is related to the acceleration in the rotational system by

$$(\frac{d\vec{v}_{in}}{dt})_{in} = (\frac{d\vec{v}_{in}}{dt})_{rot} + \vec{\omega} \times \vec{v}_{in},$$

so equation II.2 becomes

$$\vec{F} = ((\frac{d\vec{v}_{in}}{dt})_{rot} + \vec{\omega} \times \vec{v}_{in})M. \qquad (II.9)$$

Defining the velocity as (u, v, w) allows us to write

$$\begin{aligned} F_x &= (\dot{u} + qw - rv)M \\ F_y &= (\dot{v} + ru - pw)M \\ F_z &= (\dot{w} + pv - qu)M. \end{aligned} \qquad (II.10)$$

Since the aerodynamic forces and moments acting on the aircraft are functions of the angles of attack and sideslip and the Mach number, it is useful to write equation II.10 in terms of these variables. The angles of attack and sideslip are defined as

$$\alpha = sin^{-1}(\frac{w}{\sqrt{u^2 + w^2}}) \qquad (II.11a)$$

$$\beta = sin^{-1}(\frac{v}{\sqrt{u^2 + v^2 + w^2}}), \qquad (II.11b)$$

and the magnitude of the velocity is given by

$$V = \sqrt{u^2 + v^2 + w^2}. \qquad (II.11c)$$

Differentiating equation II.11c with respect to time, we find

$$\begin{aligned}\dot{V} =& \frac{1}{V}(u\dot{u} + v\dot{v} + w\dot{w}) \\ =& \cos\beta\cos\alpha\dot{u} + \sin\beta\dot{v} + \cos\beta\sin\alpha\dot{w},\end{aligned}$$

and substitution of equation II.10 for $\dot{u}$, $\dot{v}$, and $\dot{w}$ gives

$$\dot{V} = \frac{1}{M}(F_x\cos\alpha\cos\beta + F_y\sin\beta + F_z\sin\alpha\cos\beta). \qquad (II.12)$$

The differential equation for the sideslip angle can be derived by writing equation II.11b as

$$\sin\beta = \frac{v}{V}$$

and taking the derivative with respect to time to obtain

$$\dot{\beta} = \frac{1}{V\cos\beta}(\dot{v} - \sin\beta\dot{V}). \qquad (II.13)$$

Substitution of equations II.10 and II.12 into equation II.13 gives

$$\begin{aligned}\dot{\beta} = \frac{1}{MV}(&-F_x\cos\alpha\sin\beta + F_y\cos\beta - F_z\sin\alpha\sin\beta) \\ &+ p\sin\alpha - r\cos\alpha.\end{aligned} \qquad (II.14)$$

The evolution equation for the angle of attack can be found in a similiar manner. Writing equation II.11a as

$$\sin\alpha = \frac{w}{\sqrt{u^2 + w^2}}$$

and then taking the derivative with respect to time, we have

$$\begin{aligned}\dot{\alpha} =& \sec\alpha\left(\frac{\dot{w}}{\sqrt{u^2+w^2}} - \frac{w}{\sqrt{u^2+w^2}}\frac{u\dot{u}+w\dot{w}}{u^2+w^2}\right)\\ =& \frac{1}{V\cos\alpha}(-\dot{u}\sin\alpha + \dot{w}\cos\alpha).\end{aligned} \qquad (II.15)$$

Substitution of equation II.10 into equation II.15 then gives

$$\dot{\alpha} = \frac{1}{MV\cos\beta}(F_z\cos\alpha - F_x\sin\alpha) + q - \tan\beta(r\sin\alpha + p\cos\alpha). \qquad (II.16)$$

II.3 Euler Angles

The Euler angles specify the orientation of the aircraft in inertial space and determine the direction of gravity relative to the aircraft axis system. There are an infinite number of combinations of rotations that lead to the same final orientation, but the Euler angles are commonly used in aircraft dynamics. The Euler angle convention for specifying an angular orientation is to start with the aircraft axes aligned with the inertial axes and then yaw about the aircraft z-axis, followed by pitch about the aircraft y-axis and finally roll about the aircraft x-axis.

The effect of each rotation can be computed by a linear transformation. If the (X, Y, Z) are the inertial coordinates and (x,y,z) are the aircraft coordinates, the effect of yawing the aircraft by ψ degrees can be computed with the relation

$$\begin{pmatrix} x \\ y \\ z \end{pmatrix} = \begin{pmatrix} \cos\psi & \sin\psi & 0 \\ -\sin\psi & \cos\psi & 0 \\ 0 & 0 & 1 \end{pmatrix} \begin{pmatrix} X \\ Y \\ Z \end{pmatrix} \qquad (II.17)$$

which can be written symbolically as

$$\vec{x} = T_\psi \vec{X}. \qquad (II.17a)$$

The coordinate transformation for a pitch rotation is

$$\begin{pmatrix} x \\ y \\ z \end{pmatrix} = \begin{pmatrix} \cos\theta & 0 & -\sin\theta \\ 0 & 1 & 0 \\ \sin\theta & 0 & \cos\theta \end{pmatrix} \begin{pmatrix} X \\ Y \\ Z \end{pmatrix} \qquad (II.18)$$

or

$$\vec{x} = T_\theta \vec{X}, \qquad (II.18a)$$

and the coordinate transformation for a roll rotation is

$$\begin{pmatrix} x \\ y \\ z \end{pmatrix} = \begin{pmatrix} 1 & 0 & 0 \\ 0 & \cos\phi & \sin\phi \\ 0 & -\sin\phi & \cos\phi \end{pmatrix} \begin{pmatrix} X \\ Y \\ Z \end{pmatrix} \qquad (II.19)$$

or

$$\vec{x} = T_\phi \vec{X}. \qquad (II.19a)$$

Thus, if $\vec{X}$ is a vector relative to the inertial axis system, then its components in the aircraft axis system are given by

$$\vec{x} = T_\phi T_\theta T_\psi \vec{X}. \qquad (II.20)$$

The components of the gravity vector in the aircraft axis system can be computed with equation II.20. In the inertial reference system, the gravity vector is given by

$$\vec{g} = \begin{pmatrix} 0 \\ 0 \\ g \end{pmatrix},$$

so the components in the aircraft axis system are

$$\vec{g} = \begin{pmatrix} -\sin\theta \\ \cos\theta\sin\phi \\ \cos\theta\cos\phi \end{pmatrix}. \qquad (II.21)$$

Note that the yaw angle does not affect the direction of the gravity vector relative to the aircraft axis system. This is a result of applying the yaw rotation first. Since the inertial and aircraft z-axes are initially alligned, rotating about the aircraft z-axis is the same as rotating about the gravity vector so its orientation relative to the aircraft is unchanged.

The rate of change of the Euler angles can be related to the rotation rates relative to the aircraft axis system by coordinate transformations, but care must be exercised in determining these transformations because the Euler angle rotations are relative to a nonorthogonal coordinate system. Yaw rotations are around the inertial z-axis, so equation II.20 can be used to show that the components of $\dot{\psi}$ in the aircraft axis system are given by

$$\begin{pmatrix} \omega_x \\ \omega_y \\ \omega_z \end{pmatrix} = \begin{pmatrix} -\sin\theta \\ \sin\phi\cos\theta \\ \cos\phi\cos\theta \end{pmatrix} \dot{\psi}. \qquad (II.22)$$

Pitch rotations are around an axis rotated ψ degrees from in the inertial Y-axis so only a roll rotation is required to determine the components of $\dot{\theta}$ in the aircraft axis system. Using equation II.19 gives the relation

$$\begin{pmatrix} \omega_x \\ \omega_y \\ \omega_z \end{pmatrix} = \begin{pmatrix} 0 \\ \cos\phi \\ -\sin\phi \end{pmatrix} \dot{\theta}. \qquad (II.23)$$

Roll rotations are around the aircraft x-axis so no transformation is required and

$$\begin{pmatrix} \omega_x \\ \omega_y \\ \omega_z \end{pmatrix} = \begin{pmatrix} 1 \\ 0 \\ 0 \end{pmatrix} \dot{\phi}. \qquad (II.24)$$

Summing equations II.22-24 gives

$$\begin{pmatrix} p \\ q \\ r \end{pmatrix} = \begin{pmatrix} -\sin\theta & 0 & 1 \\ \sin\phi\cos\theta & \cos\phi & 0 \\ \cos\phi\cos\theta & -\sin\theta & 0 \end{pmatrix} \begin{pmatrix} \dot{\psi} \\ \dot{\theta} \\ \dot{\phi} \end{pmatrix},$$

which can be inverted to give

$$\begin{aligned}\dot{\psi} &= (q\sin\phi + r\cos\phi)\sec\theta \\ \dot{\theta} &= q\cos\phi - r\sin\phi \\ \dot{\phi} &= p + (q\sin\phi + r\cos\phi)\tan\theta.\end{aligned} \tag{II.25}$$

REFERENCES

1. Culick, F. E. C., "Building a 1903 Wright 'Flyer' – By Committee," AIAA 26th Aerospace Sciences Meeting, 1988, AIAA Paper No. 87-0094.
2. Howard, F., *Wilbur and Orville - A Biography of the Wright Brothers*, New York, Ballantine Books, 1987.
3. Adams, William M., "Analytic Prediction of Airplane Equilibrium Spin Characteristics," NASA TN D-6926, November 1972.
4. Chambers, J. R., Bowman, J. S., and Anglin, E. L., "Analysis of the Characteristics of a Twin-Jet Swept-Wing Fighter Airplane," NASA TN D-5409, September 1969.
5. Nelson, R. C., *Flight Stability and Automatic Control*, New York, McGraw-Hill Book Company, 1989.
6. Phillips, W. H., "Effect of Steady Rolling on Longitudinal and Directional Stability," NASA TN No. 1627, June 1948.
7. Stone, R. W., "Estimation of the Maximum Angle of Sideslip for Determination of Vertical-Tail Loads in Rolling Maneuvers," NASA Report No. 1136, 1953.
8. Pinsker, W. J. G., "Critical Flight Conditions and Loads Resulting from Inertia Cross-Coupling and Aerodynamic Stability Deficiencies," A.R.C. Technical Report C.P. No. 404, 1958.
9. Rhoads, D. W., and Schuler, J. M., "A Theoretical and Experimental Study of Airplane Dynamics in Large Disturbance Maneuvers,"

Journal of Aeronautical Sciences, July 1957, pp. 507-526.

10. Welch, J. D., and Wilson, R. E., "Cross-Coupling Dynamics and the Problems of Automatic Control in Rapid Rolls," Journal of Aeronautical Sciences, October 1957, pp. 741-754.

11. Westerwick, R., "The Roll Coupling Problem – A Mathematical Approach," Aeronautical Engineering Review, December 1957, pp. 48-51.

12. Gates, O. B., and Minka, K., "Note on a Criterion for Severity of Roll-Induced Instability," Journal of the Aero/Space Sciences, May 1959, pp. 287-290.

13. Schy, A. A., and Hannah, M. E., "Prediction of Jump Phenomena in Roll-Coupled Maneuvers of Airplanes," Journal of Aircraft, Vol. 14, No. 4, April 1977, pp. 375-382.

14. Young, J. W., Schy, A. A., and Johnson, K. G., " Pseudosteady-State Analysis of Nonlinear Aircraft Maneuvers," NASA Technical Paper 1758, 1980.

15. Irving, H. B., "Simplified Presentation of the Subject of Spinning of Aeroplanes," A.R.C. R.M. No. 1535, 1933.

16. Scher, S. H., and Anglin, E. L., "Analytical Investigation of Effect of Spin Entry Technique on Spin and Recovery Characteristics for a 60 Degree Delta-Wing Airplane," NASA TN D-156, December 1959.

17. Grantham, W. D., and Scher, S. H., "Analytical Investigation and Prediction of Spin and Recovery Characteristics of the North American X-15 Airplane," NASA TM X-294, October 1960.

18. Grantham, W. D., and Grafton, S. B., "Effects of Aircraft Relative Density on Spin and Recovery Characteristics of Some Current Configurations," NASA TN D-2243, March 1965.

19. Anglin, E. L., "Relationship Between Magnitude of Applied Spin Recovery Moment and Ensuing Number of Recovery Turns," NASA TN D-4077, August 1967.

20. Tischler, M. B., and Barlow, J. B., "Determination of the Spin and Recovery Characteristics of a General Aviation Design," Journal of Aircraft, Vol. 18, No. 4, April 1981, pp. 238-244.

21. Guicheteau, P., "Bifurcation Theory Applied to the Study of Control Losses on Combat Aircraft," AGARD/FMP Symposium on "Combat Aircraft Maneuverability," Florence, October 1981.

22. Carroll, J. V., and Mehra, R. K., "Bifurcation Analysis of Nonlinear Aircraft Dynamics," J. Guidance, Vol. 5, No. 5, September-October 1982, pp. 529-536.

23. Planeaux, J. B., "High-Angle-of-Attack Dynamic Behavior of a Model High-Performance Fighter Aircraft," AIAA Atmospheric Flight Mechanics Conference, Minneapolis, August 1988, Paper No. 88-4368.

24. Jahnke, C. C., and Culick, F. E. C., "Application of Dynamical Systems Theory to Nonlinear Aircraft Dynamics," AIAA Atmospheric Flight Mechanics Conference, Minneapolis, August 1988, Paper No. 88-4372.

25. Guckenheimer, J., and Holmes, P., *Nonlinear Oscillations, Dynamical Systems, and Bifurcations of Vector Fields*, New York: Springer-Verlag, 1983.

26. Wiggins, S., *Global Bifurcations and Chaos*, New York: Springer-Verlag, 1988.

27. Ioos, G., and Joseph, D. D., *Elementary Stability and Bifurcation Theory*, New York: Springer-Verlag, 1980.

28. Keller, H. B., "Numerical Solution of Bifurcation and Nonlinear Eigenvalue Problems," in *Applications of Bifurcation Theory* (Edited by: P. H. Rabinowitz), New York: Academic Press, 1977.

29. Doedel, E. J., and Kernevez, J. P., "Software for Continuation Problems in Ordinary Differential Equations With Applications," Preprint, CALTECH.

30. Wylie, C. R., *Advanced Engineering Mathematics*, New York: McGraw-Hill Book Company, 1975.

31. Press, W. H., Flannery, B. P., Teukolsky, S. A., and Vetterling, W. T., *Numerical Recipes – The Art of Scientific Computing*, New York: Cambridge University Press, 1988.

32. Hacker, T., and Oprisiu, C., "A Discussion of the Roll-Coupling Problem," *Progress In Aerospace Science*, Vol. 15, 1974, pp. 151-180.

33. Chambers, J. R., Yip, L. P., and Moul, T. M., " Wind-Tunnel Investigation of an Advanced Canard Configuration," NASA Langley Research Center, Virginia, March 1983.

34. Ericsson, L. E., "The Various Sources of Wing Rock," AIAA Atmospheric Flight Mechanics Conference, Minneapolis, August 1988, Paper No. 88-4370.